# Applications of Ground-based Mobile Atmospheric Monitoring: Real-time Characterization of Source Emissions and Ambient Concentrations

A Thesis

by

**J. Douglas Goetz**

Submitted to the committee

of

Dr. Peter DeCarlo
Dr. Michael Waring
Dr. Sabrina Spatari
Dr. Raluca Ellis
Dr. Prakash Bhave

in partial fulfillment of the

requirements for the degree

of

Doctor of Philosophy

in Environmental Engineering

March 2017

# TABLE OF CONTENTS

# List of Table

## List of Figures

# Abstract

Gas and particle phase atmospheric pollution are known to impact human and environmental health as well as contribute to climate forcing. While many atmospheric pollutants are regulated or controlled in the developed world uncertainty still remains regarding the impacts from under characterized emission sources, the interaction of anthropogenic and naturally occurring pollution, and the chemical and physical evolution of emissions in the atmosphere, among many other uncertainties. Because of the complexity of atmospheric pollution many types of monitoring have been implemented in the past, but none are capable of perfectly characterizing the atmosphere and each monitoring type has known benefits and disadvantages. Ground-based mobile monitoring with fast-response in-situ instrumentation has been used in the past for a number of applications that fill data gaps not possible with other types of atmospheric monitoring. In this work, ground-based mobile monitoring was implemented to quantify emissions from under characterized emission sources using both moving and portable applications, and used in a novel way for the characterization of ambient concentrations. In the Marcellus Shale region of Pennsylvania two mobile platforms were used to estimate emission rates from infrastructure associated with the production and transmission of natural gas using two unique methods. One campaign investigated emissions of aerosols, volatile organic compounds (VOCs), methane, carbon monoxide (CO), nitrogen dioxide ($NO_2$), and carbon dioxide ($CO_2$) from natural gas wells, well development practices, and compressor stations using tracer release ratio methods and a developed fenceline tracer release correction factor. Another campaign investigated emissions of methane from Marcellus Shale gas wells and infrastructure associated with two large national transmission pipelines using the "Point Source Gaussian" method described in the EPA OTM-33a. During both campaigns ambient concentrations of methane, CO and other pollutants were continuously monitored while driving throughout the region. A smoothing technique was developed to remove contributions of direct unmixed emissions to produce a dataset that can be used in comparison with other monitoring techniques (e.g. stationary, aircraft). Finally, a portable mobile lab equipped with fast-response aerosol instrumentation including an Aerosol Mass Spectrometer (AMS) was used to characterize non-refractory aerosol and black carbon emissions from common, but under characterized emission sources in South Asia (i.e. brick kilns, cookstoves, open garbage burning, irrigation pumps). Speciated submicron aerosol emission factors, size distributions, and mass spectral profiles were retrieved for each emission source. This work demonstrates that ground-based mobile laboratory measurements are useful for characterizing emissions and ambient concentrations in authentic conditions outside of the conventional laboratory environment, and in ways not possible with other atmospheric monitoring platforms.

# Chapter 1: Ground-based Mobile Atmospheric Monitoring

Gas and particle phase atmospheric pollution are known to impact human and environmental health as well as contribute to climate forcing (IPCC, 2013) Many types of atmospheric pollution have been attributed to acute health effects, cardiovascular and respiratory disease, and increased risk of mortality (Brook et al., 2004;Dockery, 2001;Goldberg et al., 2006;Jerrett et al., 2009;Laden et al., 2000;Lipsett et al., 2011;Pope et al., 2004;Pope et al., 2009). Because of the harmful effects of atmospheric pollutants most are regulated in the United States and other developed countries through ambient standards like the National Ambient Air Quality Standards (NAAQS), or are listed as Hazardous Air Pollutants (HAPs). Additionally, emissions of atmospheric pollutants in the United States are often regulated, controlled, and monitored by federal and state agencies (EPA). Although many atmospheric pollutants are regulated, uncertainty still remains regarding the impact of pollutants on human health and environmental health, both domestically and globally, and their impact on climate forcing (IPCC, 2013). Much of the uncertainty regarding primary atmospheric emissions stems from under characterized or difficult to characterize sources such as newly developed emission sources (e.g. unconventional natural gas extraction (Field et al., 2014)), small but prevalent sources (e.g. vehicles (Canagaratna et al., 2010;Rogers et al., 2006;Zavala et al., 2009), cooking and heating (Fullerton et al., 2008)), temporally inconsistent sources (e.g biomass burning (Andreae, 1991)), and how natural sources (e.g. volcanic activity, mineral dust, sea-spray, biogenic) interact with anthropogenic sources (Andreae, 2007). Additional uncertainty arises from the chemical and physical evolution of primary emissions in the atmosphere (Canagaratna et al., 2010;DeCarlo et al., 2010) and in particular the creation of secondary pollutants such as ozone (Hakami et al., 2004) and secondary organic aerosol (Hallquist et al., 2009;Pandis, 1992).

To constrain uncertainty in atmospheric pollution and better understand exposure pathways many different monitoring techniques have been employed to quantify ambient concentrations and characterize emissions. Common monitoring types include stationary monitoring (single fixed receptor), stationary monitoring networks (multiple fixed receptors), ground-based mobile monitoring (unfixed receptor), aerial mobile monitoring (high altitude unfixed receptor), and satellite remote sensing. Of the listed monitoring types each has its own benefits and disadvantages when considering spatial and temporal properties of measurements. Conceptually, satellite remote sensing provides measurements at the largest spatial scale, but at the expense of spatial resolution and a low sampling rate. Stationary monitoring typically has high temporal continuity, but lacks in scale and spatial resolution because of its fixed location. A network of fixed monitoring sites has the same benefit of high temporal continuity, but also increases the spatial scale monitored and improves the spatial resolution compared to a single fixed site. However, the benefits of monitoring networks are often offset by the increased need of monitoring resources (e.g. instrumentation, manpower)

and increased analysis time. Additionally, fixed site monitoring is not always suitable for quantifying emissions from difficult to characterize sources. With the development of fast-response in-situ instrumentation mobile monitoring has become a viable option to balance the spatial and temporal deficiencies of fixed site and satellite monitoring (Kolb et al., 2004). Mobile monitoring, which could be as simple as a portable lab or as complex as an airplane equipped with instrumentation, provides increased spatial resolution (platform dependent) compared to fixed site and satellite monitoring and allows for measurement techniques not possible with continuous fixed site monitoring. Alternatively, mobile monitoring does not provide the same spatial scaling as satellite remote sensing and has limited temporal continuity compared to fixed site methods. Conceptually, between aerial or ground-based mobile monitoring, aerial monitoring has lower spatial resolution because measurements take place at higher speeds and often sample at well-mixed altitudes at or above the boundary layer height and therefore often do not measure contributions from individual sources.

Ground-based mobile monitoring has been implemented for a number of different monitoring applications as seen in the literature review shown in Table 1.1. Generally, a ground-based mobile platform is designed as a vehicle (e.g. automobile, bicycle, train) equipped with an external inlet system connected to 1 Hz or greater fast-response instrumentation and powered by the vehicle or an alternative power supply (e.g. batteries or generator) (Bush et al., 2015;Drewnick et al., 2012;Hagemann et al., 2014;Herndon et al., 2005a;Kolb et al., 2004). Open path remote sensing designs have also been implemented as see in Tao et al. (2015). Ground-based mobile platforms are often also equipped with high-precision GPS to record the geoposition of each atmospheric measurement (Bush et al., 2015). Additionally, some mobile laboratories are outfitted with meteorological equipment to measure wind conditions, temperature, pressure, and other parameters needed for data analysis (Brantley et al., 2014a;Brantley et al., 2014b).

Ground-based mobile monitoring can largely be classified into three applications of measurement as described by Brantley et al. (2014a), though significant overlap exists between the categories: 1. general ambient air quality surveying, 2. near source evaluation, 3. emissions quantification. Additionally, each application type can be organized by whether the mobile platform was used as a moveable portable laboratory (i.e. stationary during monitoring) or truly mobile laboratory (i.e. not stationary during monitoring) (Table 1.1).

**Table 1.1 Literature review of ground-based mobile measurements.**

| Study type | | Article Information | Objectives |
|---|---|---|---|
| overview | design | Kolb et al., 2004 | description of automotive mobile lab design and application |
| | | Drewnick et al. 2012 | description of automotive mobile lab design and application |
| | | Bush et al., 2015 | description of automotive mobile lab design and application |
| | | Hagemann et al., 2014 | description of train based mobile lab design and application |
| | | Tao et al., 2015 | design of open path remote sensing |
| | | Herndon et al., 2005 | summary of characterizing emissions and ambient concentrations |
| | data processing | Brantley et al. 2014 | data-processing strategies for mobile datasets |
| surveying | spatial distribution | Bukowiecki et al., 2002 | distribution of urban trace gases and aerosols in Zurich, Switzerland |
| | | Phillips et al., 2013 | distribution of natural gas pipeline leaks in Boston |
| | | Weiden-Reinmüller, 2014 | urban plume tracking near Paris, France |
| | | Jackson et al., 2014 | distribution of natural gas pipeline leaks in Washington, DC |
| | ambient (portable) | Lin et al., 2012 | formaldehyde monitoring in two locations New York City |
| | on road concentrations | Jiang et al. 2005 | black carbon and PAHs from vehicles in Mexico City |
| | | Rogers et al. 2006 | VOC from vehicles in Mexico City |
| | | Wang et al. 2009 | on road pollutants before and during Beijing Summer Olympics |
| | | Shields et al. 2013 | traffic related exposure in Mexico City |
| near source evaluation | near road concentrations | Weber et al. 2008 | particle concentrations in urban neighborhoods |
| | | Hu et al., 2009 | air pollution downwind of freeway in the early morning |
| | | Durant et al. 2010 | near-highway pollution gradients in winter |
| | | Sun et al. 2012 | near-highway emissions in New York City |
| | | Canagaratna et al., 2012 | evolution of near-highway aerosol |
| | | Massoli et al. 2012 | near-highway pollution gradient |
| emissions quantification | emissions (portable) | Onasch et al. 2009 | chemical properties of aircraft exhaust |
| | | Dallmann et al. 2012 | automobile emissions characterization at exit of tunnel |
| | direct emissions (mobile) | Shorter et al. 2005 | chase NOx emissions from New York City buses |
| | | Herndon et al. 2005 | chase emissions from curb-side passenger buses |
| | | Zavala et al. 2009 | chase emissions from vehicles in Mexico City |
| | | Wood et al. 2012 | combustion efficiency of chemical flares in Houston |
| | tracer ratio methods | Lamb et al. 1995 | development of tracer ratio methods |
| | | Allen et al. 2013 | direct measurement of methane verified using tracer ratio |
| | | Goetz et al. 2015 | VOC and other pollutant emissions estimated using tracers |
| | | Roscoli et al. 2015 | methane emissions estimated using tracer gases |
| | Gaussian modeling | Brantley et al. 2014 | application of point source Gaussian technique |
| | regional modeling | Buzcu-Guven et al., 2012 | uses a mobile dataset in adjoint neighborhood scale model |

Previous studies that have implemented mobile laboratories for ambient surveying have investigated either spatial distribution of pollutants, urban ambient concentrations, or on-road concentrations and distributions (Table 1.1). Phillips et al. (2013) and Jackson et al. (2014), for example, mapped and quantified natural gas leaks by mobile methane monitoring in two US cities. Bukowiecki et al. (2002) utilized a mobile lab to quantify differences in aerosol and trace gas concentrations between urban, suburban, and rural land use types in Switzerland. Another European study implemented a mobile laboratory to track and quantify an urban plume from Paris, France (von der Weiden-Reinmüller et al., 2014). In addition to spatial distributions mobile surveys have also been used to characterize on-road concentrations in urban areas to understand temporal and spatial trends and to identify emission sources (Jiang et al., 2005;Rogers et al., 2006;Wang et al., 2009). Many of the on-road studies are useful to quantify pollution exposure to urban residents and drivers (Shields et al., 2013). Because of the high spatial resolution of mobile ambient surveying the listed studies demonstrate that mobile monitoring is a useful measurement technique for monitoring in locations uncharacterized by stationary monitoring and to distinguish individual emission sources.

Near source evaluation studies have investigated how pollutants evolve both physically and chemically as they travel downwind (e.g. pollution gradients) and how areas are impacted by a proximate emission source (Table 1.1). Many of the near source studies investigated emissions from urban highways to characterize atmospheric contributions from vehicular exhaust. Canagaratna et al. (2010) and Massoli et al. (2012) used Aerosol Mass Spectrometers (AMS) and other instrumentation to evaluate aerosol gradients downwind of New York City highways. Another mobile gradient study by Durant et al. (2010) found that near-highway pollutant concentrations change rapidly within a short distance of the highway due to atmospheric mixing and chemical reactions. Evidence from the near source studies provided in Table 1.1 suggest that spatial ground-based mobile monitoring is well suited to evaluate rapidly changing properties of atmospheric pollutants because of the fine-scale spatial resolution of the measurements technique.

In addition to ambient and near source measurements ground-based mobile monitoring studies have utilized the platform to characterize a variety of emission sources in both portable and non-stationary labs (Table 1.1). Emission studies like Onasch et al. (2009) and Dallmann et al. (2012) demonstrate that portable laboratories are ideal platforms for characterizing emission sources in authentic conditions outside of the conventional laboratory space. Similarly, non-stationary platforms have been shown to be effective at characterizing emissions source in true operating conditions. For example, mobile chase studies have investigated tail-pipe emissions from buses and other vehicles while on-road under normal operating conditions (Durant et al., 2010;Herndon et al., 2005b;Shorter et al., 2005;Zavala et al., 2009). Additionally, many mobile emission studies have investigated large in-place operating sources (e.g. landfills, oil and natural gas facilities) by real-time plume interception (Brantley et al., 2014b;Goetz et al., 2015;Roscioli et al.,

2015;Wood et al., 2012;Yacovitch et al., 2015). In several studies mobile plume interception datasets have been used in conjunction with tracer ratio methods or atmospheric modeling to estimated emission rates or trace gases and aerosols from emission sources (Allen, 2013;Brantley et al., 2014b;Goetz et al., 2015;Lamb, 1995;Roscioli et al., 2015;Yacovitch et al., 2015). The listed emission studies demonstrate that ground-based mobile measurements are effective at characterizing difficult to measure emission sources and consequently helps constrain uncertainty in emission inventories and atmospheric models.

The following chapters provide methodology, results, and interpretation from three separate ground-based mobile monitoring campaigns. The work demonstrates the application of several known mobile monitoring techniques including ambient monitoring, near source measurements, and emission quantification of aerosols and trace gases in the Marcellus Shale region of Pennsylvania and emission quantification of under characterized sources in Nepal. This work also presents novel methods for the analysis of ground-based mobile monitoring datasets. In addition to presenting technical findings the following chapters will also describe how each study is associated with ground-based mobile monitoring and will discuss the completion status of each study.

# Chapter 2: Tracer Ratio Emission Estimates of Marcellus Shale Natural Gas Sites

## 2.1 Relevance and Status

This chapter combines ground-based mobile monitoring with the release of tracer gases to characterize emissions from Marcellus Shale natural gas infrastructure. The methodology is similar to other tracer ratio studies (Lamb, 1995;Roscioli et al., 2015) but also includes the development of a factor that corrects for releasing tracers at the fenceline instead of the location of site emission. The fenceline tracer release correction factor is a useful tool for studies to utilize when direct excess to the investigated emission source isn't possible. Measurements of emission rates of methane and other atmospheric pollutants from difficult these difficult to measure sources are crucial to build a body of statistics to fully understand the impacts of Marcellus Shale development. From a regional perspective, top-down approaches (typically aircraft based) for estimating emission rates have consistently exceeded regional bottom-up emission inventories (Zavala-Araiza et al., 2015b). The mobile measurements conducted in this work help reconcile differences that has been observed between the top-down and bottom up approaches by providing authentic variability in emission rates from in operation production and gathering infrastructure associated with unconventional natural gas development. The results demonstrate that ground-based mobile measurement methods are advantageous for characterizing emissions from difficult and under measured sources. This work in this chapter is published in a peer-reviewed journal as:

Goetz, J. D.; Floerchinger, C.; Fortner, E. C.; Wormhoudt, J.; Massoli, P.; Knighton, W. B.; Herndon, S. C.; Kolb, C. E.; Knipping, E.; Shaw, S. L.; DeCarlo, P. F., Atmospheric Emission Characterization of Marcellus Shale Natural Gas Development Sites. Environmental Science & Technology 2015, 49, (11), 7012-7020.

## 2.2 Summary

Limited direct measurements of criteria pollutants emissions and precursors, as well as natural gas constituents, from Marcellus shale gas development activities contribute to uncertainty about their atmospheric impact. Real-time measurements were made with the Aerodyne Research Inc. Mobile Laboratory to characterize emission rates of atmospheric pollutants. Sites investigated include production well pads, a well pad with a drill rig, a well completion, and compressor stations. Tracer release ratio methods were used to estimate emission rates. A first-order correction factor was developed to account for errors introduced by fenceline tracer release. In contrast to observations from other shale plays, elevated volatile organic compounds, other than $CH_4$ and $C_2H_6$, were generally not observed at the investigated sites. Elevated submicron particle mass concentrations were also generally not observed. Emission

rates from compressor stations ranged from 0.006 to 0.162 tons per day (tpd) for $NO_x$, 0.029 to 0.426 tpd for CO, and 67.9 to 371 tpd for $CO_2$. $CH_4$ and $C_2H_6$ emission rates from compressor stations ranged from 0.411 to 4.936 tpd and 0.023 to 0.062 tpd, respectively. Although limited in sample size, this study provides emission rate estimates for some processes in a newly developed natural gas resource and contributes valuable comparisons to other shale gas studies.

## 2.3 Background and Motivation

The Marcellus shale is the largest shale gas resource in the contiguous United States (1). Found in the Appalachian region, the Marcellus basin has an area of 240,000 $km^2$ underlying parts of Maryland, New York, Ohio, Pennsylvania, and West Virginia (Kargbo et al., 2010;Allen, 2013) and it is estimated to contain 84 billion cubic feet of technically recoverable natural gas (Coleman, 2011). The US Energy Information Agency estimated that the Marcellus shale gas resource could support up to 90,000 individual wells (Energy Information Administation, 2012); four times more than any other shale gas resource in the United States, and approximately eight times the number of Marcellus wells as of 2012 (HPDI, 2012;Energy Information Administation, 2012).

As the development and production of unconventional natural gas resources continues there has been growing concern about its impact on the environment and human health due to the potential degradation of local and regional air quality (AQ) (Moore et al., 2014). Likewise, there has been significant debate regarding the extent of greenhouse gas emissions from the entire lifecycle of shale gas compared to other fossil fuels like coal (Weber and Clavin, 2012;Stephenson et al., 2011;Mohan et al., 2011;Howarth, 2011;Dale, 2013;Burnham et al., 2011). Natural gas (NG) is known to produce less carbon dioxide ($CO_2$), nitrogen oxides ($NO_x$), sulfur dioxide ($SO_2$), black carbon (BC), and other pollutants than oil or coal combustion per unit of energy (Hayhoe, 2002). A study by de Gouw et al. (2014) found that since 1997 emissions from fossil fuel power plants in the United States have decreased their $CO_2$ emissions by 23% and $NO_x$ emissions by 40% due in part to the replacement of coal by NG systems. However, the extent of AQ relevant emissions from upstream shale gas activities like extraction, processing, and transmission is poorly known.

The shale gas extraction process includes minor but widely distributed transitory emission sources including well pad construction, horizontal well drilling, hydraulic fracturing, and well completion (6). Off-road diesel (e.g. generators, pumps, and drill rigs) and on-road diesel (e.g. trucking and transport) engines are used throughout the extraction process. Heavy-duty diesel engines are known to emit a variety of pollutants including carbon monoxide (CO), $CO_2$, $NO_x$, $SO_2$, organic and inorganic particulate matter (PM), BC, heavy metals, and volatile organic compounds (VOC) (Shah et al., 2006; Lowenthanl et al., 1994; Graham et al., 2008; Durbin et al., 2008). Well completion, one of the final steps before production, involves the recovery of residual liquids and sand, or flowback, from the hydraulic fracturing process. The flowback can contain dissolved gases such as methane ($CH_4$) and other

components of NG. Once the flowback is recovered, the gases contained in the flowback are either directly emitted to the atmosphere, flared, or the NG is reclaimed and emissions are reduced by a "green completion" process. An environmental impact statement indicates that flowback gas flaring can emit criteria pollutants, VOC, and hazardous air pollutants (HAPS), with the quantity of $SO_2$ and HAPS increasing with heavier hydrocarbon content (e.g. wet gas) (NYS DEC, 2011). A recent study that investigated $CH_4$ emissions from shale gas operations throughout the United States, found that emissions from well completions had a wide range of values (from 0.01 to 17 Mg) suggesting that the quantity emitted is likely controlled by variable factors such as completion procedures (Allen et al. , 2013).

The routine production and distribution aspect of Marcellus shale development involves small but persistent sources of both combustion and NG related emissions including production well pads, pipelines, compressor stations, and gas processing facilities. On an annual per well basis, it is estimated that production sites in the Marcellus Basin emit between 46-1200 kg VOC, 520-660 kg $NO_x$, 9.9-50 kg $PM_{2.5}$, and 3.1-4.0 kg $SO_x$ (Litovitz, 2013). Allen et al. (2013) estimated that equipment leaks from the natural gas production sector are responsible for an average of 291 Gg of $CH_4$ per year nationally. Since few measurements of AQ relevant pollutants have been made in the Marcellus Shale region, these estimates are typically based on emissions from other plays. Compressor stations generally utilize NG fired compressor engines that run continuously to transport gas from local well sites to larger pipelines. A review of air quality permits for compressor stations in Pennsylvania shows that a single facility can have an average of 4 compressor engines (with a range of 1 to 12), each with a power capacity ranging from 800-3,500 bhp (Rupakheti et al., 2016). Compressor stations also typically have other sources of emission including process equipment such as glycol dehydrators and in-line heaters. In a similar review of Pennsylvania air quality permits, Litovitz et al. (2013) found that if operating at full capacity a compressor station in Pennsylvania has the potential to emit 11-45 Mg of VOC and 46-90 Mg of $NO_x$ per year.

As much of the Marcellus shale production is recent there has been scant research into the characteristics and potential impacts of emission sources on AQ. Additionally, there is very limited ambient AQ monitoring coverage in the Marcellus region, particularly in rural areas with high densities of NG development activity (2014). Carlton et al. (2014) suggest that the data gap in air quality monitoring in the Marcellus Shale basin could be limiting air quality management for the region. The objective of this study is to improve the current understanding of potential regional air quality impacts through the characterization of the emissions of criteria air pollutants, hazardous air pollutants, and greenhouse gases from emission sources associated with Marcellus shale development by the use of real-time mobile measurements. This study investigates both transient and persistent sources of emission, with the goal of characterizing emissions from several sites that are part of the shale gas extraction and distribution process.

## 2.4 Methods

The Aerodyne Research Inc. Mobile Laboratory (AML) (2004) was used during the summer of 2012 to collect ambient air data in two regions of Pennsylvania within the Marcellus Shale Basin with NG development activity. The first campaign took place in Northeast Pennsylvania (NE) centering on Sullivan and Bradford counties in August of 2012. The second took place in September 2012 in several counties of Southwestern Pennsylvania (SW). The sampling locations were chosen because these areas are known to have a high-density NG activity (See Figure 2.1). Furthermore, the two areas are known to have compositional differences in NG, with dry gas (mostly $CH_4$) in the NE and both wet gas ($CH_4$ with other light hydrocarbons) and dry gas in the SW (PA DEP, 2011).

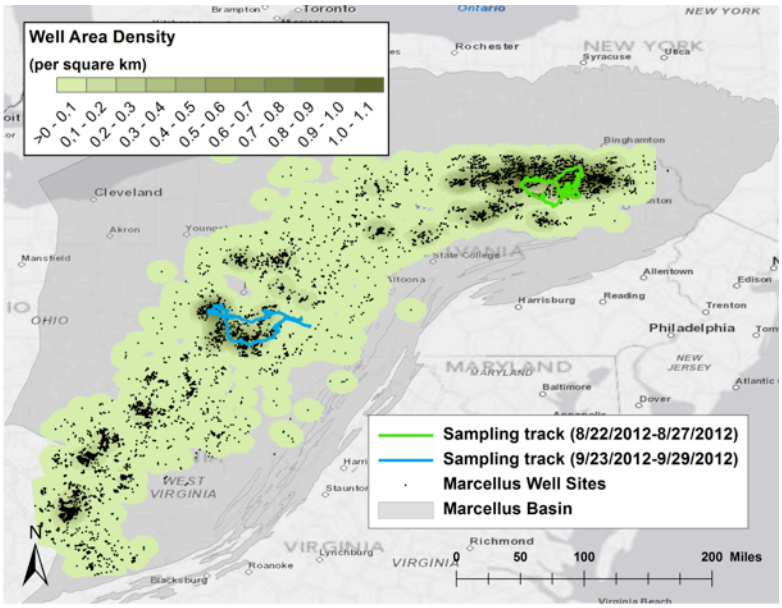


**Figure 2.1 The Marcellus Shale Basin**
The Marcellus Shale Basin (grey) with well area density (per km2) classified in green with a raster cell size of 2 km and a neighborhood radius of 15 km. Mobile lab sampling tracks are indicated for the SW (blue) and NE (green) study areas. Production wells active in 2012 are indicated with black dots.

Mobile measurements were made at specifically targeted sites of interest and while driving in areas of high development and production activity. A master list of potential sites of interest was created to identify facilities representing all major steps of shale gas extraction, production, and distribution. The master site list was developed from publicly available Pennsylvania databases and contained 54 compressor stations of various sizes, 460 wells where

drilling had recently commenced (SPUD), approximately 3800 wells that were know to be in production, and other site types all within the study area (Rupakheti et al., 2016;PA DEP, 2011). A refined list was developed after pre-measurement surveys that verified site activity, and adequate road conditions and topography. Subsequently, final site selection was made on each measurement day, and decisions were based primarily on local meteorology and drive time. Site selection was not based on the observation of emission downwind of the site. Tracer release ratio methods based on work by Lamb et al. (1995) were utilized to estimate the emission rate of measured pollution species at each targeted site similar to other recent studies (Allen et al., 2013), although without site access. Tracer release ratio experiments were conducted 17 times at 13 separate sites over the course of both measurement campaigns. Table 2.1 indicates the assigned name of the site, site type, the relative size, and the number of tracer release experiments performed at each site. The table also shows the sampling duration of each site, the average downwind distance of the measurements from the site, and the average correction factor applied to the emission estimates, which will be discussed later in this work.

**Table 2.1. 2012 Tracer Release Site List**

| Source Type | Site Name[a] | Region | Capacity (bhp)[c] | Experiments | Sample Duration (Hr) | Sample Downwind Distance (m) | Corr. Factor |
|---|---|---|---|---|---|---|---|
| Compressor Station | C-A | SW | 5285 | 1 | 2.5 | 1100 | 1.27 |
| | C-B | NE | 5360 | 1 | 1.1 | 480 | 0.67 |
| | C-C | SW | 8165 | 1 | 1.8 | 980 | 0.58 |
| | C-D | NE | 9000 | 1 | 1.7 | 1020 | 1.54 |
| | C-E | SW | 14000 | 1 | 2.0 | 660 | 0.88 |
| | C-F | NE | 14200 | 2 | 1.2, 2.3 | 730, 710 | 2.68,1.89 |
| | C-G | NE | 15300[b] | 1 | 1.5 | 900 | 2.98 |
| | C-H | NE | 16560 | 2 | 1.0 | 500 | 1.30 |
| Wells in Production | W-A | SW | 7 wells | 1 | 2.5 | 750 | 1.48 |
| | W-B | SW | 9 wells | 1 | 2.2 | 700 | 1.06 |
| | W-C | SW | 9 wells | 1 | 2.0 | 560 | 0.61 |
| Gas Processing | P-A | SW | N/A | 1 | 2.0 | N/A | N/A |
| Well Drilling | T-A | NE | N/A | 1 | 1.0 | 890 | 1.28 |
| Completion | T-B | NE | N/A | 2 | 3.3 | 650 | 1.66 |

a. See Appendix A for more information about tested facilities.
b. Electric powered compressor station.
c. 1 bhp is equivalent to 746 watts (W).

### 2.4.1 Instrumentation

For this study the AML was deployed to measure most regulated pollutants, including criteria pollutants and HAPs, and major constituents of NG. All of the instruments equipped on the AML utilized real-time rapid response measurements, typically with sampling rates of ~1 Hz. A list of calibration procedures for the instrumentation equipped on the AML can also be found in the Appendix B.

Quantum Cascade Laser (QCL) trace gas monitors: Select gas phase species including methane ($CH_4$), ethane ($C_2H_6$), acetylene ($C_2H_2$), carbon monoxide, and nitrous oxide ($N_2O$) were measured using three Aerodyne Research Inc. QCL trace gas monitors. The QCL monitors use tunable infrared laser direct absorption spectroscopy (QCL-TILDAS) and have measurement sensitivity ranging from 0.3 to 1 ppbv (2004). It is important to note that $C_2H_6$ was only measured in the SW because the development of the QCL-TILDAS for the measurement of $C_2H_6$ occurred after measurements in the NE.

Thermo Scientific 42i NO/$NO_2$ monitor: The nitrogen oxide species, NO and $NO_y$, were measured using commercial chemi-luminescence analyzers. For this study, $NO_y$ (total reactive nitrogen) was assumed to be $NO_x$ (NO+NO2) because we directly measured primary emissions plumes, which contain negligible secondary reactive nitrogen species (Dunlea et al., 2007).

Cavity Attenuated Phase Shift $NO_2$ monitor: Nitrogen dioxide ($NO_2$) was directly measured using an Aerodyne Research, Inc. cavity attenuated phase shift $NO_2$ monitor (CAPS-$NO_2$) (Kebabian et al., 2008). Because of technical issues, CAPS-$NO_2$ measurements were only available for the campaign in the SW.

Licor 6262 $CO_2$ monitor*:* Carbon dioxide ($CO_2$) was measured using a non-dispersive infrared unit.

TSI Condensation Particle Counter 3022: Particulate number concentration was measured using a condensation particle counter.

Aerodyne Research Inc. Soot-Particle Aerosol Mass Spectrometer (SP-AMS): Submicron particulate matter mass ($PM_1$) and composition, including non-refractory aerosols and black carbon, were measured using an SP-AMS (Onasch et al., 2012). This data was gathered on a 1 second timescale.

Proton-Transfer Reaction Mass Spectrometer (PTR-MS): A PTR-MS measured oxygenated and unsaturated volatile organic compounds including NG constituents, HAPs, and biogenic species (de Gouw and Warneke, 2007). A full list of masses monitored by the PTR-MS and their corresponding detection limits can be found in Table 2.2. For this study the PTR-MS had a sampling period of ~3 seconds.

Additional Measurements on the AML: In addition to ambient air monitoring instrumentation, the AML was also equipped with high precision GPS and meteorological instruments to establish position, bearing, driving speed, wind

direction, wind speed, temperature, pressure, and other parameters necessary for data analysis. All instrument data was processed and analyzed using Igor Pro 6.34, (Wavemetrics, Lake Oswego, OR).

**Table 2.2. Ion Mass and Limit of Detection (LOD) of Compounds Monitored by the PTR-MS.**

| Mass (amu) | Major chemical species monitored | LOD (ppbv) |
|---|---|---|
| 21 | O-18 isotope $H_3O^+$ reagent ion | --- |
| 34 | $O_2^+$ O-18 isotope | --- |
| 33 | methanol | 3.8 |
| 39 | O-18 isotope $H_3O^+(H_2O)$ reagent ion | --- |
| 42 | acetonitrile | 0.4 |
| 43 | propene, fragment ion of acetic acid and larger alkenes | 1.5 |
| 45 | acetaldehyde | 1.9 |
| 49 | methyl mercaptan | 0.2 |
| 57 | butenes, fragment ion of butanol and larger alkenes | 1.7 |
| 59 | acetone | 1.4 |
| 61 | acetic acid | 1.2 |
| 69 | isoprene | 0.7 |
| 71 | methacrolein + methyl vinyl ketone, fragment ion of larger alkenes | 0.6 |
| 79 | benzene | 0.7 |
| 93 | toluene | 0.3 |
| 107 | C2-benzenes | 0.5 |
| 121 | C3-benzenes | 0.5 |
| 137 | monoterpenes | 0.2 |

## 2.4.2 Tracer Release Ratio Measurements

Dual tracers were implemented at targeted sites to estimate whole site emissions. For each tracer ratio experiment $N_2O$ and $C_2H_2$ were used as tracer gases and were released at a fixed rate from tanks attached to the bed of a stationary pick-up truck at a height of 3 m. They were chosen because they are routinely available in industrial grade, cost effective, and inert on the time scale of these experiments. The relative detection sensitivity of the QCL monitors to $C_2H_2$ and $N_2O$ are adequate and exceptional, respectively. Typically, $N_2O$ was released at a rate of 24 standard liters per minute (SLPM) and $C_2H_2$ was released at 5 SLPM. However, at some sites the tracer gases were released at different fixed rates because of site conditions. The flow rate from each tank was controlled by Alicat® MC-series mass flow controllers. A high-precision GPS was used to determine the location of each tracer release. 1 Hz measurements of wind speed and wind direction were recorded at a height of 3 m at the tracer release point.

At each site, the location of tracer release was chosen in order to be as close as feasible to the presumed emission release point. For this study we did not have access to the tested facilities and therefore were unable to release tracer gases on-site, and co-located with emission sources. Consequently, we released tracers at the fenceline and attempted to position the tracers so the direction of their plume was in line with the expected site emission plume based on prevailing wind conditions. Once the tracer was positioned and activated at a site, the AML would make ambient measurements while driving on the downwind roads in the vicinity of the site. Out of plume measurements were used to characterize the non-plume "background" concentrations of the measured species and to distinguish other emission sources in the area. Downwind of the site and tracer release location, the AML transected the tracer-containing emission plumes. Five or more transects through emission plumes were made, which typically took ~2 hours (Table 2.1). The resulting downwind source and dual tracer plume measurements above the background were used to estimate the emission rate of pollution species at each site (Lamb et al., 1995;Allen et al., 2013). The background concentration for each plume transect was determined by the average of ten measurements before the plume intercept and ten measurements after the plume. This background value was then subtracted from plume transect measurements to determine a Δppbv value (See Figure 2.2). A first-order correction factor was determined for each plume transect to correct for the fact that tracers were not co-located with sources as described below. This method allows for the identification of point source emissions, but is not ideal for identifying large area sources that would appear as an elevated background value rather than a distinct plume.

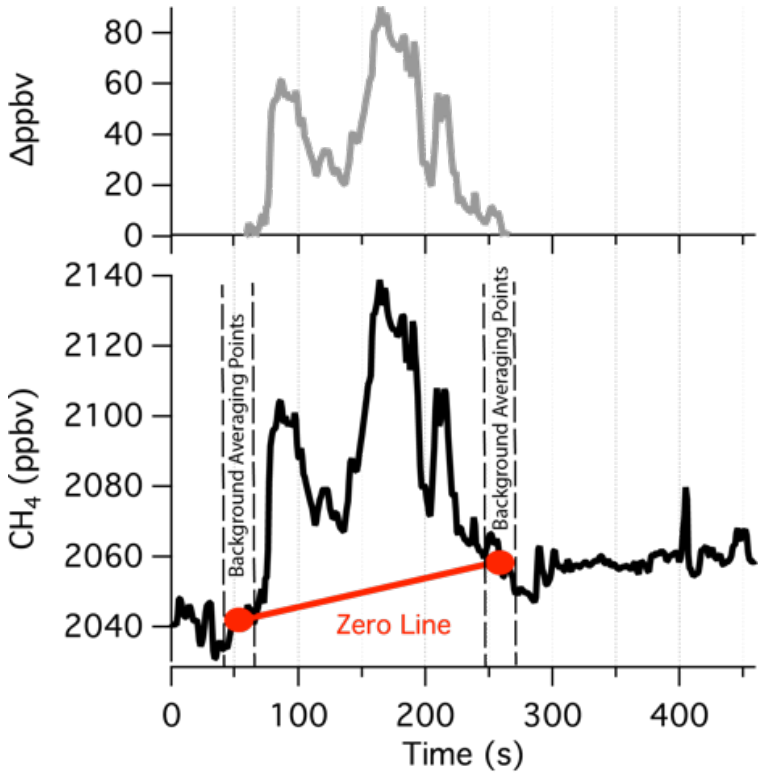


**Figure 2.2 Time Series of Emission Plume**
Time series of an emission plume transect measured from a Marcellus Shale well site in production (bottom panel) with the resulting Δppbv based on the background zero line (top panel). The 10-second background averaging points used to create the zero line are indicated with dashed lines. The calculated zero line used for background subtraction is indicated in red.

### 2.4.3 Site Emission Rate Calculation

Two techniques were used to estimate site emission rates of the measured pollution species. The first technique utilizes an orthogonal distance linear regression analysis of the downwind plume Δppbv values of the source emission versus the downwind plume Δppbv values of the dual tracer to determine the emission ratio of emitted pollutant species to tracer for each plume intercept (Figure 2.3c). The second technique utilizes the downwind plume-integrated mixing ratios (Δppbv*s) of the source emission and the tracer to determine an emission ratio for each plume intercept at each site (Figure 2.3b). Average emission ratios for each measured species for each site were calculated as follows. Based on a preliminary survey of regression method (RM) results, only plume transects where the regression analysis of the species of interest versus the $N_2O$ tracer resulted in a correlation coefficient (Pearson's R) greater than

0.60 were included in the average emission ratio calculation. Using the integration method (IM), only plume transects with an average Δppbv value greater than 3 times the instrument noise were accepted. Site emission rates were then calculated by multiplying the known tracer release rate by the average emission ratio for the site. It should be noted that $N_2O$ was used as the primary tracer species for analysis because of it had lower noise and background variability compared to $C_2H_2$.

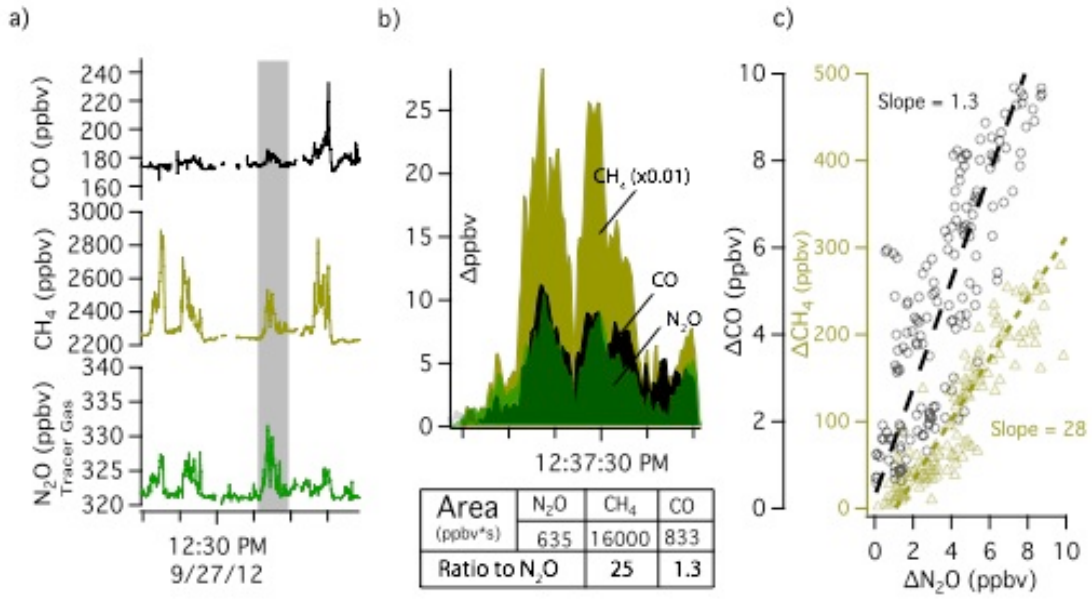


**Figure 2.3. Example of Tracer Release Ratio Methodology**
a) Time series of CO, $CH_4$, and $N_2O$ (tracer gas) during tracer release at a Marcellus Shale site with one plume intercept highlighted in gray. b) Time series of select plume intercept with crosswind integrated concentration denoted and emission ratios. c) Regression analysis of plume intercept with resulting emission ratios denoted. The Pearson's R value for the ΔCO regression is 0.86 and the $\Delta CH_4$ regression is 0.92

## 2.4.3 Fenceline Tracer Release Correction Factor

Because we performed fence line tracer release at each site, the release location was offset spatially from the site emission source. The tracer offset distance was different for each site with an average of ~200 meters, and ranged from 40 to 750 meters. Because of the tracer offset with the emission source, errors in emission rate estimates depend on the distance between the tracer release and source, the distance downwind where the tracer and emission plume is encountered and the direction of the offset with respect to the wind. For example if the tracer release location is offset about 50m to the South of the site with a southerly wind as shown in Figure 2.4, the tracer plume will have a larger

crosswind concentration and have undergone more horizontal and vertical dispersion compared to if the tracer were perfectly collocated with the site. If the tracer release is positioned downwind of the site, the crosswind concentration will be lower compared to a situation where the release is at the site emission source. Alternatively, if the tracer was located directly to the west or east 50m away and the wind continues from the South then the tracer plume will have the same decrease in ground level concentration due to vertical dispersion as if it were collocated with the site, but the plumes would be offset in space perpendicular to the wind direction (Figure 2.4). Therefore, if wind direction and wind speed are constant an important metric for understanding error due to tracer offset is the orthogonal distances from the plume transect location to the tracer release location and the orthogonal distance to the Marcellus site.

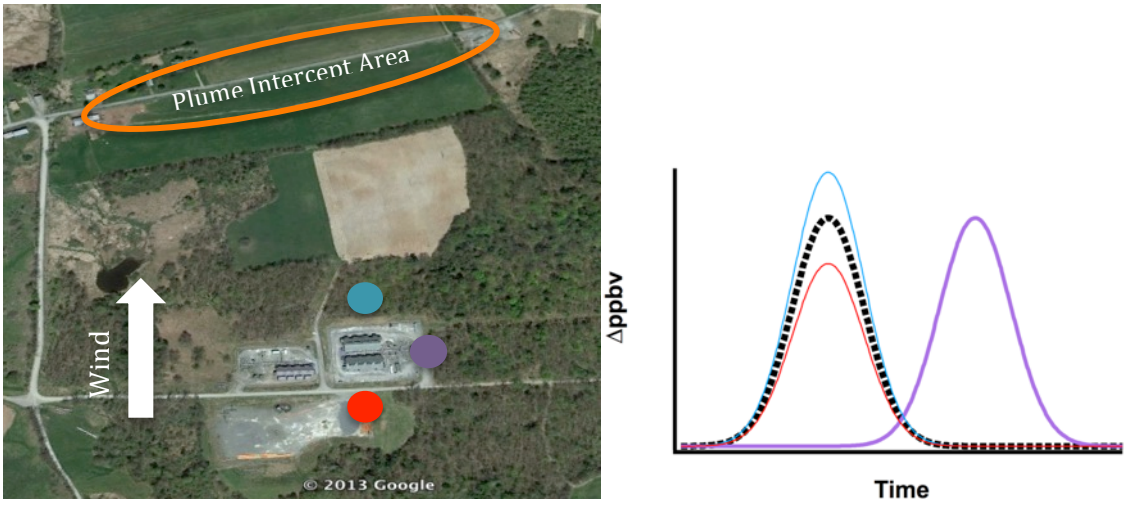


**Figure 2.4 Motivation for the Development of a Fenceline Tracer Release Correction Factor**
a) Example diagram of upwind (red), crosswind(purple), and downwind (blue) tracer release positions and plume intercept area at a compressor station. b) Theoretical plume intercept time series if the tracer was positioned on site (dashed), upwind (red), crosswind (purple), and downwind (blue) with the vehicle traveling from left to right in the plume intercept area.

The change in plume concentration at the sampling height of the AML due to tracer offset can be estimated using Gaussian plume dispersion theory. In a Gaussian plume dispersion equation that accounts for ground reflectance there are several key parameters including emission rate (Q), wind speed (u), emission height (H), distance downwind (x), distance adjacent to the centerline of the plume (y), measurement height (z), the vertical dispersion coefficient ($\sigma_z$), and the horizontal dispersion coefficient ($\sigma_y$) (Beychock, 2005). Equation 2.1 shows the Gaussian plume dispersion equation used in this work where C is the concentration at point x,y. The dispersion coefficients have been determined empirically, and the Pasquill stability classes of A through F can be used to approximate dispersion (Beychock, 2005).

$$C = \frac{Q}{u\,\sigma_z\,\sigma_y\,2\pi} e^{-y^2/2\sigma_y^2}\left[e^{-(z-H)^2/2\sigma_z^2} + e^{-(z+H)^2/2\sigma_z^2}\right] \quad (2.1)$$

Using the Gaussian plume equation, the crosswind concentration of generic plume intercepts at different distances downwind can be made by setting all parameters except for x and y which are held constant. For this work a model environment was created where $N_2O$ was emitted in a fixed wind direction at a rate of 24 slpm at a height of 3m and the receptor height was 3m. For each Pasquill stability class, and for wind speeds ranging from 1 to 10 m/s, the concentration in 1000 meter perpendicular plume transects was calculated (Figure 2.5). This was done for every 100m downwind of the emission point for up to 1000m. For each scenario, the plume intercept crosswind integrated concentration was found. The integrated plume concentration was used to produce curves for each stability class of integrated plume area versus distance downwind for each meteorological scenario (Figure 2.5). For each curve a double exponential distribution (functionally similar to the Equation 2.1) was fit to each wind speed curve. Each fit was tested using a Kolmogorov-Smirnov goodness-of-fit test to determine the goodness of fit for the double exponential distribution to the model data. It was determined that the fits matched the data well with D values significantly lower than the critical value.

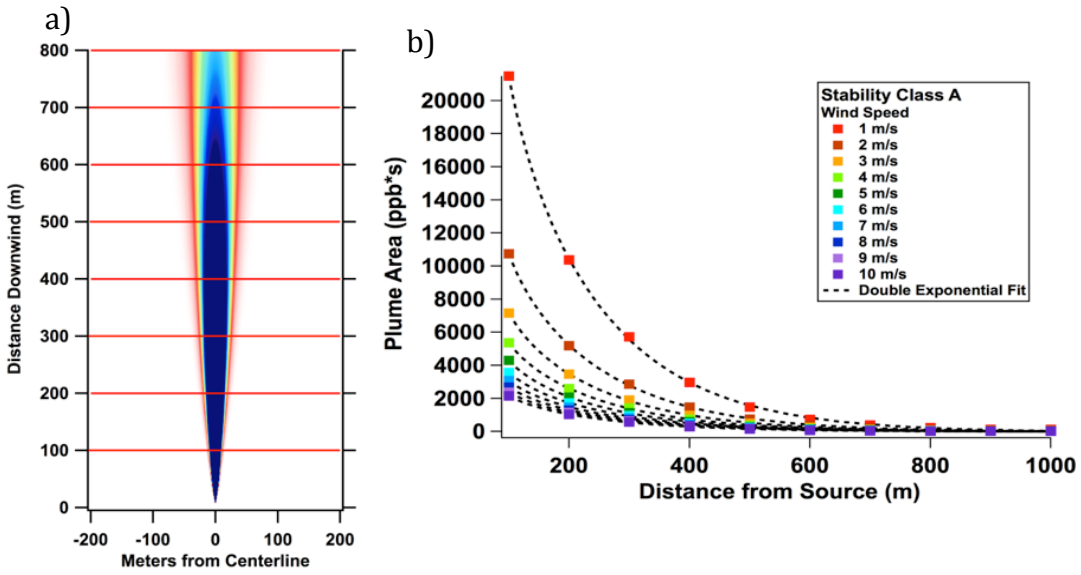


**Figure 2.5 Modeling Environment for Correction Factor**
a) Example of generic plume intercepts at intervals of 100m downwind for a model Gaussian plume with a Pasquill stability class A and a wind speed of 1 m/s. b) Plume intercept crosswind integrated concentration versus the distance of the intercept from the source. Values for different wind speeds and double exponential fit lines are included.

The parameters from the double exponential fits were used to produce a first-order correction factor for tracer offset. The correction factor is simply the ratio of the plume intercept cross wind integrated concentration of the tracer if it were released on-site ($Y_s$) to the plume intercept cross wind integrated concentration when the tracer is released from its true position ($Y_t$). Since this ratio is unknown, the correction factor (CF) can be estimated by using a ratio calculated from the double exponential fit equations for the given meteorological conditions (i.e. windspeed and stability class) and the orthogonal distances from the plume intercept to the site ($x_s$) and tracer release location ($x_t$) (Equation 2.2).

$$CF = \frac{Y_s}{Y_t} = \frac{y_{o+}\ A_1\ \exp\left[{}^{-X_S}/_{\tau_1}\right] + A_2\ \exp\left[{}^{-X_S}/_{\tau_2}\right]}{y_{o+}\ A_1\ \exp\left[{}^{-X_t}/_{\tau_1}\right] + A_2\ \exp\left[{}^{-X_t}/_{\tau_2}\right]} \qquad (2.2)$$

The correction factor, calculated for each plume intercept at each site, was then used to modify the measured emission ratio for each site intercept to reflect changes due to offset distance (Equation 2.3).

$$Emission\ Rate\ =\ Emission\ Ratio\ x\ \frac{1}{CF}\ x\ Tracer\ ER \qquad (2.3)$$

Here Emission Rate refers to the emission rate of the species of interest (e.g. CO, CH4, NOx, etc.) in liters per minute. The Emission Ratio is determined from the regression of the species of interest with the tracer (typically $N_2O$), and the Tracer ER referring to the emission rate in liters per minute of the tracer species used to determine the Emission Ratio. The resulting correction factors based on the average meteorological conditions and orthogonal distances at each tracer release site can been seen in Table 2.1, which ranges from ~0.5 to 3.0. The major sources of uncertainty in the correction factors come from meteorological parameters (i.e. wind speed and stability class) and topography at each site. The first-order correction factor is a useful tool for reducing uncertainty in tracer ratio methods due to fenceline tracer release.

## 2.5 Emission Rates

The emission rate results for $CH_4$, $C_2H_6$, CO, $CO_2$, $NO_x$, VOC, and $PM_1$ with correction factors applied are presented in the following sections. All emission rate values are shown in metric tons per day (tpd). The results indicate

that the RM was often not applicable for some pollution species at some sites because none of the plume transects met the criteria ($R > 0.6$) to be included in the average emission rate results. An error assessment of the different emission ratio techniques was performed using the known release ratios of the dual tracers (Figure 2.6) Factor error (FE), or the observed tracer ratio divided by the known tracer release ratio for each plume intercept, is a useful metric for the comparison of error between the two emission ratio methods. The dual tracer results show that the integration method (IM) for determining emission ratios produced a larger error distribution compared to the RM (Figure 2.6). Gaussian fits of the *log(FE)* reveal that there is a slight positive bias associated with both methods (Figure 2.6). Although the regression method (RM) produces a tighter error distribution, it is not necessarily the better method for estimating emission rates with fenceline tracer release because of site-specific characteristics. For example, if the tracer plume is offset crosswind from the site emission plume then the RM will produce results with poor correlation and possibly be excluded from the site averaging. Similarly, if the intercepted tracer plume has a dissimilar shape than the site plume it could yield results with a poor correlation. The IM, however, does not have the same restrictions and therefore is possibly better suited for fenceline tracer release. Although the error assessment indicates that the RM has a smaller error distribution than the IM, comparisons to literature and other discussion points are made with IM results because it contains the larger dataset.

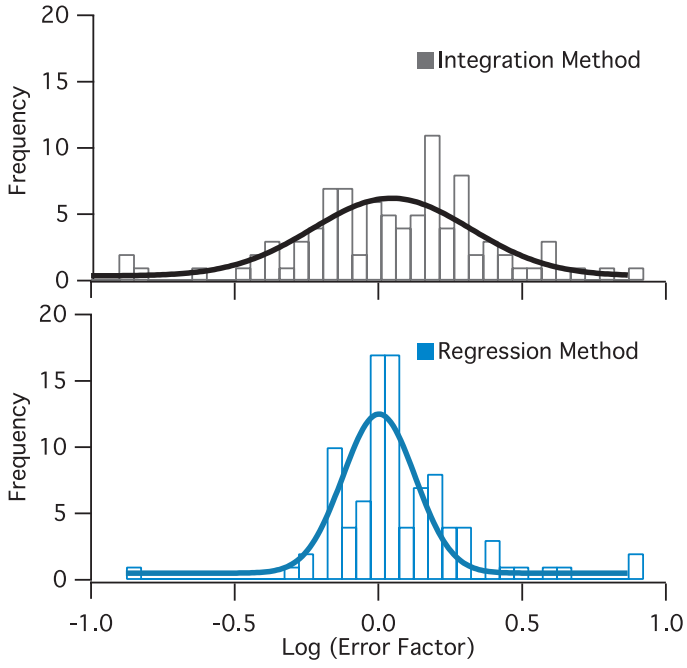


**Figure 2.6. Histogram of the log of the factor error and Gaussian fits for the two emission ratio methods.**

The ambient VOC concentrations for many of the compounds monitored by the PTR-MS were at or near the mobile mode detection limit for the instrument. Most notably, we did not observe elevated levels of any of the light aromatic compounds (benzene, toluene etc.) that have been previously observed in oil and NG emissions (Pétron et al., 2012;Gilman et al., 2013;Warneke et al., 2014). With the exception of $CH_3OH$, which was observed at one compressor station and has been observed at NG well pads (Warneke et al., 2014), all of the other VOCs detected have been attributed to on-road engine exhaust. The absence of light aromatics in NG emissions observed the Marcellus basin is not surprising because the play does not have associated oil deposits, and consequently non-alkane VOCs are not expected to be widely present (NYS DEC, 2011). It should be noted that $CH_4$ and $C_2H_6$ were the only short-chain alkanes measured in this study, therefore we cannot comment on emissions of other alkanes that have previously been observed in other NG plays (Pétron et al., 2012;Gilman et al., 2013). Enhancements in particle number concentration with sizes > 7 nm were observed downwind of most compressor and transient activity well sites. Conversely, enhancements in the submicron mass concentration of organic, nitrate, sulfate, ammonium and chloride aerosols were not observed at any site, with the exception of a single plume intercept at one compressor station in which elevated organic aerosol concentrations were observed. The absence of significant enhancement of $PM_1$ mass with enhancements in number concentration suggests that particulate emissions from these sites were mostly ultrafine particles which do not contribute significant mass, and are likely from NG combustion (Bond et al., 2006). In-situ mobile measurement of $C_2H_6$ in conjunction with $CH_4$ was found to be useful tool for the location and characterization of NG related emissions, as discussed in Yacovitch et al. (2014).

Compressor stations and transient sites (e.g. drill site and completion) were observed to be the largest emitters of most of the measured species (i.e. $CH_4$, CO, $NO_x$, $CO_2$), followed by producing well sites. Production well pads were expected to have the lowest emissions because they have fewer potential emissions sources (e.g. combustion sources) compared to other site types, and handle lower volumes of NG compared to compressor stations (NYS DEC, 2011). The following results provide a source type analysis and insight into their role on local air quality. Results from the single gas processing facility tested are not included due to an unsuccessful tracer release experiment associated with site size and topography. The IM results for emission factors will be presented first with values derived from the RM following in parentheses if available.

### 2.5.1 Well Sites

Three well sites located in the SW in Washington County were sampled using the tracer release method. The sites are within 2 miles of each other, they are of similar in size, and coincidentally operated by the same company. The

variability between these sites is informative, but it is important to note that it might not be representative of the variability of all sites of this type in the Marcellus Basin. Emission rate results are reported in Table 2.3.

The W-A well pad was the smallest of the well sites investigated with tracer release. The pad had 7 individual wells and ancillary site equipment. The W-A well pad was observed to have the second largest $CH_4$ emissions of the well sites with a value of 0.204 (0.219) tpd for the IM and (RM) analyses, respectively (Table 2.3). Ethane had an estimated emission rate of 0.120 (0.082) tpd. This well site appears to produce relatively wet gas as indicated by the high content of $C_2H_6$ at roughly 35% of $CH_4$ emissions. Combustion emissions (e.g. CO, $CO_2$, $NO_x$), $PM_1$, and VOC were not observed at the site.

The W-B well pad had 9 individual wells and ancillary site equipment. The site had the smallest correction factor with a value of 1.06 ± 0.02 and had the lowest $CH_4$ emission of any site at 0.081 (0.084) tpd. Ethane emissions were found to be 0.025 tpd by both emission ratio estimation methods. Ethane to $CH_4$ molar emission ratios found here were ~30%. Like the previous well site, combustion products and VOC other than $CH_4$ or $C_2H_6$ were not observed.

**Table 2.3 Emission rate estimates for Production Well Pads**

| Site Name | $CH_4$ | $C_2H_6$ | CO | $CO_2$ | $NO_x$ | $PM_1$ | VOC |
|---|---|---|---|---|---|---|---|
| Well Site | | | | | | | |
| W-A | **0.204(0.219)** ± 0.28(0.13) | **0.120(0.082)** ± 0.19(0.05) | - | - | **-** | - | - |
| W-B | **0.081(0.084)** ± 0.08(0.05) | **0.025(0.025)** ± 0.01(0.01) | **-** | - | - | - | - |
| W-C | **0.340 (0.036)** ± 0.49(0.01) | **0.416(0.043)** ± 0.81(0.03) | **0.034(0.043)** ± 0.03(0.05) | **83.6** ± 105 | **0.021** ± 0.01 | - | - |
| Well Drilling | | | | | | | |
| T-A | **0.923** ± 0.66 | § | **0.200(0.156)** ± 0.20(0.13) | **152** ± 125 | **0.047(0.042)** ± 0.02(0.03) | * | - |
| Completion | | | | | | | |
| T-B | **7.72(10.1)** ± 8.54(10.0) | § | **0.386(0.102)** ± 0.81(0.09) | **250(669)** ± 250(490) | **0.072(0.044)** ± 0.13(0.04) | * | - |

The values were estimated using the integration and (regression) methods reported in tons per day (tpd). Bold print represent the mean emission rate estimated at the site, and the standard deviation is represented by the non-bold values. A dashed line (-) represents undetected species and the symbol (§) represents unmeasured species. The symbol (*) indicates that in-plume elevated particle number concentrations were observed.

The W-C well pad also had 9 individual wells and site equipment. This well pad is notable because of its large $C_2H_6$ emissions. Using the IM, $C_2H_6$ emissions were estimated to be of 0.416 tpd, which was significantly larger than either of the nearby well sites. The $CH_4$ emission rate at the site, using the IM, was estimated to be 0.340 tpd. Based on the IM emission rate results W-C had a large $C_2H_6$ to $CH_4$ emission ratio with a value of ~120%. The RM

yielded markedly lower emission values of 0.043 and 0.036 tpd for $C_2H_6$ and $CH_4$, respectively. The considerable differences between the two methods are a result of the exclusion of several plume transects with large emissions ratios from the final site averaging using the RM. The excluded plume transects did not meet the averaging criteria for the RM (> 0.6 R value), but did meet the averaging criteria for the IM (>3*instrument noise). The low correlation between the dual tracer plume and the site emission plume is likely due to site specific characteristics as described in the dual tracer error assessment. Therefore, for this site the IM values should be considered the more complete emission estimate.

The molar ratio of $\Delta C_2H_6$ and $\Delta CH_4$ for the transects at the W-C site yielded different values for the same site, with some transects resulting in ratios <0.2 and others resulting in ratios >0.85. The differences in $\Delta C_2H_6$ to $\Delta CH_4$ ratios indicate that there may have been transient emissions (e.g. flash emissions, possibly from a condensate tank) that were not emitting during the full tracer release experiment, which took ~ 2 hours. Variability in emission characteristics was seen throughout the study for many of the investigated sites.

Unlike the other well sites, CO, $CO_2$, and $NO_x$ were observed at the W-C site with emission rates of 0.034 (0.043), 83.60, and 0.021 tpd, respectively. To the best of our knowledge this study is the first to quantify the emissions of criteria pollutants from Marcellus shale gas well pads. However, estimates based on other data have been reported (Litovitz et al., 2013). Although there are differences in VOC and PM emission estimates by this study and Litovitz et al. (2013), the $NO_x$ emission rate from W-C is within a factor of 2 of 0.0128 - 0.0162 tpd for a 9 well site estimated by Litovitz et al.

In comparison to another study that investigated well pad emissions our results indicate that the average $CH_4$ emissions at the tested well pads were about 16, 4, and 23 times greater than the upper range ($\mu+1\sigma$) of well pad equipment leak estimates in Allen et al. (2013). This large disparity between the two studies suggests that there are other factors such as operating practices, production volume decline, location of leaks, scheduled versus unscheduled monitoring, as well as the number and representativeness of sites sampled that may be important considerations when compiling a bottom up inventory.

### 2.5.2 Transient Sites

The T-A well pad in Bradford County was being developed at the time of our sampling and was in the drilling stage, although the state of the drill rig (e.g. drilling, stopped, etc.) was unknown. The drill site emissions were 0.200 (0.156) tpd of CO, 152.8 tpd of $CO_2$, and 0.047 (0.042) tpd of $NO_x$ (Table 2.3). Compared to engineering emission factors for a drill rig in Roy et al. (2013), and assuming the drill rig had the average power rating of 4000 bhp, our calculated $NO_x$ emission rate is about 10 times less than the engineering estimate (38). Similarly, there are emission factors for PM and

VOC from drill rigs, but we did not observe elevated concentration of either pollutant type downwind of the drill rig. The lower emissions from the drill site we sampled compared to engineering emission factors could indicate that the drill rig was not operating at full capacity, that there was pollution control on the site, or that the values in Roy et al. (Roy, 2013) are overestimated.

Unexpectedly, $CH_4$ emissions were observed at the drill site with an estimated emission rate of 0.923 tpd (Table 2.3). The $CH_4$ emissions were likely associated with a gas "kick", or when a gaseous zone is encountered during drilling and the NG is directed to a mud-gas separator then vented away from the drill rig (NYS DEC, 2011). Similar results were observed in the Marcellus Shale play by Caulton et al. (2014) via aircraft measurements. That study concluded that wells in the drilling phase in a portion of Southwestern Pennsylvania had a $CH_4$ flux of 2.94 ± 0.95 tpd (Caulton et al., 2014).

A flow-back flaring event, denoted in this work as T-B, was observed at a well pad in Sullivan County. Two tracer release experiments were performed at this site; however, the results from one experiment are not shown because it was unsuccessful due to unfavorable and variable wind conditions. Because of the large buoyancy of the hot flare, two distinct emission plumes were observed during the successful tracer release experiment. Plume-1, thought to be direct emissions from the temporary flare, was located ~1,500 m downwind. Plume-2, thought to be from ground-based fugitive losses, NG leakage not combusted by the flare, and emissions from site process equipment, was located with the dual tracer plume <500 m downwind of the site.

Plume-1 was observed to have elevated mixing ratios of CO and $CO_2$, with no enhancements in $NO_x$, and decreased concentrations of $CH_4$, $CH_3OH$, and acetone relative to the background. The modified combustion efficiency, or $\Delta[CO2]/(\Delta[CO2] + \Delta[CO])$, for the flare plume was determined to be greater than 0.99, indicating that the flare efficiently combusted flowback gases (40). Alternatively, the ground-based $NO_x$ emissions in Plume-2 were observed to have average center plume mixing ratio of 19 ppbv and a maximum 1 Hz value of 140 ppbv over a 3-hour sampling period. The emission factors obtained from the dual tracers and Plume-2 indicated large emission rates of combustion species, with CO emissions at 0.386 (0.102) tpd, $CO_2$ at 251 (669) tpd, and $NO_x$ at 0.072 (0.044) tpd (Table 2.3). There was large variability in transect emission ratios for each species, which indicates that the site emissions were not constant throughout the sampling period. Although the emission rate of the temporary flare is unknown, the large emission rates of incomplete combustion species from the ground-based operations compared to the relatively efficient flaring of flowback gases suggests that the ground-based emission sources could have a larger impact on local air quality compared to the temporary flaring during completion events.

The largest $CH_4$ emissions measured in the study were observed at this site in Plume-2 with a value of 7.7 (10.1) tpd with a median center-plume $\Delta CH_4$ mixing ratio of 1.3 ppmv and a maximum of 38 ppmv. The daily $CH_4$

emission rate observed at this completion event, if constant over the entire event, was significantly in excess of any completion event observed by Allen et al. (2013) ($\mu$ = 1.7 Mg; 95% CI = 0.67-3.3 Mg), because well completion events can often last several weeks.

### 2.5.3 Compressor Sites

Site size information for all of the compressor stations investigated in the study was found in PA DEP air quality permits. Permits from the closest available date before our measurements were used to gather site information. Sites are permitted to operate based on the full capacity of the site equipment. It is not known whether any of the compressor stations investigated were operating at full capacity during our sampling period. Additional site information can be found in Appendix A. Eight compressor stations of various sizes were investigated in this study. Compressors stations C-B, C-D, C-F, C-G, and C-H were located in Bradford County in NE Pennsylvania. Two tracer release experiments were conducted at the C-F compressor station. Compressor stations C-A, C-C, and C-E were located in the SW study area, located in Greene, Fayette, and Westmoreland counties, respectively. All compressor stations investigated utilize NG fired compressor engines with total power capacities ranging from 5285 – 16560 bhp, with the exception of C-G which is equipped with an electric powered 15300 bhp centrifugal turbine. All of the sites had various amounts of process equipment (e.g. glycol dehydrators, separators, in-line heaters, liquids tanks), and air quality controls, which was verified by PA DEP air quality permits and by visual inspection.

Emission rates of measured combustion related species from the tested compressor stations are shown in Figure 2.7. Carbon monoxide emission rates ranged from 0.029 (0.005) to 0.426 (0.229) tpd with a median emission rate of 0.09 (0.145) tpd. The largest CO emission rate was observed at the largest compressor station (C-H). The tested compressor stations had a minimum $NO_x$ emission rate of 0.005 (0.011) tpd, a median of 0.029 (0.042) tpd, and a maximum of 0.141 (0.115) tpd. Unlike CO, the largest emitter of $NO_x$ was C-A, which was the smallest compressor station, suggesting that site processes other than compressor engines and differences in pollution control may play a large part in the magnitude of site emissions. The electric powered compressor station (C-G) had the lowest $NO_x$ emissions, as expected. However, the observation of combustion emissions at site C-G indicates that site process equipment plays a role in the total emissions from compressor stations. Carbon dioxide emission rates ranged from 68.0 (52.7) to 371 (128) tpd, with a median emission rate of 111 (90.2) tpd. Elevated particle number concentrations were observed at 6 of the compressor stations where particle number was measured, and undetected at the C-G compressor station. Center-plume number concentrations above the background ($\Delta$conc.) ranged from 75 to 9600 #/cm$^3$ with a median of 1400 #/cm$^3$. Elevated $PM_1$, however, was only observed in the emission plume of the C-A compressor station. The emission plume contained only organic aerosol and had an emission rate of 0.419 (0.548) tpd. As

previously mentioned, no VOC enhancements, other than $CH_4$ and $C_2H_6$, were observed downwind of any compressor station, with the exception of $CH_3OH$ at the C-F compressor station. Methanol was observed in the site plume during both tracer release experiments at the site. The emission rate of $CH_3OH$ at the first tracer release experiment at the site had an estimated value of 0.384 (0.432) tpd and the second had a value of 0.300 tpd. The relatively similar emission values for $CH_3OH$ for tracer release experiments that occurred several days apart suggest that the emission source was likely not from a transitory site process and instead was from a constant process (e.g. antifreeze). Additionally, similar emission rates from a constant source like pipeline antifreeze provides evidence for the success of our tracer ratio methods.

Methane emission rates ranged from 0.411 (0.565) to 4.94 (5.06) tpd with a median emission rate of 1.09 (1.18) tpd. The largest emission rates and the largest variability between plume transects was observed at the C-H compressor station, which has the largest compression power of the tested facilities. The observed $C_2H_6$ emission rates at the tested facilities ranged from 0.023 (0.021) to 0.062 (0.047) tpd with a median emission rate of 0.033 (0.027) tpd. The emission ratio of $C_2H_6$ to $CH_4$ at the three compressor stations where $C_2H_6$ was measured had an average of ~0.04.

There was no significant relationship between emission rates of the measured chemical species and the compression power at the site. Although a positive trend was observed between total permitted compressor power and $CH_4$ emissions indicating that there may be a relationship between the volume of NG a facility handles and fugitive losses. However, the role of compressor power in site emissions is unclear because of the small sample size of this study and also because information about the operating state of compressor stations studied was not available to us. There are likely many other factors besides compression power that lead to differences in emission rates. Future sampling at these sites and others throughout the region is key to understanding how factors like size, operation state, NG processing, pollution control, and age affect the emission rates of pollutants from compressor stations in the Marcellus Shale region.

While this study adds critically needed measurements to the existing literature, the extent to which the results can be generalized to the Marcellus basin as a whole remains uncertain. Although the sample size of this study is too small to make statistical conclusions about different emission source types, it provides crucial comparisons to recent literature about emissions from NG well pads, pads with active drilling, and completions. Additionally, we have shown that in contrast to other unconventional NG gas resources there are few emissions of non-alkane VOCs (as measured by PTR-MS) from Marcellus shale development. The low emission of non-alkane VOC in the Marcellus play indicates that emission estimates should not be generalized across shale plays in regional models or in emission inventories. The study has also provided useful methodology for quantifying emissions from NG development without the advantage of

site access. Based on the results from this study we recommend that future studies increase the monitoring time at each site in order to better characterize daily variability in emission composition and quantity.

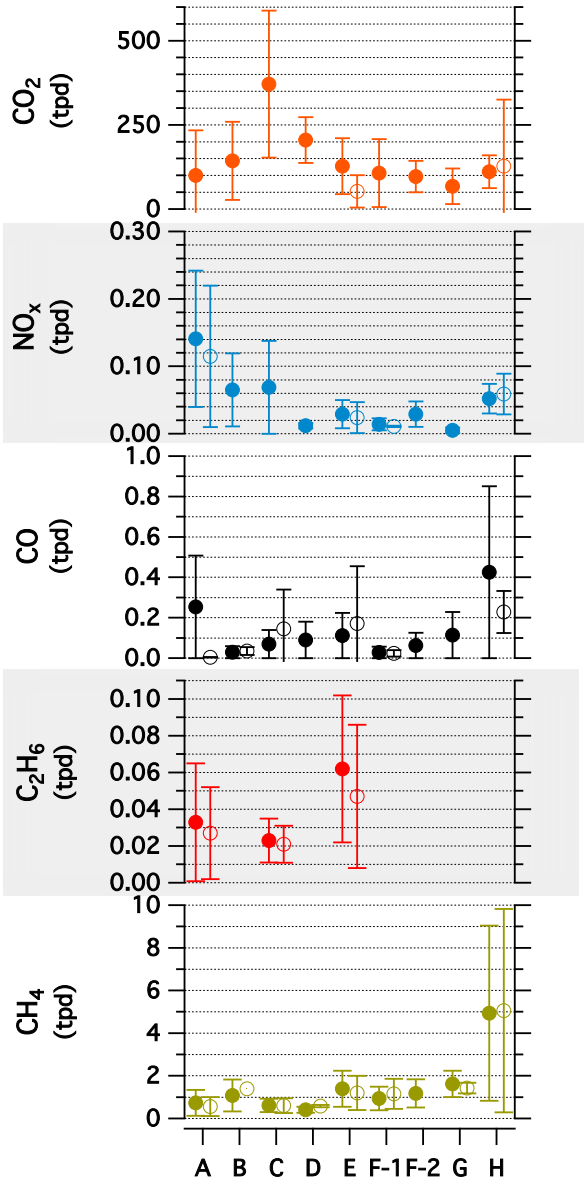


**Figure 2.7. Emission Rates of $CH_4$, $C_2H_6$, CO, $NO_x$, and $CO_2$ from the Investigated Compressor Stations**
Values are reported in metric tons per day. The average integration method results are represented by a solid circle. The average regression method results are represented with open circles when applicable. The standard deviations for both methods are represented with caps and whiskers.

# Chapter 3: Point Source Gaussian Emission Estimates and observations from the Marcellus Shale Natural Gas Transmission Sector

## 3.1 Relevance and Status

This work uses ground-based mobile monitoring in conjunction with Gaussian dispersion principles to estimate methane leak rates from natural gas production and transmission infrastructure in the Marcellus Shale region of Pennsylvania. The methodology is from an EPA other test method and Brantley et al. (2014b). This study is the first to produce results using this methodology for use on estimating emissions from Marcellus Shale infrastructure. The analysis and results of this work are completed and have been drafted into a report for the funding agency. Again, like with the tracer ratio results presented in Ch. 3, the emission rate results from this work give important statistics can further develop emission inventories and help reconcile differences observed between top-down and bottom-up regional methane emission estimates. There are no current plans to publish this work in an academic journal, however the results may be used for comparisons to future work.

## 3.2 Summary

The DML was used August 2015 to make ground-based mobile measurements in the Marcellus region with the goals of estimating methane emission rates from sources in the NG transmission sector (mainly the Transco and TGP pipelines), quantify pipeline leaks, and characterizing background concentrations in the region. An additional goal was to estimate emissions from Marcellus Shale production and gathering sites if found along the sampling route and conducive to sampling. Methane emission rates from the studied sites were estimated using the EPA OTM33a method, also known as the Point Source Gaussian method. Emission rates were calculated for 8 of the 11 compressor stations investigated and were within the range observed by other studies. However, emission at the TGP 319 and Tuesa-Thomas compressor stations were found to be significantly lower than previous observations by the authors in 2012 using tracer release methods. The meter stations studied were observed to have emissions consistent with observations by recent study that generated a larger dataset (Lamb et al., 2015). The methane emission estimates from the transmission sites that have proposed modifications due to pipeline expansion projects can now serve as a pre-modification baseline for a number of sites or serve as a baseline to determine the effect of aging infrastructure. The Marcellus shale well pads were observed to have emissions ~10 times greater than the well-based leak rate estimated by Allen et al. (2013). Finally, methane leaks from the Transco and TGP pipeline were assessed using the local background values as a baseline. It was estimated that nearly 18% of the methane enhancements above the local

background observed within 100 meters of the pipelines were due to emissions from pipelines, pipeline infrastructure, or other sources of methane.

## 3.3 Background and Motivation

Natural gas is a globally important fossil fuel. In the United States, natural gas (NG) comprised a 27% share of the total primary energy consumption in 2013 with large demand from the electric power industry, chemical industry, and residential use (Energy Information Administation, 2015a). The recent development of unconventional natural gas resources like gas rich tight sandstone, coal, or shale has dramatically increased the domestic production potential due to advances in extraction technology (Kargbo et al., 2010). The extraction of unconventional NG resources has raised both air quality and climate concerns due to the emissions of air pollutants (i.e. volatile organic compounds, particulate matter, carbon monoxide, nitrogen oxides) and climate forcing compounds (i.e. methane and carbon dioxide) (Field et al., 2014). With the increase in domestic production and subsequent decrease in price of NG coupled with changes in environmental regulations the demand for NG by the electrical power sector has increased over the past decade and is projected to increase with the decline of coal-fired power generation (Energy Information Administation, 2015a). Additionally, the Energy Information Administration (2015a) projects that the use of compressed and liquefied natural gas in the transportation sector will increase 10% annually in the coming decades. Natural gas is known to be cleaner burning than other fossil fuels (de Gouw et al., 2014), and therefore generate less air pollutants and climate forcing compounds per unit of fuel burned, however, the air quality and climate impacts of production and transmission are not well understood.

In the Appalachian region, the development of the Marcellus Shale, the most productive unconventional NG resource in the United States (Energy Information Administation, 2015b), coupled with increased demand throughout the United States has necessitated improvements and upgrades to the NG gathering and transmission infrastructure in the region. The transmission infrastructure includes high pressure pipeline, metering facilities, and large compressor station facilities used to transmit NG long distances from production areas to end-use distribution networks (US Environmental Protection Agency, 2015b). Emissions of methane, the primary constituent of NG, from fugitive leaks or venting from pneumatic controllers have been reported from pipelines and its associated infrastructure (US Environmental Protection Agency, 2015b). Methane emissions have also been attributed to uncombusted engine exhaust and other sources at compressor stations (Subramanian et al., 2015). Additionally, compressor stations have been reported to emit EPA regulated criteria pollutants such as carbon monoxide (CO) and nitrogen dioxide ($NO_2$) (Goetz et al., 2015).

The addition of pipelines and increased compressor power to transmission infrastructure in the Appalachian region, as proposed by several pipeline expansion plans such as the Leidy Southeast Expansion, Leidy South Project, the Atlantic Sunrise Project, and Constitution pipeline, is expected to increase the emissions of methane and other pollutants in the region. In the summer of 2015 ground-based mobile measurements of methane were conducted to investigate atmospheric emissions from transmission infrastructure located in the Marcellus Shale dense region of Northeastern Pennsylvania. The measurements were conducted to fulfill the following objectives:

- Estimate the emission rates from sources in the natural gas transmission sector in the Marcellus region with an underlying goal of investigating sites that have undergone or will undergo upgrades due to expansion projects
- Quantify leaks from transmission pipelines at opportunity road crossings in the Marcellus shale region
- Understand background concentration levels throughout the Marcellus Shale region
- Estimate emission rates at opportunity sites associated with Marcellus Shale production and gathering

## 3.4 Sampling Plan

To complete the above objectives the Drexel Mobile Lab conducted ground-based mobile measurements of methane at targeted transmission related sites and throughout Northeastern Pennsylvania within the Marcellus Shale basin. Measurements took place for 5 days in August 2015 and continuous measurements were made throughout each day. Figure 3.1 displays the sampling track of the DML and location of the sites investigated.

Natural gas transmission related sites located on the Transcontinental Pipe Line (Transco) and the Tennessee Gas Pipe Line (TGP) were the primary focus of the sampling plan. Compressor stations, meter stations, and pipeline road crossing were the major types of infrastructure investigated. Facilities on the Transco and TGP were studied for the following reasons:

- Both pipelines are the major transmission lines found in Northeastern PA within the Marcellus region
- Both pipelines transport Marcellus Shale produced gas and service distribution networks along the East coast of the United States
- The Transco Pipeline was part of the Leidy Southeast expansion project, which included plans for new pipeline loops, upgrades to the compressor power at several compressor facilities (stations 515, 517, 520), and modifications to meter stations within Northeastern PA with a projected in-service date of December 1, 2015 (Transcontinental Gas Pipe Line Company, 2013)
- The TGP was proposed to be part of the Kinder Morgan Northeast Direct Energy Project that included the addition of new compressor stations in Northeastern PA, modifications to an existing station (TGP 319) and additional pipeline loops (Dominion Transmission, 2015)
- Methane emission estimates will be made prior to the projected start date for these projects and other future projects providing an emission baseline that represents lower capacity facilities or older infrastructure.

Another NG transmission site investigated was a super-site in the Clinton county which contained the newly built Dominion Frinnefrock compressor station and the Dominion Leidy NG storage facility. The Frinnefrock station is part of the Dominion Leidy South project, however, based on contact with operators at the time of sampling the Frinnefrock facility was not operational (on standby) while sampling took place (Dominion Transmission, 2015).

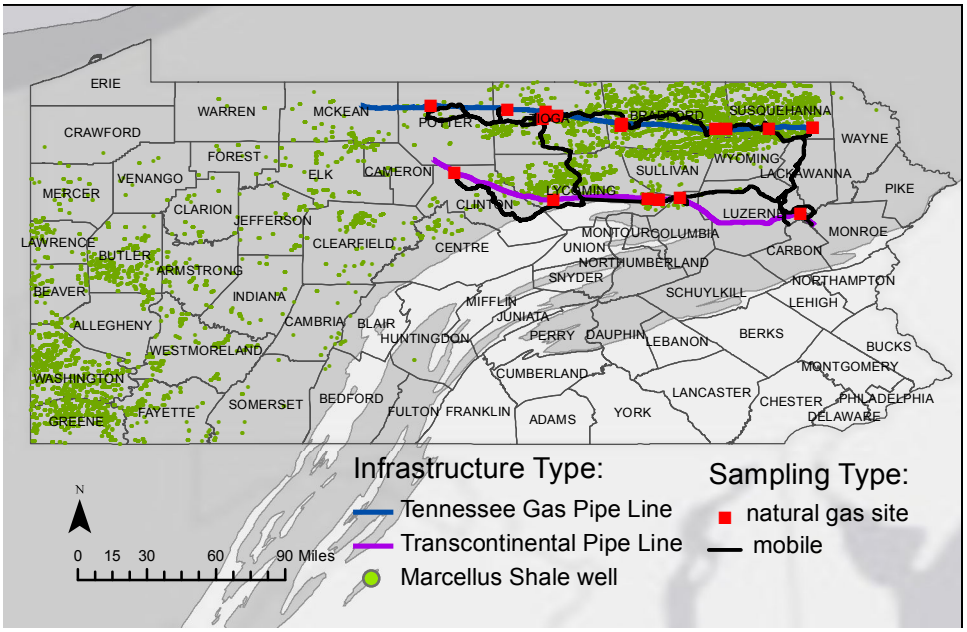


**Figure 3.1. Map of 2015 Study Area**
Map of Pennsylvania overlaid with the Marcellus Shale basin (gray), permitted unconventional wells in Pennsylvania (green), transmission pipelines within sampling area, mobile sampling track (black), and the location of sites sampled for methane emissions testing (red)

In addition to sampling at facilities associated with NG transmission the DML was also used to estimate emission rates at sites associated with Marcellus Shale natural gas production and gathering. The Marcellus Shale sites were considered "opportunity sites" because they were not part of the pre-defined sampling plan and instead were sampled if encountered while in transit to transmission sites and the topographical and meteorological conditions were conducive to downwind sampling. Table 3.1 provides information on the name (if known), location, site type, operator, and associated pipeline of the transmission and Marcellus Shale sites investigated in August of 2015.

**Table 3.1. Name, Operator, and location of sites investigated.**

| site type | name | operator | county |
|---|---|---|---|
| compressor station | 515 | Transco | Luzerne |
| | 517 | Transco | Columbia |
| | 520 | Transco | Lycoming |
| | Leidy* | Dominion | Clinton |
| | 313 | TGP | Potter |
| | 315 | TGP | Tioga |
| | 317 | TGP | Bradford |
| | 319 | TGP | Bradford |
| | 321 | TGP | Susquehanna |
| | Tuesa-Thomas | Talisman | Bradford |
| | Teel | Williams | Susquehanna |
| meter station | unknown -1 | Transco | Lycoming |
| | unknown -2 | TGP | Tioga |
| | unknown -3 | TGP | Bradford |
| well pad | Buck | XTO | Lycoming |
| | Nestor | SWEPI | Tioga |
| | Sampson | SWEPI | Tioga |

* The Leidy facility includes Dominion Leidy Storage and the Frinnefrock compressor station

## 3.5 Methods

The Drexel Mobile Lab (DML) was used for stationary ambient monitoring of methane downwind of the investigated sites and to perform mobile surveying around the sites to locate emission plumes and determine background concentrations. When applicable, the data collected at each site were used to estimate point source emissions by the method described in the EPA Other Test Method 33a (OTM-33a) (Thoma, 2014). In addition to ambient monitoring at the listed NG sites, mobile measurements were made between sites to evaluate leaks from pipelines and other NG infrastructure, and to characterize local-background concentrations of methane within the sampling track found in Figure 1. The following sections provide information about the instrumentation utilized on the DML and a brief description of OTM-33a.

### 3.5.1 Instrumentation

The DML is a late 1990s Ford cargo van that is equipped for gas-phase and particle-phase ambient mobile monitoring. The platform is modular in design and allows for the installation of any combination of instrumentation using a shock-mounted military grade 19-inch rack. When mobile the instrumentation is powered through the vehicles alternator and a 2000-watt DC to AC power inverter. When stationary, the instrumentation is powered by a 1000-watt

gasoline powered generator placed >100 feet downwind of the DML. The inlet system is adaptable to the instrumentation and for this study non-reactive PTFE tubing was used. The inlet was attached to PTFE gooseneck positioned in front of the vehicle and at a height of ~2 meters. The inlet was positioned to be outside the boundary layer of the vehicle. The gas-phase inlet was equipped with inline Teflon disc filters to remove particulate contamination. The inlet flow rate is adjustable based on excess flow and for this study was set to a fixed flow rate that provided an inlet residence time of ~1 second.

This work will focus on methane measurements made using a Picarro Inc. Cavity Ring Down Spectrometer (CRDS), Picarro G2401. The CRDS has a sampling rate of ~1 Hz and the mobile detection limit for methane was estimated to be <1 ppbv. The CRDS was factory calibrated prior to the measurement campaign and dilution calibrations were performed at the end of the campaign. The multi-point dilution calibrations were completed by using zero air and a custom calibration standard of methane, CO, and $CO_2$ balanced with $N_2$ produced by Airgas Inc. (Radnor, PA). The calibrations determined that the CRDS measured ~6.5% low for the campaign compared to the calibration standard for a span up to 5 ppmv for methane. All campaign measurements were adjusted to reflect the calibration results.

Ancillary instrumentation included a 1 Hz GPS, providing geopostioning with <5m precision, and a Davis Vantage Vue weather station. The weather station was fixed on the DML when conducting stationary sampling at a height of ~2.5 meters and within a meter of the inlet opening. The weather station provided wind speed, wind direction, temperature, and relative humidity data at each site at sampling rate of ~1 Hz.

### 3.5.2 Emission Rate Calculation

Methane emission rates were calculated using the EPA OTM-33a (Thoma, 2014). The method utilizes fast-response instrumentation and Gaussian dispersion principles to estimate emissions rates of a point source from a roadside sampling location. At each site, the sampling location was chosen based on several survey loops in which elevated methane concentrations found in the bearing of the prevailing wind were assumed to be part of the emission plume from the site. Each survey loop utilized the closest accessible up-wind and down-wind roads around the tested site to find the position of the emission plume, to determine if interferences exist from other sources, and to establish the background concentration outside of the emission plume. Once the location of the emission plume was determined the DML was positioned on the nearest downwind road within the plume and remained stationary within the plume for 20 to 60 minute. Sampling locations ranged between 80 to 400 meters of the emission source at the tested sites based on estimates from satellite imagery, though at large sites with multiple emission sources the downwind distance was approximated to the center of the site.

The data collected from within each plume was used in conjunction with collocated wind measurements to determine the average peak concentration within the plume based on a Gaussian distribution (Brantley et al., 2014). Methane concentrations were binned by the wind direction data in ten degree increments, which was converted into polar coordinates based on the prevailing wind direction (Figure 2). A Gaussian function was fit to the results for each site plume and the average peak concentration was used to calculate the emission rate using a simplified 2-dimension Gaussian dispersion equation (eq. 1) (no reflection). In equation 1 Q is the emission rate in grams per second (g/s), μ is the mean wind speed during stationary sampling (m/s), C is the peak average concentration, $\sigma_z$ is the vertical dispersion coefficient (m), and $\sigma_y$ is the horizontal dispersion coefficient (m) (Thoma, 2014;Brantley et al., 2014).

$$Q = 2\pi\sigma_y\sigma_x\mu C \qquad (3.1)$$

The horizontal and vertical dispersion coefficients were calculated using equation 2 for rural dispersion, which is a function of the downwind distance (x) and constants I, J, and K that are derived from a look-up table that corresponds to the estimated Pasquill stability class (Beychock, 2005).

$$\sigma = \exp\left[I + J(\ln x) + K(\ln x)^2\right] \qquad (2)$$

The Pasquill stability class for each plume was estimated using the wind speed, standard deviation of the wind direction, and degree of solar insolation. Generally, because measurements were made during the day and each sampling day had strong solar insolation the Pasquill stability class was typically estimated to be B or C.

For each plume, error was calculated based on the propagation error from the Gaussian function fit of the binned concentrations, error in downwind distance determined by the site radius, and variability in wind speed. All data processing and analysis was performed using Igor Pro 6.37 Wavemetrics, Lake Oswego, OR). A more detailed discussion of the methods used can be found in Brantley et al. (2014).

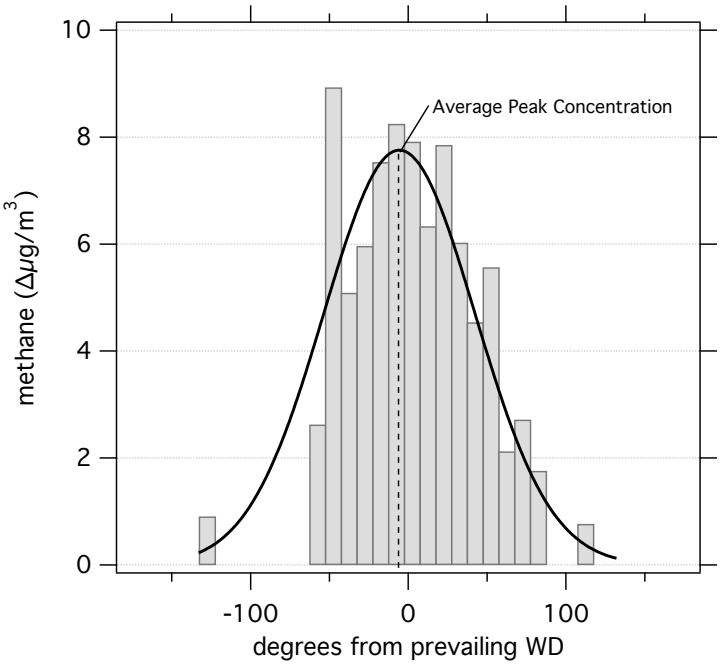


**Figure 3.2 Excess methane Concentrations Observed at the Buck Well Pad**
Histogram is from 25 minutes of sampling binned by degrees from prevailing wind direction and fit with a Gaussian function.

## 3.6 Methane Emission Rates

The calculated methane emission rates from the investigated sites can be found in Table 3.2. The downwind distance, average wind speed, and average peak concentration observed at each site can also be found in Table 3.2. Emission rate estimates are not available for several of the sites investigated including Transco 515, Transco 517, Teel compressor station, and meter station 2. Generally, emission rates at these sites could not be calculated because the topography or the road network at the site was not compatible for plume measurements because of unfavorable wind direction. Transco 515 and 517 for example had few available downwind roads given the prevailing wind direction on that sampling day and no methane plumes were encountered near the site. A site-type based discussion and overview of results can be found in the following sections. It should be noted that the uncertainty in all of the emission rate estimates is substantial primarily due to the propagated error from uncertainty in the emission source. Distinguishing the location of the largest on-site emission source would significantly reduce any spatial uncertainty.

**Table 3.2. Point Source Gaussian Derived Methane Emission Rates**

| site type | name | downwind distance ±site radius (m) | average wind speed ±1σ (m/s) | Average peak concentration ±1σ (Δμg/m$^3$) | methane emission rate ±1σ (g/s) |
|---|---|---|---|---|---|
| Compressor Station | 515 | N/A | N/A | N/A | N/A |
| | 517 | N/A | N/A | N/A | N/A |
| | 520 | 280 ±100 | 3.10 ±0.41 | 283.59 ± 200.0[1] | 7.88 ±6.79 |
| | Leidy | 300 ±150 | 0.41 ±0.47 | 755.57 ±12.98 | 16.24 ±19.09 |
| | 313 | 370 ±200 | 2.17 ±1.50 | 691.33 ±727.70[1] | 23.22 ±33.91 |
| | 315 | 240 ±100 | 1.51 ±0.78 | 86.75 ±3.11 | 0.84 ±0.66 |
| | 317 | 400 ±100 | 2.08 ±0.75 | 88.22 ±3.48 | 3.29 ±1.66 |
| | 319 | 390 ±150 | 0.34 ±0.42 | 31.41 ±8.08 | 0.18 ±0.25 |
| | 321 | 340 ±100 | 0.47 ±0.49 | 100.52 ±1.55 | 0.630 ±0.70 |
| | Tuesa-Thomas | 220 ±80 | 1.01 ±0.67 | 304.44 ±12.46 | 1.66 ±1.38 |
| | Teel | 80 ±40 | N/A | N/A | N/A |
| Meter Station | unknown -1 | 320 ±20 | 1.44 ±0.57 | 10.01 ±0.20 | 0.07 ±0.03 |
| | unknown -2 | 250 ±20 | N/A | N/A | N/A |
| | unknown -3 | 290 ±20 | 0.09 ±0.17 | 107.75 ±1.28 | 0.04 ±0.08 |
| Well Pad | Buck | 170 ±50 | 1.46 ±0.80 | 7.76 ±0.40 | 0.04 ±0.02 |
| | Nestor | 160 ±30 | 0.30 ±0.45 | 1011.5 ±85.2 | 0.95 ±1.44 |
| | Sampson | 90 ±40 | 2.45 ±1.56 | 325.8 ±13.9 | 0.76 ±0.68 |

1. Due to technical difficulties wind measurements were not available while sampling in the emission plume. To calculate the methane emission rate the average wind speed was instead estimated from other time periods while sampling at the site. The average peak concentration and standard deviation was estimated by using summary statistics from the stationary sampling at the site, no Gaussian function was used.

### 3.6.1 Compressor Stations

The transmission compressor stations investigated were found to have a large range of methane emission rates with the lowest rates observed at TGP 319 (0.18 g/s) and the largest emission rate at TGP 313 (23.22 g/s) and a mean emission rate of 7.5 g/s. All transmission compressor stations except for TGP 319 were estimated to have methane emission rates within the range of emissions observed by Subramanian et al. (2015) of 0.544-281 g/s, though generally skewed to the lower range of the study. The low emission rate at TGP 319 is significantly lower than previous measurements the site by Goetz et al. (2015), which estimated a methane emission rate of 4.75 ±1.69 g/s in 2012 using different methods. The inconsistency between this study and Goetz et al. (2015) could be due to different operational states, fixed leaks, or due to differences of methods. Additionally, the very low wind speeds and long downwind distance at TGP 319 could have added additional error to the 2015 measurement. The Leidy Storage facility was found to have the second highest emissions of the study at 16.24 ±19.09 g/s. Operation of the proximal Frinnefrock

facility is expected to increase methane in the area. An analysis of the type and quantity of infrastructure at each site could highlight why differences in emission exist between many of the transmission sites.

Of the two Marcellus Shale NG gather compressor stations only measurements at the Tuesa-Thomas compressor station were applicable for methane emission rate calculations. However it should be noted although emission rates could not be calculated at the Teel compressor station, the largest methane enhancements observed during the study of >50 ppm were observed downwind of the site. The large methane enhancements are thought to be due to on-site construction and modifications that were taking place while sampling. The calculated methane emission rate at the Tuesa-Thomas station was determined to be 1.66 ±1.38 g/s and was found to be 34 times lower than measurements made by Goetz et al. (2015). Employing the same parameters used to calculate the original emission rate, downwind methane enhancements of ~15 ppm would be required to reach the observations made in 2012, whereas a max enhancement of 2.3 ppm was observed downwind of the site in 2015. The large difference between the observations suggests site operations may have changed since 2012, though differences due to measurement techniques cannot be discounted.

### 3.6.2 Metering Stations

Little information in known about the investigated meter stations except that they service the Transco and TGP transmission lines. Based on satellite imagery it is assumed that the tested meter stations are receipt stations, or stations that meter the NG volumes from supply pipelines. Compared to the compressor stations in the transmission sector the investigated meter stations were found to have low methane emissions with rates of 0.04 and 0.07 g/s. The most recent study that also investigated emission from meter stations found methane emission rates of 0.067 g/s from facilities servicing pipelines at an inlet pressure of >300 psi and 0.031 g/s from facilities servicing pipelines at 100-300 psi (Lamb et al., 2015). Although the inlet pressure is of the tested facilities is not known, there is generally good agreement between this study and Lamb et al. (2015).

### 3.6.3 Well Pads

The tested well pads were generally found to have lower methane emissions than the compressor station and larger emissions than the meter stations (Table 3.2). The Nestor well pad has the most wells with 5, followed by the Buck well pad with 4, and the Sampson well pad that contains 3. Of the well pads tested Nestor, the site with the most wells, was found to have the largest methane emissions (0.95 ±1.44 g/s), but also had the most uncertainty compared to the other two well pads. The Buck well pad was estimated to emit 0.04 ±0.02 g/s of methane and the Sampson well pad was estimated to emit at a rate of 0.76 ±0.68 g/s. The methane emission rates estimated in this study were found to be similar to findings from one well pad in Goetz et al. (2015) (0.937 ±0.92 g/s) and were 2-4 g/s less than emissions from

the other wells investigated. Another recent study, estimated that equipment leaks from NG production sites emit an average of 0.02 g/s of methane per well (Allen et al., 2013). Given the number of wells on each site the Nestor and Sampson pads where found to have 13 and 9.5 times emissions compared to the findings by Allen et al. (2013).

## 3.7 Assessment of Pipeline Leaks

The local background assessment was used as a baseline to determine the magnitude of enhancements in the 1-Hz mobile dataset while near pipeline road crossings. See Chapter 4 for more information about the local background assessment. The analysis is limited to crossings of the Transco or TGP pipelines and only investigated enhancements within 100 meters of the pipelines. Figure 3.3 shows a cumulative distribution plot of the observed enhancements at the pipeline crossings. Because pipeline road crossings are rare and often outside of the planned route, only ~2 hours of data from the 5 days were within 100 meters of the studied pipelines. A mobile detection limit of 9 ppb (0.009 ppm) for methane was estimated as 3 times the standard deviation of a 30-minute period of data from outside the Marcellus Shale region where there are fewer point sources of methane. In this assessment any pipeline enhancements above 9 ppb are considered to be enhancements due to natural gas emissions or other sources and not from instrument noise. Based on Figure 3.3, nearly 18% of the measurements within 100 meters of the studied pipelines observed methane enhancements above the mobile detection limit. Additionally, approximately 8% of the measurements were 50 ppb above the local background concentrations and enhancements as large as 0.5 ppm were observed. The observation of enhancements above the detection limit and local background suggests that methane emissions were observed near pipeline road crossings. However, since some of the crossings were also near other types of transmission infrastructure (e.g. compressor and meter stations) it is not clear whether the observed emissions from sources other than the pipelines.

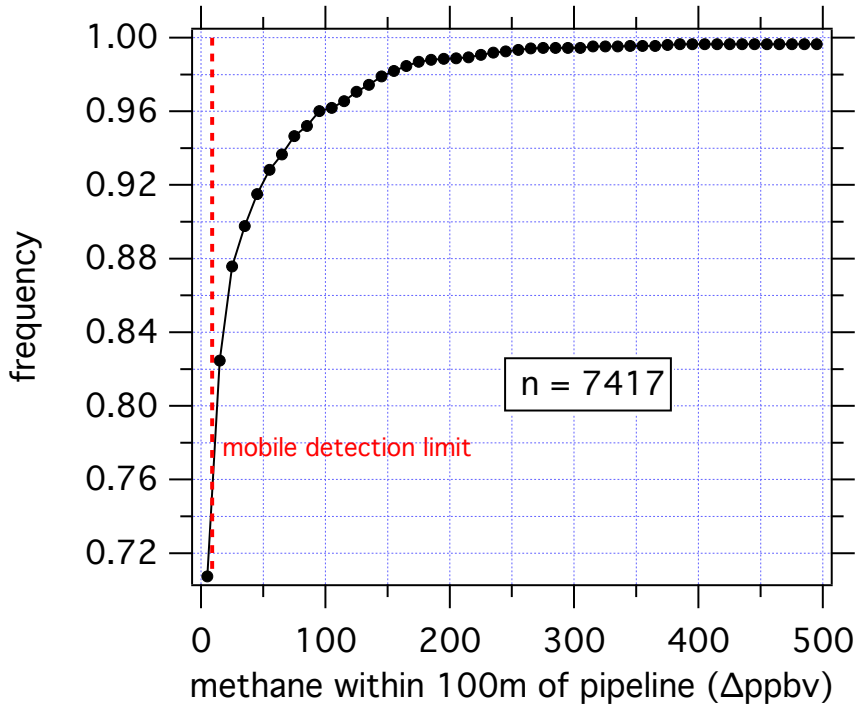


**Figure 3.3. Cumulative Frequency of Excess Methane Concentrations**
Values within 100m of transmission pipelines (markers). The methane mobile detection limit for the study is shown as a dashed line (red).

# Chapter 4: Analysis of Local Background Concentrations in the Marcellus Shale

## 4.1 Relevance and Status

This work uses ground-based mobile monitoring for ambient surveying of methane, criteria pollutants, and select volatile organic compounds in in the Marcellus Shale region of Pennsylvania. An averaging technique was developed for this work to transform mobile datasets, which are heavily influenced by on-road emission and other direct emission sources, to make comparisons to ambient measurements made by other monitoring platforms and provide baseline measurements for future studies. This work has been published by the journal Elementa: Science of the Anthropocene under the following citation:

> Goetz, J. D.; Avery, A.; Werden, B.; Floerchinger, C.; Fortner, E. C.; Wormhoudt, J.; Massoli, P.; Knighton, W. B.; Herndon, S. C.; Kolb, C. E.; Knipping, E.; Shaw, S. L.; DeCarlo, P. F. Analysis of Local-scale background concentrations of methane and other gas-phase species in the Marcellus Shale. *Elem Sci Anth*. 2016.

## 4.2 Summary

The Marcellus Shale is a rapidly developing unconventional natural gas resource found in part of the Appalachian region. Air quality and climate concerns have been raised regarding activities associated with the extraction, production, and transmission of unconventional natural gas resources. Two ground-based mobile measurement campaigns were conducted to access the impact of Marcellus Shale natural gas development on local scale atmospheric background concentrations of air pollution and climate relevant pollutants in Pennsylvania. The first campaign took place in Northeastern (NE PA) and Southwestern PA (SW PA) in the summer of 2012 using the Aerodyne Inc. Mobile Laboratory. Compounds monitored included methane ($CH_4$), ethane, carbon monoxide (CO), nitrogen dioxide, and PTR-MS measured volatile organic compounds (VOC) including oxygenated and aromatic VOC. The second campaign took place in Northeastern PA in the summer of 2015 where only $CH_4$ and CO were monitored with the Drexel Mobile Laboratory. The ground-based mobile monitoring data were transformed using interval percentile smoothing to remove bias from local unmixed emissions to isolate local-scale background concentrations that are useful for comparison to other studies using other types of monitoring platforms. Comparison were made to other ambient monitoring in the Marcellus region including a NOAA SENEX flight that conducted measurements over the Marcellus Shale region in the summer of 2013. The results show that regional background $CH_4$ mole fractions were 140 ppbv greater in SW PA compared to NE PA in 2012 and that regional background $CH_4$ increased 100 ppbv from 2012 to 2015. $CH_4$ local background mole fractions were not found to have a detectable relationship between well

density or production rates in either region. In NE PA CO was observed to have the inverse trend to $CH_4$ with a decrease of 75 ppbv over the three year period. Acetone and methanol observations were found to be at mole fractions similar to observations made by studies in rural regions and are not thought to be from natural gas activity or the oxidation of natural gas. Toluene to benzene ratios in both study regions were found to be most similar to aged rural air masses indicating that the emission of aromatic VOC from Marcellus Shale activity may not be significantly impacting local background concentrations. In addition to understanding local background concentrations the ground-based mobile measurements were useful for investigating the composition of natural gas produced on a spatial scale.

## 4.2 Background and Motivation

The Marcellus Shale is a large-scale unconventional natural gas resource that underlies part of the Appalachian region. As of January 2015 the natural gas (NG) production rate in the Marcellus region was about 16 billion cubic feet per day, or 2 times the production rate of any other unconventional NG resource in the United States and 8 times its 2010 rate (Energy Information Administation, 2015b). The Energy Information Administration estimated that shale gas production in the US is projected to increase to about 150% of 2010 values by 2040 (Energy Information Administation, 2015a). As Marcellus Shale development increases it is estimated to contribute 30-40% production share of the total US natural gas consumption east of the Mississippi River (Energy Information Administation, 2014), establishing its potential role in the US energy market.

Although the Marcellus Shale and similar NG resources are important to the future energy portfolio of the United States, there has been growing concern about the emissions of greenhouse gases (largely methane), criteria pollutants, and air toxics from all stages of shale gas development (Moore et al., 2014;Field et al., 2014). Novel extraction technologies like directional drilling and hydraulic fracturing, as well as other practices used to prepare an unconventional well for gas extraction, are known to emit pollutants associated with diesel combustion including carbon monoxide (CO), carbon dioxide ($CO_2$), nitrogen oxides ($NO_x$), sulfur dioxide ($SO_2$), particulate matter (PM), and volatile organic compounds (VOC) (Roy et al., 2013;Goetz et al., 2015). In addition to combustion products, several well development practices including directional drilling and well completion have been observed to emit methane ($CH_4$), the primary component of NG (Caulton et al., 2014;Goetz et al., 2015).

The atmospheric impacts of the above emission sources per well are typically brief because each process typically has a maximum lifetime of several weeks. Persistent sources of emissions involved in shale gas manufacturing include active well pads, compressor stations, processing facilities, liquid unloading, and pipelines, or sources associated with routine production and distribution (Roy et al., 2013;Litovitz et al., 2013;Allen et al., 2013;Goetz et al., 2015). Natural gas leaks are prevalent throughout the production and distribution stream (US

Environmental Protection Agency, 2015a;Burnham et al., 2011;Allen et al., 2013). Emissions of VOC, CO, $NO_x$, and ultrafine PM have been reported from several stages of the shale gas production sector (i.e. active well pads, compressor stations, and processing facilities) (Warneke et al., 2014;Rich et al., 2014;Pekney et al., 2014;Goetz et al., 2015).

Despite the known increase of unconventional natural gas extraction and obligatory increase in atmospheric emissions there have been limited measurements of ambient air quality in regions that could be impacted. In the Marcellus region, Carlton et al. (2014) suggest that there is an air monitoring data gap and that increased monitoring is needed to assess the air quality impact of shale gas activity. The importance of improved monitoring is further demonstrated by Ogneva-Himmelberger and Huang (2015) who determined that clusters of populations vulnerable to poor air quality (e.g. young, elderly, impoverished) are found in some areas of the Marcellus basin with high densities of shale gas activity. On a regional scale, Vinciguerra et al. (2015) observed increased ethane ($C_2H_6$), an alkane that is the second largest component of NG, downwind of the Marcellus basin corresponding to increased Marcellus Shale production rates. Another ambient air study in the Marcellus basin observed elevated methane and light alkanes near clusters of shale gas wells, but determined that the wells were only a minor source of alkenes and hazardous air pollutants (HAPs) (Swarthout et al., 2015). Similar results were observed by Goetz et al. (2015), where aromatic VOC and other HAPs were not detected at elevated levels in NG emissions from Marcellus shale infrastructure.

Although non-alkane VOC may not be readily emitted from Marcellus shale development, the impact of other primary pollutants (e.g. CO, $NO_x$, PM) and secondary pollutants (e.g. $O_3$) on regional air quality remains uncertain. Studies focusing on other unconventional NG regions have attributed high summertime (Kemball-Cook, 2010) and wintertime (Ahmadov et al., 2015;Schnell et al., 2009) ozone events to VOC emitted from NG development. In northeastern Colorado, Gilman et al. (2013) found that alkanes from oil and natural gas activity contributed to 60% of the total hydroxyl radical (OH) reactivity, an important metric that indicates a compounds potential to contribute to photochemical $O_3$ production. Given the known increase in alkanes in the Marcellus region it is likely that NG emissions from Marcellus shale activity plays an increasing role in $O_3$ production in the region and especially in areas with high $NO_x$ concentrations.

As Marcellus Shale development expands, its impact on local and regional air quality from direct emissions of criteria pollutants or ozone production will likely intensify. Therefore, ambient air quality measurements are necessary to monitor the evolution of potential impacts from increased development. Additionally, as NG production from the Marcellus Shale increases emission of climate forcing compounds like methane with likely also increase in the region. The objective of this study is to utilize ground-based mobile measurements to determine concentrations of air quality and climate relevant pollutants in the Marcellus region during the early development stages of the NG play.

Because future atmospheric measurements in the Marcellus region could be on other platform types (e.g. stationary monitoring, aircraft, etc.) methods have been developed in this study to identify "local background" concentrations in an attempt to create a cross platform metric that can be used by other researchers. Additionally, this study will interpret the local background in the context of spatial distribution and composition of natural gas emissions in two areas of the Marcellus basin with high densities of production activity.

## 4.2 Methods

This work combines results from two ground-based mobile measurement campaigns. The first campaign was conducted in the summer of 2012 using the Aerodyne Research Inc. Mobile Laboratory (AML) (Herndon et al., 2005a). The second campaign took place in the summer of 2015 with the Drexel University Mobile Laboratory (DML). Details on instrumentation and where measurements took place can be found in the following sections.

### 4.2.1 2012 Measurements Overview

The two major goals of the 2012 campaign were to characterize ambient concentrations of measured atmospheric species in areas of the Marcellus basin with high densities of shale gas activity and to characterize emissions from Marcellus Shale infrastructure. The emission characterization aspect of the study was completed using tracer release ratio methods and the results were published in Goetz et al. (2015). The ambient measurement portion of the campaign, and the focus of this work, was located in sections of Southwestern and Northeastern Pennsylvania (SW PA and NE PA). Measurements were made while driving on-road and also while the AML was parked at night. Sampling locations are shown in Figure 4.1. In NE PA, ambient sampling was conducted in Sullivan and Bradford counties and the AML sampled overnight while parked in Laporte, PA. Sampling in the region began on August 22nd and ended on August 27$^{th}$ 2012. In SW PA, measurements were made in Fayette, Green, Somerset, Washington, and Westmoreland counties between the 23rd and 29th of September 2012. Stationary overnight sampling took place in Hidden Valley, PA (Figure 4.1). In addition to being located in areas with concentrated shale gas extraction activity, the study locations were also chosen because of differences in natural gas composition. Marcellus Shale in SW PA in known to contain areas of wet-gas (methane and other light alkanes), while the remainder of the shale layer in PA is know to contain dry gas (mostly methane) (PA Department of Environmental Protection, 2011;PA Deptartment of Environmental Protection, 2011).

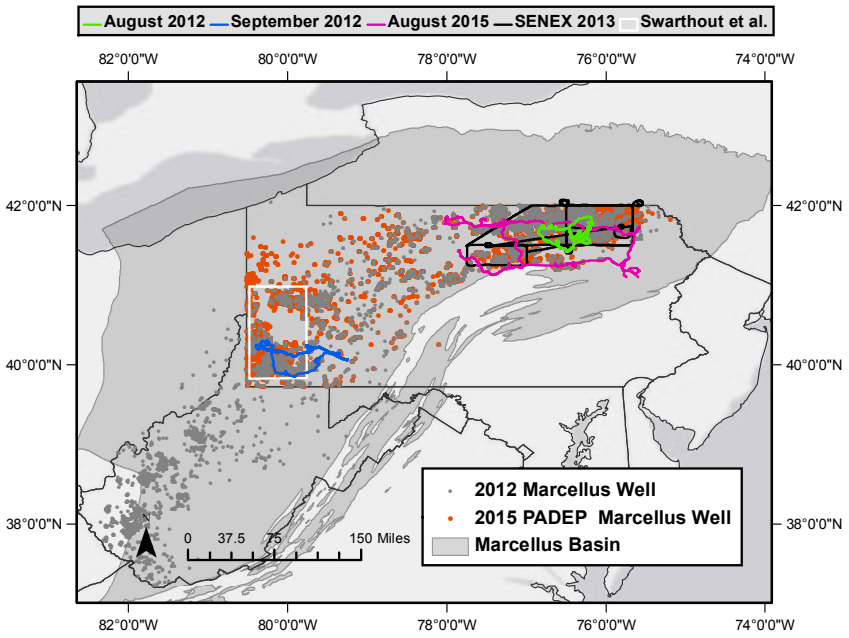


**Figure 4.1. Map of Study Region**
Mobile sampling tracks in Northeastern PA (green and pink) and Southwestern PA (blue) and NOAA SENEX flight (black). The sampling area of Swarthout et al. (2015) is shown in white. The extent of the Marcellus Basin in displayed in grey and overlaid by well sites in 2012 (red marker) and 2015 (orange marker).

### 4.2.2 AML Instrumentation

The AML was equipped with both commercial and research grade instrumentation that utilize real-time rapid response measurements, with most instruments sampling at ~1 Hz. An overview of the AML setup including layout, power setup, and inlet systems can be found in Kolb et al., 2004). A detailed list of particle and gas phase instrumentation installed on the AML for this campaign can be found in Goetz et al. (2015) and its supporting information.

This work will focus on ambient measurements of methane, ethane, CO, $NO_2$, and select volatile organic compounds. Methane, CO, and ethane were measured using Aerodyne Inc. quantum cascade laser (QCL) trace gas monitors. Mobile detection limits for the species measured by the QCL trace gas monitors were <1 ppbv. Ethane monitoring took place only in the SW PA study area because the development of a QCL monitor for ethane detection occurred after measurements were made in the northeast PA. An Aerodyne Inc. cavity attenuated phase shift monitor (CAPS) was used to measure $NO_2$. Because of a technical issue CAPS-$NO_2$ measurements were only available in SW

PA. The CAPS-$NO_2$ mobile detection limit was estimated to be ~0.25 ppbv. Various volatile organic compounds including aromatics and oxygenated hydrocarbons were measured using a proton-transfer reaction mass spectrometer (PTR-MS). A full list of compounds monitored by the PTR-MS and their associated detection limits can be found in Goetz et al. (2015). Additionally, all calibration procedures can be found in the supplemental material of Goetz et al. (2015). All measurements were adjusted based on derived calibration factors. Data processing and analysis was performed in Igor Pro 6.37 (Wavemetrics, Lake Oswego, OR).

### 4.2.3 2015 Measurements Overview

Ground-based mobile measurements using the DML were conducted in NE PA between August 3rd and the 7th of 2015. Unlike the 2012 campaign, measurements were only made during the day while driving and were not active while parked at night. The DML made ambient measurements while driving in Bradford, Clinton, Columbia, Luzerne, Lycoming, Potter, Susquehanna, and Tioga counties (Figure 4.1). All of the counties investigated are known to contain Marcellus shale NG wells and supporting infrastructure. Some measurements were in similar locations as the 2012 campaign, but generally the 2015 measurements investigated areas outside the 2012 domain. Similar to the 2012 campaign, another objective of the 2015 campaign was to estimate emission rates from Marcellus shale infrastructure. The results from the emissions portion of the 2015 campaign are not included in this work and will be available elsewhere.

### 4.2.4 DML Instrumentation

The DML is a late 1990s Ford cargo van that is equipped for gas-phase and particle-phase ambient mobile monitoring. The platform is modular in design and allows for the installation of any combination of instrumentation using a shock-mounted military grade 19-inch rack. Instrumentation is powered through the vehicles alternator and a 2000-watt DC to AC power inverter. The inlet system is adaptable to the instrumentation and for this study non-reactive PTFE tubing was used. The inlet was attached to PTFE gooseneck positioned in front of the vehicle and at a height of ~2 meters. The inlet was positioned to be outside the boundary layer of the vehicle. The gas-phase inlet was equipped with inline Teflon disc filters to remove particulate contamination. The inlet flow rate is adjustable based on excess flow and for this study was set to a fixed flow rate that provided an inlet residence time of ~1 second. The DML was equipped with a ~1 Hz GPS to provide geopostioning.

This work will focus on methane and CO measurements made using a Picarro Inc. Cavity Ring Down Spectrometer (CRDS), Picarro G2401. The CRDS has a sampling rate of ~1 Hz and the mobile detection limits for all compounds analyzed were estimated to be <1 ppbv. The CRDS was factory calibrated prior to the measurement

campaign and dilution calibrations were performed at the end of the campaign. The multi-point dilution calibrations were done by using zero air and a custom calibration standard of methane, CO, and $CO_2$ balanced with $N_2$ produced by Airgas Inc. (Radnor, PA). The calibrations for both methane and CO determined that the CRDS measured ~6.5% low for the campaign compared to the calibration standard for a span up to 2 ppmv for CO and 5 ppmv for methane. All campaign measurements were adjusted to reflect the calibration results.

### 4.2.5 Percentile Interval Smoothing

Ambient concentrations from ground-based mobile monitoring provide insight into local-scale air quality of the area monitored, but they are not useful for direct comparison to other monitoring studies because unprocessed ground-based mobile measurements are biased by a number of factors that do not impact other measurement platforms. For example, changes in topography coupled with spatial changes in local scale meteorology are factors that affect ground-based mobile monitoring, but does not have the same significance for stationary monitoring. Aircraft and satellite monitoring are largely independent of topography and typically impacted by larger scale (rather than local) meteorology. One of the largest differences between ground-based mobile ambient monitoring and other types of measurement platforms is the degree of mixing of emissions at the local scale. Depending on proximity to emission sources, a stationary ambient monitoring site can be influenced by local unmixed emissions, but the extent of that influence is typically based on wind direction and regularity of emissions. Consequently, when the sampling location is fixed, and distances to emission sources are known, background concentrations can be easily isolated from unmixed emission signals and conclusions can be made about the magnitude of emissions. Aircraft measurements are mobile, however, depending on altitude often sample air masses assumed to be well mixed vertically in the boundary layer (Peischl et al., 2015). Alternatively, the degree of emission mixing on ambient ground-based mobile monitoring is constantly changing with its location, and the magnitude of an emission source is difficult to estimate because the scale is dependent on the rate of emission, local scale meteorology and distance. Therefore, local scale mixing of emissions need to be removed from mobile datasets to make them comparable to other types of atmospheric monitoring.

In order to generate a cross platform dataset, the data in this study was transformed using percentile smoothing over a defined “averaging” time. The processing technique generates a dataset at a user selected percentile that best represents the background concentrations over a time interval with sufficient resolution to remove rapid changes in the time series due to emission source plumes and acute changes due to topographically dependent meteorology. The following methods establish how the percentile and the time interval were chosen to best represent the local-scale background concentrations in the Marcellus basin from our combined datasets.

The percentile smoothing analysis was conducted at a range of time intervals and at percentiles ranging from 5 to 60 for to determine which percentile best represents the local background for all of the atmospheric species monitored. Time intervals at multiples of 10 minutes ranging from 10 to 60 minutes were investigated. It was qualitatively determined that the 20 minute interval best provides spatial resolution with enough sampling points to well represent a local background concentrations for all species. This value may be different for other mobile platforms and is based on both platform velocity (e.g. car vs plane) and sampling rate of the measurement. The percentile that best represents the local background was determined through comparison with lognormal fits of the measurement data histograms over the same 20-minute section of data for the entire dataset. Histograms were calculated for each interval because it was assumed that the most frequent concentrations represent the local-scale background for that sampling interval. Example histograms of 20-minute sections of ethane measurements that display three common sampling scenarios encountered in the dataset are shown Figure 4.2. The figure demonstrates how the mode of the lognormal fit of each histogram approximates the most frequent value for each sampling interval. The mode of a lognormal fit of a histogram is assumed to reasonably characterize the local-scale background, however the analysis is less robust compared to percentile smoothing and can create unpredictable results when the fitted histogram is not log normally distributed. The concentration percentiles for each species were then plotted against the mode of the lognormal fit for each 20-minute interval to determine which percentile best represents the most frequent concentrations (Figure 4.3). Results from the comparison determined that percentiles between 30 and 40 were the most closely related (i.e. slope = 1) to the lognormal fits for all of the species analyzed. An example of how the $35^{th}$ percentile most closely matches the mode of the lognormal fits for ethane is shown in Figure 4.3. Based on these analysis results, 20-minute $35^{th}$ percentile smoothing is used to represent the local-scale background concentrations for the remainder of this work.

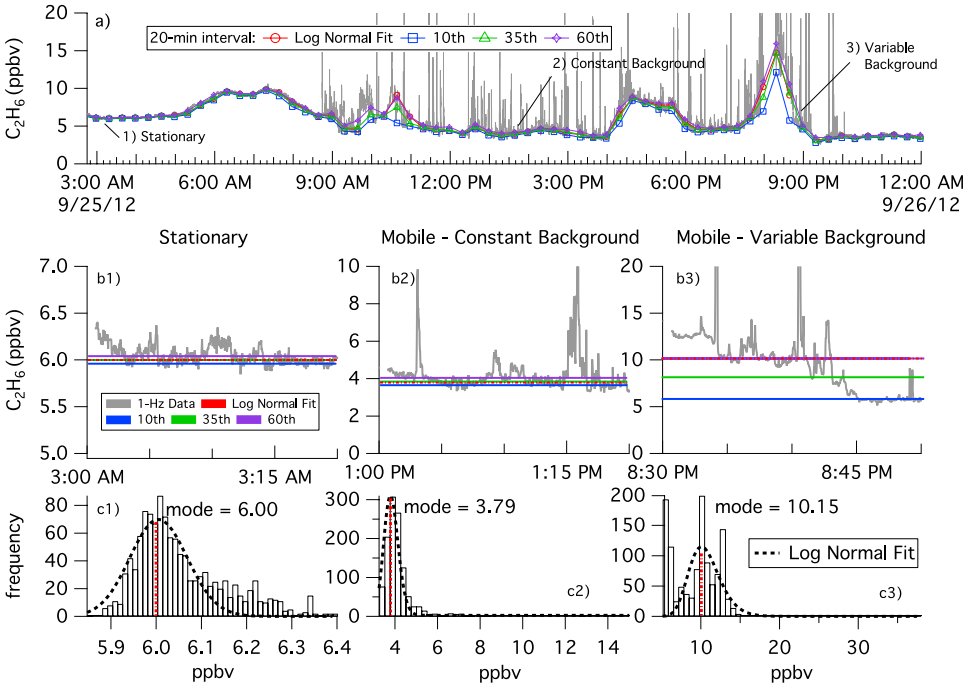


**Figure 4.2. Examples of Local Background Estimates**
Time series (lower plots) and histograms (upper plots) of ethane with examples of stationary data (left plots), mobile data with a constant background (middle plots), and mobile data with a variable background (right plots). Log normal fits of each histogram (black dotted line) and the mode of the log normal fit (red dotted line)

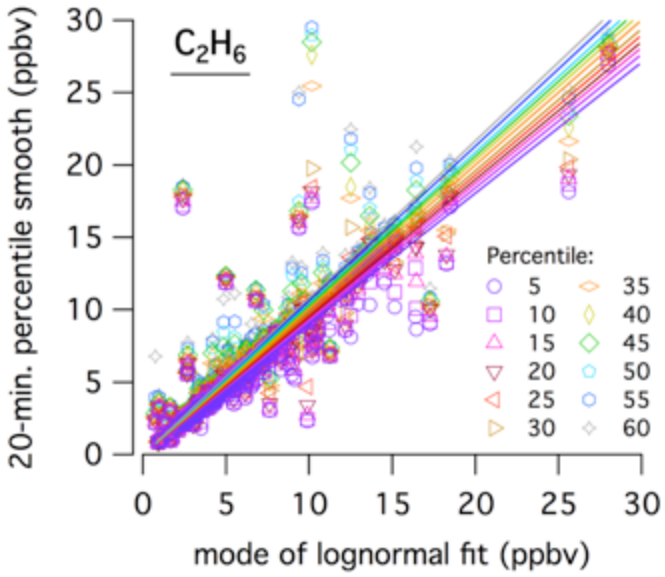


| Percentile | Slope |
|---|---|
| 5 | 0.90 |
| 10 | 0.92 |
| 15 | 0.94 |
| 20 | 0.95 |
| 25 | 0.97 |
| 30 | 0.98 |
| 35 | 1.00 |
| 40 | 1.02 |
| 45 | 1.03 |
| 50 | 1.05 |
| 55 | 1.07 |
| 60 | 1.08 |

**Figure 4.3. Correlation of percentile smoothed data to lognormal fits of the data**
Scatter plot of 20-minute percentile smoothed ethane data at percentiles ranging from 5 to 60 versus the mode of the log normal fit for the same 20-minute intervals. Linear fits of the data with results slopes are shown.

### 4.2.5 Other Sources of Data

Aside from the ground-based mobile measurements conducted on the AML and DML other data from other ambient air quality studies in Marcellus region were retrieved and used for comparison. Results from flask samples detailed in the supporting information of Swarthout et al. (2015) were used for comparisons of methane, ethane, acetone, methanol, acetonitrile, acetaldehyde, benzene, and toluene mole fractions in SW PA. Major comparisons were made between the mobile results and results from PTR-MS and Picarro CRDS measurements taken during the National Oceanic and Atmospheric Administration's (NOAA) 2013 Southeast Nexus (SENEX) field study. The SENEX campaign performed multiple flights using the NOAA WP-3D aircraft in Southeast U.S. and also directed several flights that focused on areas with unconventional natural gas activity including the Haynesville, the Fayetteville, and the Marcellus Shale regions (Peischl et al., 2015;Yuan et al., 2015). Summary statistics are derived from data collected on the July 6$^{th}$ 2013 flight when in the Marcellus region (>41.0°N latitude) and below an altitude of 2000 meters were estimated. Measurements below 2000 meters were assumed to be at or near the planetary boundary layer height and therefore to have similar characteristics to ground-based measurements (Peischl et al., 2015).

## 4.3 Local Background Concentrations

Observed ambient concentrations of CO, $NO_2$, methane, ethane, and PTR-MS measured VOC can be seen in Figure S1. The results in Figure 4.4 show the average concentrations, standard deviations (upper bounds) and minimums (lower bounds) for the monitored species in both SW PA and NE PA. The summary statistics were calculated using all on-road and stationary measurements with the exception of measurements taken while stopped in traffic, when self-sampling exhaust, and when downwind of sites sampled for the emission characterization portion of the campaign. Since most on-road measurements were included in the summary statistics, the values shown in Figure 4.4 represent both background concentrations and elevated concentrations from local emissions sources. Contributing local sources likely included on-road and off-road vehicles, manufacturing, power generation, natural gas infrastructure, biomass burning, vegetation, and agriculture, all of which was observed visually from the mobile labs.

In 2012, $CH_4$ was observed to have an average of 1.97 ppmv, and a standard deviation of 0.23 ppmv in NE PA over the 6-day sampling period. In the SW PA study area $CH_4$ was observed at 2.15 ± 0.30 ppmv over a 7-day averaging period. In 2015, $CH_4$ observed to have an average of 2.09 ppmv, and a standard deviation of 0.17 ppmv over the 5-day sampling period. Ethane, which was only measured in SW PA, was observed at 7.41 ± 24.0 ppbv. Carbon monoxide was observed to have an average mole fraction of ~240 ppbv in both study areas in 2012 and was observed to have large variability with standard deviations of 830 ppbv and 1510 ppb in NE PA and SW PA, respectively. In 2015, CO was observed at an average of 281 ppbv and had a large standard deviation of 2700 ppbv. The large standard deviation in 2015 compared to 2012 observations suggests that more direct unmixed emission plumes were observed in 2015. The average mole fraction of $NO_2$ in the SW PA was observed to be 2.90 ± 6.48 ppbv.

Although the above summary statistics are useful for characterizing concentrations observed while monitoring throughout the Marcellus Shale region they are not useful for inter-year comparisons or comparisons with other studies as described previously in section 4.2.5. Therefore the following sections provide results of local-scale background mole fractions derived from percentile interval smoothing. All discussion points are based on the analysis of the local-scale background mole fractions and not from the summary statistics of the ambient mole fractions contained in Figure 4.4.

Box and whisker plots are presented in Figure 4.5 to show local-scale background mole fractions of methane, ethane, CO, $NO_2$, methanol, and acetone estimated from interval percentile smoothing for SW PA and NE PA from both measurement campaigns. Results from other studies and other data sources are also provided for comparison to concentrations observed elsewhere in the Marcellus region, concentrations observed in other unconventional natural gas plays, and also to make comparisons to urban measurements and larger regions. Most notably, comparisons to mole fractions observed by the above mentioned SENEX campaign and Swarthout et al. (2015).

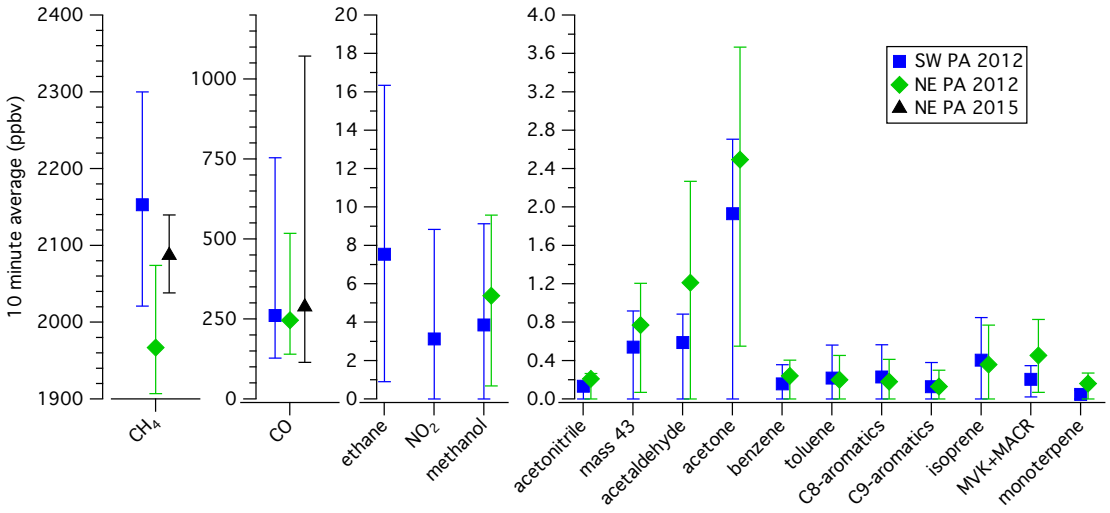


**Figure 4.4. Ambient Mole Fractions of Monitored Species**
Mobile measurements are from Southwestern PA (blue) and Northeastern PA (green) in 2012. Ambient mole fractions of species monitored in 2015 are found in black. The average (marker), standard deviation (upper whisker) and minimum (lower whisker) are displayed for each species.

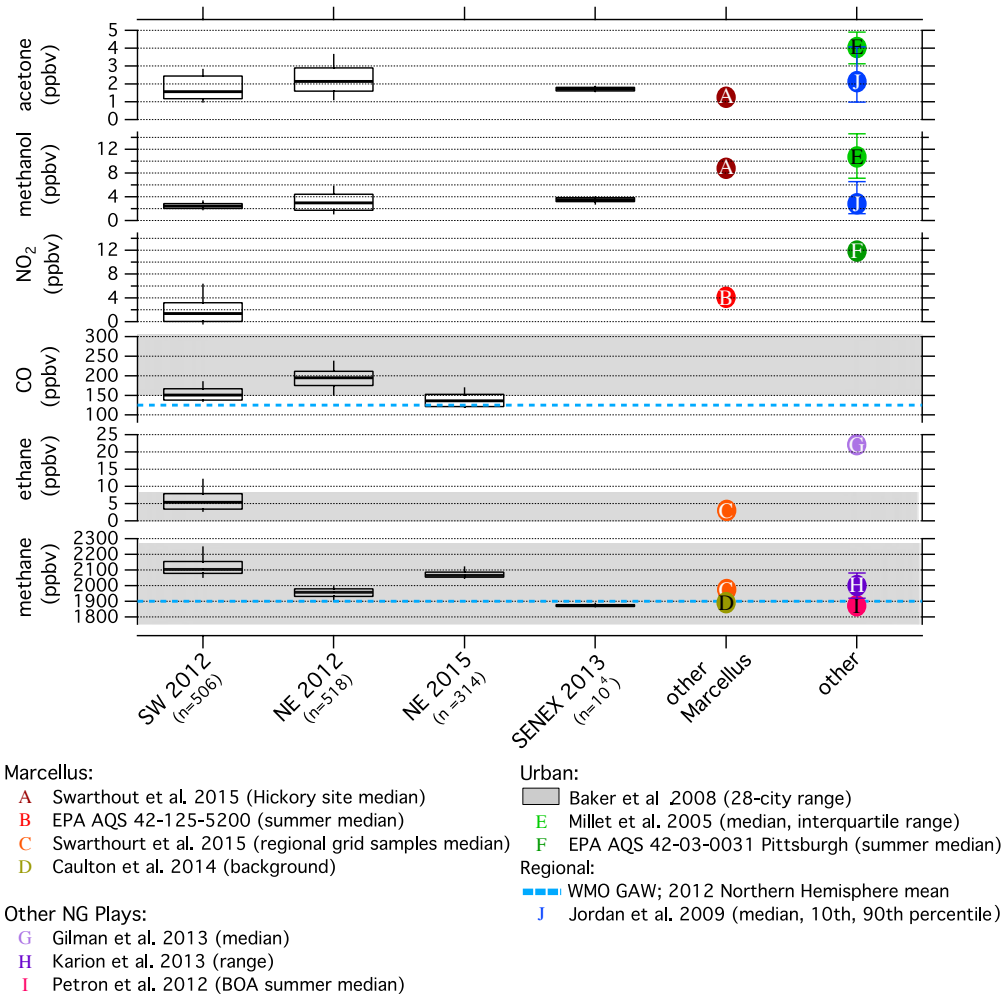


**Figure 4.5 Summary of Local-scale Background Estimates**
Box and whisker plots ($10^{th}$, $25^{th}$, $50^{th}$, $75^{th}$, and $90^{th}$ percentiles) of local-scale background estimates from Southwestern PA and Northeastern PA in 2012 for methane, ethane, CO, NO2, methanol and acetone. Also included are estimates of methane and CO from the 2015 Northeastern PA field study. Box and whisker plots for methane, acetone, and methanol from the SENEX 2013 field study are displayed. The Baker et al., 2008 28-city range is for select species is shown in grey. WMO mean is displayed as the blue dashed line. Important values from relevant studies and other data sources displayed as lettered markers (circles).

### 4.3.1 Methane

As seen in Figure 4.5, the median local-scale background mole fraction of methane was estimated to be 2100 ppbv in SW PA and 1960 ppbv in NE PA during the 2012 field study. The results indicate that the local background methane mole fractions were significantly elevated in the Southwest compared to the Northeast study area, and that similar local background mole fractions were never observed between the two areas in the summer of 2012. For example, there was approximately a 50 ppbv difference between the $10^{th}$ percentile value in SW PA and the $90^{th}$ percentile value in the NE PA in 2012. An analysis of boundary layer heights taken from the North American Region Reanalysis (NARR) model (NCEP, 2015) during the two study periods, which can be found in the Appendix C. This analysis found that the boundary layer height was typically greater during the SW PA study period compared to the NE PA study period in 2012. Furthermore, an analysis of wind speed observed by the AML, located in Appendix D, determined that the median wind speed during the NE PA study period was approximately 50% of the median of the SW PA study period, which would lead to less atmospheric dilution compared to SW PA. Because both datasets were obtained in the summertime and the SW PA study area observed larger local background mole fractions of methane in more dilute atmospheric conditions, the large differences in background mole fractions were likely due to differences in the quantity of emissions between the two study areas in 2012. Natural gas activity is a major source of methane emissions, but there are a number of other natural and anthropogenic emission sources of methane that could contribute to enhanced backgrounds in SW PA (IPCC, 2013). However, the role of other emissions sources (e.g. landfills, biomass burning, biogenic, NG distribution leaks etc.), which may be significant in some areas, is outside the scope of this work. An investigation of the influence of Marcellus Shale well density on local-scale background methane will be discussed later in this work in section 4.4.

Results from the 2015 campaign indicate that the median local-scale background of methane was enhanced by 100 ppbv compared to the 2012 Northeast study area. In addition to enhancements of the median local-scale background there were enhancements in all percentiles when comparing 2012 to 2015 datasets with no overlap in local background values. Since mobile routes differed between 2015 and 2015 measurements, we can compare measurements made in the same area to remove this potential source of error. When comparing sampling location within a 10 km proximity, the median local methane background was found to be 125 ppbv greater in 2015 compared to 2012. Additionally, analysis of boundary layer heights and wind speed during the two study periods shows that the atmosphere was likely more dilute in 2015 compared to 2012 in NE PA with boundary layer heights equal to or lower than 2012 (Appendix C) and with greater wind speeds (Appendix D). Consequently, the elevated background levels observed NE PA in 2015 were not due to less dilute atmospheric conditions in the region. The universal enhancement of methane from 2012 to 2015 suggests that emissions of methane has increased in NE PA. Since the scale of

agricultural activities have not changed significantly, it is likely that the major contributor to the elevated local backgrounds in 2015 is increased Marcellus Shale NG production.

Additional comparisons can be made between local-scale methane backgrounds in the two study areas and measurements from other studies in the Marcellus region. In NE PA, the SENEX flight provided a median methane mole fraction of 1880 ppbv in July 2013, which is lower than any local-scale background estimate made in this study. From two flights in SW PA in June 2012, Caulton et al. (2014) estimated the methane background to be 1890 ppbv. Another study that took place in June 2012 in SW PA used a regional grid of ground-based flasks and found methane to have a median value of 1970 ppbv from 144 samples (Swarthout et al., 2015). It is noteworthy that both aircraft studies observed lower methane concentrations than what was observed by ground-based measurements in this work and by Swarthhout et al. (2015), all of which took place in the summertime and within a 13 month span. The difference between the ground-based and aircraft platforms suggests that there may be some inherent systematic difference between the two measurement approaches, and assumptions of well-mixed boundary layers may not be appropriate. It is important to note that the aircraft measurements were within 20 ppbv of the World Meteorological Organization's (WMO) 2012 estimated mean for methane of 1900 ppbv for the Northern Hemisphere between 30°N and 60°N latitude (World Meterological Organization, 2013), which if correct could indicate that the methane background in the Marcellus region at that time was not elevated compared to the mid-latitude average. Alternatively, if there is a systematic difference between the two measurement approaches, and ground-based measurements are considered to be more representative of a regional air mass, then the ground-based results from this study and in Swarthout et al. (2015) demonstrate that methane in the Marcellus region is elevated compared to the Northern Hemisphere mid-latitude (30-60°N) mean.

Methane mole fractions from other unconventional natural gas regions (Karion et al., 2013;Pétron et al., 2012) and from a 28-city air study (Baker et al., 2008) can be found in Figure 4.5. All local-scale methane backgrounds estimated in this study were within the 28-city urban range, suggesting that methane concentrations in the Marcellus are more similar to urban air masses than rural, despite being a mostly rural region. It is important to note however that the 28-city study values may no longer be representative of urban methane because the study was conducted over ten years ago and therefore does not represent the increasing global background on top of which urban emissions accumulate. For example, between 2007 and 2012 the global mean mole fraction increased 29 ppbv (World Meterological Organization, 2013). Comparisons to Petron et al. (Pétron et al., 2012), demonstrate that background methane mole fractions were greater in the Marcellus region than the summertime median at Boulder Atmospheric Observatory (BAO) located in the Denver-Julesburg basin in Colorado. In the Uintah Basin in Utah, Karion et al. (2013) found that downwind methane ranged from 1920 to 2080 from one flight in February 2012. The results from the Uintah basin

flight reveals that the local-scale methane backgrounds estimated in this study are within the mole fraction range observed in another large unconventional natural gas basin.

### 4.3.2 Ethane

Ethane was observed to have a local-scale background median of 5.4 ppbv and interquartile values of 2.7 ppbv and 7.9 ppbv in SW PA (Figure 4.5). Unfortunately, because ethane monitoring was limited to SW PA comparisons cannot be made between study areas or between years to determine emission trends. Most of the local-scale ethane background estimates were within the Baker et al. 28-city range (0.5-8.74 ppbv), but the 90$^{th}$ percentile was outside the range with a mole fraction of 12.2 ppbv. Due to hydroxyl radical (OH) chemistry in the summertime ethane has been observed to have strong seasonal variability and was found to have amplitude of ~0.8 ppbv in the high Northern Hemisphere (Simpson et al., 2012). Consequently, it is difficult to estimate a global or hemispheric average. From WMO (World Meterological Organization, 2013) and Simpson et al. (Simpson et al., 2012), it was approximated that the summertime mole fraction of ethane in 2009 was ~1 ppbv in the Northern Hemisphere between 30°N and 60°N latitude. Given the approximated mid-latitude average it is likely that ethane in SW PA is enhanced compared to other rural mid-latitude locations. Further evidence that ethane is enhanced in SW PA can be found in Swarthout et al. (2015), who observed a summertime median of 2.86 ppbv. While ethane appears to be enhanced in SW PA it is not as enhanced the Denver-Julesburg Basin (median of 22 ppbv) based on measurements made at the BOA in 2011 (Gilman et al., 2013). The large differences between the two NG regions could be due to the quantity of emissions in the region, differences in NG composition, and seasonal effects. Further monitoring of ethane in the Marcellus region is needed to understand seasonal trends and how increased NG activity influences ozone production in the region.

### 4.3.3 Carbon Monoxide

The median local-scale background for CO was estimated to be 150 ppbv in SW PA (Figure 4.5). Northeastern PA in 2012 was estimated to have a local-scale background mole fraction nearly 50 ppbv larger than SW PA. The larger CO median in NE PA is unexpected because NE PA is considered the most rural of the two study areas and the counties contained in the study area have a lower population density compared to the counties in SW PA, though all counties had a population density of less than 20% of the urbanized local Allegheny County (Bureau, 2012). While both study areas were in rural areas, the median background CO was within the 28-city range of Baker et al. (2008) and above the WMO mid-latitude average of 125 ppbv (World Meterological Organization, 2013). The comparison to the 28-city study indicates that although the areas are rural there is a source of CO emissions that is

amplifying CO to urban levels. However, the larger CO local-scale background in NE PA in 2012 could partially be explained by lower boundary layer heights (Appendix C) and windspeed (Appendix D) over the study period compared to SW PA. Back trajectories for each study day were produced using NOAA's HYSPLIT (Stein, 2015;Rolph, 2016) to look at the air mass source regions as a potential explanation of CO differences between locations and years. Though not a definitive analysis, the 48 hour back trajectories show that the majority of the air masses monitored in SW PA originated in regions West of the Marcellus shale region, as seen in (Appendix E) in the supporting information. Alternatively, many of the 48 hour back trajectories calculated for the NE PA 2012 study period originated within the Marcellus Shale region or from the Atlantic Ocean and passed through the urbanized Atlantic coast. The differing source regions could explain the differences in CO local background, though more monitoring is needed to assess the role of emissions from Eastern urbanized areas on CO levels in the region.

In 2015 CO was estimated to have a median local-scale background mole fraction of 136 ppbv. The estimated background was lower than what was observed in either study area in 2012 and when investigating measurements within the same 10 km vicinity the 2015 median was ~75 ppbv lower than the 2012 median. The 2015 median was also lower than the 28-city range and the 25$^{th}$ percentile was within the 30-60°N mean (Figure 4). The comparisons suggest that NE PA in 2015 had CO backgrounds more similar to rural areas despite the observation of larger CO emission signals in the ambient dataset as seen in Figure 4.4. The significant drop in median local-scale background provides some evidence that CO emission may have decreased from 2012 to 2015 in the NE PA, though the lower median background in 2015 can also be explained by the increased boundary layer height, increased wind speed, and differences in air mass source regions estimated for that study period. The supposed trend in CO emissions corresponds with a decrease in Marcellus Shale spuds, or the point at which a new NG well is drilled, in Pennsylvania over the same time period. New unconventional NG wells have decreased at a rate of ~170 wells per year in Pennsylvania, though 2011 and 2014 were outside that trend, and the total spuds in 2015 were only 58% of the total for 2012 (Pennsylvania Department of Environmental Protection). A decrease in new NG well development would induce a decrease in the use of heavy duty diesel trucks, direction drilling, hydraulic fracturing, flow-back flaring, well pad construction all of which are sources of CO emissions and is one possible explanation for the decreased CO levels. However, while spuds have decreased in PA, the total production in the Marcellus Basin has more than doubled (110% increase from 2012 to 2015) (Energy Information Administation, 2015b). The increase in production with the coupled decrease in spuds suggests that distribution infrastructure (i.e. compressor stations, pipelines, processing facilities) is starting to become accessible to many of the started and capped wells in the region. Increased CO monitoring combined with emission inventories are needed to understand the evolving role of CO emissions from well pad development and distribution infrastructure on air quality in the Marcellus region.

### 4.3.4 Nitrogen Dioxide

Nitrogen dioxide, a criteria pollutant under the National Ambient Air Quality Standards (NAAQS), was estimated to have a median local-scale background of 1.4 ppbv in SW PA. The median was lower than the 2012 summertime median of 4.0 ppbv at an US Environmental Protection Agency (USEPA) monitoring station (AQS 42-125-5200) located in rural Washington County in an area with a high density of Marcellus Shale well pads (U.S. Environmental Protection Agency). Additionally, the SW PA median was ~10 ppbv lower than the 2012 summertime median at a USEPA monitoring station located in Pittsburgh, PA (AQS 42-03-0031) (U.S. Environmental Protection Agency). Though comparisons to other studies are difficult because of the short lifetime of $NO_2$ in daytime hours, the values shown in Figure 4.5 provide a baseline that represents mole fractions observed in the early development of the Marcellus Shale.

### 4.3.5 Acetone

Acetone is known to be prevalent in the troposphere and is emitted by solvents, vehicles, biogenic sources, oceans, biomass burning, and secondary production from propane oxidation (Jordan et al., 2009). Past measurements in the troposphere have observed ambient mole fractions ranging from 0.2-3 ppbv (Jacob et al., 2002). Globally, the largest sources of acetone are terrestrial vegetation (35%) exchange with oceans (28%), and oxidation of propane (22%) (Jacob et al., 2002). In the Marcellus region the major sources are expected to be vegetation and the oxidation of propane from NG leaks.

In SW PA acetone was estimated to have a median local-scale background of 1.6 ppbv (Figure 4.5). Based on measurements in NE PA in 2012 acetone was estimated to have a median local scale background of 2.1 ppbv. Similar results have been observed by the SENEX 2013 field study in Northeastern PA (median of 1.7 ppbv) and by Swarthout et al. (2015) in SW PA at their Hickory monitoring station (median of 1.3 ppbv) located within an area of with a high density of NG activity. The analogous results from field studies indicate that the acetone mole fractions were consistent throughout the Marcellus region in the summertime of 2012 and 2013 and acetone was likely emitted from a constant source or was transported from other regions. The local background estimates were also similar to findings from Jordan et al. (2009), who observed a summertime median mole fraction of 2.1 ppbv at a rural monitoring site in New Hampshire. Further evidence that the local-scale background estimates are most similar to rural concentrations can be found in Millet et al (2005), who observed large acetone mole fractions in the summertime in Pittsburgh. Given that propane has an atmospheric lifetime of 10 days due to OH oxidation (Atkinson, 2000), which allows for significant transport outside the region, and that acetone measurements are not enhanced compared to literature values it is likely natural gas development is not significantly adding to acetone concentrations in the Marcellus region. Future acetone

measurements collocated with propane measurements would be valuable in constraining the role of propane oxidation in acetone production in the Marcellus region and how it compares to biogenic production.

### 4.3.6 Methanol

Methanol is ubiquitous in the atmosphere and emissions have been attributed to terrestrial vegetation, plant decay, biomass burning, oxidation of methane, and direct anthropogenic sources (Wells et al., 2012;Singh et al., 2000;Holzinger et al., 2005). Methanol has also been observed from unconventional NG wells in the Uintah Basin in Utah and from a compressor station in the Marcellus Basin because of its use as a pipeline anti-freeze (Warneke et al., 2014;Goetz et al., 2015). Methanol was estimated to have a local-scale background median of 2.5 ppbv in SW PA and 3.0 ppbv in NE PA in 2012. In 2013 methanol observed by the SENEX field study was slightly larger with a median mole fraction of 3.5 ppbv, but generally methanol followed the same trend in the three field studies compared to acetone. Methanol observations by Swarthout et al. (2015) produced a median mole fraction of 8.96 ppbv in SW PA at their Hickory monitoring site. The observations by Swarthout et al. (2015) were more similar to the urban summertime median of 10.72 ppbv observed by Millet et al. (2005) than the rural summertime median of 2.69 observed by Jordan et al. (2009). The observations of urban scale methanol at the Hickory monitoring site and consistent rural scale concentrations observed by this study and SENEX suggest that the Hickory site likely detected methanol emissions from natural gas infrastructure that was not detected at the same extent by the other studies. The observation of methanol emissions at the Hickory site is possibly due to the intensity of NG activity in the area, but could also be due to other factors like operator practices in the study area.

### 4.3.7 Hazardous Air Pollutants

Hazardous air pollutants are atmospheric pollutants, mostly VOCs, that are known to cause cancer or serious health impacts and consequently emissions of the compounds are regulated by the US EPA (U.S. Environmental Protection Agency, 2015). The PTR-MS aboard the AML monitored several signals that are attributable to volatile organic compounds classes that have been listed as hazardous air pollutants and the complete list of monitored masses can be found in Goetz et al. (2015). The HAPs monitored in this study include oxygenated VOC such as methanol, acetonitrile, and acetaldehyde and aromatic compounds including benzene, toluene, and $C_8$-aromatics (107 amu). $C_8$-aromatics species measured at 107 amu include ethyl benzene, (m+p)-xylene and o-xylene (de Gouw and Warneke, 2007). The same HAPs were monitored by a PTR-MS on the July 6 2013 SENEX flight. Local-scale background estimates for the monitored HAPs and observations of the same compounds during the SENEX flight can be found in Figure 4.6, excluding methanol for which results were discussed previously.

Median local-scale background mole fractions of the monitored HAPs were generally larger in NE PA in 2012 compared to SW PA and the SENEX flight, with the exception of $C_8$-aromatics, which were found to have the largest mole fractions in SW PA. Acetonitrile is known to be emitted from the combustion of biomass and is often used as a biomass burning tracer (de Gouw, 2003). The presence of enhanced acetonitrile in NE PA by this study and SENEX compared to SW PA suggests that biomass burning was likely prevalent in NE PA (Figure 4.6). Median mole fractions of the HAPs found in Figure 4.6 were generally lower than observations at the Hickory site by Swarthout et al. (2015), with the exception of benzene in NE PA which was ~50 pptv greater.

Benzene in both SW PA and NE PA had median mole fractions within the Baker et al. 28-city range, but toluene was found to have medians below the urban range (Baker et al., 2008). Because aromatic compounds are often emitted from similar sources (e.g. fuel combustion, biomass burning, oil, and natural gas) and have different atmospheric lifetimes, molar ratios of the compounds can be used to understand the photochemical age of the compounds if the molar ratio at the point of emission is known (Rogers et al., 2006;Monod et al., 2001). The atmospheric lifetime for benzene, toluene, and C8-aromatic compounds due to reaction with the OH radical are estimated to be 9.4, 1.9, and <1.6 days respectively based on standard atmospheric conditions (Atkinson, 2000;Monod et al., 2001). While the dominant source or sources of aromatics in the Marcellus basin are not known, the emission ratio of common sources provided in the literature can be used to make inferences about potential sources and the age of aromatic compounds in the region. As seen in Table 4.1, the emission of toluene is greater than benzene from common emissions sources like vehicle emissions, oil wells, and NG wells, but has been found to be lower from biomass burning and from diesel combustion (Warneke et al., 2014;Monod et al., 2001;Jobson et al., 2005;Heeb et al., 1999). Molar ratios of toluene to benzene were determined to be 1.45 in SW PA and 0.77 in NE PA based on linear fits of the local-scale backgrounds (Table 4.1), though correlation was shown to be poor in SW PA with an $r^2$ of 0.24. Based on a linear fit of 1-minute averaged data the SENEX flight observed a toluene to benzene molar ratio of 0.93 ($r^2$ = 0.22). Comparisons with toluene to benzene ratios reported in different types of ambient air masses shown in Table 4.1 demonstrate that the molar ratios observed in the Marcellus region were less than what has been observed in urban and suburban air masses (Rogers et al., 2006;Parrish et al., 1998;Monod et al., 2001;Heeb et al., 2000). The toluene to benzene molar ratio in SW PA was also slightly less than the daytime summer rural ratio observed by Jordan et al. (Jordan et al., 2009), but was also within 2% of the benzene to toluene ratio observed in oil well emissions in the Unitah Basin, another unconventional fossil fuel resource located in Utah (Warneke et al., 2014). Although there are NG liquid producing wells in the Marcellus region, which could potentially contribute to enhanced toluene and benzene, evidence from another study shows that unconventional natural gas wells only contribute to ~10% of the ambient benzene and toluene in SW PA (Swarthout et al., 2015). Additionally, the molar ratio of C8-aromatics to

benzene in SW PA was estimated to be 1.6 ($r^2$ = 0.37), which is most similar to the ratio of gasoline automobile emissions than oil and NG emissions that have been observed at molar ratios <1 (Table 4.1). (Warneke et al., 2014;Heeb et al., 1999). The evidence indicates that aged emissions similar to what has been found in other rural locations, likely from vehicular emissions, may be the dominant source of aromatics in SW PA, though the contribution from other sources is unknown.

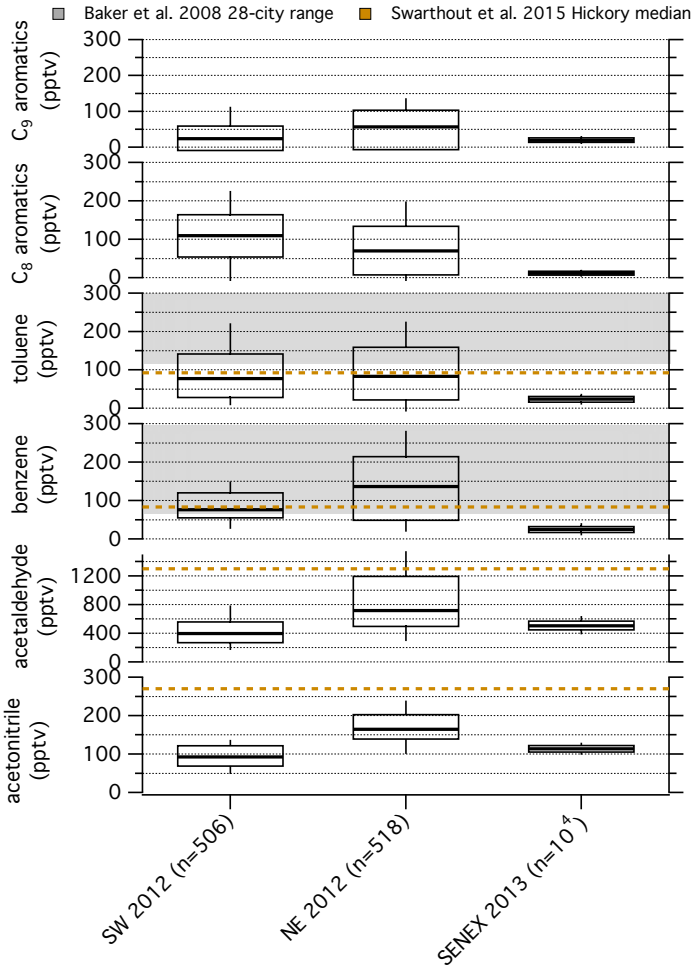


**Figure 4.6. Summary of Local-scale Background Estimates for HAPs**
Box and whisker plots ($10^{th}$, $25^{th}$, $50^{th}$, $75^{th}$, and $90^{th}$ percentiles) of local-scale background estimates from Southwestern PA and Northeastern PA in 2012 for acetonitrile, acetaldehyde, benzene, toluene, $C_8$-aromatics. Box and whisker plots of mole fractions of the same compounds monitored during the July 6 2013 SENEX flight are also included.

**Table 4.1. Molar ratios of local-scale background mole fractions in SW PA and NE PA**
1-minute average data from the July 6 2013 SENEX flight, and literature values of aromatic compounds.

| location or source | | toluene/benzene ratio ($r^2$) | $c^8$-aromatics/benzene ratio ($r^2$) |
|---|---|---|---|
| this study | SW PA | 1.45 (0.24) | 1.6 (0.37) |
| | NE PA | 0.77 (0.68) | 0.64 (0.66) |
| | SENEX (1-min mean) | 0.93 (0.22) | 0.45 (0.14) |
| emissions | natural gas wells[a] | 1.22 | 0.5 |
| | oil wells[a] | 1.42 | 0.78 |
| | biomass burning[b] | 0.45 (0.95) | |
| | automobile emissions[c] | 1.89 | 2.04 |
| | diesel emissions[d] | 0.50[aa] | 0.64[aa] |
| ambient | rural[e] (daytime summer) | 1.49 | |
| | suburban[f] (1998) | 1.72 | |
| | urban[b] | 1.93 (0.66) | |
| | urban[g] (U.S. average) | 2.27 | |
| | Mexico City[h] | 4.35 | |
| Uintah Basin | downwind of NG field[a] | 0.60 | 0.92 |

a. Warneke et al. 2014; b. Monod et al. 2001; c. Heeb et al. 1999; d. Jobson et al. 2005; e. Jordan et al. 2009; f. Heeb et al. 2000; g. Parrish et al. 1998; h. Rogers et al. 2006
aa. mean from idle and 20%, 40%, and 80% loading of generators

The molar ratios of toluene and C8-aromatics to benzene in NE PA were significantly lower than what was observed in SW PA, as seen in Table 4.1. The toluene to benzene molar ratio of 0.77 was also >35% less than any emission source listed in Table 4.1 except for biomass burning and diesel emissions. The low ratio in NE PA suggests that either the sampled air masses were well aged, that emission sources like biomass burning or diesel combustion were large contributors to background concentrations in the area, or the combination of both scenarios were true especially since the ratio is significantly lower than what has been observed in other rural areas. As previously discussed, the presence of elevated acetonitrile in NE PA suggests that biomass burning was prevalent in the region. Although biomass burning is likely a contributor to the aromatics in NE PA it does not preclude the contribution of aged NG or diesel emissions from Marcellus Shale development in the region. For example, the C8-aromatics to benzene molar ratio in NE PA was 0.64, which is similar to the ratio observed from oil and NG by Warneke et al. (2014). Warneke et al. (2014) found that the toluene to benzene ratio at the edge the NG field in the Uintah Basin was approximately half the ratio measured directly from NG wells in the basin, demonstrating that significant mixing and ageing can occur within a NG basin. The C8-aromatics to benzene ratio observed in NE PA was closest to the ratio

produced by diesel exhaust (Jobson et al., 2005) demonstrating that on and off road diesel engines used in well pad development and transport may have an impact on air quality in the region.

Further monitoring of HAPs is needed to understand their air quality impacts in the Marcellus Basin and how concentrations evolve over time. Yet the estimated local-scale background the mole fractions of benzene and toluene in the Marcellus Basin in the summer of 2012 were below or within the lower range of urban levels. Furthermore, molar ratios of light aromatics to benzene have shown that the monitored areas do not have urban characteristics and that aromatic emissions from NG production are not obvious. These results coincide with results by Goetz et al. (2015), where HAPs were not detected above detection limits from Marcellus Shale production and infrastructure.

## 4.4 Well Area Density and Production

In addition to being useful for comparisons to other studies, local-scale background estimates from ground-based mobile monitoring are suitable for discerning relationships between spatial parameters and ambient concentrations. One spatial parameter that is thought to be a useful proxy for the intensity of NG extraction activity is the density of permitted NG wells in an area. Permits for unconventional NG wells in the Marcellus region in 2012 were retrieved from the HDPI database (HPDI, 2012), an independent clearinghouse for oil and natural gas data. Marcellus Shale well permit information for the Pennsylvania in 2015 was retrieved from the PADEP (Pennsylvania Department of Environmental Protection).

Well locations retrieved from permit information were used to determine the density of unconventional NG wells within 2.5 km of the sampling track for all of the sampling locations in NE PA and SW PA. Figure 4.7 shows the cumulative frequency of the unconventional well density when the sampling location was at least within 2.5 km of 1 well for SW PA and NE PA in 2012 and 2015. Based on Figure 4.7 it is apparent that measurements in SW PA (2012) and NE PA in 2015 were taken in locations with more even distributions of well density compared to NE PA in 2012. While areas with the largest densities of unconventional wells (>4.0 $km^{-2}$) were sampled in NE PA in 2012 the density range was not well distributed and nearly 75% of the sampling locations were within 2.5 km of ~20 (1 $km^{-2}$) unconventional wells.

The disparity in distributions of unconventional well density observed between the 2012 and 2015 sampling tracks may be responsible for the lower methane local-background concentrations estimated in NE PA in 2012 compared to the other sampling campaigns. However, when the methane local-scale background for each study area is plotted against unconventional well density there does not appear to be any relationship between well density and increasing mole fractions (Figure 4.8). Notably, local-scale background methane does not increase when comparing low

well density areas (≤ 0.5 km$^{-2}$) to high well density areas (≥ 2.5 km) in any study region from our sampling data. The results are contradictory to findings by Swarthout et al. (Swarthout et al., 2015) who observed increased methane mole fractions in areas with more unconventional wells. The data does however illustrate increased methane mole fractions in areas with unconventional well densities ranging from 0.5 to 1.5 km$^{-2}$ in SW PA. The increased methane mole fractions in mid-range density areas in SP WA suggest that factors other than well area density likely affected local-background concentrations in the Marcellus regions.

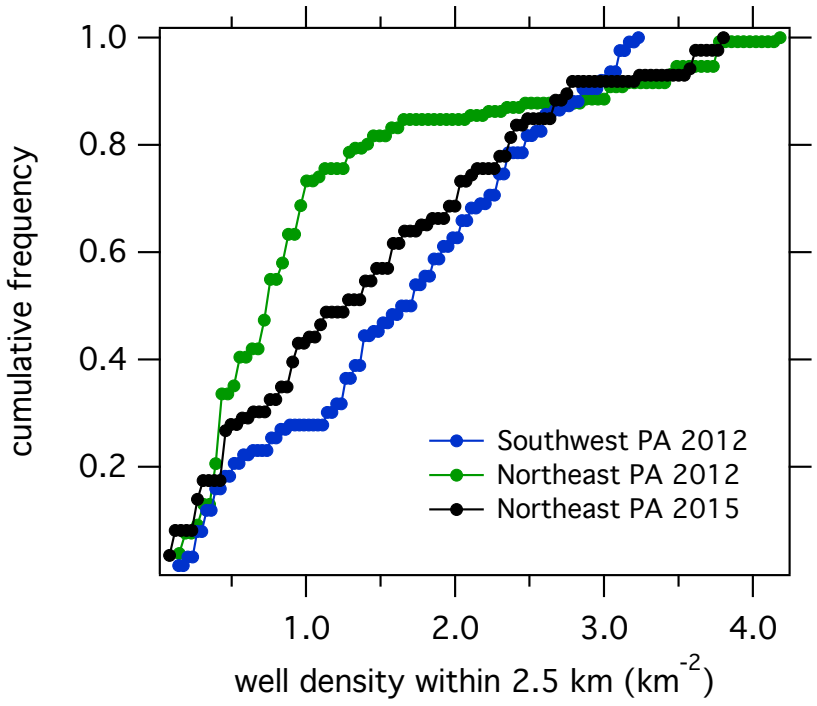


**Figure 4.7. Cumulative Frequency of Observed Unconventional Well Density**
Cumulative frequency of unconventional well density (km$^{-2}$) within 2.5 km of the sampling locations with more than 1 well within 2.5 km in Southwestern PA (blue), Northeastern PA in 2012, (green), and Northeastern PA in 2015 (black)

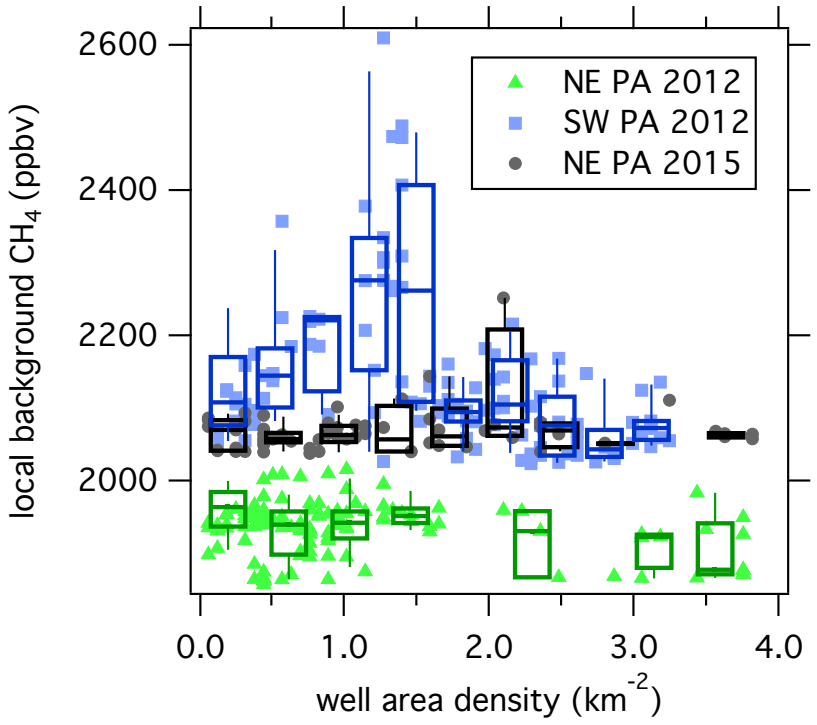


**Figure 4.8. Correlation of the Methane Local-scale Background to Well Area Density**
Scatter plot of methane local-scale background estimates for NE PA and SW PA versus the unconventional well area density within 2.5km of each sampling location. Box and whisker plots ($10^{th}$, $25^{th}$, $50^{th}$, $75^{th}$, $90^{th}$ percentiles) are used to approximate trends within 10 well density bins. Any bin containing less than 3 data points is not included as a box and whisker.

Similar results were observed when comparing the local-scale background estimates for ethane to unconventional well density in SW PA (Figure 4.9). The primary source of ethane in the atmosphere is emissions from fossil fuel activities (e.g. natural gas leaks from production, transmission and processing) (Simpson et al., 2012). Because natural gas production is a major source of ethane, the elevated methane in mid-range well density areas in SW PA was most likely due to NG sources and not other sources of methane emission (e.g. biological and combustion). Since we do not observe a relationship between the background mole fractions of methane and ethane and well area density, the elevated mole fractions observed throughout the study may be due to emissions from other natural gas infrastructure (e.g. compressor stations, processing plants, pipelines) or due to atypically large emissions rates of NG from a few wells commonly called "super-emitters".

Recent attention has been given to the prevalence of super-emitters, or NG production sites that account for the majority of emissions in an area (Zavala-Araiza et al., 2015a;Yacovitch et al., 2015). Evidence of super-emitters or large emissions from other natural gas infrastructure is seen when investigating the relationship between the

background mole fractions of methane in SW PA and the production rate of unconventional wells in the area (Figure 4.10). Natural gas production rates of actively producing unconventional wells from June through December of 2012 were obtained from the PADEP (PA Departement of Environmental Protection, 2012). If the leak rates of NG corresponded to production at a site there would likely be an observable relationship between production and local-scale background concentrations of methane in an area. However, based on Figure 4.10 it is clear that background methane does not have a clear relationship with the mean NG production rates of actively producing wells within 2.5 km of the sampling locations. Additionally, some of the largest methane background estimates were in locations with low NG production rates and low well density. While the above results provide inferences to major NG emission sources in the Marcellus region, further ambient observations combined with emission rate measurements are needed to evaluate the role of super-emitters and their impact on emission inventories in the region.

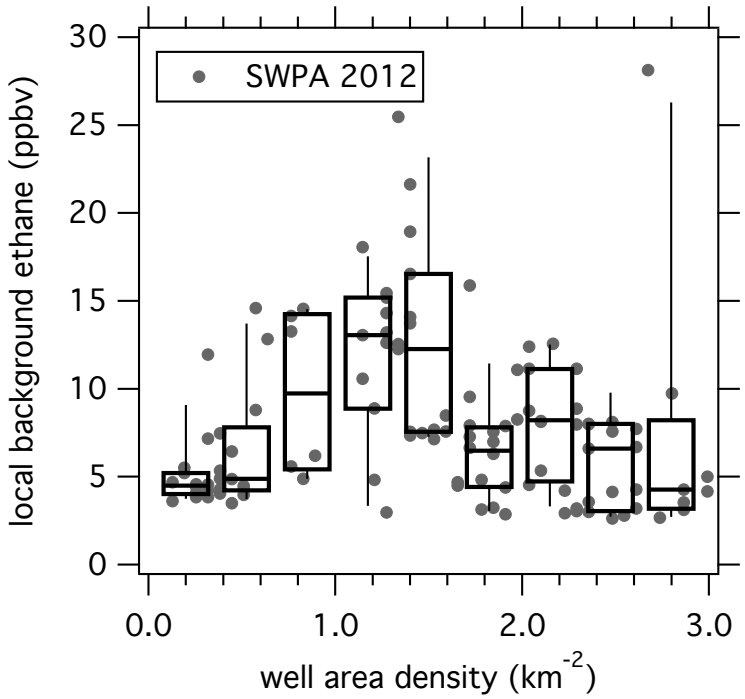


**Figure 4.9. Correlation of the Ethane Local-scale Background to Well Area Density**
Scatter plot of local-scale background mole fractions ethane in SW versus the unconventional well area density within 2.5km of each sampling location. Box and whisker plots ($10^{th}$, $25^{th}$, $50^{th}$, $75^{th}$, $90^{th}$ percentiles) are used to approximate trends within 10 well density bins. Any bin containing less than 3 data points is not included as a box and whisker.

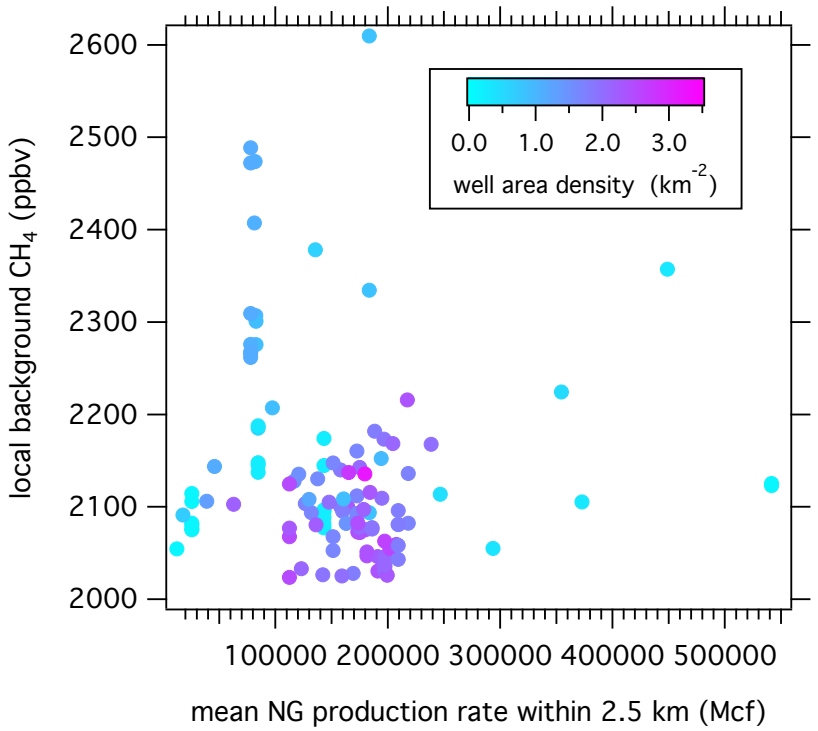


**Figure 4.10. Methane Local-scale Background to Mean Natural Gas Production Rates**
Scatter plot of local-scale background mole fractions of methane in SW PA versus the mean production rate of NG (Mcf) from July to December of 2012 of wells within 2.5 km of the sampling locations. The markers are colored by the well area density within the same sampling locations.

## 4.5 Characteristics of Natural Gas Emissions

Molar enhancement ratios of ethane to methane have been used in the past for methane source identification and to characterize NG composition (Yacovitch et al., 2014;Yacovitch et al., 2015;Goetz et al., 2015). Yacovitch et al. (2014), found that methane emissions attributed to biogenic sources (e.g. landfills, wastewater treatment, ruminants) are only associated with very low levels of ethane (<0.2%) and that sources from NG production and distribution had emission ratios ranging from 1% to >30% depending on the source of the NG emissions. Using this standard, methane enhancements observed in this study are investigated to determine sources and spatial characteristics of NG emissions in parts Marcellus Shale region.

The ethane to methane enhancement ratio (Δppbv/Δppbv) of plumes encountered throughout SW PA was determined by subtracting the continuous local-background estimates from the enhancements encountered throughout SW PA during within the same time interval. The 1-Hz measurements of the encountered emissions are plotted in

Figure 4.11. Emissions from biogenic sources were assumed to have molar ratios <0.01 and NG emissions were attributed to any emissions with ethane to methane enhancement ratios greater than 0.01. Any enhancement of methane due to a combustion source was removed by using CO emissions as a combustion tracer. Based on Figure 4.11, it is clear that methane attributed to NG was observed with a large distribution of ethane enhancements and that molar emission ratios ranged from ~0.01 to >0.40. The wide distribution of emission ratios suggests that a variety of NG emissions sources were sampled while surveying in SW PA, that there is spatial variability in NG composition, or the combination of the two possibilities. Although a wide distribution of enhancement ratios were observed only 28% of the observations were found to have ratios greater than 0.055, indicating that raw dry-gas or pipeline grade NG emissions were prevalent in SW PA (Yacovitch et al., 2014). In other work, large ethane to methane enhancement ratios have been observed from wet-gas (>0.06) NG wells, NG processing plants (>0.30), and chemical feedstock facilities (Yacovitch, 2014). Additionally, Goetz et al. (2015) observed molar ratio enhancements >0.85 from suspected condensate tank flashing emissions at one investigated well pad. The enhancement ratios above 0.06 demonstrate that emissions from wet-gas or NG processing was observed by the AML.

We find that the majority of large enhancements from NG encountered in SW PA with ethane to methane molar ratios above 0.05 were located in subregion 1, located in Washington County, PA (Figure 4.12b). Additionally, ~65% of the enhancements due to NG emissions in subregion 1 had ethane to methane ratios above 0.06. In subregions 2 and 3 it was determined that <10% of the enhancements encountered were found to have molar emission ratios greater than 0.06. Though subregion 2 was observed to have larger enhancements of both ethane and methane than subregion 3 and the large enhancements were found to have ratios of ~0.025 (Figure 4.12b). The low frequency of molar enhancements above 0.06 in subregions 2 and 3 indicate that the areas predominately emit dry-gas or pipeline quality NG. However, the major source of the low ethane NG is unknown.

The contrast in ethane to methane enhancement ratios between subregion 1(high ethane to methane ratios) and the other subregions indicate that the sources of NG emissions or the composition of produced NG is not homogenous throughout SW PA. Further evidence of this is illustrated with well production data from the same time period that highlights that the high condensate (natural gas liquids) producing wells are located in subregion 1, whereas subregions 2 and 3 produced little or no NG liquids (Figure 12a) (PA Departement of Environmental Protection, 2012). Therefore, the high ethane to methane enhancement ratios observed in SW PA by the AML were due to emissions in a wet-gas producing sub-section of the region. Because ethane and other light alkanes contained in the wet-gas are known to contribute more strongly to photochemical ozone production, areas in the Marcellus Shale basin known to contain wet-gas like, subregion 1 in Washington County PA, should be considered to be more at risk for ozone events than other parts of the basin. The above results demonstrate that ground-based mobile sampling is an effective tool for

characterizing the spatial distribution of natural gas emissions. Further air quality monitoring and modeling inside and outside of wet-gas producing areas of the Marcellus basin is needed to assess the influence of wet-gas and NG liquids production on ozone production in the region.

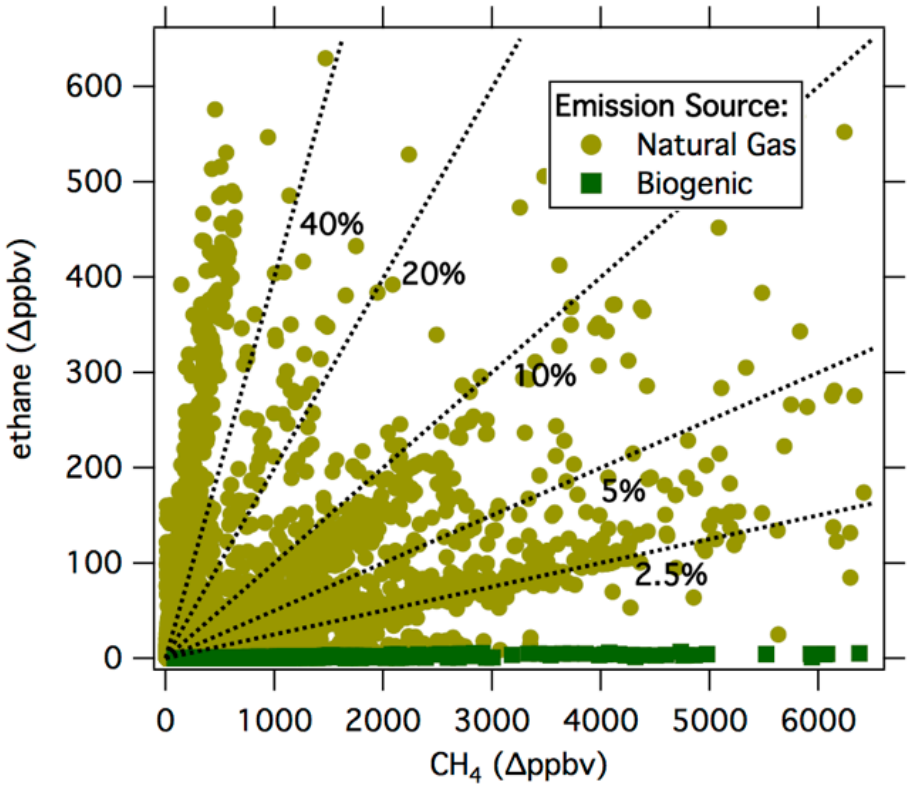


**Figure 4.11. Correlation of Excess Ethane to Excess Methane in SW PA**
Scatter plot of 1-Hz molar enhancements (Δppb) of ethane and methane attributed to biogenic (green) and natural gas sources (gold). Enhancement ratios are displayed as dotted lines.

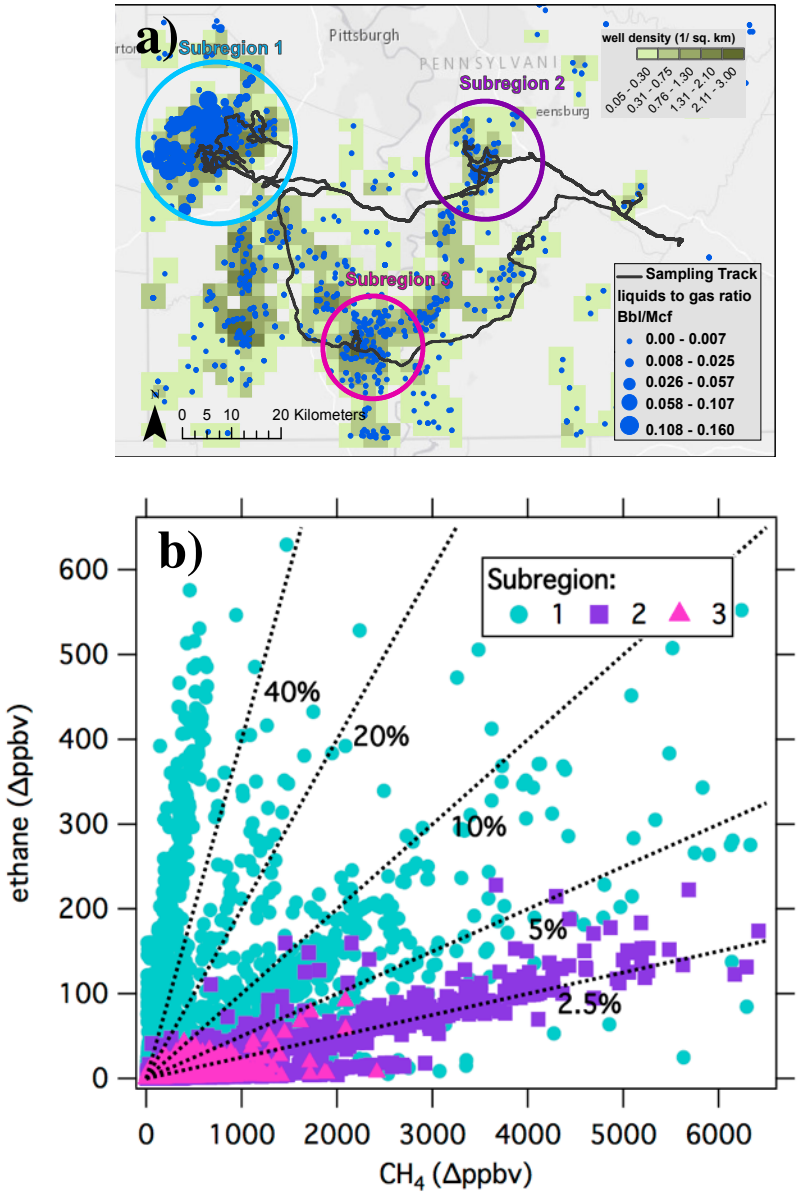


**Figure 4.12. Correlation of Excess Ethane and Excess Methane by Subregion**
a) map of Southwestern PA study are with the sample track (black trace) and Marcellus Shale well locations (blue markers) displayed. The well locations are sized by the condensate liquids production (barrel) to the natural gas production (million cubic feet) ratio (Bbl/Mcf). Well area density is displayed in green. b) Scatter plot of 1-Hz molar enhancements (Δppb) of ethane and methane attributed divided into three major spatial sub-regions. Enhancement ratios are displayed as dotted lines.

## 4.6 Conclusions

Ground-based mobile monitoring has been used to understand the concentrations and sources of climate relevant pollutants, combustion products, and compounds that have previously been associated with natural gas production and distribution in the Marcellus Shale basin. The mobile datasets from 2012 and 2015 were transformed to remove biases from topography and local unmixed emission sources to generate a dataset that represents local-scale background concentrations. Data from the NOAA SENEX flight over the Marcellus Shale region and literature values were used to make comparisons to other observations and to characterize concentrations observed in this study.

Methane was observed to be at higher concentrations in SW PA than NE PA in 2012 demonstrating that there is spatial variability in methane concentrations across the region. In 2015 methane mole fractions were observed to be ~125 ppbv greater than what was observed in 2012, indicating the background concentrations have likely increased due to increased emissions in the region. However, methane levels were not influenced by well area density or by average production rates at the mobile sampling locations. Methane, ethane, and CO mole fractions were all within urban levels and above estimated mid-latitude Northern Hemispheric backgrounds. Though CO mole fractions were decreased by ~60 ppbv in 2015 compared to 2012 in NE PA. Because the Marcellus Shale region is primarily rural, emissions from Marcellus Shale development may be responsible for the enhanced concentrations in the region. While ethane was found to be elevated in the region, other VOC monitored (i.e. oxygenated VOC and aromatics) did not appear to follow the same trend, with the exception of benzene and acetonitrile in NE PA, which is thought to be due to biomass burning emissions. Methanol and acetone concentrations in 2012 were observed to be at rural levels and the primary source of the compounds was thought to be biogenic emissions and not primary emissions from NG infrastructure or the oxidation of NG. Additionally, the observed toluene to benzene molar ratios in SW PA and NE PA were less than what has been observed in urban air masses and were inferred to be most similar to aged rural air masses, though low toluene to benzene ratios have also been observed in the Uintah Basin.

In addition to being used to understand background concentrations the mobile local-background estimated were used as a baseline to characterize ethane and methane enhancements observed in SW PA. It was determined that methane enhancements due to NG in SW PA were found with a large distribution of ethane enhancements indicating that differing emission sources or NG composition exists in the region. However, the majority of the NG emissions (72%) were found to have ethane to methane molar enhancement ratios similar to dry-gas. An analysis of three subregions in SW PA determined that wet-gas like emissions almost exclusively found in an area of Washington County, PA.

Overall the ground-based mobile monitoring was found to be useful tool for understanding ambient concentrations and emissions of relevant atmospheric pollutants during the early phases of NG development in the

Marcellus Shale region. Future ambient monitoring is needed to understand how ambient concentrations change as the shale play increases in NG production and the construction of new wells declines. Additional monitoring is also needed to understand the potential impact of aging NG production and distribution infrastructure as Marcellus Shale production matures.

# Chapter 5: Speciated Emission Factors and AMS Mass Spectral Profiles of South Asian Combustion Sources

## 5.1 Relevance and status

This chapter contains recent work from the collaborative Nepal Ambient Monitoring and Source Testing Experiment (NAMaSTE) that investigated trace gas and aerosols emissions from under characterized combustion sources found in urban and rural Nepal and investigated ambient air quality in Kathmandu in April of 2015. This work focuses on emission measurements made with fast response aerosol instrumentation and supporting trace gas instrumentation. The work demonstrates how ground-based mobile monitoring in a portable application can be used to quantify emissions from difficult to monitor combustion sources under typical, and out of lab, operating conditions. A manuscript has been finalized based on work from this chapter and is out to co-authors for review. The manuscript will likely be published in Atmospheric Chemistry and Physics and has the following citation:

> Goetz, J. D., Giordano, M. R., Stockwell, C. E., Christian, T. J., Maharjan, R., Adhikari, S., Bhave, P. V., Praveen, P. S., Panday, A. K., Jayarathne, T., Stone, E. A., Yokelson, R. J., and DeCarlo, P. F.: Speciated On-line PM1 from South Asian Combustion Sources: Part I, Fuel-based Emission Factors and Size Distributions, in manuscript, 2017.

## 5.2 Background and Motivation

South Asia is a culturally and geographically diverse region that is inhabited by nearly 25% of the world's population (United Nations, 2014). Although rapid urbanization is occurring throughout South Asia (Ellis and Roberts, 2016), much of the population lives in rural areas with limited access to public utilities (Palit and Chaurey, 2011;Bhattacharyya, 2007). Because of limited or inconsistent utility supplies, solid biofuels (e.g. wood, charcoal, agricultural residue, dung) are readily used in the region for residential cooking and heating and often in the indoor environment (Winijkul and Bond, 2016;Streets et al., 2003;Pandey et al., 2014;World Health Organization, 2006). Biofuels are also used throughout South Asia in the industrial sector for brick making, in agriculture, and other activities (Pandey et al., 2014). Because of the atmospheric emissions from the combustion of solid fuels, heavy biofuel use in South Asia has air quality implications that range from indoor exposure (Chen et al., 1990) to regional outflow (Lawrence and Lelieveld, 2010) and leads to uncertain climate forcing impacts (Ramanathan et al., 2005;Venkataraman et al., 2005). In addition to biofuel, solid and liquid fossil fuel combustion from on-road vehicles, generators, diesel pumps, brick kilns, and coal-fired power generation are important sources of trace gas and aerosol emission sources in the region (Lawrence and Lelieveld, 2010;Pandey et al., 2014;Reddy and Venkataraman, 2002).

The combustion of solid fuels (e.g. biomass and coal) is often inefficient and has been observed to emit varying and often harmful levels of aerosols and trace gases. Fine aerosol emissions ($PM_{2.5}$) from solid fuel burning contain organic compounds, black carbon (BC), inorganic compounds ($SO_4$, $NO_3$, Cl), and trace metals (Sheesley et al., 2003;Shahid et al., 2015;Roden et al., 2009;Kortelainen et al., 2015;Jayarathne et al., 2017;Bruns et al., 2015). Additionally, aerosol emissions from solid fuels like wood, dung, crop residue, and coal have been observed to contain polycyclic aromatic hydrocarbons (PAHs), which are known carcinogens (Sheesley et al., 2003;Jayarathne et al., 2017;Bruns et al., 2015;Chen et al., 2005). Gaseous emissions from solid fuel burning include organic compounds like carbon dioxide ($CO_2$), carbon monoxide (CO), methane ($CH_4$), and non-methane hydrocarbons (NMHC), and other compounds such as nitrogen oxides ($NO_x$) and inorganic acids (Stockwell et al., 2014;Stockwell et al., 2015;Stockwell et al., 2016). In the indoor environment the use of solid fuels for cooking and heating leads to high levels of exposure to the above mentioned aerosols and trace gases (Chen et al., 1990) and poor indoor air quality from solid fuel burning is one of the leading factors that contribute to the global burden of disease (Fullerton et al., 2008;Chafe et al., 2014;Agrawal and Yamamoto, 2015;World Health Organization, 2006). In South Asia, Lim et al. (2012) ranked household air pollution from solid fuel burning as the primary risk factor for populations in the region. The health impacts from poor indoor air quality due to solid fuel combustion demonstrates the importance of understanding emissions to quantify and potentially mitigate exposure.

On the local and regional scale, solid biofuel burning and fossil fuel combustion as well as other sources like open garbage burning and mineral dust have led to significant air quality impacts in South Asia. For example, many cities in India have been observed to have large exceedances of the U.S. National Ambient Air Quality Standards (NAAQS) for $PM_{10}$ (aerosol <10 $\mu$m) and nitrogen dioxide ($NO_2$) (Guttikunda and Goel, 2013;Guttikunda et al., 2014). In the Kathmandu Valley in Nepal, emissions of $PM_{10}$, volatile organic compounds (VOCs), and other pollutants from the above-mentioned combustion sources combined with topography induced entrapment has led to poor air quality in the area (Panday and Prinn, 2009;Sarkar et al., 2016) and the formation of secondary pollution like ozone ($O_3$) (Putero et al., 2015). On a broader scale, the densely populated Indo-Gangetic Plain region is known for the generation of atmospheric brown clouds that are formed from the confinement of persistent anthropogenic aerosol emissions by reduced vertical mixing that is due to wintertime boundary layer dynamics (Gautam et al., 2007;Nair et al., 2007). Outflow of wintertime atmospheric brown cloud formations has atmospheric impacts on South Asia and regions downwind (Gustafsson et al., 2009;Ramanathan et al., 2005). Lelieveld et al. (2001) found that winter monsoonal outflow from South Asia affects air quality in an area of 10 million $km^2$. Additionally, there is evidence that aerosol outflow from South Asia impacts regional climate from direct and indirect radiative forcing, which is thought to lead to

stabilization of the troposphere, changing monsoonal patterns, and retreat of Himalayan glaciers (Lawrence and Lelieveld, 2010).

Regional emission inventories have shown that South Asia is responsible for a large portion of the aerosol emissions from the Asian continent and that regional emissions have been increasing. For example, Ohara et al. (2007) found that South Asia was responsible for nearly 48% of Asian organic aerosol emissions and 38% of the BC emissions in the year 2000. Kurokawa et al. (2013) found that $PM_{2.5}$ emissions increased by 40% and 30% from 2000 to 2008, for India and other parts of South Asia, respectively. Although aerosol emission from South Asia are known to be prevalent compared to other parts of Asia, the role that biofuels and fossil fuel emissions play on aerosol loading in the region remains uncertain. One of the early Asian emissions inventories, Streets et al. (2003), found that of the regions in Asia, BC and organic aerosol emissions from South Asia had the highest percentage of uncertainty and that the uncertainty derives from unknowns about biomass burning (e.g. biofuels and agricultural residue burning) emissions and liquid fuels consumption in the region. The unknowns in solid biofuel emissions in South Asia have produced significant differences between bottom-up and top-down estimates of BC in the region as well as differences between emission inventories that weigh the relative contribution of biomass burning and fossil fuel combustion to BC emissions in the region (Lawrence and Lelieveld, 2010). Uncertainty concerning biofuel emissions is largely due to the fact that emission sources that are prevalent in South Asia are not well characterized, both chemically and by quantity.

The above background reveals that aerosol emissions from biofuel and fossil fuel combustion associated with prevailing sources in South Asia need to be further investigated. Better characterizing aerosol emission from South Asian combustion sources can aid in understanding the impacts of residential exposure, provide key insights for local and regional air quality management, and constrain uncertainty about climate impacts. The goal of this study is to investigate aerosol emissions from prevalent emission sources found in South Asia and to provide some regional context for emission inventories. This study will focus on speciated submicron aerosol ($PM_1$) emission factors and size distributions of primary aerosol emissions measured during the Nepal Ambient Monitoring and Source Testing Experiment (NAMaSTE) that took place in Nepal in 2015.

## 5.3 Methods

The NAMaSTE took place in April 2015 in and around the urbanized Kathmandu Valley, in the Dhading District in Central Nepal, and in the rural Teria region of Southern Nepal, which is part of the Indo-Gangetic plains. As the name of the experiment suggests, NAMaSTE had two major components: (1) ambient monitoring of aerosol and trace gases in the Kathmandu Valley and (2) characterization of aerosol and gas-phase emissions from sources that are prevalent in South Asia. This work is part of emissions testing portion of NAMaSTE with in-the-field on-line $PM_1$

measurements of emission sources. A list of the investigated emissions sources can be found in Table 1. Detailed descriptions of the investigated sources can be found in the companion paper Stockwell et al. (2016). Additional source sampling was planned, but the campaign was cut short by the Nepal Gorka earthquake that occurred on April 25 2015. It should be noted that although the sample number is limited, and duplicate tests were not performed for many of the emission sources, this work provides critical real-world observations to the limited body of literature that is primarily comprised of laboratory measurements.

**Table 5.1. Emission Sources, Type, Location, and Fuel type of NAMaSTE Sites**

| Emission Source | Source Type | Location | Fuel Type[a] | Samples[b] |
|---|---|---|---|---|
| **Brick Kilns** | Forced-draft Zigzag | Dhading District | Coal (Baggase) | 1 |
| | Batch Style Clamp | Kathmandu Valley | Coal (Sawdust and HW) | 1 |
| **Motorcycles** | 4-stroke – idling | Kathmandu Valley | Gasoline | 4 |
| **Pumpset** | Irrigation | Tarai Region | Diesel | 2 |
| **Cookstoves** | 1-Pot Mudstove | Tarai Region, RETS | HW, Sticks, Dung | 3(3) |
| | 2-Pot Mudstove | Tarai Region | HW and Dung | 1 |
| | Chimney Stove | RETS | HW, Sticks, Dung | (3) |
| | Natural Draft Stove | RETS | HW, Dung | (2) |
| | Forced-draft Stove | RETS | Charcoal, HW | (2) |
| | Biolite Stove | RETS | Charcoal Briquettes | (1) |
| | Bhuse Chulo | RETS | Sawdust | (1) |
| | Biogas | RETS | Biogas | (1) |
| | 3-stone Cooking Fire | RETS | HW, Sticks, Dung | (3) |
| **Open Garbage Burning** | Mixed Garbage | Kathmandu, Tarai Region | | 2 |
| | Metalized Plastic | Kathmandu Valley | | 1 |
| | Plastic | Kathmandu Valley | | 1 |
| **Agricultural Residue Burning** | Mixed[c] | Tarai Region | | 1 |
| | Wheat straw | Tarai Region | | 1 |
| | Grass | Tarai Region | | 1 |
| | Mustard | Tarai Region | | 1 |

Note: 'RETS' is the Nepal Renewable Energy Test Station cookstove lab.
a. primary fuel (secondary or starter fuel)
b. field sample (RETS lab sample)
c. rice, wheat, mustard, lentil, grasses

### 5.3.1 Experimental Setup

Source measurements were performed by directly sampling the exhaust plume from each source with an attempt to sample at an adequate distance from the point of emissions (typically > 1 m) and outside of the center of the plume to collect cooled and dilute emissions. Emissions were sampled in a well-mixed condition instead of directly from the point of emissions in order to obtain end state gas-particle partitioning of an emission plume, and for cookstoves, to simulate indoor ambient exposure. For example, in residences with cookstoves, sampling took place at the far end of a room or by sampling from the open eave of a building. Sample air was collected through ¼" copper tubing of varying length between 1 to 5 meters, which depended on site accessibility, that was connected to an on-line aerosol and gas sampling system. The longest inlet length was implemented at the forced-draft zigzag kiln to collect emissions from downwind of a >10 meter tall stack. The on-line sampling system was either setup in the bed of the truck that transported the equipment or was setup in a safe location nearby the emission source. The system was powered using a gasoline generator, which was placed downwind of the emission source in each experiment typically at a distance of ~15 m.

The on-line sampling system was made up of two major components, the undiluted flow system and the diluted flow system (Fig. 5.1). The undiluted flow system contained aerosol-free $CO_2$ monitoring. The diluted flow system was comprised of an inline HEPA filter bypass (for periodic zero calibrations), a Dekati Ltd. Axial Diluter (DAD-100), and a $PM_{2.5}$ cyclone, which fed to on-line aerosol and gas phase instrumentation. Excess flow was controlled with a needle valve and diaphragm pump. The axial diluter was calibrated to provide 15.87 SLPM of dilution air at a pressure of 3500 mbar. All dilution air was obtained from ambient background air outside the plume at each site and filtered to remove aerosols prior to injection in the dilution system. Dilution factors were calculated in the field by monitoring sample and dilution volumetric flow rates and later were verified using molar ratios of $CO_2$ from the undiluted flow systems to $CO_2$ from the diluted flow system. The axial diluter was typically operated at a dilution factor between a range of 1:1 to 1:22, with an average of ~1:10. The large range of dilution factors used in this experiment was due to the varying downwind distance and source strength between the investigated emission sources. Lab experiments conducted after NAMaSTE found that the sampling system has a $PM_1$ transmission rate of 97.6% for ammonium nitrate aerosol. The calculated system transmission rate was for dilution factors from 1:1 to 1:15. Transmission was determined to be independent of the dilution factor for non-volatile aerosol.

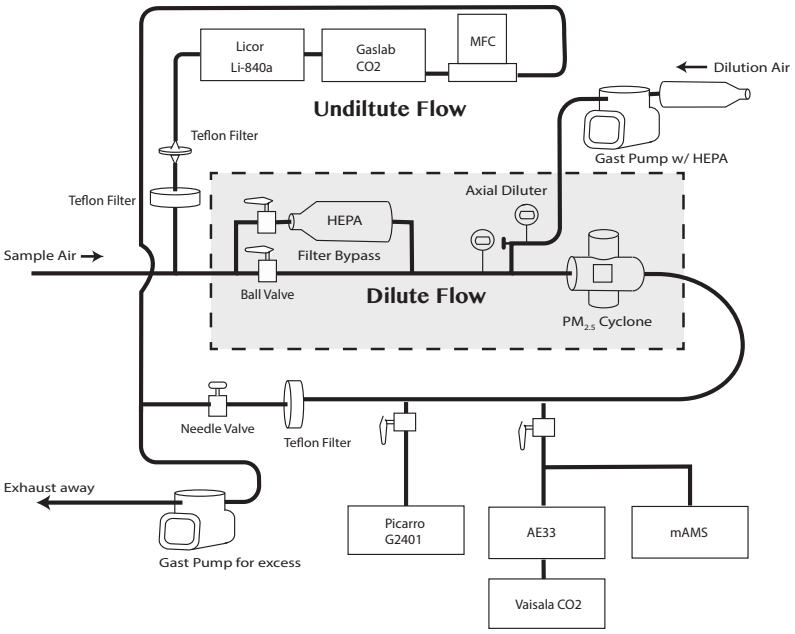


**Figure 5.1. Diagram of the NAMaSTE Real-time Aerosol Sampling Platform**

## 5.3.2 Instrumentation

*mAMS*: Sub-micron non-refractory aerosol (e.g. organics, sulfate, nitrate, chloride, ammonium) mass, composition, and size was measured using a mini Aerosol Mass Spectrometer (mAMS). The mAMS is a version of the Aerodyne Research, Inc. Aerosol Mass Spectrometer that is a functionally similar to the unit mass resolution (UMR) Time-of-Flight-AMS (c-TOF-AMS) (Drewnick et al., 2005), but with a smaller time-of-flight spectrometer and a smaller vacuum chamber with a pump system that utilizes a single split flow turbo molecular pump. The mAMS has the same body, turbo pump system, and time-of-flight mass spectrometer as the Time-Of-Flight Aerosol Chemical Speciation Monitor (TOF-ACSM) (Fröhlich et al., 2013), but contains a chopper system (Jayne et al., 2000) and a more advanced data acquisition card for particle time-of-flight sizing. The mAMS used is this work operates with a pseudo-random multi-slit chopper system (ePTOF) that has increased signal to noise (~50% particle throughput) compared to single slit chopper systems with ~2% throughput, and employs Hadamard Transform for signal inversion (Campuzano Jost, 2014). Because of it's enhanced throughput the ePTOF is ideal for rapidly changing concentrations like those observed with source emissions in this work. It should be noted that although we categorize the aerosol detected by the mAMS as submicron, transmission of aerosol between 1 μm to 2.5 μm through the aerodynamic lens of the instrument does

occur and similar lenses have been characterized to have 2.5 um transmission efficiencies of less than 50% (Zhang et al., 2004).

The mAMS operated in both mass spectrum mode (MS) and particle time-of-flight mode (ePTOF) for the entirety of the source experiments with the exception of several Nepal Renewable Energy Test Station (RETS) laboratory cooking fires in which the chopper system was not operational. The MS and ePTOF sampling alternated every 5 seconds and the data from both modes was saved every 10 seconds for an effective sampling rate of 0.10 Hz. Mass spectra were acquired from 10 m/z to 300 m/z for all data collected.

Ion efficiency calibrations were conducted twice in April while the instrument was in Nepal. Other in-country calibrations of the mAMS were planned, but were not possible because of the Gorka Earthquake. Velocity calibrations were conducted using polystyrene latex spheres (PSLs) after the campaign at the Drexel lab at inlet pressures of 0.76 bar and 1.01 bar. The velocity calibrations were conducted at the above pressures to model particle time-of-flight velocity at the atmospheric pressures observed in the high-altitude Kathmandu Valley and in the Tarai Plains.

All data processing and analysis was done in Igor Pro 6.3 (Wavemetrics, Lake Oswego, OR) using standard TOF-AMS analysis software SQUIRREL v1.57I and PIKA v1.16I. Although the mAMS is an UMR spectrometer, the data was processed using high-resolution peak fitting in the PIKA module to reduce fragmentation table errors due to high organic loading. High-resolution treatment of UMR data has previously been performed by other researchers using the TOF-ACSM (Fröhlich et al., 2013). A collection efficiency of 0.5 was applied to all of the data sets. Test dependent detection limits of the aerosol species measured by the mAMS were calculated from HEPA bypass filter periods, which occurred at least twice per emissions test for a period of 10 minutes each. The detection limits were defined as 3σ of the combined filter periods for each source experiment.

*Aethalometer*: A Magee Scientific AE33 aethalometer was used to measure light absorbing carbonaceous aerosol concentrations. The AE33 is a dual-spot filter based monitor that measures light attenuation by aerosols on a Teflon filter tape at 8 wavelengths (370, 470, 525, 590, 660, 880 and 950 nm) and unlike previous aethalometer models the AE33 allows for real-time filter loading compensation (Drinovec et al., 2015). In this work, attenuation at 880nm was used to measure black carbon mass. Attenuation at 370nm was used to measure ultraviolet absorbing BC (UVBC) which is comprised of black carbon aerosol and light-absorbing organic aerosol. Delta-C, defined as the excess concentration of UVBC above BC measured at 880nm ([Delta-C]=[370nm]-[880nm]), is used as an approximation of light absorbing organic aerosol or "brown carbon". Delta-C has been used in previous work for the source apportionment of organic aerosol from biomass burning (Olson et al., 2015;Wang et al., 2012). Filter periods were used to zero calibrate the instrument. The AE33 operated at a sampling rate of ~1 Hz and was averaged to 0.10 Hz to match

the sampling scheme of the mAMS. Black carbon aerosol measured by the aethalometer in this work was assumed to have diameters <1 μm based on the morphology of fresh biomass burning and fossil fuel emissions observed by other studies (China et al., 2013;Gong et al., 2016;Torvela et al., 2014).

*Gas-phase instrumentation*: Gas phase instrumentation included a Picarro Cavity Ring Down Spectrometer (CRDS) Model G2401, a Licor $CO_2$ and $H_2O$ monitor (Li840A), a Vaisala $CO_2$ monitor (GMP343), and a Gaslab Inc. high range $CO_2$ monitor. The Picarro CRDS was implemented as the primary diluted measurement of $CO_2$, CO, and $CH_4$ while the Vaisala was used as a backup dilution measurement of $CO_2$. The Licor $CO_2$ monitor was used as the primary undiluted $CO_2$ measurement and was used to measure the dilution ratio. The Licor monitor was also implemented as a calibration reference for the other $CO_2$ monitors because $CO_2$ standard calibrations could not be conducted while the instrumentation was in Nepal and the Licor monitor had recently been factory calibrated. Unfortunately, the $CH_4$ and CO measurements also could not be calibrated because of a contaminated calibration standard. However, comparisons to whole air sample measurements taken at similar times reveal that $CH_4$ measured 1% low and that CO measured up to 30% high.

### 5.3.3 Combustion Metrics

For each source experiment time-resolved and test-integrated emission factors (EF) were calculated in units of g per kg of fuel using the carbon mass balance approach proposed Ward (1990). Emission factors for each aerosol species was calculated using Eq. (1), where $\Delta n$ is the excess concentration of aerosol species of interest above the background, $EF_n$ is the emission factor of species $n$ in g $kg^{-1}$ of fuel, $f$ is the carbon mass fraction of the fuel, $\Delta[C]$ is the excess concentration of total carbon above the background.

$$EF_n = f \frac{\Delta n}{\Delta[C]_{CO_2} + \Delta[C]_{CO} + \Delta[C]_{CH_4} + \Delta[C]_{NMHC} + \Delta[C]_{PM}} \qquad 5.1$$

For total excess carbon we assume that carbon emissions from NMHC and aerosols are minor compared to the major gaseous components of emissions, as observed in other studies (Akagi et al., 2011;Stockwell et al., 2016;Stockwell et al., 2015), and therefore only the excess carbon concentrations of $CO_2$, CO, and $CH_4$ are used to calculate EFs. For each fuel the carbon mass fraction was retrieved from Stockwell et al. (2016). In Stockwell et al. (2016) the carbon mass fraction was either measured directly or assumed based on literature values. The $f$ for each fuel can be found in the supporting information in Tables G1-G4.

Another combustion metric used in this work is the modified combustion efficiency (MCE). The modified combustion efficiency assumes that >90% of emissions is comprised of CO and $CO_2$ and that complete combustion generates only $CO_2$. The MCE is defined here as the ratio $\Delta CO_2/(\Delta CO_2+\Delta CO)$. Because the Picarro CRDS measured CO could not be calibrated, MCE values shown in this work are from Fourier transform infrared spectroscopy measurements made by (Stockwell et al., 2016). Time-resolved Picarro CRDS derived MCE values are only used to fill data gaps or as secondary evidence of trends.

Organic carbon (OC) is used to make comparisons to other studies that derive organic carbon (OC) EFs from off-line thermal-optical methods. Because the organic aerosol (OA) mass measured with the mAMS includes organic carbon as well as other elements found in organic compounds (e.g. hydrogen, oxygen, nitrogen, sulfur), OC in this work is estimated based on oxygenation of bulk OA. Assuming oxygen comprises the majority of non-carbon mass of OA, organic fraction of m/z 44 (*f*44) has been found to be a useful approximation of the oxygenated organic mass of aerosol when high-resolution mass spectral elemental analysis is not available (Aiken et al., 2008). Oxygen-to-carbon atomic ratios (O:C) were estimated based on work by Canagaratna et al. (2015) using median *f*44 values from each emission test. Organic aerosol to organic carbon ratios (OA:OC), which is equivalent to organic matter to organic carbon (OM:OC), were determined based on the linear relationship between OA:OC and O:C found Aiken et al. (2008). Median and interquartile values for *f*44, O:C, and OA:OC for each emission source can be found in Table 5.2. It should be noted that the large *f*44 associated with the coal-fired zigzag brick kiln was due to the presence of nitrogen containing organic ions at m/z 44 ($C_2H_6N^+$) and not due to oxygenated organics as discussed in the companion paper Goetz et al. (2017a). Because the O:C of the zigzag kiln emissions cannot be determined based on *f*44, the O:C statistics of the coal-fired clamp brick kiln emissions are used to approximate OC emission factors for the zigzag kiln emissions.

**Table 5.2. *f*44, O:C, and OA:OC of the field-tested emission sources.**

| Emission Source | *f*44 | O:C[a] | OA:OC[b] |
|---|---|---|---|
| Clamp Brick Kiln | 0.009 (0.012) | 0.116 (0.132) | 1.326 (1.347) |
| Zigzag Brick Kiln | 0.167 (0.027) | | |
| Mixed Garbage | 0.015 (0.015) | 0.144 (0.142) | 1.361 (1.359) |
| Metalized Plastic | 0.019 (0.013) | 0.161 (0.133) | 1.383 (1.347) |
| Mixed Plastic | 0.021 (0.013) | 0.170 (0.134) | 1.394 (1.349) |
| Motorcycles | 0.003 (0.004) | 0.092 (0.096) | 1.296 (1.301) |
| Irrigation Pumps | 0.010 (0.009) | 0.120 (0.116) | 1.332 (1.326) |
| Hardwood[c] | 0.032 (0.020) | 0.217 (0.166) | 1.453 (1.389) |
| Sticks and Twigs[c] | 0.024 (0.013) | 0.181 (0.136) | 1.408 (1.352) |
| Dung[c] | 0.015 (0.012) | 0.142 (0.132) | 1.359 (1.346) |
| Dung and Hardwood[d] | 0.024 (0.011) | 0.182 (0.126) | 1.410 (1.339) |
| Agricultural Residues[e] | 0.025 (0.017) | 0.186 (0.152) | 1.414 (1.371) |

a. Based on linear relationship to *f*44 from Canagaratna et al. (2015) (y = 4.31x + 0.079)
b. Based on linear relationship to O:C from Aiken et al. (2008) (y = 1.260x +1.180)
c. Fuel used in single-pot traditional mudstove
d. Fuel used in two-pot traditional mudstove
e. Combined values for mustard, grass, wheat, and mixed residue piles (rice, wheat, mustard, lentil, and grasses)

## 5.4. Results and Discussion

This work presents on-line $PM_1$ fuel-based EFs and size resolved EFs from the field-tested emission sources provided in Table 5.1. Mass spectral profiles and wavelength absorption dependence of aerosol emissions from the investigated combustion sources can be found in Part II of this study (Goetz et al., 2017b). This work compliments other NAMaSTE works that performed measurements simultaneously at the tested emission sources. Stockwell et al. (2016) provides fuel-based EFs of $CO_2$, CO, $CH_4$, trace gases, and analysis of aerosol optical properties. Jayarathne et al. (2017) conducted filter-based $PM_{2.5}$ measurements and gives EFs of organic and elemental carbon, water-soluble organic carbon and inorganic ions, as well as off-line GC-MS analysis of trace organic aerosol components. In addition to providing stand-alone results, the on-line $PM_1$ results derived in this work contribute source specific in situ summary statistics of EFs that give support to the test integrated values of Jayarathne et al. (2017) and allows for comparisons of on-line and off-line aerosol measurement techniques.

A summary of the on-line fuel-based $PM_1$ EFs of the field-tested emission sources can be found in Fig. 5.2. Tabulated EFs including percentiles, average and standard deviation, and test integrated EFs for the field-tested emission sources shown in Table 5.1 can be found in Appendix G. The tables also contain MCE values for each field-tested emission source from (Stockwell et al., 2016) and uncalibrated Picarro CRDS derived MCE values from this work. Emission factors from the cookstoves tested at the RETS laboratory are not included in this work because of poor

venting in the RETS lab that elevated background concentrations and elevated gas phase concentrations to the dilution system, which produced unreliable results. Submicron aerosol, or $PM_1$, was calculated as the sum of the observed aerosol components measured in this study, which included non-refractory species like primary OA, sulfate, nitrate, chloride, and ammonium measured by the mAMS in addition to BC measured by the aethalometer. Polycyclic aromatic hydrocarbons are not included in the sum because they are already included as part of the OA total. Emissions of other refractory aerosol species (e.g. trace metals, mineral dust) and slow vaporizing aerosol species are not included in the $PM_1$ calculation.

The largest $PM_1$ EFs observed in this study were from open garbage burning and the diesel powered irrigation pumps. Plastic burning associated with open garbage burning had a median EF of 13.73 g per kg of fuel. Median EFs ranging from about 3 to 9 g $PM_1$ $kg^{-1}$ were observed from open burning of other refuse (mixed and chip bags) and emissions from the diesel irrigation pumps. Biomass burning emissions from the field-tested cookstoves and agricultural residue burning generally had $PM_1$ EFs between 1 to 2 g $kg^{-1}$ with the exception of dung and hardwood burning in the 2-pot traditional mudstove (3.15 g $kg^{-1}$) and wheat residue burning (3.38 g $kg^{-1}$) (Fig. 5.2). Generally, the $PM_1$ emissions from the above mentioned sources were primarily comprised of OA followed by BC. The coal-fired brick kilns were observed to have similar $PM_1$ EFs to the biofuel burning, but with lower median fractions of OA and BC and significantly larger fractions of sulfate. The lowest EFs were observed from idling motorcycles. It should be noted that the median is considered to be the most representative statistic of the observed EFs because the majority of the emission profiles were not normally distributed. Histograms of the 10 second resolved OA EFs indicate that the emission distributions generally do not have definable distributions and the median often falls in a location where the bulk of the data is found in histogram space (Appendix F). The average and test integrated EFs appear to overestimate the central tendency of the emission profiles.

Mass size distributions of the aerosol species observed by the mAMS were calculated at a range of 30 nm to 2 μm and normalized by the median EF of each emission source to produce size-resolved EFs in mg per g of fuel (Fig. 5.3 and Fig. 5.4 right axis). The size-resolved emission factors were also binned into aerodynamic diameter size cuts common with aerosol impact samplers (32, 56, 100, 180, 320, 560, 1000, 1800 nm) and plotted as stacked bars to produce Lundgren style cumulative size distributions (Kleeman et al., 1999) and normalized by the median non-refractory submicron EF (Fig. 5.3 and Fig. left axis). The Lundgren style plots provide a better understanding of aerosol composition at each size and offers more interpretable results for model inputs compared to the species segregated continuous distributions. The size-resolved results for open garbage burning, agricultural residue burning, and the field measured traditional mudstoves can be found in Fig. 5.3. Size-resolved emission factors of sources primarily associated

with fossil fuel combustion can be found in Fig. 5.4. The following subsections contain a source-type examination of the EF results.

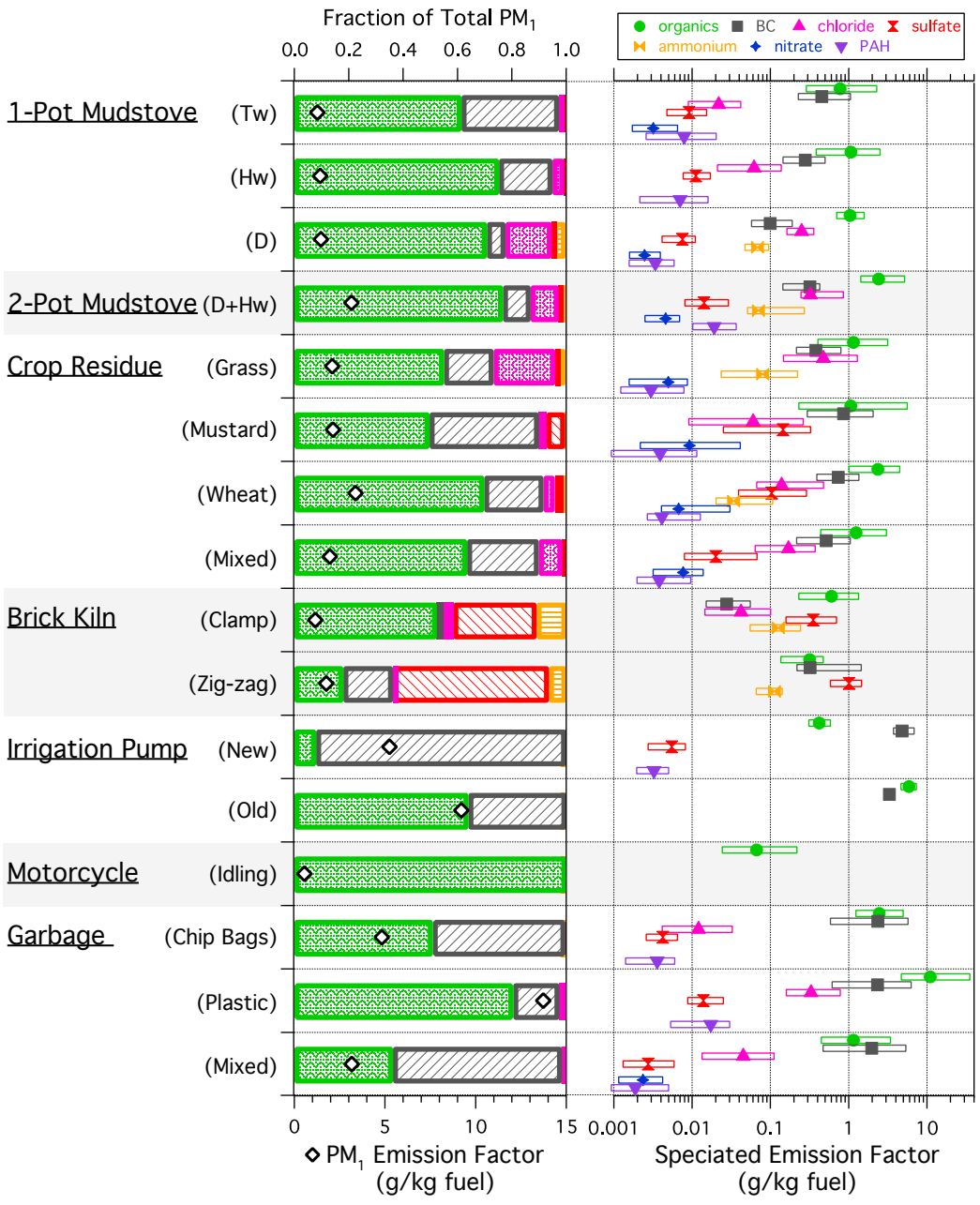


**Figure 5.2 Summary of $PM_1$ Fuel-based Emission Factors**
Compositional fractions of the investigated emission sources are included. The colors of the horizontal bar chart correspond with the species colors designated by markers in the speciated emission factor panel. The markers represent the median and the speciated bars represent the 25th and 75th percentile of the combined emission factor observations for each emission source.

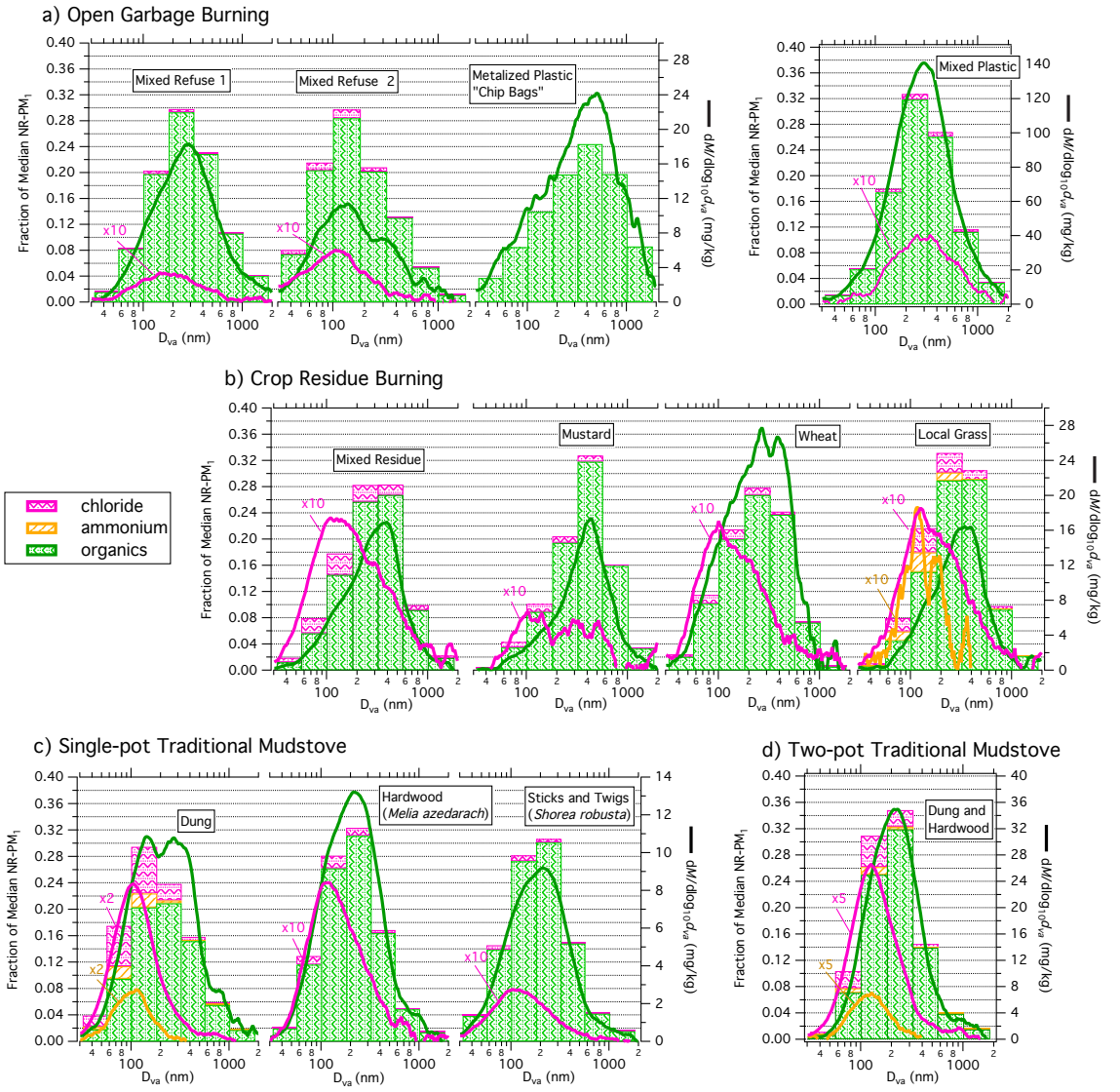


**Figure 5.3. Size-resolved emission factors of Biomass Burning Sources**
(a) open garbage burning, (b) agricultural residue burning, and (c) cooking with a traditional mudstove. All sizes are shown as vacuum aerodynamic diameters. Continuous species specific mass size distributions normalized by the median emission factor are shown as solid lines. Cumulative binned mass size distributions normalized by the total non-refractory submicron aerosol mass ($NR\text{-}PM_1$) are shown as stacked bars. The distributions bins are between 32, 56, 100, 180, 320, 560, 1000, 1800 nm. All sizes are shown as vacuum aerodynamic diameters.

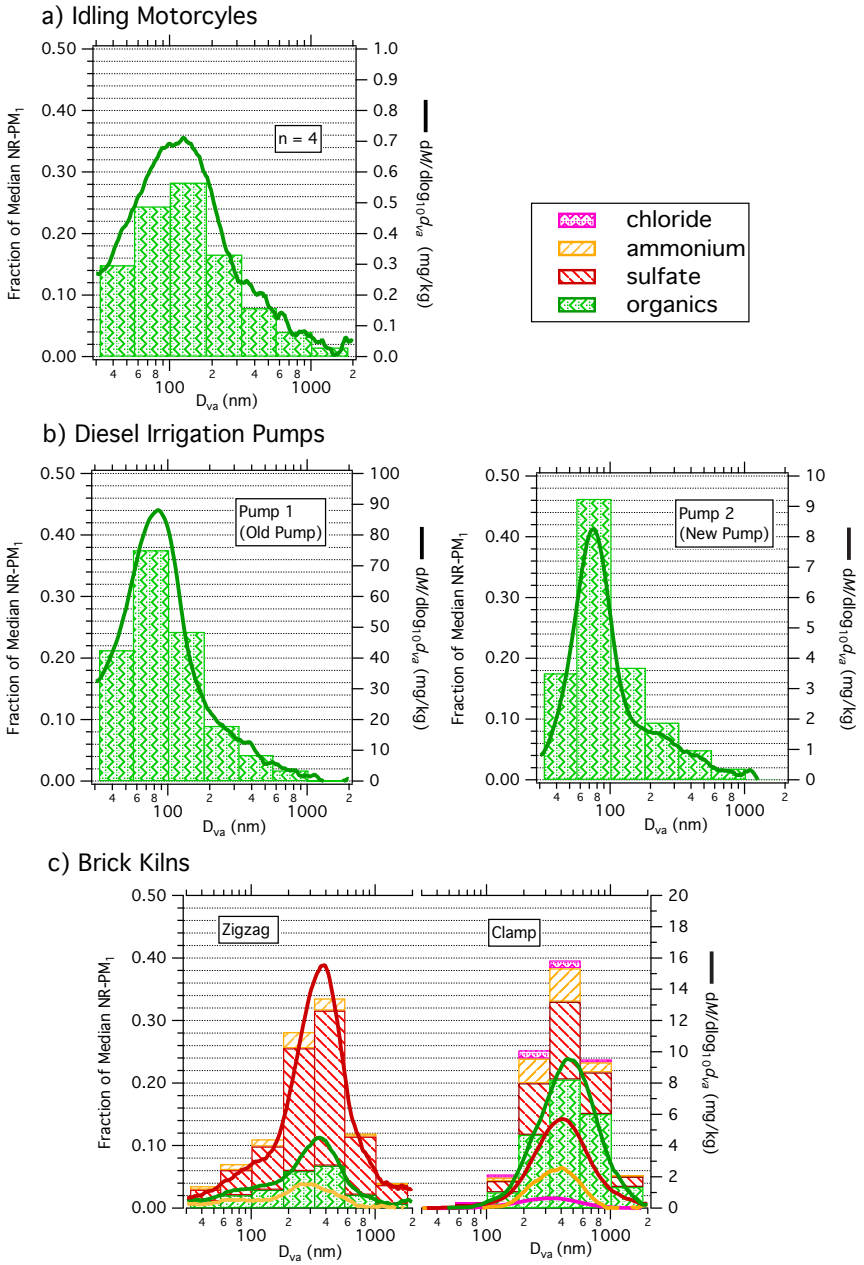


**Figure 5.4. Size-resolved Emission Factors of Fossil Fuel Sources**
(a) idling motorcycles, (b) diesel powered irrigation pumps, and (c) brick kilns. All sizes are shown as vacuum aerodynamic diameters. Continuous species specific mass size distributions are shown as solid lines. Cumulative binned mass size distributions are shown as stacked bars. The distributions bins are 32, 56, 100, 180, 320, 560, 1000, 1800 nm.

### 5.4.1 Open Garbage Burning

The three types of open garbage burning that were tested in NAMaSTE include mixed refuse, plastic, and metalized plastic or "chip bags" (Table 5.1). We sampled mixed refuse emissions in two separate burns and both mixes were comprised of unknown fractions of plastic bags, metalized plastic, food waste, paper, and yard waste that were collected from local sources. Mix 1, which was sourced and burned in the Kathmandu Valley, was slightly damp producing inefficient burn conditions with an average MCE of 0.937 (Stockwell et al., 2016). Mix 2 was residential waste burning sampled in the Tarai Plains and was more efficient than Mix 1 with an average MCE of 0.980 (Stockwell et al., 2016). The two mixes were found to have a combined median $PM_1$ EF of 3.168 g $kg^{-1}$ with an approximate median OA fraction of 0.36 and median BC fraction of 0.62 (Fig. 5.2). Trace aerosol species were found to have median EFs in mg $g^{-1}$ of 45, 3, 2, and 2 for chloride, sulfate, nitrate, and PAHs, respectively. The two mixes differed primarily in BC emissions where Mix 1 had a $PM_1$ EF of 1.815 g $kg^{-1}$ with a BC fraction of 0.10 and Mix 2 had a $PM_1$ EF of 4.699 g $kg^{-1}$ with a BC fraction of 0.77. The mixes were also found to have large variability in emissions with combined $PM_1$ EFs having a $10^{th}$ percentile of 0.174 g $kg^{-1}$ and a $90^{th}$ percentile of 14.557 g $kg^{-1}$ (Table G3). Additionally, the two mixes had distinct OA size distributions with Mix 1 having a lognormal mode vacuum aerodynamic diameter, hereafter named "mode diameter", at 260 nm and Mix 2 having a mode diameter at 145 nm (Fig. 5.3). The variability in emissions between the mixes demonstrates that open garbage burning is a difficult to characterize emission source because of the inherent heterogeneity of residential garbage and because of the uncontrolled nature of open burning.

Open garbage burning is considered to be a globally important source of aerosol pollution, but there has been limited field measurements of open garbage burning EFs (Wiedinmyer et al., 2014). In NAMaSTE the filter-based measurements of Jayarathne et al. (2017) found an organic carbon (OC) EF of 8.42 g $kg^{-1}$ with an error of 0.63 g $kg^{-1}$ for Mix 2. Based on the estimated OA:OC for open garbage burning (1.361; Table 2) the OC EF measured by Jayarathne et al. (2017) for Mix 2 was about 11 times greater than median on-line EF measured in this work. Off-line measurements of the damp garbage burning (Mix 1) produced an estimated OC ER ~50 times greater than the online OC EF estimated in this work. Measurements of open burning of landfills in Mexico reported OM ranging from 3.6 g $kg^{-1}$ to 14.0 g $kg^{-1}$ with an average of 5.27 g $kg^{-1}$ (Christian et al., 2010). The overlap in variability between the our results and the literature values suggest that differences in the material burned is possibly responsible for the large range of EF values found between studies. Because the size distributions indicate that the OA emission were <1 μm, the large differences between the OA and the $PM_{2.5}$ OC in NAMaSTE are possibly due to differences in gas-particle partitioning of semi-volatile organic compounds resulting from differences in dilution (Lipsky and Robinson, 2006).

Assuming that BC measured by the aethalometer and thermal-optical measurements of elemental carbon (EC) are approximately equivalent, there is good agreement in the observed aerosol emissions from open garbage burning. The NAMaSTE filter-based measurements found an average EC EF of 1.85 g $kg^{-1}$ (Jayarathne et al., 2017). Stockwell et al. (2016) found BC EFs for open garbage burning to be 0.561 g $kg^{-1}$ for Mix 1 and 7.43 g $kg^{-1}$ for Mix 2 using photoacoustic measurements. The similarities between the different BC measurements made in NAMaSTE for garbage burning provide confidence in the BC observations. Furthermore, because of the low volatility of BC the congruent results further suggest that gas-particle partitioning is responsible for the large differences between the off-line and filter-based measurements of organic aerosol.

As seen in Fig. 5.2, the segregated plastic burn was observed to have the largest OA EF of any source investigated (11.047 g $kg^{-1}$) in the study and contained some of the largest EFs for chloride (0.331 g $kg^{-1}$) and PAHs (17 mg $kg^{-1}$). The open plastic burning had a BC EF of 2.335 g $kg^{-1}$ and a sulfate EF of 0.221 g $kg^{-1}$ (Fig. 5.2). The OA emissions were observed to have a size distribution with a lognormal mode diameter of 280 nm (Fig. 5.3).

The metalized plastic burning was observed to have a median $PM_1$ EF of 4.827 g $kg^{-1}$ and was comprised of 51% OA and 49% BC, with nominal quantities of inorganic aerosol and PAH (Fig. 5.2). The relatively large fraction of BC observed with metalized plastic burning compared to other garbage burning tests is likely due to the efficient burn conditions (MCE = 0.989), but differences in chemical composition cannot be discounted. Unlike the other open garbage burning tests there were relatively low emissions of particulate chloride and Stockwell et al. (2016) did not observe gas-phase hydrogen chloride (HCl) above detection limits. The size distribution of the metalized plastic emissions had the largest mode of the sampled open garbage burning with a diameter of 380 nm and large fraction of aerosol with diameters greater than 560 nm (~28%; Fig. 5.3).

Chloride in the form a gaseous HCl and water soluble particulate Cl has been observed from open garbage burning in Mexico and has been attributed to the combustion of polyvinyl chloride (PVC) plastic (Christian et al., 2010). The high levels of chloride observed in the plastic burning emissions and mixed refuse emissions that were not observed with metalized plastic burning is therefore likely from the combustion of PVC plastic. Analysis of average mass spectra from open garbage burning indicates that the non-refractory chloride measured by the mAMS was between 80-85% particle phase HCl. A comparison with undiluted gas phase EFs from Stockwell et al. (2016) shows that the particle phase HCl was 1.2%, 2.5%, and 0.4% the extent of gas phase HCl emission factor for Mix 1, Mix 2, and plastic burning, respectively. The low quantity of particle phase chloride under dilute conditions compared to gas phase HCl under less dilute conditions suggests that condensation of HCl in fresh open garbage burning emissions is minor.

### 5.4.2 Engine Exhaust

Sampling of engine exhaust from idling motorcycles and diesel powered ground water crop irrigation pumps took place during NAMaSTE (Table 5.1). Testing of gas and diesel generators also took place during the campaign (Jayarathne et al., 2017;Stockwell et al., 2016), but the generators were not sampled by the on-line sampling system used in this work. Two ~5 kVA irrigation pumps were sampled including a Kirloskar (model unknown) that had been in operation for 3 years and a Field Marshall model R170a that had been purchased within three months of the emissions test. The older pump (Pump 1) was observed to have a median $PM_1$ EF of 9.212 g $kg^{-1}$ with an OA fraction of 0.64 and a BC fraction of 0.36 (Fig. 5.2). Inorganic aerosol was not observed from Pump 1. The median organic mass distribution of Pump 1 had a mode diameter of ~80 nm and nearly 38% of the organic emissions were found in the 56 to 100 nm size bin (Fig. 5.4). The newer pump, Pump 2, was observed to have a lower $PM_1$ EF than Pump 1 with an EF of 5.248 g $kg^{-1}$. Pump 2 emissions had an organic fraction was 0.08, a BC fraction of 0.92, and a nominal fraction of sulfate (Fig. 5.2). Additionally, Pump 2 had the largest BC EF of any of the emission sources investigated in this study (median = 4.823 g $kg^{-1}$). The Pump 2 organic size distribution indicates that the Pump 2 organic emissions were similar to Pump 1 (mode diameter = 75 nm), but with a larger fraction of aerosol found in the 56 nm bin (Fig. 5.4). Emissions of PAHs were observed from Pump 2 with an EF of 3 mg $kg^{-1}$ and were not observed from Pump 1. The PAH EF from Pump 2 was approximately equivalent to EFs that have previously been observed from heavy-duty diesel trucks in the United States (Marr et al., 1999). Stockwell et al. (2016) found that Pump 1 and Pump 2 had an MCE of 0.987 and 0.996, respectively. Because the diesel fuel used by the irrigation pumps was likely sourced from the same location, and therefore was similar in composition, the large differences observed between the investigated pumps were likely due to differences in efficiency induced by operational age or by model.

The filter-based measurements of Jayarathne et al. (2017) observed similar organic emission factors with an average OM EF of 7.01 g $kg^{-1}$, but measured significantly lower EC compared to the BC EFs in this work. Stockwell et al. (2016) estimated similar BC EFs with 405 nm photoacoustic measurements but did not observe the same increase in BC with Pump 2 and in fact observed a 13% decrease in BC between Pump 1 and Pump 2. The FTIR measurements, however, did observe a decrease in gas phase organics between from Pump 1 to Pump 2 and there was a 200% increase in nitric oxide (NO) between the two pumps (Stockwell et al., 2016). The decreased OA EF combined with elevated MCE and elevated emission factors of NO, BC, and PAHs associated with the newer irrigation pump suggests that the air quality and climate impacts of irrigation pumps can likely change over the lifetime of a pump. Additionally, the complex differences between the three NAMaSTE measurements of black carbon highlight how differences in methodology can produce unaccountable differences in measured emissions factors. To our knowledge NAMaSTE is the first to characterize emissions from diesel powered irrigations pumps. Although there is uncertainty in the extent of

black carbon emissions, the large $PM_1$ emission factors associated with the tested pumps suggest that ground water pumping for irrigation could be an important source of aerosol pollution in South Asia.

Four idling gasoline powered 4-stroke motorcycles were sampled in this study. Sampling included 2 Honda CBZs, a Bajaj Pulsar, and a Bajaj Discover. The vehicles were sampled directly after servicing. Pre and post service sampling of idling motorcycles was part of NAMaSTE sampling plan, but the mAMS was not operational for the pre-service period of the experiment. Information about the reduction of aerosol and gas phase emissions resulting from servicing can be found in the NAMaSTE companion papers (Jayarathne et al., 2017;Stockwell et al., 2016). The combined post-servicing results from the four motorcycles investigated this work indicate that organics were the only aerosol component observed above the background. The median OA EF was 0.067 g $kg^{-1}$ with a $10^{th}$ percentile of 10 mg $kg^{-1}$ and a $90^{th}$ percentile of 1.329 g $kg^{-1}$ (Fig. 5.2). The mass size distributions indicate that the mode diameter the motorcycle emissions was 107 nm and nearly 53% of the mass had a diameter between 56 nm and 180 nm (Fig. 5.4).

The OA EFs observed were two orders of magnitude lower than OC observations by (Jayarathne et al., 2017) and observations by U.S. based motorcycle studies (Bond et al., 2004). The low OA emissions factors observed by this study are thought to be due to large and variable backgrounds CO, $CH_4$, $CO_2$ at the motorcycle shop where testing was performed. The large unstable backgrounds were likely due to poor venting of emissions from the tested motorcycles and vehicle emissions from the bordering congested Kathmandu road that likely affected the gas-phase concentrations of the aerosol-free air injected into the dilution system. The OA EF from this work should therefore be used with caution. Alternatively, the size distributions and mass spectra derived from the mAMS data are independent of the error in the emission factor calculation due to elevated gas-phase carbon concentrations. Another study that investigated Asian motorcycle emissions found a similar size distribution range for $PM_{2.5}$, but observed a bimodal distribution with modes above and below 100 nm (Yang et al., 2005). A study of 4-stroke Asian motorcycles found that the $PM_{2.5}$ size distribution of idling motorcycles had the largest mode diameter of the operation cycles investigated and that the distributions shift to smaller sizes when the motorcycles were operated at 15 and 30 km per hour (Chien and Huang, 2010). The results from the above studies suggest that the OA size distributions we observed were at the middle to upper range of OA sizes for motorcycle emissions and that the mode of the distribution would likely shift to ultrafine sizes when the motorcycles are operated above idle.

### 5.4.3 Brick Kilns

Brick kilns are a poorly characterized but important source of aerosol emissions in South Asia (Weyant et al., 2014). In NAMaSTE we investigated emissions from two kilns in Nepal that represent two distinct classifications of brick kilns. In the Kathmandu Valley we sampled emissions from a batch-style clamp kiln. In central Nepal we investigated emissions from a zigzag brick kiln. Although we were not able to obtain a large sampling set, the results presented here and in other the NAMaSTE works are the first to characterize the aerosol and gas phase composition of brick kiln emissions in South Asia.

Clamp kilns are a traditional and inefficient brick firing technology that uses intermittent firing (single batch per firing) and are not designed with a chimney or draft system (Manadhar, 2013). Because of the design of the clamp kiln, we sampled uncontrolled emissions from cracks at the top of the kiln. The investigated kiln was co-fired with coal and hardwood. Over the ~2 hour time span in which sampling took place the median $PM_1$ EF was 1.153 g $kg^{-1}$ with quartile values of 0.205 g $kg^{-1}$ and 4.545 g $kg^{-1}$. The $PM_1$ median was comprised of 54% OA, 30.6% sulfate, 10.9% ammonium, 3.64% chloride, and 2.4% BC (Fig. 5.2). PAHs were not observed above detection limits. The speciated size distributions of the clamp kiln emissions show that the organic component had the largest mode diameter at 453 nm and the mode diameter of each inorganic component decreased in the same rank order as the fraction of $PM_1$ mass (Fig. 5.4). Chloride, for example, was found to have the lowest mode diameter at ~140 nm less than the OA mode. It is uncertain if the size differences between the aerosol components are due differences in volatilization times within the ePTOF system or because of physically distinct sizes due to external mixing. Regardless of the differences in the estimated mode diameters, nearly 87% of the non-refractory mass was found in a size range between 180nm and 1000nm, and ultrafine mass was virtually zero (Fig. 5.4).

Zigzag brick kilns are a subset of fixed chimney bull's trench kiln (FCBTK) and an established kiln type in Nepal (Manadhar, 2013). The kilns utilize continuous firing with bricks stacked in a zigzag pattern to optimize efficiency and use force draft or natural draft with a fixed chimney. In NAMaSTE we sampled from a force draft zigzag kiln with a stack of ~10m. The kiln was fired with coal and sugar cane residue (bagasse) was used as a starter fuel. More details on the operation of the investigated brick kilns and why they were chosen for sampling can be found in Stockwell et al. (2016). At the zigzag kiln, the on-line sampling system was in operation for ~4 hour sampling period, but unfortunately because of the heat of the kiln, the mAMS was only operational for portion of the sampling period (~0.5 hours). However, because of the continuous design of the kiln, the emissions were expected to have low temporal variability over the sampling period. The median $PM_1$ EF of the kiln was 1.760 g $kg^{-1}$ comprised of 57% sulfate, 18% BC, 18% OA, and 6% ammonium. The zigzag kiln is the only investigated emission source to have sulfate as the dominant component of the $PM_1$ emissions. Additionally, the

mass distributions shown in Fig. 4 indicate that sulfate aerosol with diameters between 180 nm and 560 nm comprised 63% of the sulfate distribution and approximately 36% of the total $PM_1$ mass. Sulfate and OA were found to have a mode diameter of ~345 nm and the ammonium mode was lower at 285 nm. Based on the distributions alone it is unclear if the inconsistency between the sulfate mode and the ammonium mode was due to external mixing or mAMS measurement error.

Like the clamp kiln, PAHs were not observed above detection limits from the zigzag kiln. The PAH detection limit at the zigzag kiln was estimated to be 42.3 ng $m^{-3}$ and the clamp kiln PAH detection limit was 90 ng $m^{-3}$. The observation of PAH concentrations below detection limits from the coal-fired kilns is unexpected because PAHs have previously been observed in coal emissions measured by an AMS in China and were proposed as tracer compounds for coal burning (Hu et al., 2013). PAH aerosol was also not readily observed at the zigzag kiln by the NAMaSTE filter-based measurements, but were observed from the clamp kiln (Jayarathne et al., 2017). More PAH measurements at brick kiln are needed to understand if low PAH emissions are ubiquitous with coal fired brick kilns and to investigate the mechanisms associated with low PAH formation.

Although the two brick kilns had roughly similar $PM_1$ EFs and size distributions, the two coal-fired kilns had major differences in efficiency and in the chemical composition of emissions. The zigzag kiln had lower OA emissions and markedly enhanced BC and sulfate EFs compared to the clamp kiln. Additionally, the mass spectral profiles of the brick kiln OA emissions indicate that significant molecular differences existed between the kiln emissions primarily because the zigzag kiln emissions contained nitrogen containing organic compounds that were not present with in the clamp kiln emissions (Goetz et al., 2017b).The differences in OA and BC between the two kilns are thought to be due to the enhanced combustion efficiency of the zigzag kiln (MCE = 0.994) compared to the clamp kiln (MCE = 0.950) (Stockwell et al., 2016). Evidence from mass spectral data indicates that emissions of levoglucosan, a biomass burning tracer compound, were limited at the clamp kiln compared to other biofuel sources suggesting that coal was the dominant fuel inside the kiln and wood burning was limited at the time sampling took place (Goetz et al., 2017b;Jayarathne et al., 2017). Therefore, the difference in average MCE between the kilns was likely because of kiln design and not due to differences in fuel type. The role of kiln design on combustion efficiency was expected as the forced-draft system of the zigzag kiln is designed for enhanced fuel and production efficiency compared to the less advanced clamp kiln. Alternatively, fuel quality explains the differences in sulfate EF observed between the two fuels. Elemental analysis indicated that the zigzag kiln coal was composed of 1.28% sulfur and the clamp kiln was composed of 0.68% (Stockwell et al., 2016). The enhanced sulfate EF at the zigzag kiln was therefore likely due to the enhanced sulfur content of the coal used at the site.

Of the limited reports of brick kiln emissions the results presented above agree well with what has previously been observed by kilns with the same fuel type. Weyant et al. (2014), conducted measurements at three South Asian zigzag kilns that operated with 100% coal and found an average $PM_{2.5}$ fuel-based EF of 0.93± g $kg^{-1}$ and an average BC EF of 0.43 g $kg^{-1}$. Assuming that the $PM_{2.5}$ observed by the Weyant et al. (2014) is roughly equivalent to $PM_1$ based on the observed mass distributions from this study, the results from this study correspond well with previous zigzag kiln observations. Observations of biomass fueled clamp kilns by Christian et al. (2010) in Mexico found an average OM EF of 0.25 g $kg^{-1}$ and an EC EF of 1.05 g $kg^{-1}$ produced under burning conditions with an average MCE of 0.968. The order of magnitude difference in BC EF from the mostly coal-fired clamp kiln investigated in NAMaSTE compared to the EC EF from the biomass fueled clamp kilns in Mexico combined with enhanced MCE at the Mexican kilns, suggests that coal burning kilns with lower efficiency produce lower BC aerosol emissions compared to biofuel burning kilns on a per unit of fuel basis. The use of coal for brick making in place of biofuels could therefore potentially reduce the climate impact of inefficient traditional brick firing operations. However, the role of other light absorbing aerosol emissions from brick kilns needs to be better quantified before fuel recommendations can be made for the mitigation of short-term climate forcers. For example, the clamp kiln emissions investigated in this study had strong ultraviolet absorption (Goetz et al., 2017b;Stockwell et al., 2016) and based on Delta-C estimates made with the aethalometer nearly 35% of the OA emissions were light absorbing aerosol, demonstrating that the light absorbing properties of brick kiln emissions cannot be determined from BC quantification alone.

### 5.4.4 Agricultural Residue Burning

Emissions from the open burning of crop residues common in the Indogangetic Plains were investigated in NAMaSTE. In this work, segregated mustard, grass, and wheat straw burning emissions were sampled in addition to a mixture of residues that included grass, wheat and rice straw, lentils, and mustard. The mixed residue was found to have a median $PM_1$ EF of 1.95 g $kg^{-1}$ with compositional fractions of 0.64 OA, 0.26 BC, 0.08 chloride and nominal fractions of nitrate and sulfate (Fig. 5.2). Mustard and grass residues were observed to have similar $PM_1$ EFs at 2.136 g $kg^{-1}$ and 2.091 g $kg^{-1}$, respectively. The two segregated residues, however, had different aerosol compositions. Mustard was found to have reduced OA and chloride EFs, and enhanced BC and sulfate EFs compared to the mixed residue. The grass was found to have slightly lower EFs for OA, BC, and nitrate, but with significantly larger EFs of chloride (0.475 g $kg^{-1}$) and ammonium (80 mg $kg^{-1}$) (Fig. 5.2). Wheat straw residue was observed to have the largest $PM_1$ EF of

the tested crop residues (3.378 g $kg^{-1}$) with a median OA EF approximately double the mixed residue. Organic aerosol emissions from wheat straw burning had the largest variability of crop residues with a $10^{th}$ percentile of 0.424 g $kg^{-1}$ and a $90^{th}$ percentile of 18.78 g $kg^{-1}$. Black carbon, sulfate, nitrate, ammonium, and chloride were all observed above the background from wheat straw burning. Polycyclic aromatic hydrocarbons were observed from the entirety crop residue burning experiments with EFs of about 4 mg $kg^{-1}$.

The mass distributions for the crop residue burns can be seen in Fig. 5.3. The majority of the OA mass from the burns was found in the accumulation mode (between 0.1 and 1 $\mu$m) and less than 15% of the OA mass was found below 100 nm. Wheat burning OA was observed to have the lowest mode diameter of the investigated residues (240 nm) and had the largest percentage of mass below 100nm. Grass burning and the mixed residue OA emissions were observed to have mode diameters at 300 nm and mustard burning OA had a mode diameter of 400 nm. The differences in OA mass distributions are thought to be due to differences in fuel type and not due to differences in burn conditions since the average MCEs were roughly equivalent at ~0.955 for all of the residue burns except for mustard burning which had an MCE of 0.920 (Stockwell et al., 2016). Aside from OA, chloride was also observed to have distinguishable mass distributions from the crop residue burns and an ammonium distribution was observed from grass burning. The chloride emissions were found to have mode diameters that ranged between 130 nm to 175 nm and the ammonium distribution from grass burning emissions had a roughly equivalent mode diameter to the chloride emissions. Similar chloride mass distributions with modes centered between 100 nm and 180 nm were also observed from sugarcane residue burning in Brazil (da Rocha et al., 2005). The significantly lower inorganic mode diameters compared to the mode diameters of the OA emissions indicate that the aerosol components were externally mixed. The non-refractory chloride measured by the mAMS was estimated to be between 82% and 87% particle phase HCl. Additionally, for grass burning HCl comprised up to 23% of the median non-refractory aerosol mass. Particle phase chloride emissions were also observed by the filter-based measurements conducted by Jayarathne et al. (2017). Similar particle phase chloride emission factors have also been observed with grass burning samples (0.305 g $kg^{-1}$) and agricultural waste samples (0.164 g $kg^{-1}$) from Africa (Keene et al., 2006). Conversely, gas phase HCl emissions from crop residue burning were not observed above detection limits by Stockwell et al. (2016). The preponderance of externally mixed particle phase chloride suggests condensation of HCl is occurring within the crop residue plumes, and that unlike what was observed with garbage burning the inorganic chlorine mass is mostly found in the particle phase. Gas phase organic chlorine primarily in the form of chloromethane ($CH_3Cl$), however, was reported from the gas-phase measurements (Stockwell et al., 2016). The presence of both inorganic and organic chlorine emissions as large fractions of $PM_1$ mass from agricultural residues, combined the large emission rates of aerosol produced from residue

burning in parts of South Asia (Pandey et al., 2014), suggests that crop residue burning is likely a major source of atmospheric chloride in South Asia and globally.

There have been limited field measurements of open crop residue burning aerosol emissions and the majority of the lab measurements have been off-line and filter-based. Lab experiments that have sampled crop residue burning of have reported EC EFs between 0.12-0.52 g $kg^{-1}$ and OC values between 0.17 - 4.69 g $kg^{-1}$ (Andreae and Merlet, 2001;Cao et al., 2008;Hays et al., 2005;Venkataraman et al., 2005). Based on the previous reports, the OC EFs for crop residue burning, based on an estimated OA:OC of 1.414 (Table 5.2), are within the lower range of OC EF observations; the BC EFs are in the upper range or above the referenced EC emission factors. Black carbon EFs above the referenced EC range were also observed with the NAMaSTE photoacoustic BC measurements and the off-line thermal-optical measurements (Jayarathne et al., 2017;Stockwell et al., 2016). Conversely, the off-line NAMaSTE measurements observed an OC EF of 6.314 g $kg^{-1}$ from the mixed crop residue emissions placing the measurements above other filter-based results for crop residue burning (Jayarathne et al., 2017). The contradictory results between the on-line and off-line organic aerosol NAMaSTE measurements combined with the similarities between the BC EFs indicates that differences in dilution likely play a large role in the phase partitioning of semi-volatile organic compounds (Lipsky and Robinson, 2006). Given the enhanced dilution of the on-line $PM_1$ measurements (~1:5) compared to the off-line filter based measurements, we suggest that the on-line OA EFs are more representative of ambient crop residue emissions, whereas, the off-line crop residue burning OM EFs are likely more representative what would be observed on the residential scale with the use of crop residue for heating and cooking fires.

### 5.4.5 Traditional Mudstove

We investigated aerosol emissions from three separate traditional mud cookstoves found in homes within Tarai region of Nepal (Table 5.1). The stoves were fueled with biomass common to South Asia local fuel including hardwood, sticks and twigs, and dung. The hardwood and sticks were from local sources and the dried dung logs were provided to the stove operators by the NAMaSTE team, as dung burning was not common in the region where sampling took place.

Emissions from the hardwood-fueled stove were sampled during an evening cooking cycle where lentils, rice and curry were cooked in a pressure cooker heated by the stove. The hardwood fuel was primarily Bakaino (*Melia azadarach*). The hardwood fueled stove produced a median $PM_1$ EF of 1.421 g $kg^{-1}$ over the ~1 hour burn period (Fig. 2). The $PM_1$ was comprised of 75% OA, 20% BC, 4.4% chloride, and <1% sulfate (Fig. 2). The observed PAH EF was 7 mg $kg^{-1}$. Figure 5.3 indicates that hardwood burning had an OA mode diameter of 200 nm and a chloride mode

diameter of 133 nm. Like the agricultural residue samples previously discussed, the chloride aerosol and OA appear to be externally mixed based on the differences in mass distributions. Nearly 84% of the OA mass was found in the accumulation mode. Similar size distributions have been observed elsewhere with oak and pine wood burning (Kleeman et al., 1999).

Emissions from a separate cookstove fueled with stick and twigs of *Shorea robusta,* and ignited with plastic, were sampled during a morning cook cycle (Table 5.1). During the 1-hour long cook cycle lentils, roti, curry, and rice was prepared. It should be noted that the ignition and start-up phase of the stick burning started ~15 minute prior to sampling and therefore plastic burning was likely not part of the sampled emissions. The sticks and twig burning cookstove produced a median $PM_1$ EF of 1.265 g $kg^{-1}$ that was composed of 61% OA, 34% BC, 1.7% chloride, and nominal fractions of sulfate and nitrate aerosol (Fig. 5.2). The PAH EF for stick fueled cooking was 8 mg $kg^{-1}$. Stick burning had the highest MCE of the tested cookstove fires (0.933) (Stockwell et al., 2016), and the more efficient burn conditions are thought to be responsible for the enhanced median BC EF and reduced median OA EF compared to the hardwood fueled stove. The stick fueled stove did however have larger variability in $PM_1$ emissions compared to the hardwood fueled stove, which was likely generated because of the differences in burn cycle due to the low density and inconsistency of stick fuel compared to hardwood logs (Fig. 5.2). Although differences in emission factors existed between the wood biomass fueled stoves, the two burns produced similar mass distributions. Like the hardwood fuel cooking, the stick fueled cooking was found to have an OA mode diameter of ~190 nm and chloride emissions had a mode diameter of 123 nm (Fig. 5.3).

The single-pot mudstove that was fueled with sticks and twigs was later separately fueled using cow dung logs. The dung logs were ignited with kerosene and the stove was operated for ~30 minutes and without cooking. The measured dung burning median $PM_1$ EF was 1.466 g $kg^{-1}$ and was composed of 70% OA, 17% chloride, 6.8% BC, 4.6% ammonium and less than 1% sulfate and nitrate (Fig. 5.2). Dung burning had the lowest PAH EF of the investigated biomass fuels with a median of 3 mg $kg^{-1}$, a $10^{th}$ percentile of mg $kg^{-1}$, and a $90^{th}$ percentile of 15 mg $kg^{-1}$ (Fig. 5.2). Also it should be noted that the dung burning had the lowest variability in OA emissions of the sampled biomass in NAMaSTE (Fig. 5.2). Compositionally, the dung fueled cookstove emissions were distinct from the wood burning emission because of the lower BC emissions, the greatly enhanced chloride emissions, and because of the presence of ammonium containing aerosol. Significant chloride and ammonium emissions were also sampled by the off-line filter measurements and gas-phase HCl was not measured above detection limits indicating that particle phase chloride was dominant with dung burning (Jayarathne et al., 2017;Stockwell et al., 2016). Additionally, because of the increased fraction of ammonium, a cation molecule, compared to the measured inorganic anions (i.e. sulfate, nitrate, chloride), it can be inferred that dung fueled cooking with a traditional mudstove is more neutralized to wood biomass

fueled cooking. By summing the anion concentrations of all the dung burning sampled in NAMaSTE (RETS samples included) to estimate a predicted ammonium concentration that represents full ionic neutralization, the anionic mass from dung burning ranged from 35% to 50% neutralized and the field samples were 45% neutralized. Whereas, with wood fueled cookstoves, ammonium wasn't detected above AMS detection limits in any sample indicating that little aerosol neutralization occurred. However, although the evidence suggests that dung burning was more neutralized, the dung burning emissions were ultimately more acidic on a per mass of fuel basis since the chloride EF from dung burning was an order of magnitude greater than wood burning.

In addition to having unique emission factors, the dung-fired mudstove was found to have a unique mass distribution compared to wood burning. The OA mass distribution was observed to be bimodal with an estimated mode diameter at 150 nm and 270 nm, and a valley at ~200 nm (Fig. 5.3). Based on the 2-dimensional time series of the organic mass distribution found in Fig. 5.5 (top panel) it's clear that the two distinct OA distributions materialize at different time periods during the dung-burning test. The two distinct distributions appear to correspond with the two identified modes from the average distribution in Fig. 5.3, with the larger mode diameter occurring at the start of the burn and the smaller mode diameter occurring shortly after ignition of the dung (Fig. 5.5). Additionally, during the ignition phase of the burn, the highest OA and BC EFs were observed and the MCE derived from the uncalibrated Picarro CRDS was at its highest point. Two minutes after ignition the inorganic components appeared in the emissions, the OA and BC EFs decreased, and the OA distribution shifted to smaller sizes (Fig. 5.5). The MCE, however, did not appear to follow the same abrupt trend and remains constant with a relative value of ~0.97, suggesting that the dung remained in a flaming phase. Because the MCE did not follow the same trend as the aerosol, it is thought that the kerosene that was used to ignite the dung was responsible for the larger mode diameter of the OA distribution and for the absence of inorganic mass at the start of the burn. However, without further samples, it is unclear if the same trends in size and mass would occur with different starter fuels.

Although we did not sample other exclusively dung-fueled cookstoves in the field, we did sample cooking with a 2-pot traditional mudstove that was co-fired with dung and hardwood, and started with hardwood (Table 5.1). The 2-pot stove was used to cook rice, lentils, and curry during the evening cook cycle at a village restaurant. The co-fired stove did not show the same bimodal mass distribution as the single- pot dung-fueled stove and was observed to have a unimodal distribution that was most similar to the hardwood fueled cookstove. However, unlike hardwood burning the co-fired mass distribution was found to have large fractions of ammonium and chloride aerosol (Fig. 5.3). Organic aerosol emitted from the co-fired stove emissions was estimated to have a mode diameter of 206 nm. Inorganic aerosol was estimated to have a mode diameter of ~125 nm. Again, like the other cookstove emissions the differences between the organic and inorganic modes suggest that the aerosol components were externally mixed. Although

differences in mode diameter existed between the aerosol components, the non-refractory distribution was fairly narrow and 67% of the mass was found between 100 nm and 320 nm. Because the authors are not aware of other studies that have characterized the aerosol size distributions of dung emissions in the field, we cannot comment on the universality of the distributions observed from the NAMaSTE samples. However, under more dilute conditions (~1:45) produced in a lab, Venkataraman and Rao (2001) found a mass median aerodynamic diameter of dung-fired emissions between 600-780 nm. The larger central tendency of the highly dilute dung burning emissions suggests that the mass distributions observed in this study would likely shift to larger diameters under more dilute conditions downwind of the cookstoves. It is important to note however that an effort was made to sampled well mixed emissions from inside the building in which sampling took place. If our well-mixed assumption holds true then the mass distributions observed in this study are more representative of residential exposure, whereas the Venkataraman and Rao (2001) size distributions are likely more representative of local or regional ambient aerosol sourced from dung-fueled cookstoves.

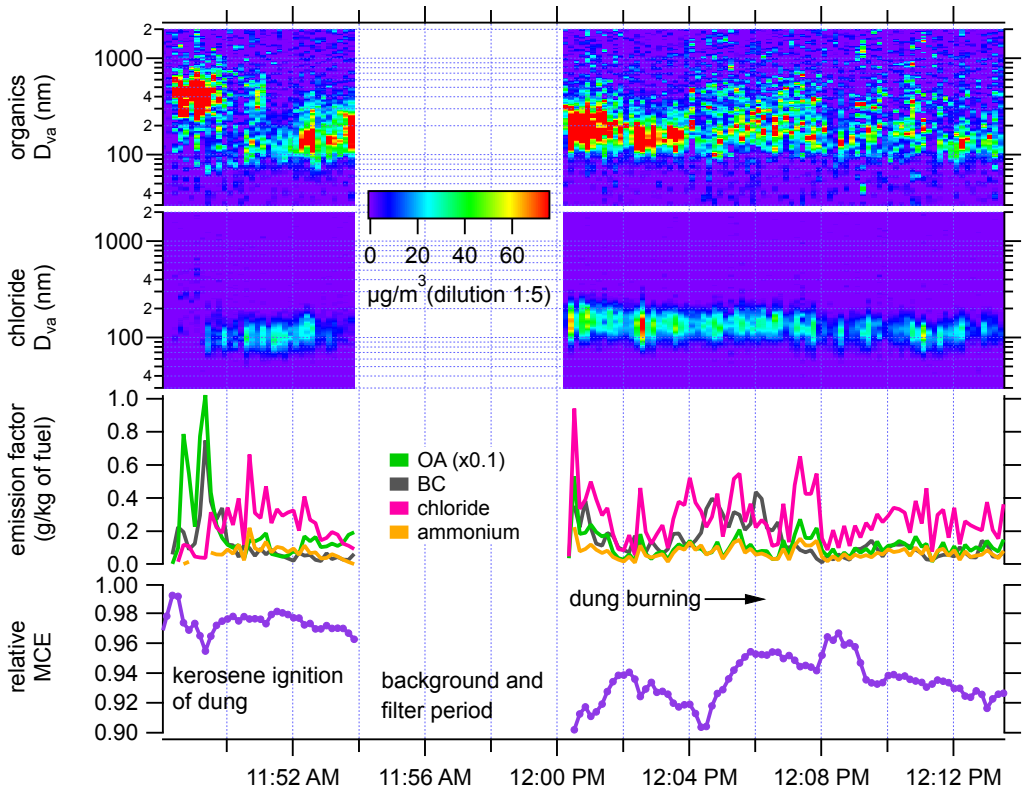


**Figure 5.5 Dung-fired Cookstove Timeseries**
Time Series of the modified combustion efficiency (bottom panel), aerosol emission factors, and chloride and organic mass size distributions (top panels) for the dung burning emissions from a 1-Pot traditional mudstove. The 2-d time distributions are colored by the size-resolved dilute concentration as indicated by the color ramp.

The dung and hardwood fueled two-pot traditional mudstove was found to have enhanced aerosol emission factors compared to the tested single-pot stoves. With an average MCE of 0.912 (Stockwell et al., 2016), the 2-pot stove was observed to have a median $PM_1$ EF of 3.151 g $kg^{-1}$. The median $PM_1$ was composed of 77% OA, 10% BC, 10% chloride, 2% ammonium, and nominal fractions of sulfate and nitrate (Fig. 5.2). The co-fired cookstove had the largest median PAH EF of any of the investigated emission sources in this study (19 mg kg-1), and was only surpassed by plastic burning in the 90$^{th}$ percentile (Fig. 5.2). The general increase in aerosol emissions between the dung-fired single-pot stove and the co-fired two-pot stove was unexpected because few differences between the two sources were observed by the filter-based measurements of Jayarathne et al. (2017) or the gas-phase measurements of Stockwell et al. (2016). The two-pot results, however, were closer to the EFs observed by the filter-based measurements indicating that differences in dilution between the cookstove tests may be due to the extent of ambient dilution (e.g. distance from source or air exchange rate) since the controlled dilution factor for all of cooking experiments was ~1:5. Nevertheless, unaccounted for differences in cookstove operation or the composition of fuels cannot be discounted.

### 5.4.6 Delta-C

Delta-C carbon estimated by the aethalometer was used as an approximation of light absorbing organic carbon emissions, or brown carbon (BrC), from the investigated emission sources. Delta-C emissions were observed from the biomass combustion sources and from the clamp kiln, but weren't observed above the background from open garbage burning, the zigzag kiln, or from the engine exhaust experiments. Summary statistics of the Delta-C EFs can be found in Appendix G. The ratio of Delta-C to OA (g $g^{-1}$) was used to estimate the light-absorbing fraction of the OA emissions. Figure 5.6a shows that the largest median Delta-C fractions were observed from the field-tested cookstoves ranging from 55-70% of OA. Of the cookstove emissions, the largest light absorbing fraction from dung burning (0.70). Assuming that ratios are conserved in poorly vented background conditions, then like the field-tested cookstoves, the traditional stoves fueled with a mix of dung, sticks, and hardwood tested at RETS observed an average Delta-C fraction of 0.62. The crop residue burning emissions were observed to have median Delta-C to OA ratios that ranged from 0.18-0.55 (Fig. 5.6a). The crop residue samples were also observed to have the most variability with especially low 10$^{th}$ percentiles that were <0.02. The presence of light absorbing organic aerosol from the biomass burning samples was expected as BrC has been previously attributed to the combustion of biomass (Saleh et al., 2014). The Delta-C fraction from the clamp kiln (median = 0.30), however, was unexpected since it was previously inferred that hardwood was a minor component of the kiln fuel and Delta-C wasn't observed from the other coal-fired kiln.

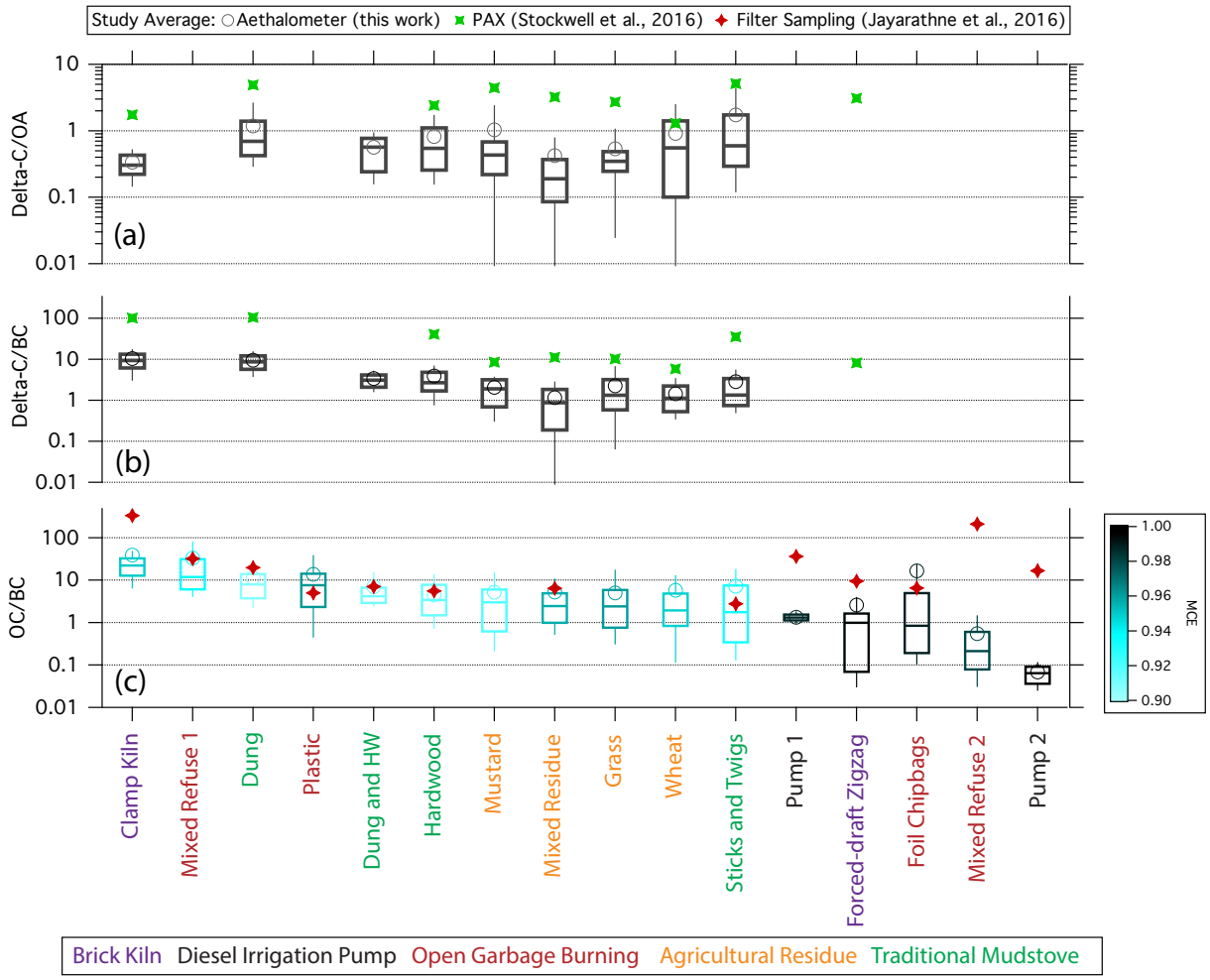


**Figure 5.6. Box and Whisker Plots of the Emission Factor Ratios**
(a) the Delta-C (BrC) to organic aerosol ratio (OA) (g/g), (b) Delta-C (BrC) to black carbon (BC) ratio (g/g), and (c) the organic carbon (OA) to black carbon ration (g/g) for each emission source. The box and whisker plots are ranked by the median organic aerosol to black carbon ratio. PAX derived brown carbon (BrC) to OA ratios (avg. g/ avg. g.) and black carbon ratios (g/g) from Stockwell et al. (2016) are found in panel a and b, respectively. Off-line filter based organic matter to elemental carbon ratios (g/g) from Jayarathne et al. (2017) are found in panel c. The organic aerosol to black carbon ratios are colored by average MCE values from Stockwell et al. (2016).

Estimates of BrC from (Stockwell et al., 2016) using an on-line dual-wavelength (405 and 870 nm) photoacoustic extinctiometer system (PAX) indicated that the PAX measured BrC had significantly larger EFs compared to the OA and Delta-C measured in this work. The PAX BrC to OA (average EF used) ratio ranged from 1.3 to 5.1 for the emission sources from which Delta-C emissions were observed, and the average BrC to OA ratio was 3.5. The results indicate that either the PAX was overestimating BrC emissions or the mAMS was underestimating OA emissions. It's assumed that underestimation of OA by the mAMS would be due to mischaracterization of the OA collection efficiency or by errors in ion efficiency quantification. The possible overestimation of BrC by the PAX system could be due to error in the calculation of light absorbing aerosol mass prompted by using an incompatible mass absorption coefficients (MAC) or by error in the absorption coefficient ($b_{abs}$) measurements. A comparison of BC EFs between the PAX and the aethalometer demonstrates that the PAX BC mass quantification based on a MAC of 4.74 $m^2$ $g^{-1}$ at 870 nm used by Stockwell et al. (2016) agree well with BC mass measured by the aethalometer at 880nm (Fig. 5.7a). Although some large differences existed between the BC EFs observed at the zigzag kiln and at the stick fueled mudstove, linear regression of the results provides a linear slope of 1.14, and the subsequent correlation coefficient ($r^2$) of 0.70 indicated that there was limited scatter between the two instruments (Fig 5.7a.). The results therefore eliminate BC mass quantification as factor responsible for the differences between mAMS observed OA and PAX estimated BrC. Furthermore, given that BrC in other work has been observed to be composed of extremely low volatility organic compounds (Saleh et al., 2014), the evaporation of semivolatile organics by dilution also likely does not explain the large differences observed between the PAX BrC and OA EFs. When the PAX was on the dilution sampling system, for example, the average BrC to OA ratio was ~2, compared to the average Delta-C to OA ratio of 0.42 for the same sources. Additionally, there were several instances where the PAX measurements produced larger BrC EFs than the OC measurements of Jayarathne et al. (2017). Ultimately, because of the limited experimental controls available to us in the field we cannot provide more than speculation on why differences in organic aerosol mass existed between the different measurement techniques. More comparisons between on-line and off-line measurement techniques like those used in NAMaSTE, but in a controlled lab environment, are needed to address the disparity in organic aerosol mass quantification observed in this study.

Median Delta-C to BC ratios, (Delta-C/BC) which in this case are equivalent to the fractional difference between BC mass measured at 370 nm and at 800 nm by aethalometer and a metric for ultraviolet mass absorption, were found to range between 0.87 and 9.35 for the emission sources in which Delta-C was observed (Fig. 5.6b). The lowest median Delta-C/BC ratios were observed from the crop residue burning experiments with an average of 1.30. The field-tested mudstove emission were found to have an average Delta-C/BC of 3.93 and the dung burning experiment had a significant mass fraction observed in the 370 nm channel with a ratio of 8.67 (Fig. 5.6b). The clamp

kiln emissions had the largest ratio at 9.35, indicating that the strongest 370 nm mass absorption was observed from the coal-fired kiln. Similar trends were observed by the PAX system with BrC and BC, but with significantly larger ratios (Figure 5.6b) (Stockwell et al., 2016). Analysis of optical wavelength dependence indicates that the dung burning and clamp kiln emissions had the largest ultraviolet absorption dependence of the investigated emission sources, with average PAX derived Angstrom absorption exponents (AAE) of ~4 (Stockwell et al., 2016). Therefore, based on the high Delta-C, BrC, and AAE from dung burning and the coal-fired clamp kiln compared to other sources investigated in NAMaSTE, shortwave light absorption by OA is an important property of their emissions and should be considered when evaluating the climate impact of the two sources. Furthermore, the distinct optical properties of the two emission sources combined with atmospheric tracers could aid in ambient source identification and apportionment of dung burning or coal-fired clamp kilns in South Asia.

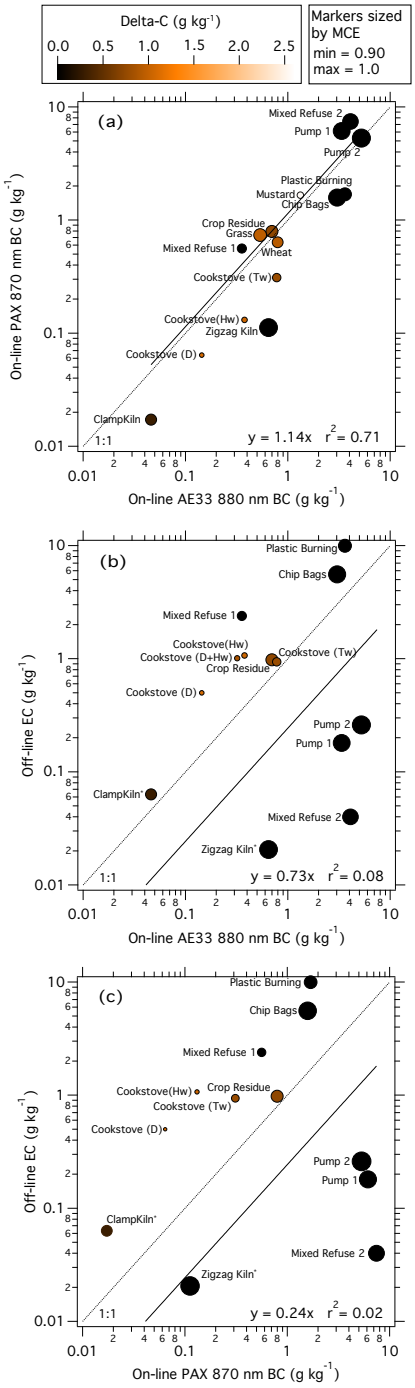


**Figure 5.7. Intercomparison of Black Carbon Emission Factors**
(a) on-line PAX 870 nm measured black carbon emission factors from Stockwell et al. (2016), (b) off-line thermal-optical measured elemental carbon emission factors from Jayarathne et al. (2017) versus on-line AE33 aethalometer 880nm measured black carbon emission factors in units of g kg of fuel$^{-1}$. Panel (c) provides a scatter plot of the off-line EC measurements versus the on-line PAX 870 nm measurements. Linear regression curves are displayed as solid lines with the resulting equation and correlation coefficient displayed in each respective panel. Markers are colored by the median Delta-C emission factor for each emission source and sized by the modified combustion efficiency from Stockwell et al. (2016). (*) indicates that the off-line measurements were below detection limits. Cookstove fuel types are hardwood (Hw), dung (D), and sticks and twigs (Tw).

### 5.4.6 OA/BC

The large instrument suite used in NAMaSTE provided unique insight into the chemical composition of emissions from prevalent emissions sources found in South Asia, but also generated complex and sometimes diverse results. As discussed briefly with the above results, some differences in aerosol emission factors have been observed between the on-line results presented in this work and the emission factor results found by the other NAMaSTE measurements. The differences observed between the instrumentation are thought to be due to the inherent differences between measurement techniques and also likely due to sampling methodology. Here we investigate the mass ratio of organic carbon to black carbon (OC/BC) from the emission sources studied in NAMaSTE. The mass ratio provides an internally consistent parameter to assess the aerosol composition between emission sources and also offers a metric to make comparisons of aerosol composition across the NAMaSTE instrumentation and relevant results in the literature. The OC to BC mass ratio of the field-tested emission sources can be found in Fig. 5.6c. The figure displays box and whisker percentiles in addition to the average ratio for each emission source, and the ratios are displayed in rank order by the median OC/BC. Additionally, the box and whiskers for each emission source in Fig. 5.6c are colored by the average MCE from Stockwell et al. (2016). Generally, the lowest OC/BC values appear to correspond with the highest observed MCEs (Fig. 5.6c). The trend between OC/BC and MCE matches observations from biomass burning emissions that have taken place in the field (Kondo et al., 2011) and in the lab (Christian et al., 2003).

The largest median OC/BC was observed at the coal-fired clamp brick kiln with a value of 22.1 (Fig. 5.6c). Conversely, the OC/BC observed at the zigzag brick kiln was ~1 and the lower percentiles ranged to below 0.1 (Fig. 5.6c). Similar results were observed with other South Asian coal-fired zigzag kilns by off-line filter based measurements with OC/EC ratios ranging from 0-0.29 (Weyant et al., 2014). Clamp kilns investigated in Mexico saw similarly low OC/EC emissions with an average of 0.16 (Christian et al., 2010). The lower OC/EC observed with clamp kilns in Mexico compared to the clamp kiln investigated in this study was likely due to fuel type as previously discussed.

The median ratios did not follow any specific trend based on source type, although the agricultural residue burning samples were grouped with median OC/BC ratios between 1.93 and 3.01 (Fig 5.6c). Literature based results provide an estimated range of 1.8-8.2 for OC/EC for crop residue burning (Andreae and Merlet, 2001;Cao et al., 2008;Hays et al., 2005;Sahai et al., 2007). The upper OC/BC percentiles of the crop residue emissions observed by this study agree well with what has been observed in the literature. Additionally, the off-line filter based measurements of Jayarathne et al. (2017) are in agreement with an estimated OC/EC of 6.44 (Figure 5.6c).

Open garbage burning produced mixed results with Mix 1 and plastic burning emissions containing median OC/BC >5 and Mix 2 and metalized plastic chip bags containing OC/BC below 1 (Fig 5.6c). Based on the median EFs, the differences between Mix 1 and Mix 2 are largely due to enhanced BC emissions observed from Mix 2. The differences between the plastic burning samples were primarily due to enhanced OA emissions mixed plastic compared to the chip bags (Fig. 5.2). Based on the plastic burning results, it's possible that Mix 1 was composed of a larger percentage of mixed plastic compared to the Mix 2, although differences in burn conditions could also be a factor. Christian et al. (2010) also observed estimated OC/EC >1 (2.3-28.5) from open garbage burning in Mexico. The combined OC/BC range from this study and Christian et al. (2010) suggests that considerable variability in emissions exist with the open garbage burning.

The diesel powered irrigation pumps observed the most consistently low OC/BC of the source types but were observed to produce noticeably different ratios. As discussed in Section 5.3.2 emissions from Pump 2, the newer more efficient pump, had considerably reduced OA EFs compared to the older Pump 1 (Fig. 2). Here the reduced OA

associated Pump 2 is responsible for the lower OC/BC compared to Pump 2. Although previous reports of OC/BC from diesel irrigation pumps do not exist outside of NAMaSTE, the observed OC/BC correspond well with observations from diesel powered military generators which emitted an estimated OM/BC range 0.23-6.25 (Zhu et al., 2009). Additionally, OC/EC observed from U.S. diesel vehicle primary emissions under dilute conditions (>1:8 dilution) were found to be less than 1 (May et al., 2014). Although we only sampled two irrigation pumps in NAMaSTE, the results indicate that the aerosol emissions are similar to what has been observed from other diesel combustion sources by other studies. However, a better understanding of inter-pump variability in aerosol emissions is needed before emission factors from other more common (and likely more controlled) emission sources can used as a supplement for field tested diesel powered irrigation pump emissions.

The wood fueled traditional mudstoves were observed to have emissions with OC/BC close to what was observed from the crop residue burns and the filter-based measurements of Jayarathne et al. (2017) were within 43% of the on-line measured values (Fig 5.6c). The median OC/BC from the hardwood fueled stove was found to be 3.43 and the stick burning stove emissions had an OC/BC of 1.77. The OC/BC observed from the wood-fired traditional stoves in Nepal are within the estimated OC/EC range of 1.22-11.5 from similar wood-fired stoves investigated in Guatemala (Roden et al., 2006). Additionally, OC/BC of the hardwood fired cookstoves tested at RETS ranged from 0.34-4.72 from traditional stoves with and without chimneys, natural draft improved stoves, a Bhuse Chulo, and a three stone fire, with the largest OA/BC observed from the three stone fire. Another study that investigated South Asia residential biofuels found an average OC/EC of 0.5 for low burn rate fuelwood and an OC/EC of 3.8 for high burn rate fuelwood (Venkataraman et al., 2005). The results suggest that the NAMaSTE emission results provide further confidence in the aerosol composition results that have been reported by other studies with larger sample numbers.

The field-tested dung fueled mudstoves were found to have some of the largest OC/BC observed in the study. The 100% dung fueled test was observed to have a median OC/BC of 7.94 and the co-fired dung and hardwood test has a median OC/BC of 4.20 (Fig 5.6c). The filter-based measurements by Jayarathne et al. (2017) were found to have a similar trend to the on-line measurements but with larger OC/BC ratios because the filter-based measurements observed a larger mass of organic aerosol from each test (Fig 5.6c). One dung-fueled RETS test was observed to have OC/BC ratio closer to the co-fired field tested stove with an average of 3,73. Co-fired dung and hardwood tests at RETs produced an average OC/BC of 3.79. Other studies that have investigated dung burning emissions in the lab have observed OC/EC ratios of greater than 20 and closer to have has been observed by Jayarathne et al. (2017). Therefore, it's possible that the on-line results presented in this study underestimated the organic aerosol mass contained in dung burning emissions.

With many of the aerosol emission factor results it has been discussed how differences exist between the on-line EFs from this work and the companion paper Jayarathne et al (2017). Many of the large differences are thought to be due to detection method in addition to differences in sample dilution which is know to effect the detection of organic aerosol because of the volatility of some organic components emitted from biomass burning and engine exhaust (May et al., 2013;May et al., 2014). As seen in Fig. 5.6c, there is some agreement between in OC/BC between the on-line and undiluted off-line measurements and in particular there is agreement with many of the biomass burning emission sources. However, there are significant differences between the fossil fuel combustion samples (e.g. brick kilns and diesel pumps) and excluding the relatively low MCE clamp kiln, the large differences in OC/BC appear to correspond with emission sources with large MCE values (Fig 6c). Based on Figure 7b, there is significant scatter between on-line BC EFs ($r^2$ = 0.08) and off-line EC EFs, and EC EFs from the some of the high MCE sources are underestimated compared to the BC EFs from the aethalometer. Additionally, although the sample size is limited, sources that contain

Delta-C emissions generally had larger off-line measured BC EFs compared to the on-line measurements and mostly fall closest the 1:1 line (Fig. 5.7b). Similar results were also observed when comparing the off-line EC EFs to on-line BC measurements using a PAX by Stockwell et al. (2016) (Fig 5.7c). The results suggest that there were likely two processes that contributed to the large differences in off-line and on-line BC EFs and were partially responsible for inconsistent OC/BC: (1) black carbon mass from high MCE sources was quantified differently between off-line and on-line detection methods, and (2) the presence of light absorbing organic carbon impacted BC (or EC) detection. Similar processes have been observed with ambient measurements that compared thermal-optical transmittance derived EC to BC from an aethalometer, where urban haze events were found to have larger aethalometer measured BC concentrations and biomass burning events were observed to have larger off-line measured EC concentrations (Jeong et al., 2004). Jeong et al. (2004) attributed the differences in BC and EC quantification to the use of an incorrect mass absorption cross section value at 880 nm to calculate the absorption coefficients with the aethalometer. However, in NAMaSTE the agreement between the PAX and AE33 indicates that the manufacturer selected mass absorption cross section of the AE33 at 880 nm (7.77 $m^2$ $g^{-1}$; (Drinovec et al., 2015)) was likely applied correctly. The enhanced off-line EC EFs compared to BC for sources that had Delta-C emissions could also be explained by insufficient characterization of organic matter charring by the OC/EC analyzer used in Jayarathne et al. (2017). Ultimately, the source of variability between the on-line and off-line detection methods cannot be fully elucidated in this work and further experimental controls that were not available in the field are needed to fully characterize these differences.

As previously suggested, another factor thought to be responsible to the on-line versus off-line differences in OC/BC was the degree of phase partitioning of semi-volatile organic compounds. In other emission testing work, Lipsky and Robinson (2006) determined that OC mass in low-load diesel and wood burning emissions decreases with increasing dilution. Figure 8 investigates the fractional difference between the test integrated OC values from this work and the off-line OC values from Jayarathne et al. (2017) as a function of the controlled dilution factor implemented by the on-line sampling system. The test integrated emission factors were used to reduce error due to differences in the calculation of emission factors. Based on Fig. 8, there was no obvious relationship between differences in OC EFs and on-line dilution factors. For example, with both irrigation pumps, in which controlled dilution wasn't used, it was expected that the OC EFs would have the lowest fractional difference between on-line and off-line measurements. However, the irrigation pumps were found to have both the lowest fractional difference (0.40), and one of the highest fractional differences (0.92) of the investigated emission sources (Fig. 5.8). It is possible that other factors may have also influenced OC detection (e.g. uncontrolled dilution, composition, measurement methods). Again, further experimental controls were needed in the field to fully characterize the influence on dilution. Quantification of aerosol phase semi-volatiles with a thermodenuder or by other methods is recommended for future field experiments like NAMaSTE to help provide mass closure between organic aerosol detection methods.

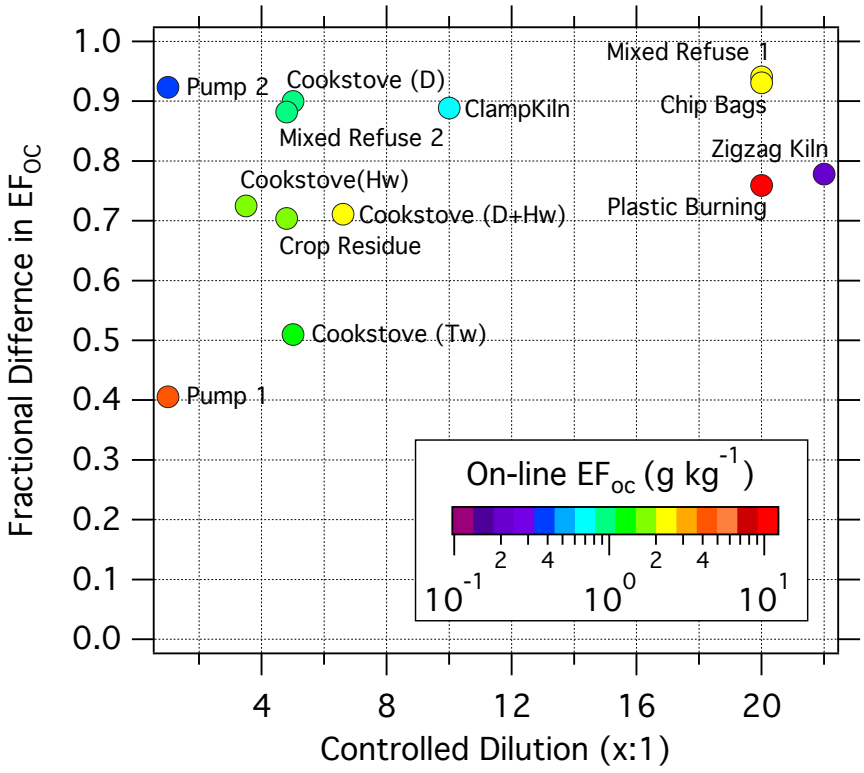


**Figure 5.8. Investigation of OC and Dilution Factors**
Fraction difference between the on-line test integrated from this study and off-line organic carbon emission factors from Jayarathne et al. (2017) ($EF_{oc}$) versus the controlled dilution factor implemented with the on-line sampling system. Markers are colored by the on-line test integrated $EF_{oc}$ in g $kg^{-1}$. Cookstove fuel types are hardwood (Hw), dung (D), and sticks and twigs (Tw).

## 5.5. Conclusions

On-line $PM_1$ measurements of emissions from prevalent but under characterized emission sources in South Asia using a mAMS and aethalometer were conducted as part of the NAMaSTE. With controlled dilution sampling, fuel-based emission factors of major aerosol species were derived from the time resolved measurements of the field-tested emission sources. Additionally, mAMS measured average mass size distributions were generated from each emission source. The field-tested emission sources included traditional mudstoves, agricultural residue burning, brick kilns, open garbage burning, ground water pumps used for irrigation, and idling motorcycles. Open garbage burning, a globally important but poorly understood emission source, was found to have some the largest and most variable in $PM_1$ emissions of the sources investigated in NAMaSTE. Like previous open garbage burning observations, particle

phase chloride was observed from the combustion of PVC plastic, but based on other compliment measurements chlorine mass was primarily in the gas phase as HCl. Diesel powered irrigation pumps were also observed to large $PM_1$ emission factors compared to other investigated sources. The on-line measurements indicate that the two pumps that were sampled produced similar OA size distributions (mode diameter ≈ 80 nm), but produced significantly different OA emission factors. Differences in efficiency due to age or model are thought to be responsible for the different OA EFs from the pumps. Idling motorcycles were observed to have the lowest $PM_1$ emission factors of the investigated sources, however, significant error was likely introduced due to the large and variable gas phase background concentrations observed where sampling took place. The OA size distributions obtained from the motorcycle emissions agreed well with what has been observed from emissions of other Asian motorcycles. The two mainly coal-fired brick making kilns were observed to have similar $PM_1$ emissions on a per mass of fuel basis but with some unique difference in composition which is though to be due to differences in design. The traditional and less efficient clamp kiln had larger OA emission factor compared to more efficient zigzag kiln and the organic mass was made up of a large fraction of light absorbing organic aerosol. The zigzag kiln was observed to have a larger sulfate EF due to the sulfur content of the coal used for firing, and the organic aerosol was found to contain nitrogen-containing species. Polycyclic aromatic hydrocarbons were not observed above the mAMS detection limits from either of the coal-fired brick kilns. Crop residue burning EFs were found to be within the range of other crop residue experiments found in the literature. Interestingly, chlorine emissions externally mixed from organic aerosol were observed from the crop residue experiments and unlike observations from open garbage burning, a significant fraction of chlorine mass was found in the particle phase. Aerosol emissions from traditional mudstoves used for cooking fuel with hardwoods and dung were investigated in the field. For all of the cookstove experiments, organic aerosol was the dominant aerosol component in the emission with OC/BC ranging between 1.7 and 7.9. Like crop residue burning, chloride aerosol was observed from all of the cooking experiments and was externally mixed from the organic aerosol based on the size distribution data. Ammonium emissions were observed with dung burning suggesting that the emissions were neutralized to some extent, but on a per mass of fuel basis the aerosol emissions from dung fueled cooking were likely acidic compared to wood fueled cooking. Additionally, the largest PAH EF was observed from the two-pot mudstove fueled with hardwood and dung.

In addition to examining size distributions and speciated emission factors, mass ratios of light absorbing organic aerosol (Delta-C), black carbon, and organic aerosol were summarized for the investigated emission sources. The agricultural residue burning, wood and dung fueled cooking, and the clamp kiln were all observed to have estimated light absorbing aerosol fractions above 50% of the total organic mass. The clamp kiln and dung burning emissions were observed to have the highest ultraviolet wavelength dependence and a similar trend was observed from the aerosol optical analysis by the companion paper Stockwell et al. (2016). Ratios of organic carbon to black carbon were examined to make comparisons of composition between the emission sources and make comparisons to the filter-based aerosol measurements by the companion paper Jayarathne et al. (2017). It was determined that OC/BC measurements made by this work corresponded well with other studies that have investigated similar sources indicating that the on-line emission factors presented in this work help affirm previous results. The aerosol size and composition results from this work have added important results to the literature for some prevalent emission sources found in South Asia. Additionally, the NAMaSTE results as a whole have expanded the body of knowledge about South Asia combustion sources and provide key results that will help constrain uncertainty in emission inventories and indoor exposure models.

# Chapter 6: AMS Mass Spectral Profiles of South Asian Combustion Sources

## 6.1 Relevance and status

Like Chapter 5, this work is based on measurements conducted as part of the Nepal Ambient Measurements and Source Testing experiment (NAMaSTE) with on-line aerosol and gas-phase instrumentation. This chapter focuses on mass spectral profiles retrieved from an aerosol mass spectrometer that was part of aerosol sampling system. The mass spectral profiles are important results that can be used for comparison to other similar emission measurements or used in ambient source apportionment studies conducted with an AMS in South Asia and in the developing world. The work presented in this chapter is currently in manuscript form and will be distributed to co-authors by the time this dissertation is published. The manuscript will likely be submitted to Atmospheric Chemistry and Physics and currently have the following citation:

> Goetz, J. D., Giordano, M. R., Stockwell, C. E., Christian, T. J., Maharjan, R., Adhikari, S., Bhave, P. V., Praveen, P. S., Panday, A. K., Jayarathne, T., Stone, E. A., Yokelson, R. J., and DeCarlo, P. F.: Speciated On-line PM1 from South Asian Combustion Sources: Part II, AMS Mass Spectral Profiles and Wavelength Dependence, in preparation, 2017.

## 6.2 Background

Aerosol emissions from prevalent but poorly understood combustion sources in South Asia impact indoor health (Chen et al., 1990), influence local and regional and regional air quality (Guttikunda et al., 2014;Lelieveld et al., 2001;Ohara et al., 2007;Panday and Prinn, 2009) and have uncertain direct and indirect climate forcing impacts (Lawrence and Lelieveld, 2010). The persistent use of solid fuels in the form of biomass or coal is common throughout South Asia in the industrial sector (Pandey et al., 2014;Reddy and Venkataraman, 2002;Weyant et al., 2014) and is predominant for residential cooking and heating in the region (Venkataraman et al., 2005;World Health Organization, 2006). Because solid fuel combustion is a strong emitter of gaseous and particle phase pollution, residential solid fuel use has been ranked the primary risk factor for disease in South Asia (Lim et al., 2012) and is a major source of emissions for the region (Streets et al., 2003). In addition to solid fuel combustion, the combustion of petroleum-based fuels with light and heavy-duty vehicles is a major source of aerosol pollution in Asia and has been increasing (Kumar et al., 2015;Kurokawa et al., 2013). However, because the chemical characteristics and extent of primary aerosol emissions from solid biofuel and fossil fuel combustion in South Asia are poorly understood there is uncertainty in the relative contribution of the two emission sources, which has led to differences in emission inventories as well as contradictory results from top-down and bottom-up regional emission estimates (Gustafsson et al., 2009;Lawrence and

Lelieveld, 2010). The uncertainties in the aerosol emission inventories of South Asia indicate that there is a need for improved source apportionment in the region. Additionally, the limited source apportionment studies that have been conducted reveal that variability in the chemical profiles of aerosol emissions from South Asian combustion sources have led to additional unknowns in apportionment models (Chowdhury et al., 2007;Stone et al., 2010).

To expand the current understanding of atmospheric pollution in South Asia, field research was conducted as part of the Nepal Ambient Monitoring and Source Testing Experiment (NAMaSTE) in Nepal in 2015. As indicated by it's name, the NAMaSTE had two major components: (1) ambient monitoring in the Kathmandu Valley to investigate ambient air quality and for source apportionment modeling, and (2) to characterize aerosol and gas-phase emissions from important and under characterized emission sources in South Asia. The investigated sources included brick-making kilns, agricultural residue burning, traditional and improved cookstoves operated with a variety of fuels, open garbage burning, diesel powered ground water pumps used for crop irrigation, and idling motorcycles. Detailed descriptions of the investigated emission sources can be found in the companion papers Stockwell et al. (2016) and Jayarathne et al. (2017). The objective of this work is to use on-line aerosol measurements to characterize the chemical composition of submicron aerosol ($PM_1$) from the investigated emission sources and to evaluate molecular tracer compounds. In this work, aerosol mass spectrometry is used to report the composition of non-refractory $PM_1$. This work is completed in tandem with Part 1 of the study, which assessed speciated $PM_1$ emission factors using on-line aerosol and gas-phase instrumentation (Goetz et al., 2017b). Other NAMaSTE companion papers that were involved with the source testing aspect of the campaign include Stockwell et al. (2016), who reported gas-phase emission factors and aerosol optical properties, and Jayarathne et al. (2017), who reported off-line filter-based emission factors of fine aerosol ($PM_{2.5}$), organic carbon, elemental carbon, and trace organic and metal aerosol components. This work bridges between the NAMaSTE source testing and ambient source apportionment work by Werden et al. (in preparation) that took place in the Kathmandu Valley in Nepal. Additionally, the AMS mass spectral profiles reported in this work are important standards for similar ambient measurements that may take place in South Asia in the future.

## 6.3 Methods

The NAMaSTE source sampling took place in April 2015 in several regions of Nepal including the Kathmandu Valley, Central Nepal, and the Tarai region that is part of the Indo-Gangetic Plain bordering India. Engine exhaust sources included two diesel powered ground water pumps that are used for crop irrigation and four idling four-stroke motorcycles sampled directly after servicing. We sampled two brick kilns, which included a traditional batch style clamp kiln and a more advanced continuous firing forced draft zigzag kiln (Manadhar, 2013). Both kilns were

fueled with coal, but the clamp kiln was also co-fired with hardwood and bagasse was used as a starter fuel at the zigzag kiln. Several types of open garbage burning were sampled including two mixed refuse piles, segregated plastics, which was primarily composed of plastic films, and segregated metalized plastic or foil "chip bags". The refuse mixes were composed of unmeasured quantities of paper, cardboard, plastics, food waste, yard waste, and other common household garbage. Biomass burning sources included crop residue burning, and cooking stoves. The agricultural residue included a mix of wheat straw, lentils, mustard, and grasses. Other segregated burns included wheat straw, mustard, and locally sourced grasses. Cooking stoves were sampled in the field at residences in the Tarai region and in a lab setting at the Nepal Renewable Energy Test Station (RETS). The field-tested samples include two single-pot traditional mudstoves fueled with either hardwood (mostly Baikano), sticks and twigs (mostly *Shorea robusta*), or dung logs, and one two-pot traditional mudstove co-fired with hardwood and dung logs. None of the field-tested stoves had a chimney and all tests but the single-pot dung-burning test were conducted during either the morning or evening cook cycles. The cooking typically consisted of rice, lentils, and curry. Meat cooking or deep-frying were not sampled during these tests which indicates that the food cooking likely had little impact on the organic aerosol emissions compared to the fuel. It should be noted that an attempt was made to sample well mixed emissions from the field-tested cookstoves similar to what a resident would typically exposed to during a cook cycle. The lab-tested traditional cookstoves included a single-pot mudstove, and a three stone cooking fire. Each traditional stove was fueled with fuelwood, dung, or a mix of the two. The lab-tested improved cookstoves include a mudstove with a chimney fueled with hardwood and dung, an Envriontech natural draught stove fueled with hardwood and dung, a forced draft stove fueled with hardwood, a bio-briquette charcoal stove, a Bhuse Chulo fueled with sawdust and hardwood, and a biogas stove. Details on sampling durations and sampling methods at each emission source can be found in Part 1 of this study (Goetz et al., 2017b), whereas details on the operation and fuels of each source can be found in the companion paper (Stockwell et al., 2016). The on-line sampling was conducted with a dilution system to simulate end-state particle-to-gas partitioning of semivolatile organic compounds contained in a cooled and dilute emission plume. Dilution factors ranged from ~20:1 to 1:1 with an average a 10:1 and where chosen based on plume proximity and source strength.

### 6.3.1 Instrumentation

Aerosol mass spectral profiles were retrieved using an Aerodyne Inc. "mini" aerosol mass spectrometer (mAMS). The mAMS is functionally similar to a unit mass resolution time-of-flight aerosol mass spectrometer (c-TOF-AMS) (Drewnick et al., 2005), but with a more compact vacuum chamber and a smaller time-of-flight mass spectrometer. Additionally, the body, the split-cell turbo vacuum pump, and electronics are similar to an Aerodyne Inc.

time-of-flight aerosol chemical speciation monitor (TOF-ACSM) (Fröhlich et al., 2013), but the mAMS contains a chopper system for particle time-of-flight sizing and aerosol signal control in addition to a more advanced data acquisition card. The mAMS was operated in mass spectrum mode and all mass spectra were averaged to an effective sampling rate of 0.1 Hz. All mass spectra were collected at a mass to charge (m/z) range of 10 to 295 at unit mass resolution (UMR). The tungsten vaporizer was operated at 600ºC. All data processing and analysis was done in Igor Pro 6.3 (Wavemetrics, Lake Oswego, OR) using standard TOF-AMS analysis software SQUIRREL v1.57I and PIKA v1.16I. Although the mAMS is an UMR spectrometer, the data was processed using high-resolution peak fitting in the PIKA module to reduce fragmentation table errors due to high organic loading. High-resolution treatment of UMR data has previously been performed by other researchers using the TOF-ACSM (Fröhlich et al., 2013). Coincident carbon dioxide ($CO_2$) measurements using a Picarro Inc. cavity ring down spectrometer (CRDS) were used for time-dependent correction of gas-phase loading at m/z 44.

## 6.4 Results and Discussion

The average UMR mass spectral profiles of organics, sulfate, nitrate, chloride, and ammonium of the field-tested emissions can be found in Fig. 6.1 as fractions of total non-refractory submicron aerosol (NR-$PM_1$) mass. The mass spectral profile for a charcoal-fueled cookstove sampled at RETS can also be found in Fig. 6.1 and was included because charcoal burning was not sampled in the field. Generally, organic aerosol comprised the largest fraction of the non-refractory emissions with the exception of sulfate at the coal-fired zigzag kiln (Fig. 6.1p). Inorganic chloride and ammonium were found to make up a large fraction of NR-$PM_1$ emissions from the traditional biomass burning sources (e.g. crop residue burning and biomass fueled cookstoves) and the clamp kiln. Open garbage burning was also observed to have a significant fraction of chloride and the engine exhaust sources were observed to have negligible fractions of inorganic aerosol. Fuel-based emission factors and size distributions for the measured NR-$PM_1$ species can be found in the companion paper (Goetz et al., 2017b). A discussion of the mass spectral profiles for each source type can be found below.

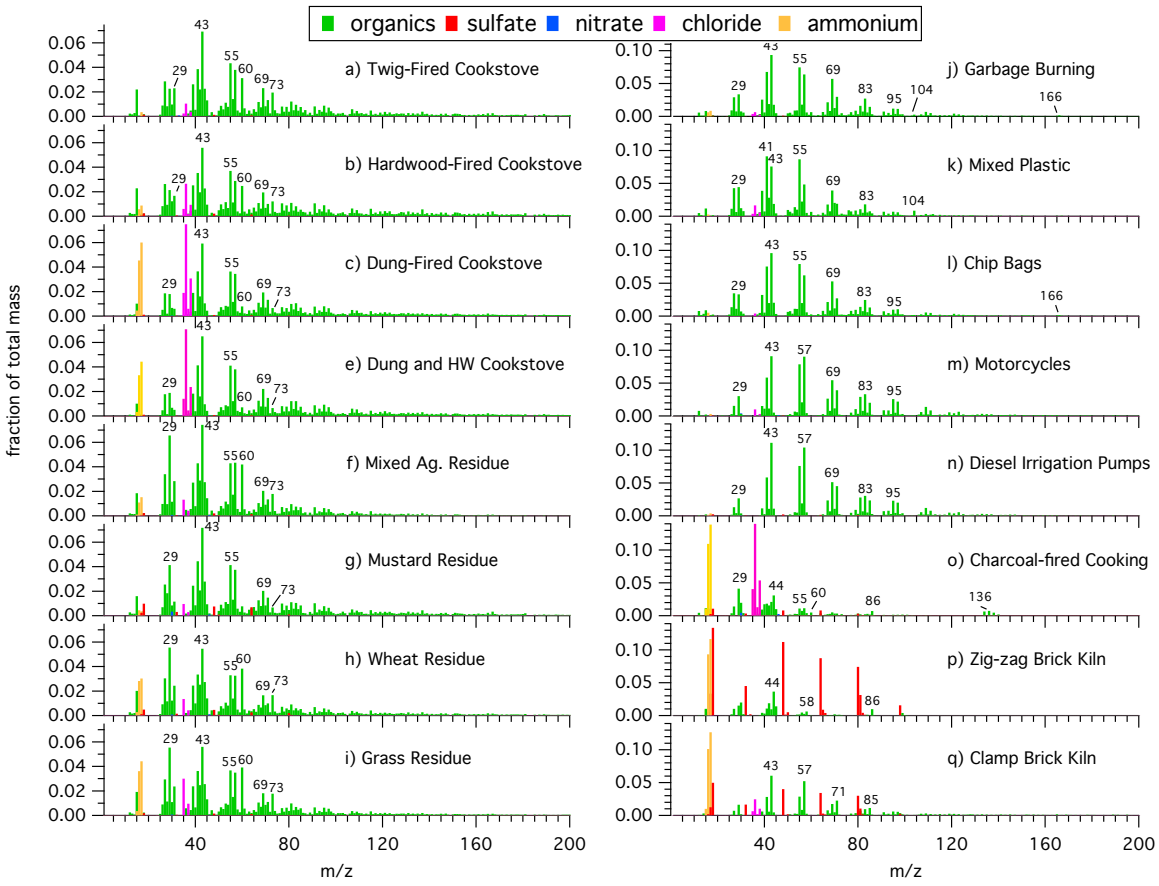


**Figure 6.1. Average Mass spectra of Non-refractory Submicron Aerosol Emissions**
Displayed as a function of average total mass from NAMaSTE field-tested emission sources measured with the mAMS.

## 6.4.1 Wood-fueled Cookstoves

Figure 6.2 shows the average NR-$PM_1$ mass spectra for the wood-fired cookstove emissions measured in the field and at RETS. The mass spectra indicate that similar fragmentation patterns existed with the organic fraction and that there were dissimilarities in the inorganic fraction between the stove types. The differences in the inorganic fractions and specifically with ammonium and chloride are thought to be due to the differences in the elemental composition of the fuel. However, differences in phase partitioning due to variance in dilution could also be a contributing factor. The organic aerosol fragmentation followed what has previously been observed by other studies with biomass burning and with wood burning specifically (Alfarra et al., 2007;Ng et al., 2011;Schneider et al., 2006).

For example, organic mass spectral peaks at m/z 29 ($C_2H_5^+$ and $CHO^+$), m/z 55 ($C_4H_7^+$ and $C_3H_3O^+$), m/z 57 ($C_4H_9^+$ and $C_3H_5O^+$), m/z 69 ($C_5H_9^+$ and $C_4H_5O^+$), 60 ($C_2H_4O_2^+$), m/z 73 ($C_3H_5O_2^+$), 91 (benzyl ion, $C_7H_7^+$), m/z 115 ($C_9H_7^+$ and $C_8H_3O^+$) and m/z 137 (likely $C_8H_7O_2^+$) have previously been observed from wood burning (Schneider et al., 2006). Levoglucosan, a by-product from the pyrolysis of cellulose, has been shown to produce the organic ion fragments at m/z 29, 60, and 73, and is a well-documented tracer compound for biomass burning (Alfarra et al., 2007;Simoneit et al., 1999). Ion fragments m/z 55 and 69 make up part of the UMR ion series $C_nH_{2n-1}^+$ and $C_mH_{2m-1}CO^+$, and m/z 29 and 57 make up part the ion series $C_nH_{2n+1}^+$ and $C_mH_{2m+1}CO^+$. Both ion series are typically produced from electron impact ionization (EI) of saturated hydrocarbon compounds including alkanes, alkenes and cycloalkanes (Mohr et al., 2009). Ions found at m/z 91, m/z 115, and m/z 137 are thought to be from the combustion of lignin, a fiberous compound that in found in plants, and have previously been observed from aerosolized lignin powder mass spectrum retrieved from the AMS mass spectral database (Ulbrich et al., 2009;Ulbrich et al., 2017)

The organic profiles from the two field-tested single-pot mudstoves indicate that there was excellent correlation in organic aerosol composition between the stick and twig fueled emissions and the hardwood fueled emissions (Pearson's r = 0.99). A linear fit of the data did however produce a slope of 1.09 with the y-intercept held to zero, indicating that some small differences in the profiles existed. The linear fit slope >1 was because a 6% greater organic fraction was found at amu values between 100 to 200 in the hardwood burning emissions compared to the stick burning emissions. The fractional differences in mid-range amu values between cookstoves were likely related the burn conditions observed with the two stoves. Gas-phase measurements by Stockwell et al. (2016) found that the average modified combustion efficiency (MCE = $\Delta CO_2/(\Delta CO+\Delta CO_2)$), denoted as MCE, were observed to be 0.914 for hardwood burning and 0.933 for stick and twig burning. The MCE estimates suggest that the less complete combustion observed with the hardwood-fueled cookstove was responsible for the enhanced organic fraction between m/z 100 and m/z 200. Conversely, a slightly larger organic fraction was found at amu values above 200 from stick burning compared to hardwood burning (0.2%), which have previously been associated with high molecular weight polycyclic aromatic hydrocarbons (PAH) (Dzepina et al., 2007). Indicating that stick-burning emissions had a slightly larger compositional fraction of large molecular weight organic compounds, and likely PAHs, compared to hardwood burning. High molecular weight PAH compounds have previously been associated with bark burning (Weimer et al., 2008) and therefore the larger fraction observed with stick burning was likely due to the larger fraction of bark contained in the stick and twig fuel compared to the hardwood fuel.

Comparisons of the hardwood-fueled traditional and improved cookstoves at RETS to the field-tested hardwood fueled stove indicated that there is good correlation between the tests with Pearson's r values ranging from 0.87 to 0.93 (Fig. 6.2). Additionally, the linear regression slopes >1.16 indicates that some differences existed between

the emission sources. One major difference between the field and lab mass spectra was the enhanced organic m/z 29 fraction observed with the lab-tested stoves. The field-tested stove observed an average *f*29 (fraction of m/z 29 to total organic mass) of 0.023 and m/z 43 was the dominant organic peak in the mass spectrum. The lab-test stove emissions, however, were observed to have the largest organic peak at m/z 29 and the average *f*29 ranged from 0.067-0.087 for the improved cookstoves and was 0.082 for the three-stone traditional stove. In addition to differences in individual organic peaks, the lab-tested cookstoves were observed to have a reduced fraction of organics at amu values greater than 100. The percentage of organic mass above m/z 100 ranged from 13% to 18% with the lowest percentages observed from the three-stone fire and the forced-draft improved stove compared to the 26% observed from the field-tested stove. The lab-test stoves were observed to have more efficient burn conditions with average MCE values ranging from 0.955-0.984 (Fig. 6.2) (Stockwell et al., 2016). Therefore, the lower fraction of high molecular weight ion fragments combined with the larger *f*29 values observed from the lab-tested stoves suggests less complex and more easily fragmented organic functional groups were contained in the lab tested aerosol emissions compared to the field-tested stove, which was likely due to the increased efficiency of the lab tested stoves. Figure 6.2 shows that similar results were observed in comparisons between the field-tested stoves and lab tests of Puerto Rican hardwood burning and average ambient observations of biomass burning organic aerosol (BBOA) (Ng et al., 2011), both of which were retrieved from the AMS mass spectral database (Ulbrich et al., 2009;Ulbrich et al., 2017). The results reveal that real-world residential cooking with a single-pot traditional mudstove fueled with wood produces some unique mass spectral characteristics compared to other types of wood burning. The emissions of more complex organic functional groups by traditional mudstoves and possibly increased emissions of PAHs should therefore be considered in indoor exposure modeling and in source apportionment studies.

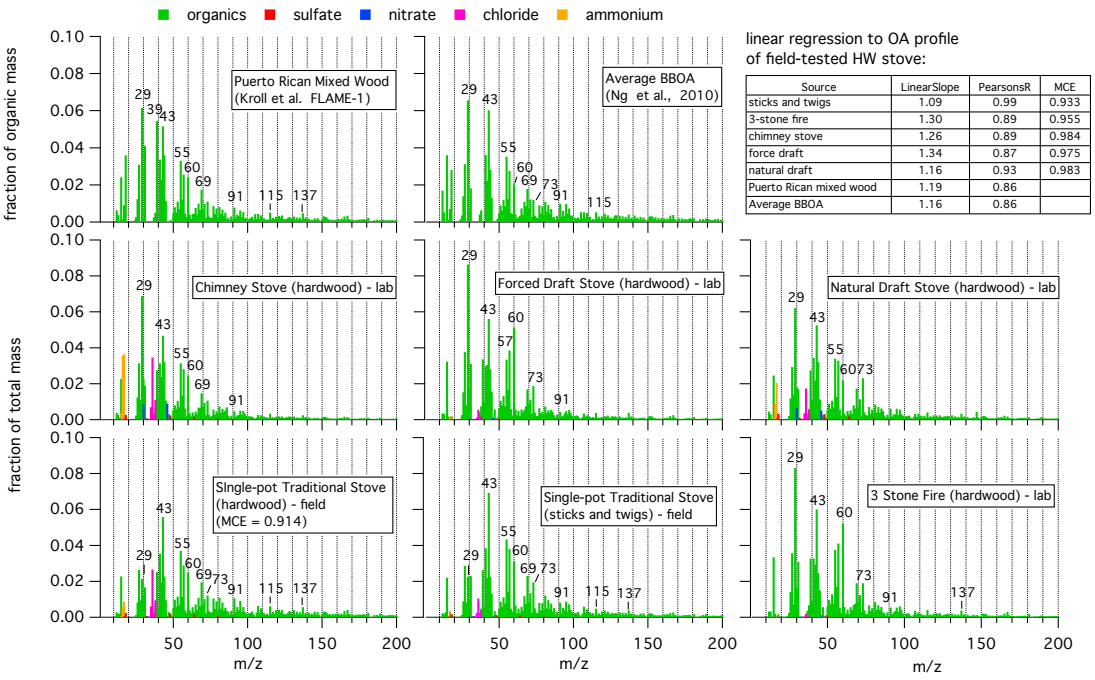


**Figure 6.2. Hardwood Burning Mass Spectra**
Average mass spectra for non-refractory submicron aerosol emissions from NAMaSTE field-tested and lab-tested wood-fueled cookstoves measured with the mAMS. The inset table provides linear fit slopes and Pearson's r values from comparisons to the field-tested hardwood stove organic mass spectra. Modified combustion efficiency (MCE) values are retrieved from Stockwell et al. (2016).

## 6.4.2 Dung-fueled Cookstoves

The mass spectral profiles for emissions from the field and lab-tested cow dung fueled cookstoves and profiles for wood and dung co-fired cookstoves can be found in Figure 3. The dung burning emissions are characterized as containing large fractions of inorganic ammonium and chloride (Fig. 6.3). Based on the average mass spectra from the dung-fueled cookstoves the chloride content ranged from 9-23% of the total NR-$PM_1$ mass with an average of 15%. The ammonium ion content ranged from 7-20% of total NR-$PM_1$ mass with an average of 12%. In comparison, the field-tested hardwood-fueled stove emissions were observed to contain 1.5% ammonium and 4.3% chloride, and lower fractions were observed from most of the other hardwood-fueled stoves (Fig 6.2.). The observed inorganic fraction from the dung-fueled stoves appeared to be independent of sampling location, stove type, and dung content of the fuel. In addition to containing large fractions of chloride, the chloride itself was composed of >80% HCl (m/z 36 and the

isotope at m/z 38) suggesting that there was some amount of acidity associated with the aerosol emissions. The size distribution data presented in the companion paper show that the chloride aerosol was found at similar sizes to the ammonium aerosol indicating that the components were likely internally mixed and the chloride was neutralized to some extent by the ammonium cations (Goetz et al., 2017b).

The organic aerosol profiles from dung-fueled emissions were found to have similar patterns to wood burning emissions but with some key differences (Fig. 6.1). Based on the eight dung-burning samples from both the field and lab, organic aerosol mass spectra had major peaks associated with the ion series $C_nH_{2n-1}^+$, $C_mH_{2m-1}CO^+$, $C_nH_{2n+1}^+$, and $C_mH_{2m+1}CO^+$ (Fig. 6.3). The dung burning samples also had notable peaks from ions at m/z 60, m/z 73, m/z 91, and m/z 115, which had previously been observed with the wood burning (Fig. 6.1), and an isolated peak at m/z 165 (Fig 6.3). Generally, the organic profiles had similar patterns and all of the samples were well correlated to the field-tested dung-fueled cookstove with Pearson's r values ranging from 0.95-0.98 (Fig 6.3). The best correlation was observed between organic emission from the two field-tested samples indicating that dung was the primary emitter from the two-pot stove and wood burning had little influence on the co-fired organic profile. Unlike with the hardwood-fueled samples shown in Figure 6.2, the burn conditions appeared to have little impact on the organic mass spectral profiles from dung burning based on MCE values obtained from Stockwell et al. (2016) and displayed in the inset table of Fig. 6.3. Additionally, the levoglucosan ions emitted from dung burning (m/z 60 and 73) were observed to comprise a smaller fraction of the total organic mass compared to hardwood burning. For example, the *f*60 from the dung burning samples had an average of 0.012, compared to an *f*60 of 0.026 from the hardwood-fueled stove emissions observed in the field. *f*73 was observed at an average of 0.009 from dung burning compared to the field-tested hardwood burning which had an *f*73 of 0.13. Since the levoglucosan ions are used as tracers for traditional biomass burning and to understand the photochemical aging of biomass burning aerosol (Cubison et al., 2011), the low fractions observed from dung burning could complicate ambient observations when dung burning is part of a source profile. It should be noted that aside from the low fraction of levoglusocan ions there are few other distinctions between organic aerosol of the field-tested wood burning samples and the dung burning samples (Pearson's r = 0.95). Although one profile characteristic that was observed from dung burning and should be considered further as an organic tracer for dung burning is a m/z 165 peak isolated from m/z 167. The ion fragment observed at m/z 165 with co-fired dung and hardwood burning produced an average organic fraction of 0.0025 and the field-tested dung burning produced an average *f*165 of 0.0029. Wood burning also produced an average *f*165 of 0.0024, but was observed to be associated with an enhanced *f*167 and produced an average *f*165/*f*167 ratio of 0.89. The ion fragment at m/z 167 has previously been observed with wood burning but the parent molecule was unidentified (Schneider et al., 2006). With dung burning, however, the same relationship between ions at m/z 165 and m/z 167 was not observed and the average *f*165/*f*167 was 1.38 for co-fired

dung burning and 1.52 for the field-tested dung-fueled cookstove emissions. Because we sampled the emission using an UMR instrument and did not have high-resolution capabilities instrument we cannot identify the organic ion responsible for enhancements at m/z 165 and further confirmation is needed before the ion pair should be considered as a standalone mass spectral tracer in ambient source apportionment. Overall, since no strong tracer ion or unique ion series appears to stand out with dung burning we suggest that combination of high inorganic fractions and large m/z 165 fractions with low detection of levoglucosan ions be used to help deconvolve wood burning and dung burning signatures in ambient datasets.

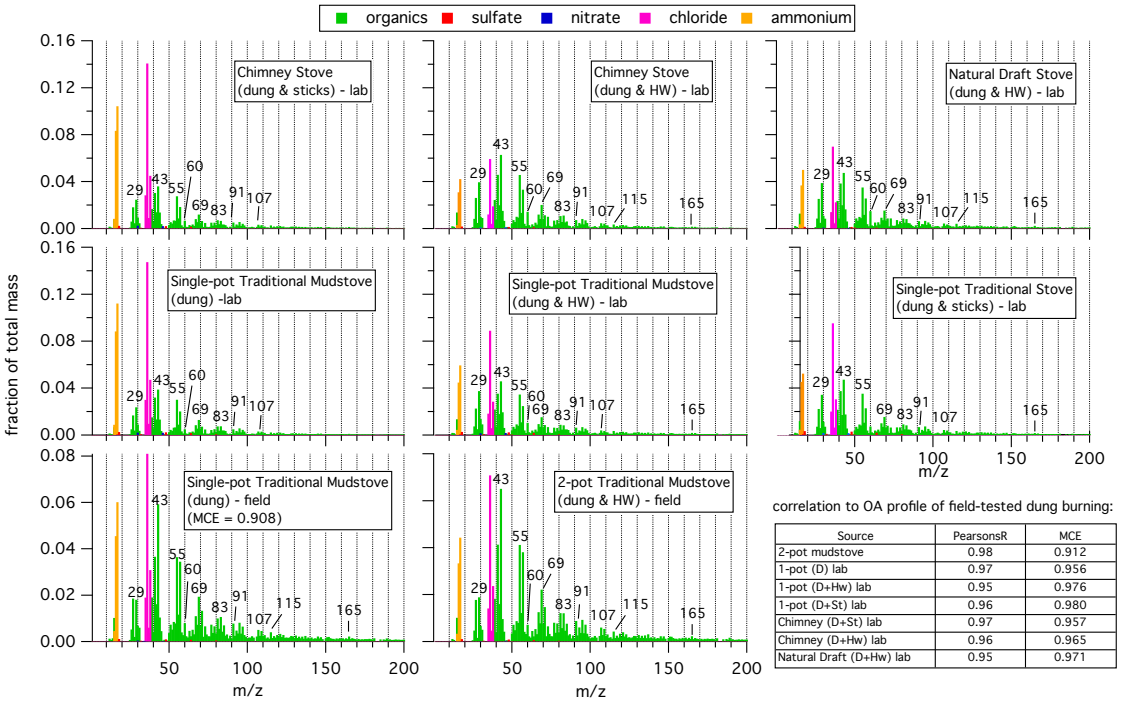


| Source | PearsonsR | MCE |
|---|---|---|
| 2-pot mudstove | 0.98 | 0.912 |
| 1-pot (D) lab | 0.97 | 0.956 |
| 1-pot (D+Hw) lab | 0.95 | 0.976 |
| 1-pot (D+St) lab | 0.96 | 0.980 |
| Chimney (D+St) lab | 0.97 | 0.957 |
| Chimney (D+Hw) lab | 0.96 | 0.965 |
| Natural Draft (D+Hw) lab | 0.95 | 0.971 |

**Figure 6.3. Dung Burning Mass Spectra**
Average mass spectra for non-refractory submicron aerosol emissions from NAMaSTE field-tested and lab-tested dung-fueled cookstoves measured with the mAMS. The inset table provides linear fit slopes and Pearson's r values from comparisons to the field-tested dung fueled stove organic mass spectra. Modified combustion efficiency (MCE) values are retrieved from Stockwell et al. (2016).

### 6.4.3 Improved Cookstoves with Other Fuels

Emissions from other improved cookstoves including a Bhuse Chulo, a biogas stove, and a biobriquette stove were sampled at RETS. Bhuse Chulo is a type of standalone insulated vertical combustion chamber stove and the stove was fueled with sawdust. The biogas stove was fueled with locally produced cow dung biogas (likely primarily composed of methane) and it is important to note that NR-$PM_1$ mass was not observed above the background when the biogas stove was operational. Therefore, we cannot comment on the mass spectral profile from biogas burning. The biobriquette stove was fueled with charcoal briquettes.

The average organic mass spectrum from the sawdust-fired Bhuse Chulo can be found in Fig. 6.4. The Bhuse Chulo emissions had similar mass spectral characteristics to what had been observed from the hardwood and stick wood-fired cookstoves and contained similar organic fragmentation patterns with amu peaks associated with the saturated hydrocarbon ion series and levoglucosan (Fig. 6.4). The Bhuse Chulo emissions, however, exhibited enhancements in the common levoglucosan peaks (m/z 29, 60, 73, etc.), and were observed to contain a lower fraction of mass at m/z values above 100 compared to the field-tested hardwood fueled cookstove (Fig 6.4c.). The average *f*60 of the Bhuse Chulo emissions was 0.036, which was 22% greater than the combined average of the wood-fired cookstoves and a larger fraction that was observed from any of the traditional cookstove experiments. The low fraction of mass above m/z 100 (15%) indicates that like the other improved cookstoves, the increased combustion efficiency compared to the traditional stoves (MCE = 0.990; Stockwell et al. (2016)) produces low molecular weight organic ions. Additionally, the sawdust-fired Bhuse Chulo was observed to have low organic aerosol emission factors compared to the tested traditional cookstoves (Jayarathne et al., 2017) and was observed to have the lowest carbon monoxide (CO) emission factor of the NAMaSTE tested solid fuel cookstoves (Stockwell et al., 2016). The low emission factor of low molecular weight organic aerosol combined with low emission factor of CO of the Bhuse Chulo suggests that from an air quality standpoint the stove is a good alternative to traditional cookstove technologies.

The NR-$PM_1$ emissions from the charcoal biobriquette stove produced unique mass spectra compared to the other NAMaSTE tested cookstoves and to our knowledge this work is the first to characterize the mass spectral profile of charcoal combustion emissions. Generally, the charcoal emissions were observed to have high inorganic fractions and the average non-refractory mass was comprised of 42.3% organic, 27.5% chloride, 25.9% ammonium, 3.9% sulfate, and 0.3% nitrate (Fig. 1o). The observed chloride and ammonium fraction were the largest of any of the combustion sources investigated in this work. In addition containing a unique inorganic fraction, the average organic spectrum was observed to have distinct fragmentation patterns. Major organic peaks included ion fragments common with biomass burning (m/z 29, m/z 57, m/z 60, etc.), but also included characteristics peaks at m/z 44, m/z 64, m/z 86, and a grouping of peaks centered at m/z 136 (Fig. 4b). Many of these organic peaks, and others not listed but observed

with charcoal emissions, were not observed to the same extent from hardwood burning (Fig. 4d). Additionally, some organic ions found at m/z values greater than 200, which have been associated with PAHs (Dzepina et al., 2007), were observed at a higher fraction from charcoal burning than wood burning (Fig. 4d). Based on the high-resolution peak fitting estimates of the UMR data, the organic ions at m/z 44, m/z 64, and m/z 84 correspond to nitrogen containing organics $C_2H_6N^+$, $C_4H_2N^+$, and $C_5H_{12}N^+$, respectively. An example of the peak fitting estimates at m/z 44 can be found in Fig. 6.5. The figure shows that $CO_2^+$, $C_2H_4O^+$, and $C_2H_6N^+$ produces a good fit to the raw UMR difference signal at m/z 44, which indicates that $C2H5N^+$ is a likely a major component of the organic signal at that position. Similar results were observed at m/z 64 and m/z 86 and the listed ions have previously been attributed to nitrogen-containing organic compounds in ambient datasets (Huffman et al., 2009;Zhang et al., 2011). Additionally, electron impact ionization of aliphatic primary amides have been observed to generate peaks at m/z 44 and m/z 86 (McLafferty and Turecek, 1993). We could not identify nitrogen-containing organic ions at m/z 136 because of the larger peak width at m/z 136 compared to the lower amu peaks, and the peak has not been observed with nitrogen containing organics spectra in the literature. The grouping of organic ions centered at m/z 136 remains unidentified but are possibly due to higher molecular weight nitrogen containing organic ions or are fragments of PAH compounds. More sampling of charcoal emissions are needed to understand if the mass spectral characteristics of biobriquette charcoal combustion observed in this study are ubiquitous with other types of charcoal and under different burn conditions.

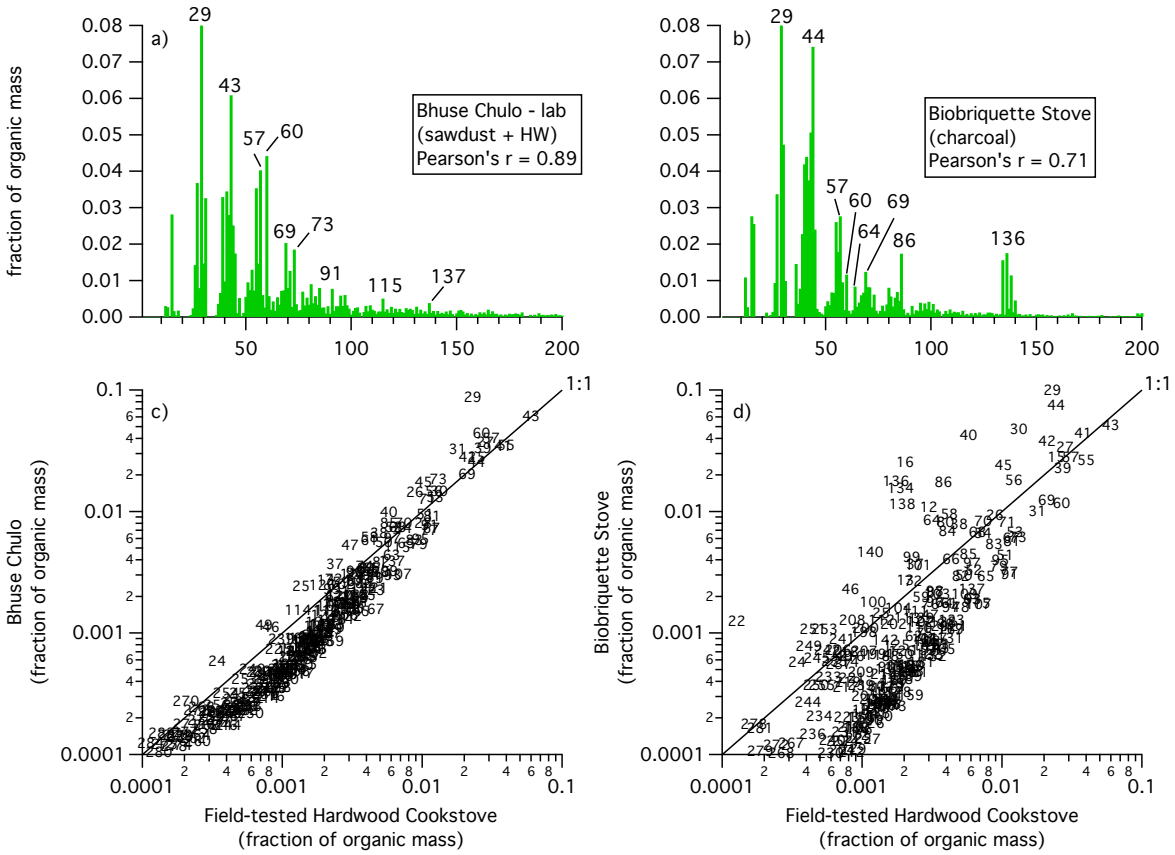


**Figure 6.4. Charcoal and Bhuse Chulo Mass Spectra**
Average mass spectra for organic submicron aerosol emissions from the Bhuse Chulo and Bio Briquette cookstove emissions measured with the mAMS (top panels). Scatter plot of the Bhuse Chulo and Bio Briquette organic mass specta versus the organic mass specta of the hardwood-fired single-pot traditional mudstove emissions measured in the field (bottom panels).

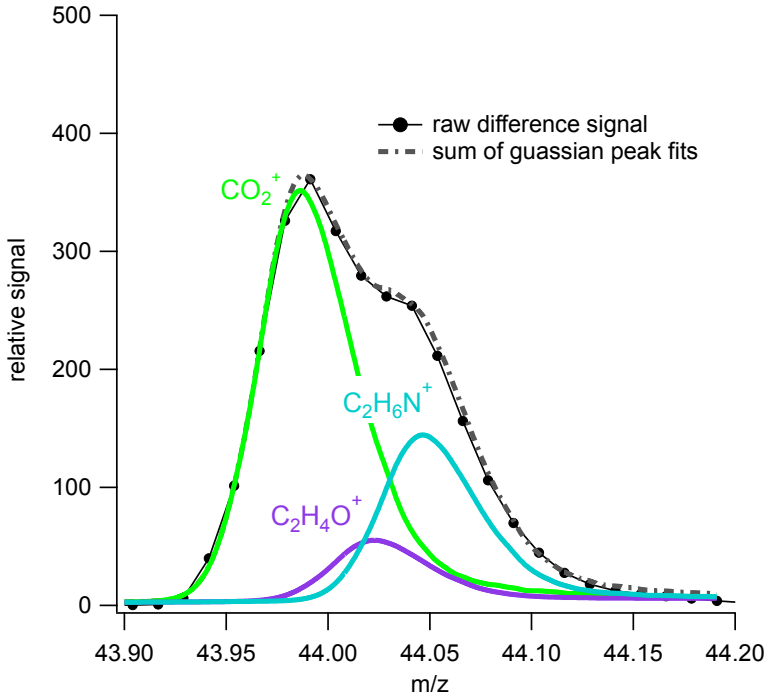


**Figure 6.5. Charcoal Burning m/z 44**

## 6.4.4 Agricultural Residue Burning

The average NR-$PM_1$ mass spectra for the agricultural residue burning samples can be found in Fig. 6.1f-i. The crop residue samples were observed to have mass spectra similar to the wood burning samples with moderate fractions of inorganic compounds and organic fragmentation that features peaks associated with cellulose and lignin combustion (Fig. 6.2). The largest inorganics fraction was observed from grass burning and the emissions were likely well neutralized with an average ammonium fraction of 0.08, an average chloride fraction of 0.04 and nominal fractions of sulfate and nitrate. Neutralized inorganic aerosol was also observed from the mixed residue and wheat residue burns. Mixed residue NR-$PM_1$ emissions were composed of 2.7% ammonium and 1.7% chloride. Wheat residue emissions were composed of 6.0% ammonium and 1.7% chloride. Mustard residue emissions were less neutralized and were observed to have inorganic fractions <0.01. The organic aerosol emissions from the crop residue burning samples were observed to have relatively similar mass spectral patterns. Comparisons of organic spectra from the segregated residue burns to the mixed residue burn reveal that the Pearson's r correlation between the samples are >0.9 with 0.94 for

mustard residue, 0.99 for wheat residue, and 1.00 for grass residue. The lower correlation associated with the mustard residue and the mixed residue was due to the lower fraction of organic ions associated with levoglucosan and the 10% greater fraction of organic ions found at amu peaks above 100.

### 6.4.5 Open Garbage Burning

The open garbage burning samples were characterized as having low inorganic aerosol fractions and organic aerosol with major mass spectral patterns that follow the saturated hydrocarbon ion series (Fig 6.1h-j). The mixed garbage samples were visually observed to contain biomass material like paper and yard waste, but the mixes were found to have small fractions of levoglucosan and lignin organic ion fragments that have been discussed with the cookstoves and with agricultural residue burning. Based on high resolution peak fitting estimate of the UMR data the garbage burning samples had larger fractions of $C_nH_{2n+1}^+$ and $C_nH_{2n-1}^+$ ions compared to their oxygenated ion series counter parts, which were observed at almost equal fractions to the alkyl ions in the biomass burning samples. Consequently, other materials contained in the mixes (e.g plastics) likely had a large influence on the organic aerosol composition from open garbage burning. The two garbage mixes were found to have differences in aerosol emission factors, which were thought to be due to differences in fuel composition and water content (Goetz et al., 2017b;Jayarathne et al., 2017). Nonetheless, the organic mass spectra for the two mixes were well correlated (Pearson's r = 0.95). The two segregated plastic burns, which included metalized plastic "chip bags" and mixed plastics, were found to have organic mass spectra that were well correlated to the combined mixed garbage samples. The Pearon's r value between the garbage mix and the metalized plastic was 0.99, and the mix was found to be slightly less correlated to the plastic burn with a value of 0.96. The good correlation between the plastic emissions and the mixed garbage combined with the low fractions of organic ions related to biomass burning indicates that plastic burning aerosol dominated the emissions from the sampled garbage mixes.

Several notable high molecular weight organic ions were observed with the open garbage burning samples. Figure 6.6 shows the organic mass spectra between m/z 100 and 295 for open garbage burning and the plastic burning samples and highlights several large organic peaks associated with each source. To identify ion peaks that were unique to garbage burning comparisons are made with mass spectral profiles that have previously been observed with biomass burning and engine exhaust. A standard hydrocarbon like organic aerosol (HOA) profile from Ng et al. (2011) and retrieved from the AMS mass spectral database (Ulbrich et al., 2009;Ulbrich et al., 2017), was used for comparison to engine exhaust. Ambient HOA has been shown to have a strong relationship with gas-phase and organic aerosol emissions from engine exhaust (Zhang et al., 2005b). As seen in Fig. 6.6, the several ion peaks are shared between

HOA and garbage burning at m/z 109 (likely $C_8H_{13}$), m/z 141, m/z 202, and m/z 239. The organic ion fragment at m/z 202 has previously been attributed to PAH compounds with the molecular formula $C_{16}H_{10}$ (i.e. pyrene, fluoranthene, acephenanthrylene) (Dzepina et al., 2007). The peak at m/z 239 has also been attributed to the PAH compounds and is thought to be the [M-1] ion of Methylbenzo[ghi]fluoranthene ($C_{19}H_{12}$) (Dzepina et al., 2007). Because open garbage burning and engine exhaust are commonplace in urban areas of South Asia, the shared UMR ion peaks should not be used as organic tracer ions for garbage burning. In comparison to biomass burning, several comparable high molecular weight ion peaks were observed. Two characteristic peaks located at m/z 252 and m/z 276 have previously been detected with NAMaSTE wood burning organic profiles and have been attributed to several PAH compounds (Dzepina et al., 2007). Another high molecular weight peak that was observed with open garbage burning and wood burning as well as many other source profiles not shown in Fig. 6.6 was m/z 281 (Fig. 6). The organic ion at m/z 281 in addition to ions detected at m/z 221, m/z 207, m/z 147, and m/z 73 have been observed from aerosolized polydimethylsiloxane and from siloxane sampling artifacts due to the use of conductive silicone tubing in sampling inlets (Timko et al., 2009). Because siloxane associated peaks have also been detected from many of the source emissions investigated in NAMaSTE, the peaks observed with the garbage burning samples were likely due to sampling artifacts from small sections of conductive tubing used with the on-line sampling inlet. Still, because organic silicon based materials were possibly present in the garbage mixes, some siloxane mass may have come from the combustion of those materials.

By eliminating ion peaks that have been detected with other sources several organic ion peaks above m/z 100 appear to be distinct to garbage burning and are likely attributed to plastic combustion. Three major peaks that were observed from metalized plastic burning and the mixed garbage were m/z 121, m/z 166, and m/z 193. Because of the large UMR peak width at amu values greater than 100, high-resolution fitting estimates could not provide insight on the organic ions found at the listed ion peaks detected from metalized plastic. However, inferences can be made based on existing literate. For example the organic ion peak at m/z 166 is thought to be due to emissions of the PAH fluorene based on standard EI mass spectra from NIST (Stein et al., 2001). NAMaSTE filter-based measurements by Jayarathne et al. (2017) and filter-based measurements in Mexico by Christian et al. (2010) have revealed that antimony (Sb) is an important marker for open garbage burning. Because Sb has a molecular weight of approximately 121 g $mol^{-1}$ it is possible that surface ionized Sb was misattributed as an organic ion at m/z 121. Detection of similar "semi-refractory" metals with conventional aerosol mass spectrometry has been discussed by Salcedo et al. (2012). Because Sb is semi-refractory and would exhibit slower vaporization in the mAMS compared to organic aerosol, we analyzed the closed m/z 121 decay rate directly after emission sampling when a HEPA filter was inline with the mAMS inlet and compared it to other closed organic signals (Fig. 7). Based on Fig. 6.7 the m/z 121 closed signal exhibited an equivalent exponential decay constant ($\tau$) to the closed organic signal at m/z 43 during the HEPA filter period directly after

sampling the metalized plastic emissions. Additionally, compared to the closed organic signal at m/z 43 for a motorcycle HEPA filter period the τ value of m/z 121 from metalized plastic emissions was almost half (Fig. 6.7). The results indicate that Sb signal from slow vaporization was likely not detected above the large organic instrument background of the mAMS. It is important to note, however, that the Sb was observed to have a τ of 1.3 s in ambient observations made with an HR-TOF-AMS by (Salcedo et al., 2012). Therefore, it is possible that the large instrument background of the mAMS caused by the reduced vacuum capabilities of the mAMS compared to other AMS instruments combined with the large mass loadings from sampling direct emissions, hampered the detection of Sb from open garbage burning. Based on the available information it is unclear if Sb detection with ambient concentrations is possible with a mAMS or TOF-ACSM, which likely limits the use of the instruments for the source apportionment of garbage burning in South Asia.

The only organic ions fragment shared between mixed plastic burning and open garbage burning that was not detected at significant fractions from other sources, including metalized plastic burning, was m/z 104. The large fraction of m/z 104 was due to the styrene ion ($C_8H_8^+$) based on comparisons to NIST EI mass spectra (Stein et al., 2001). The large organic fractions of styrene ions was likely due to the combustion of polystyrene, acrylonitrile butadiene styrene, or similar styrene containing plastics. The styrene peak was also observed from plastic no. 2 burning by (Mohr et al., 2009). Based the mass spectral profiles of open garbage burning, organic ions found at m/z 104 and m/z 166, as well as other peaks discussed above, are good candidate UMR peaks for organic tracer fragments from open garbage burning in South Asia. The use of styrene and fluorene as tracer ions broadens the list of garbage burning tracer molecules, which prior to this work has only included 1,3,5-Triphenylbenzene (TPB). Using TPB as a tracer was proposed by Simoneit et al. (2005) and was detected in NAMaSTE with off-line filter-based methods (Jayarathne et al., 2017). Ion peaks from the EI of TPB were not identified in the organic mass spectra indicating that the high molecular weight tracer compound likely produced ions outside the mass spectral range of the mAMS.

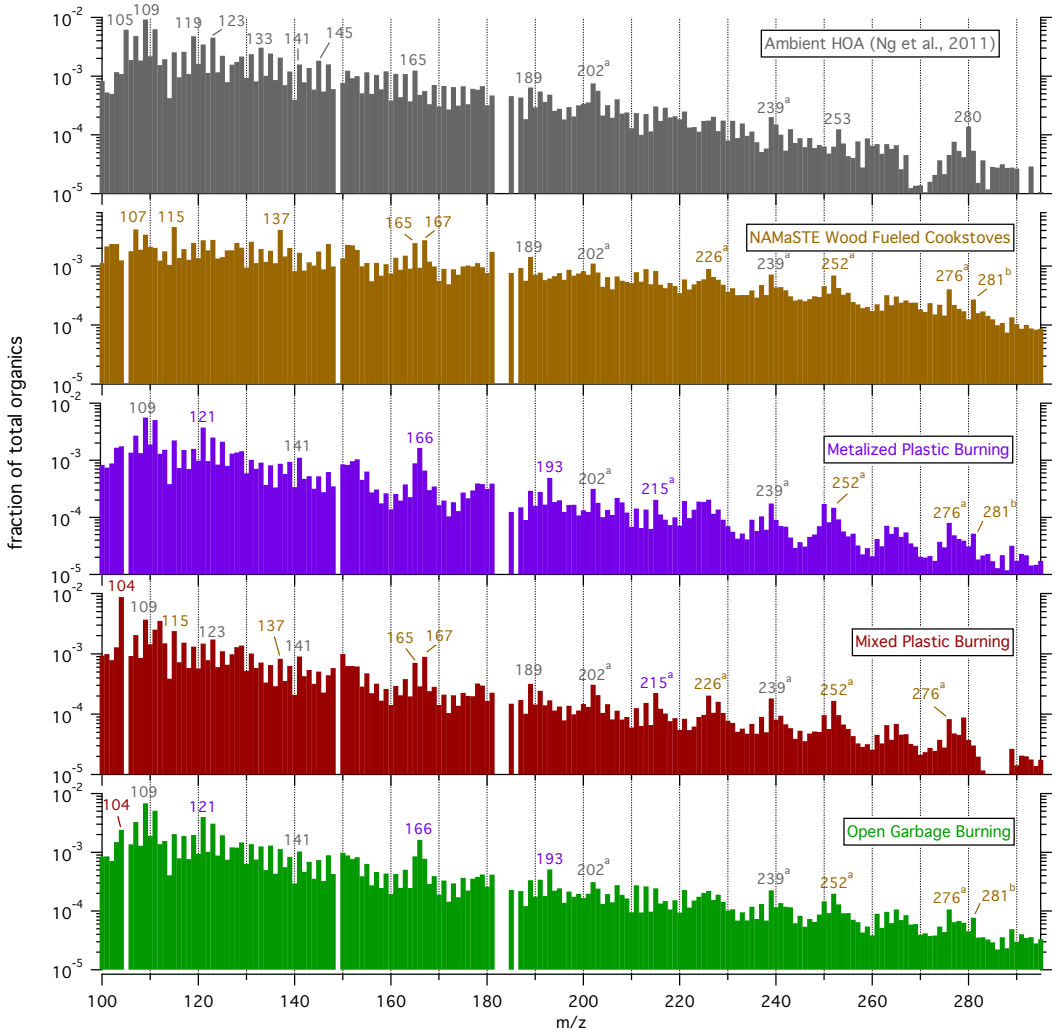


**Figure 6.6. Garbage Burning Mass Spectra**
Average organic mass spectra between m/z 100 and m/z 295 for open garbage burning, plastic burning, NAMaSTE wood fuel burning, and average HOA from Ng et al. (2011). Major peaks are colored by their associated source type. Ions with superscript (a) denote major PAH compounds. Superscript (b) denotes siloxane ions.

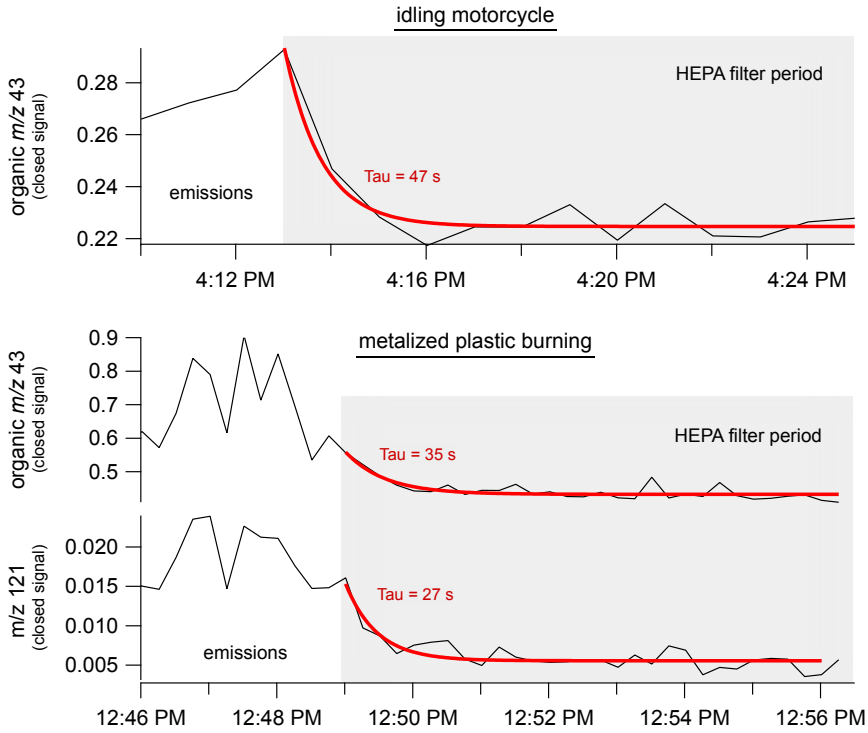


**Figure 6.7. Analysis of Slow Vaporizing m/z 121**
Time series of "closed" organic aerosol signal from an idling motorcycle and metalized plastic burning with exponential decay fit.

## 6.4.6 Engine Exhaust

Two ground water irrigation pumps and four idling motorcycles were the only liquid fuel emission sources sampled by the mAMS during NAMaSTE. Organic aerosol was the dominant fraction of the NR-$PM_1$ emissions from both source types and most inorganic aerosol components were below detection limits (Fig 6.1m-n). The irrigation pumps were diesel powered and produced ~ 5 kVA of power and had different operational lifetimes. One pump was a Kirloskar (model unknown) that was in operation for ~3 years (Pump 1) and the other was a Field Marshall model R170a (Pump 2) that had been recently purchased. Although the newer pump was observed to have a lower organic aerosol emission factor compared to the older pump (Goetz et al., 2017b), the bulk organic mass spectra of the emissions were very well correlated (Pearson's r = 1.00). The average mass spectra from the two pumps had major ion peaks associated with the saturated hydrocarbon series $C_nH_{2n+1}^+$ and $C_nH_{2n-1}^+$ and high-resolution peak fit estimates

indicate that the oxygentated ions comprised a nominal fraction the ion series (Fig. 6.1n). The largest fraction of ion fragments observed with the diesel pump emissions were at m/z 41 ($C_3H_5$+), m/z 43 ($C_3H_7^+$), m/z 55 ($C_5H_7^+$), and m/z 57 ($C_4H_9^+$) with the dominate ions being $C_3H_7^+$ and $C_4H_9^+$ (Fig 6.1n). Similar results have been observed with emissions from diesel vehicles and engine lubricating oil (Canagaratna et al., 2004;Mohr et al., 2009). The organic mass spectra from the combined pump emissions were also well correlated to the average HOA spectrum of Ng et al. (2011) with a Pearson's r of 0.97. Because of the typically low oxygenated ion content at m/z 57 compared to other ions found in the two major saturated hydrocarbon ion series, the ion peak has previously been determined to be useful for the deconvolution of ambient HOA from aged oxygenated organic aerosol (OOA) using positive matrix factorization (Zhang et al., 2005a). Based on the time-resolved mass spectra from all of the sources investigated in NAMaSTE the irrigation pumps were found to have the largest *f57* with a 10$^{th}$ percentile of 0.091, interquartile values of 0.096 and 0.115, a median of 0.105, and a 90$^{th}$ percentile of 0.133. The large *f*57 could therefore be a useful marker for diesel irrigation pumps in ambient datasets collected in agricultural regions of South Asia with limited vehicle use.

Although the bulk organic spectra between the irrigation pumps were well correlated, there were significant differences between the fractions above m/z 200. Figure 6.8 provides a scatter plot the compares the average relative fractions of organic peaks above 200 from the two pumps. The Pump 2 was found to have more than twice the fraction of m/z above 200, which included many PAH ions, and there was significant scatter between the high molecular weight mass spectra. The differences between the two pumps indicate that by unit of organic aerosol mass that the new pump produced more PAH compounds compared to older pump. Similar results were observed between comparisons of mass specta from a diesel rental truck emissions (Mohr et al., 2009) and average HOA (Ng et al., 2011) with the Pump 2 organic spectra above m/z 200 (Fig. 6.8). Based on the emission factor results, Pump 2 was observed to be more efficient have a larger PAH emission factor compared to the older pump (Goetz et al., 2017b;Stockwell et al., 2016). The results indicate that PAH fractions could be useful to make inferences concerning the efficiency of diesel engines or for understanding the influence of high efficiency diesel on ambient measurements. However, differences in PAH fractions due to fuel type, engine type, and oxygenation of ambient organic aerosol cannot be discounted.

The four gasoline powered idling 4-stroke motorcycles did not produce inorganic fractions above detection limits and based on the average organic mass spectra the emissions produced spectral patterns almost identical to the diesel emission (Fig. 6.1m). The average organic mass spectrum was dominated by ions associated with the ion series $C_nH_{2n+1}^+$ and $C_nH_{2n-1}^+$. Based on estimated high-resolution peak fitting of the UMR data, $C_4H_9^+$ found at m/z 57 the most abundance organic ion. The time-resolved data indicates *f*57 had a more narrow range compared to the irrigation pumps with a 10$^{th}$ percentile of 0.088 and a 90$^{th}$ percentile of 0.10, with a median at 0.099. Overall, the average organic mass

spectrum from the motorcycle emissions was well correlated to the average diesel irrigation pump profile with a Pearson's r of 0.98. Furthermore, the average idling motorcycle profile was found to have a similar percentage of ions above m/z 100 (~15%) compared to the irrigation pump profile. The results indicate that from a compositional perspective the liquid fueled engines investigated in NAMaSTE produced similar organic aerosol.

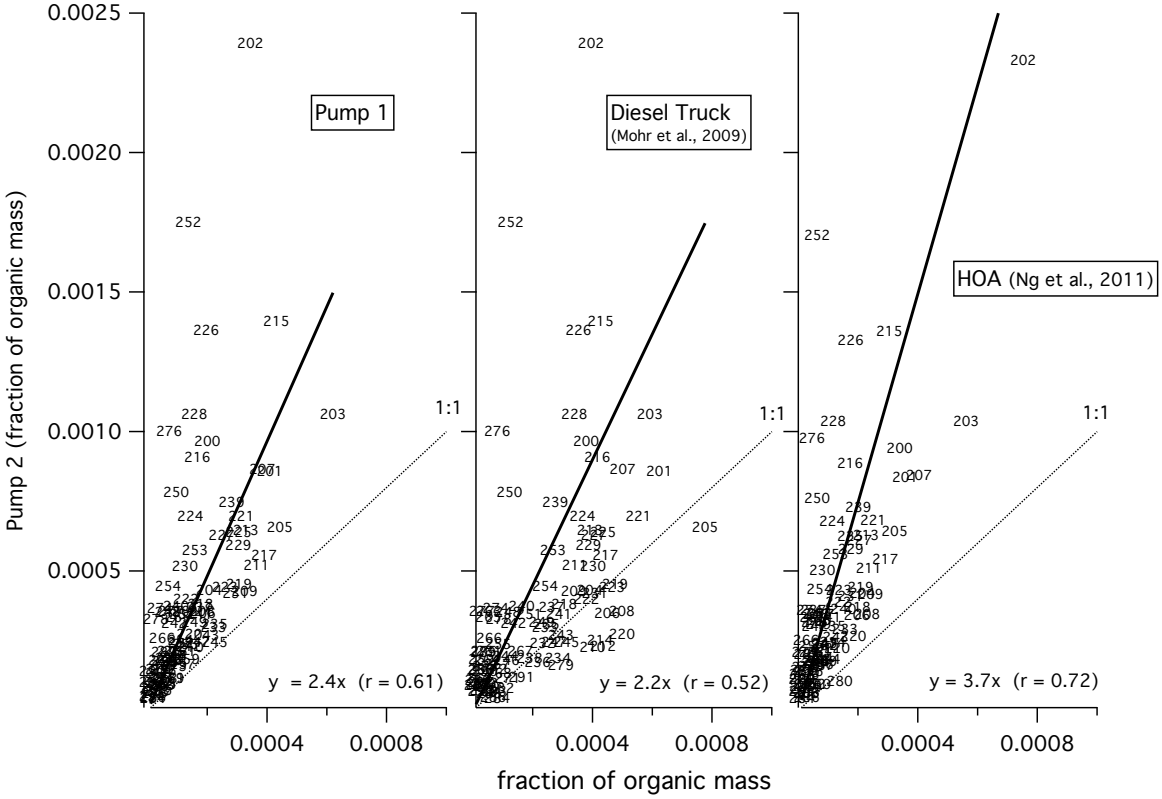


**Figure 6.8. Comparison of Irrigation Pump Mass Spectra**
Scatter plots that compare average organic mass spectrum above m/z 200 from Pump 2 to the organic spectra from other sources. Linear slopes and Pearson's r values are provide in each panel.

## 6.4.7 Brick Kilns

Emissions from a low efficiency batch-style clamp brick kiln that was fired with coal and hardwood were sampled in NAMaSTE. The average mass spectral profile from the kiln emissions shows that inorganic aerosol was a major component of the total NR-$PM_1$ mass at approximately 50% (Fig. 6.1n). Ammonium was the primary inorganic component at ~24.0% of the total mass, followed by sulfate (21.0%), chloride (4.3%), and nitrate (<1%). The large

ammonium fraction indicates that some percentage of the sulfate fraction was likely neutralized and in the form of ammonium sulfate $(NH_4)_2SO_4$ and the remaining fraction was likely in the form of sulfuric acid. The average organic aerosol profile contained patterns that were similar to HOA and engine exhaust (Fig. 6.1) with large fractions observed with the $C_nH_{2n-1}^+$ and $C_nH_{2n+1}^+$ ion series from alkyl fragments. Based on peak fitting estimates very low fractions of the $C_mH_{2m+1}CO^+$ and $C_mH_{2m-1}CO^+$ were observed. The average *f*43 was 0.12 and the average *f*57 was 0.10. Also, like engine exhaust significant fractions of $C_nH_{2n-3}^+$ ions were observed and specifically m/z 67, 71, and 81 (Fig. 6.1q). Large fractions of $C_nH_{2n-3}^+$ have previously been attributed to EI of cycloalkanes (McLafferty and Turecek, 1993). Unlike engine exhaust, however, the alkyl fragment series at $C_5$ and $C_6$ $C_nH_{2n+1}^+$ ions were observed comprise a larger fraction of the organic mass compared to their $C_nH_{2n-1}^+$ counterpart (Fig. 6.1n). Similar alkyl fragmentation has previously been observed with aerosolized diesel fuel (Canagaratna et al., 2004). The clamp kiln emissions were also found to have a 10% larger fraction of high molecular weight organic ions above m/z 100 compared to the average diesel irrigation pump emissions. The low estimated fractions of oxygenated ions at m/z 43, m/z 55 and other ions in the saturated hydrocarbon ion series suggests that the wood fuel may have been limited compared to coal since oxygenated ions in the series are common with the NAMaSTE sampled wood-burning emissions and with BBOA (Ng et al., 2011). Further evidence for the low fraction of wood fuel is demonstrated by the low fraction of levoglucosan ions (average *f*60 = 0.0007) observed in the clamp kiln emissions. There have been limited measurements of coal burning aerosol with AMS instrumentation and to our knowledge this work is the first to characterize direct emissions. One study that deconvolved ambient measurements in China to produce a PMF spectra for coal combustion found characteristic organic peaks at m/z 128 (molecular ion for naphthalene) and m/z 152 ($C_7H_6NO_3^+$ and $C_9H_{12}O_2^+$), and m/z 178 ($C_{14}H_{10}$) (Hu et al., 2013). Based on the average organic mass spectrum from the clamp kiln emissions *f*128 was 0.0035, *f*152 was 0.0026, and *f*178 was 0.002, and none of the listed m/z stood out as prominent peaks. The results indicate that factors like coal type and quality in addition to plume aging may influence the relative contribution of the tracer ions observed by (Hu et al., 2013).

Emissions from the more efficient coal-fired zigzag brick kiln were observed to have inorganic profiles most similar to the clamp kiln emissions. Large inorganic fractions were observed in the NR-$PM_1$ mass spectra with sulfate contributing to the majority of mass with 57% of the total (Fig. 6.1p). Other inorganic components contributed significantly less mass with ammonium at 24%, and nitrate and chloride contributing to <1% of the total. The lower fraction of ammonium compared to sulfate associated with zigzag kiln emissions indicates that sulfuric acid was a large component of the aerosol emissions. The larger fraction of sulfate detected from the zigzag kiln compared to the clamp kiln was likely due to the sulfur content of the fuel since similar sulfate ratios were observed between the average mass spectra and with the fuel-based emission factors from the kilns (Goetz et al., 2017b). Additionally, elemental analysis

of the fuel conducted in (Stockwell et al., 2016) indicates that the zigzag kiln coal was 1.28% by weight and the clamp kiln coal was 0.68% by weight. Further investigation of brick kilns is needed to access the impact of coal quality and fuel type on aerosol emissions. However, based on the substantial fraction of inorganic aerosol emissions from the brick kilns, large inorganic mass loadings found in ambient datasets with nearby brick kilns should considered as a molecular marker for brickmaking.

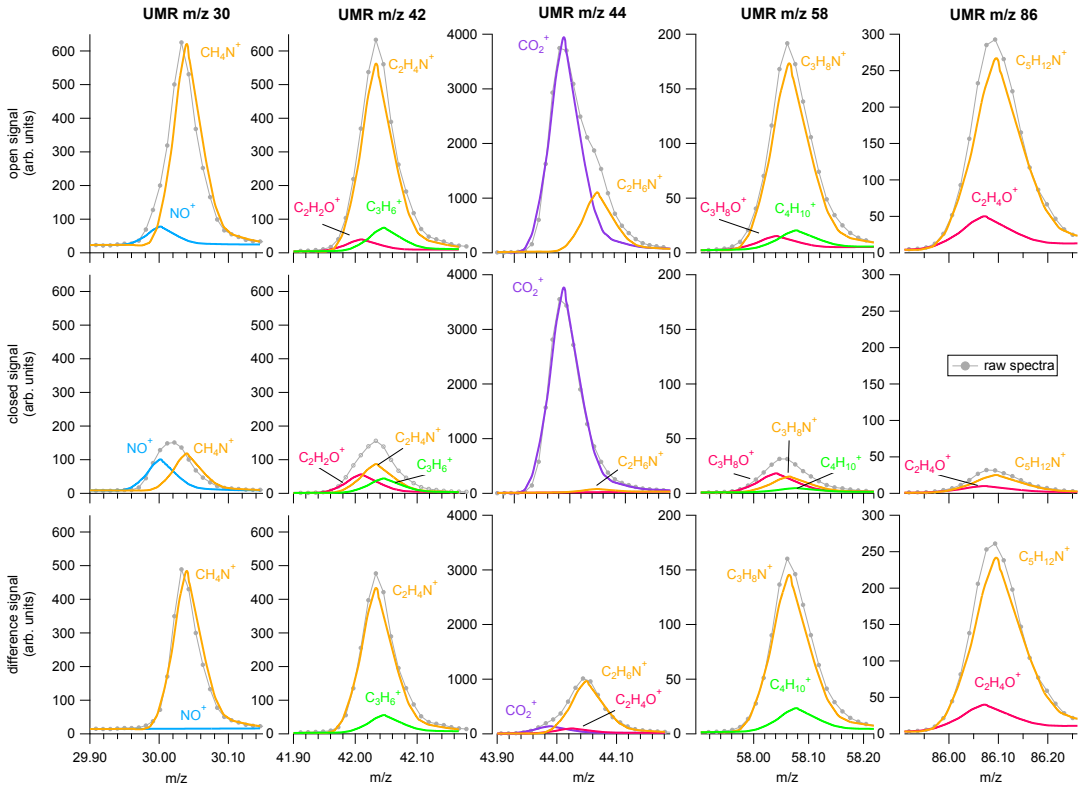


**Figure 6.9. Zig-zag Kiln Peak Fitting**
Average open, closed, and difference high-resolution peak fitting estimates of major UMR peaks associated with zigzag brick kiln emissions.

Based on the mass spectral data the organic aerosol emissions from the zigzag brick kiln were the most unique of the investigated emission sources in NAMaSTE because of large fractions of nitrogen containing organic compounds. Dominant organic peaks included m/z 30, m/z 42, m/z 44, m/z 45, m/z 58, and m/z 86 (Fig. 6.1p). High-

resolution peak fitting estimates indicate that the peaks are associated with the ion series $C_mH_{2m}N^+$ and $C_mH_{2m+2}N^+$. Figure 6.9 gives the chopper open, chopper closed (instrument background), and difference signal (used to calculate aerosol mass) peak fitting estimates for some major m/z peaks detected from the zigzag emissions. The peak fit estimates indicate that the difference signal m/z 30 is due to the organic ion $CH_4N^+$ and not the $NO^+$ as is common with the detection of inorganic nitrate. Although there isn't peak separation between the two ions as would be observed with a high-resolution spectrometer, the wide peak of m/z 30 closed that isn't observed in the difference signal combined with the strong signal with a mode at m/z 30.03 suggests that $CH_4N^+$ was the dominate ion associated with m/z 30 (Fig 6.9). Following the remaining $C_mH_{2m+2}N^+$ series, the peak fits indicate that the major ions detected at m/z 44 was $C_2H_6N^+$, m/z 58 was $C_3H_8N^+$, and 86 was $C_5H_{12}N^+$ (Fig. 9). Non-nitrogen containing ions were also estimated to make up a fraction of the listed UMR peaks but always at lower values. Some of the nitrogen containing organic peaks were also observed with charcoal burning but at much lower fractions and the peaks were attributed to aliphatic primary amides or similar compounds. The mechanism responsible for the formation of amides or other nitrogen containing compounds from coal and charcoal burning is unknown. Additionally, why the compounds were observed with the zigzag kiln emissions and not clamp kiln emissions, both of which were from coal combustion, is unknown. Further characterization of coal-fired brick kilns is needed to understand if emissions of nitrogen containing organics are pervasive with high-efficiency brick making technologies. If amide associated ions are common with other brick kilns they could be a useful molecular markers for coal-fired brick making depending on their atmospheric stability.

## 6.5 Conclusions

Mass spectral profiles of NR-$PM_1$ from the emissions prevalent but under characterized combustion sources in South Asia were investigated as part of the NAMaSTE. Emission sources included field and lab tested cook stoves, agricultural residue burning, open garbage burning, diesel powered irrigation pumps, idling motorcycles, and brick making kilns. Generally, large inorganic aerosol fractions were detected from the biomass burning sources (cookstoves and crop residue) and the coal-fired brick making kilns. Ammonium and chloride were major components of the biomass burning emissions, sulfate was a major component of the brick making emissions and the dominant fraction detected with the coal-fired zigzag kiln. Significant chloride fractions were also observed with open garbage burning and have been attributed to plastic burning. Biomass burning organic tracer fragments were prevalent with wood burning and agricultural residue burning, and were present but observed at lower fractions from dung fueled cooking. Additionally, lab-tested improved wood-fired cooking stoves emissions were observed to contain larger fractions of levoglucosan tracer fragments as well as reduced high molecular weight organic ions compared to their field-tested

traditional counterparts. Charcoal burning emissions produced a unique mass spectral profile with enhanced chloride and ammonium as well as unique organic peaks associated with nitrogen containing organic ions (m/z 44, 64, 86). Additionally strong organic signal was detected with an ion group centered at m/z 136 and was not able to be identified. Open garbage burning was found to have several unique organic ion peaks that were not associated with HOA or BBOA profiles and were attributed to plastic burning. Mixed plastic burning was found to have marker at m/z 104, which was attributed to styrene ions and metalized plastic was found to have an organic marker associated with the fluorene ion (m/z 166). Both plastic burning markers should be considered complimentary garbage burning tracers to Sb and 1,3,5-Triphenylbenzene. The diesel powered irrigation pump and idling motorcycle emissions were found to be well correlated to HOA and contain similar organic peaks that have previously been observed with other engine exhaust profiles. The newer of the irrigation pumps, however, produced emissions with a larger fraction of PAH compounds compared to the older less efficient pump. Finally, the two coal-fired brick kilns produced unique mass spectral profiles compared to the other emission sources and compared each other. The emissions from the kilns were not observed to contain large fractions of organic ions previously associated with deconvolved ambient organic profiles of coal burning. Additionally, high-resolution peak fitting estimates indicate that like charcoal burning the zigzag kiln emissions contained ions associated with nitrogen containing organics. The mass spectral profiles characterized in this work provide important information about the composition of non-refractory submicron emissions from poorly understood emission sources common to South Asia. The collected profiles can aid in the source apportionment aerosol pollution in South Asia and in the developing world.

# Chapter 7: Thesis Conclusions

As discussed in Chapter 1, ground-based mobile monitoring has been used in the past for ambient monitoring, near-source evaluation, and emissions quantification of important gas and aerosol phase atmospheric pollutants and climate forcing compounds. The ambulatory capabilities of ground-based mobile monitoring platforms combined with fast response in-situ instrumentation allow for high spatial and temporal resolution measurements that aren't possible with other types of measurement platforms (e.g. stationary, aircraft, space-based). In this thesis, methods and results from four separate measurement campaigns have demonstrated that ground-based mobile measurements are capable of characterizing atmospheric pollution in under monitored regions, provide insight into how factors associated with unconventional natural gas activity influence ambient concentrations, and characterize emissions from poorly understood emission sources in both developed and under developed regions of the world.

In the Marcellus Shale region of Pennsylvania, ground-based mobile monitoring was used to its fullest extent and important findings were acquired regarding emissions from the production, gathering and transmission sectors of the Marcellus Shale natural gas play. The results show that ground-based methodology like tracer ratio methods and point-source Gaussian methods (OTM-33a) are capable of estimating emission rates from natural gas infrastructure without site access and in areas with complex terrain; something not possible to the same extent with other measurement types. Because of the high spatial and temporal resolution of the mobile measurements, variability of emissions in authentic operating condition was obtained and provides critical results for emission inventories and chemical transport models. In addition to emissions quantification, mobile ambient measurements in the Marcellus region provided a first look at ambient concentrations of greenhouse gases, criteria pollutants, and hazardous air pollutants during the early development period of the Marcellus Shale. This work not only provides an early development baseline, but also characterizes under monitored areas in the region, demonstrating the strength and utility of ground-based mobile monitoring compared to conventional stationary monitoring sites.

In Nepal during the NAMaSTE campaign, the portable application of ground-based mobile monitoring was used to characterize and quantify aerosol emissions from prevalent, but poorly understood emission sources in South Asia including open garbage burning, brick making kilns, traditional cookstoves, diesel irrigation pumps, and others. Many of the investigated emission sources are thought to be important contributors to indoor exposure, local and regional pollution, as well as global budget of climate forcing compounds. This work provided some of the first on-line aerosol measurements of the investigated emission in authentic operating conditions in the field. The results demonstrate that ground-based mobile monitoring with real-time instrumentation is a useful tool to obtain genuine variability in emissions that can be used for emission inventories and various types of atmospheric modeling.

Ultimately, ground-based mobile monitoring is still in its infancy and this work provides two novel approaches to analyzing mobile datasets that advance the field of mobile monitoring. The development of a first-order correction factor for fenceline tracer release offers unique analysis methodology for studies that cannot acquire site access. The correction factor therefore opens to researchers the ability to investigate emissions from uncooperative or inaccessible industries. Similarly, the development of the percentile interval smoothing of mobile ambient datasets provides new means of investigating ambient datasets and to make comparisons to more traditional monitoring methods. The development of these new analysis methods, in addition to some of the results given in the above chapters, provide impetus for future studies in the Marcellus Shale region and across the globe.

# Appendix A: Tracer Release Site Information

## Compressor Stations

| Identifier | Region | Compressor Engines | Dehydrators | Other Process | Pollution Control |
|---|---|---|---|---|---|
| C-A | SW | (3) 1340 bhp NG fired (1) 1265 bhp NG fired | (1) 15 MMscf/day (1) 5 MMscf/day | (1) 0.275 MMbtu/hr reboiler (1) 0.125 MMBtu/hr reboiler (4)100 bbl prod. water tanks | (4) oxidation catalyst w/ air/fuel ratio controllers (2) thermal oxidizers |
| C-B | NE | (4) 1340 bhp NG fired | (1) 75 MMscf/day | (1) 1.0 MMBtu/hr reboiler | (4) oxidation catalyst |
| C-C | SW | (1) 1,265 bhp NG fired (5) 1,380 bhp NG fired | (2) 30 MMscf/day (1) 10 MMscf/day | (2) 0.5 MMBtu/hr reboiler (1) 0.25 MMBtu/hr reboiler (2) 200 bbl prod. water tank | (4) oxidation catalyst w/ air/fuel ratio controllers (1) dehy. flare |
| C-D | NE | (2) 4,500 bhp centrifugal turbine | N/A | Boiler, heaters, and storage tanks | N/A |
| C-E | SW | (5) 1,380 bhp NG fired (2) 3,550 bhp NG fired | (1) 35 MMscf/day (1) 150 MMscf/day | (5) prod. water tanks | (7) oxidation catalyst w/ air/fuel ratio controllers |
| C-F | NE | (8) 1,775 bhp NG fired | N/A | N/A | N/A |
| C-G | NE | (1) 15.300 bhp electric centrifugal turbine | N/A | N/A | N/A |
| C-H | NE | (12) 1,380 bhp NG fired | (3) 35 MMscf/day | | (12) oxidation catalysts |

(N/A) Unknown based on accessed documentation
Information for these sites were obtained from the Pennsylvania Bulletin and from PA Department of Environmental Protection permit reviews

## Production Well Pads

| Identifier | Number of Wells | Gas Production 2012 (Mcf) | Liquids Production (Bbl) |
|---|---|---|---|
| W-A | 7 | 1,704,000 | 31,000 |
| W-B | 9 | 3,051,000 | 10,000 |
| W-C | 9 | 3,044,000 | 72,000 |

Information for these sites were obtained from PA Department of Environmental Protection oil and gas reporting

# Appendix B: AML Calibration Procedures

PTR-MS

The PTR-MS measurements in this study were quantified using calibrated response factors or those estimated from reaction kinetics. Response factors were evaluated from calibration experiments performed daily by dynamically diluting a certified multi-component gas standard (Apel Reimer). The compounds found in the standard and the mixing ratio of each compound found in the standard can be found in Table SI-2. For components not present in the gas standard response factors were deduced from previous laboratory studies, which included acetone, toluene, C2benzenes and C3benzenes. All other species were quantified from response factors derived assuming a reaction rate constant of 2x10-9 ml/s and a reaction time of 0.106 ms. Sample concentrations represent the difference of the ambient measurement and instrument background responses. Instrument background response was determined by periodically by purging the sample line with VOC free air. The VOC free air was produced by passing ambient air through a heated Platinum catalyst. Because the background response is expected to only drift slightly between background measurements, the background signal was linearly interpolated between the measurements.

**Table B-2** Apel Reimer Calibration Standard

| Compound | Mixing Ratio (ppbv) |
|---|---|
| Acetylene | 508 |
| Acetaldehyde | 533 |
| Methanol | 981 |
| i-pentane | 511 |
| isoprene | 489 |
| acetonitrile | 514 |
| benzene | 513 |
| 2,2-trimethylpentane | 529 |
| alpha pinene | 504 |
| decane | 100 |
| dodecane | 100 |
| tridecane | 96 |

]

QCL Trace Gas Monitors

The QCL monitors were used to measure $CH_4$, $C_2H_6$, CO, $N_2O$, and $C_2H_2$. The $C_2H_6$ measurements were calibrated using calibration experiments that occurred before and after the study period in Southwest PA that utilized a

custom calibration standard. It was determined that the $C_2H_6$ had a measurement error of ~7% (high). Methane, $N_2O$, and $C_2H_2$ were calibrated using a custom dilution standard. Methane was expected to be one of the most commonly encountered compounds because we were measuring natural gas infrastructure, therefore a dilution standard calibration experiment was conducted once daily during the study and sometimes calibrations were performed twice daily. Similarly, dilution standard calibration experiments were conducted once or twice daily for $N_2O$ and $C_2H_2$ because they were used as tracer gases. The resulting calibration factors from the dilution standard experiments for $CH_4$, $C_2H_2$, and $N_2O$ were applied to the mobile measurements. The CO calibration experiments were not implemented during the study, but experiments were conducted three months prior to the study using a custom dilution standard and the CO measurement was found to have an error of <1%. Instrument noise was also measured periodically by sampling zero air gas in place of ambient air.

Chemiluminescence NOx Monitor

Similar to CO, NOx and NO calibration experiments were not conducted during this study. However, dilution standard calibration experiments were conducted 3 months prior to this study and it was determined that the NO had an average measurement error of 27% and NOx had an average measurement error of 13%. The NOx monitor measurements were adjusted to account for these errors.

CAPS-NO2 Monitor

Using the same standard as the CO and NOx calibrations, two $NO_2$ calibration experiments were conducted 3 months prior to this study. It was determined that NO2 had a measurement error of 8% (high).

SP-AMS

The SP-AMS calibrations were conducted for both non-refractory aerosols and for refractory black carbon aerosols. Non-refractory aerosols measurements were calibrated using an ammonium nitrate solution. Black carbon measurements were calibrated using a "regal black" solution. Both calibration types were implemented before and after the measurements in Northeastern PA and once during the Southwestern PA study period. PM measurements were conducted at 1 second time resolution for the majority of the campaign because of the transient nature of plume measurements conducted in a mobile laboratory. A slower mode of operation which acquired both MS and particle-time-of-flight (pToF) modes over 1 minute time periods to obtain chemically resolved mass loadings and average size distributions while in a slowly changing environment was also used during periods when the lab was stationary. BC and organic species mass concentrations were obtained from the SP-AMS mass spectra following methods outlined by Onasch et al. (2012). Mass spectral intensities (in units of Hz) are converted to mass units ($\mu gm^{-3}$) using factors that account for species-dependent ionization efficiencies and laser-particle beam overlap. The relative ionization efficiency (RIE) for refractory black carbon was determined by calibration to be .13, .22 and .18 at different points in time during this campaign and the RIE is interpolated with respect to these calibration points. A collection efficiency (CE), which

accounts for incomplete particle and laser beam overlap as well as the particle shape and size was determined to be .49 by comparison of Multi Angle Absorption Photometer (MAAP; Thermo Fisher Model #5012) BC and SP-AMS BC measurements.

## Appendix C: Planetary Boundary Layer Height

The planetary boundary layer (PBL) height for each study period in the Marcellus Shale region was estimated using the National Oceanic and Atmospheric Administration's National Centers for Environmental Prediction (NCEP) North American Region Reanalysis (NARR) model (NCEP, 2015). The NARR model provides 8 times daily geospatial climate data at a 32 kilometer resolution over the North American region and assimilates monitoring observations for reanalysis (NCEP, 2015). The NARR modeling products include surface meteorological data, and data at multiple atmospheric pressure levels. For this study only the PBL product was used. The PBL height for each study region was estimated using two techniques based on the availability of the data formatted into individual 3-hour rasters, which were not available for 2015. The first technique estimated a location specific PBL based on the geoposition and time of each mobile measurement. The mobile data was then binned based on the 3-hour NARR modeling periods (0z, 3z, 6z, 9z, 12z, 15z, 18z, 21z) and the median of each bin calculated. The second approach was to estimate a region-wide PBL based on a composite average for each sampling week resolved to each 3-hour modeling period.

The results for both techniques for the 2012 measurements can be found in Figure S2. The results from the PBL height estimates in 2012 shows that the PBL was generally higher in Southwestern PA (SW PA) in September 2012 than in Northeastern PA (NE PA) in August 2012. Though based on the composite averages the PBL was similar in both regions in the midday and afternoon local time (15z, 18z, 21z) when the PBL is at its highest (Figure C.1). Comparisons of the NE PA PBL show that the PBL was generally higher when sampling in 2015 than in 2012 (Figure C.2). The results also indicate that early morning (local time) PBL height composite averages were similar for both study periods. Median location specific PBL heights are not show in Figure C.2 because independent 3-hour model outputs were not available for 2015.

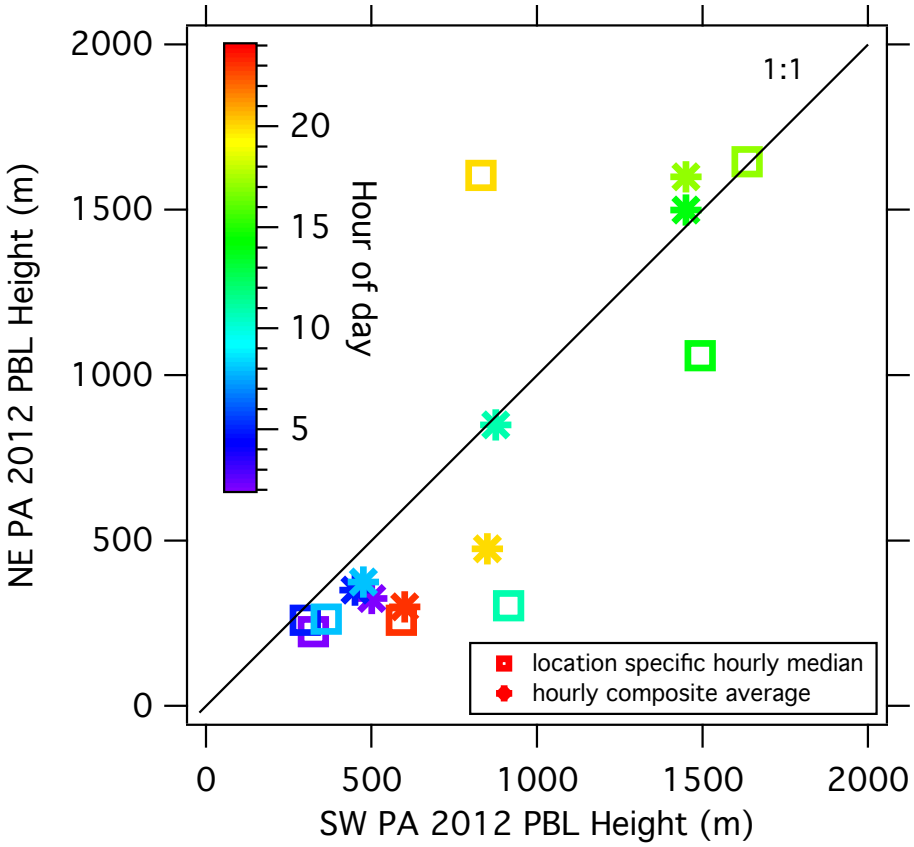


**Figure C.1.** Three hour planetary boundary layer (PBL) height estimated for the Northeastern PA and Southwestern PA during the 2012 study period. The median of the location specific PBL for each model time period is shown as square markers. The region wide mean PBL for each model time period is displayed as asterisks. The color scale denotes the model time period.

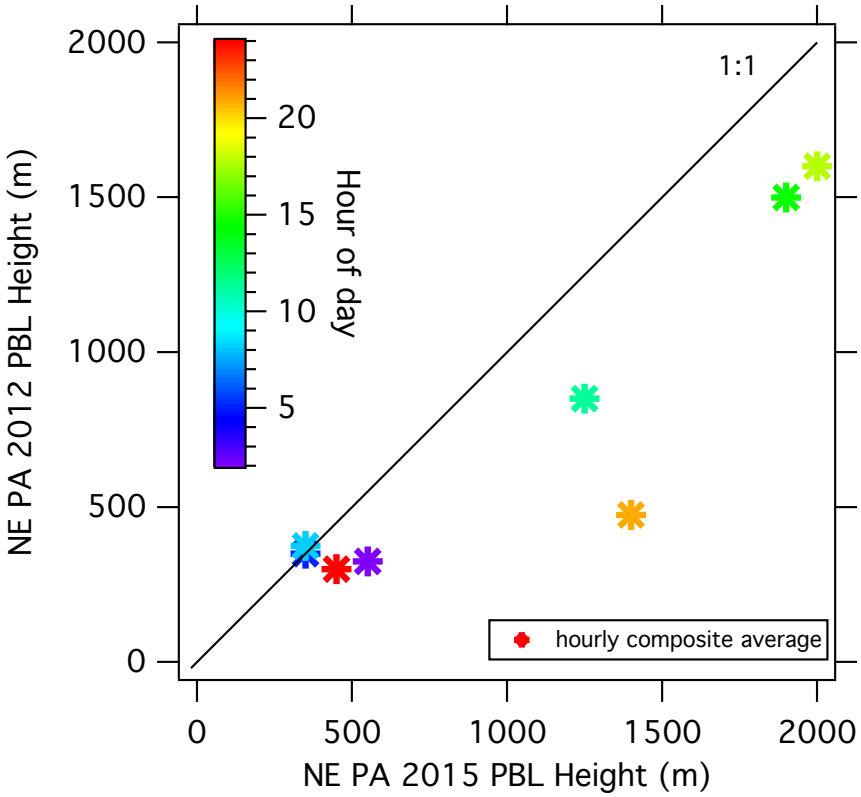


**Figure C.2.** Three hour planetary boundary layer (PBL) height estimated for the Northeastern PA 2012 study period versus the same for the 2015 study period. The region wide mean PBL for each model time period is displayed as asterisks. The color scale denotes the model time period.

# Appendix D: Wind Speed

The wind speed for each study period in the Marcellus Shale region is summarized in Figure D.1. In 2012, the Aerodyne Inc. Mobile Lab (AML) was equipped with a sonic anemometer and wind direction and speed was monitored continuously while driving and during stationary sampling. The box and whisker plots in Figure D.1 show the $10^{th}$, $25^{th}$, $50^{th}$, $75^{th}$, and $90^{th}$ percentiles of the AML measured wind speeds for NE PA and SW PA in 2012. The median wind speed observed in NE PA in 2012 was 0.5 m/s and 0.9 m/s in SW PA. The mean wind speed for the same study periods was 0.88 m/s and 1.46 for NE PA and SW PA in 2012, respectively. Mobile wind speed was not monitored in NE PA in 2015 and therefore summary statistics from ground-based observation cannot be made. To estimate the wind speed during the study period daily averages and maximums were retrieved from the Williamsport Regional Airport (KIPT) found on the Weather Underground History website (www.wunderground.com). The mean wind speed for the 2015 study period was estimated to be 2.1 m/s and the mean maximum wind speed was estimated to be 6.5 m/s (Figure D.1). A similar analysis for the NE PA 2012 study period from the same airport found a mean wind speed of 1.4 m/s and a mean maximum wind speed of 6.0 m/s for the study period. The Williamsport airport was chosen because it is centrally located in NE PA and has most recorded observations in the region. Wind speeds at the Allegheny County Airport (KAGC) were found to have a mean of 2.42 m/s and a mean maximum of 5.87 m/s during the SW PA study period. Generally, the strongest wind speeds were observed during the SW PA study period followed by 2015 study period. However, there is little difference between the mean maximum wind speeds of the three study regions.

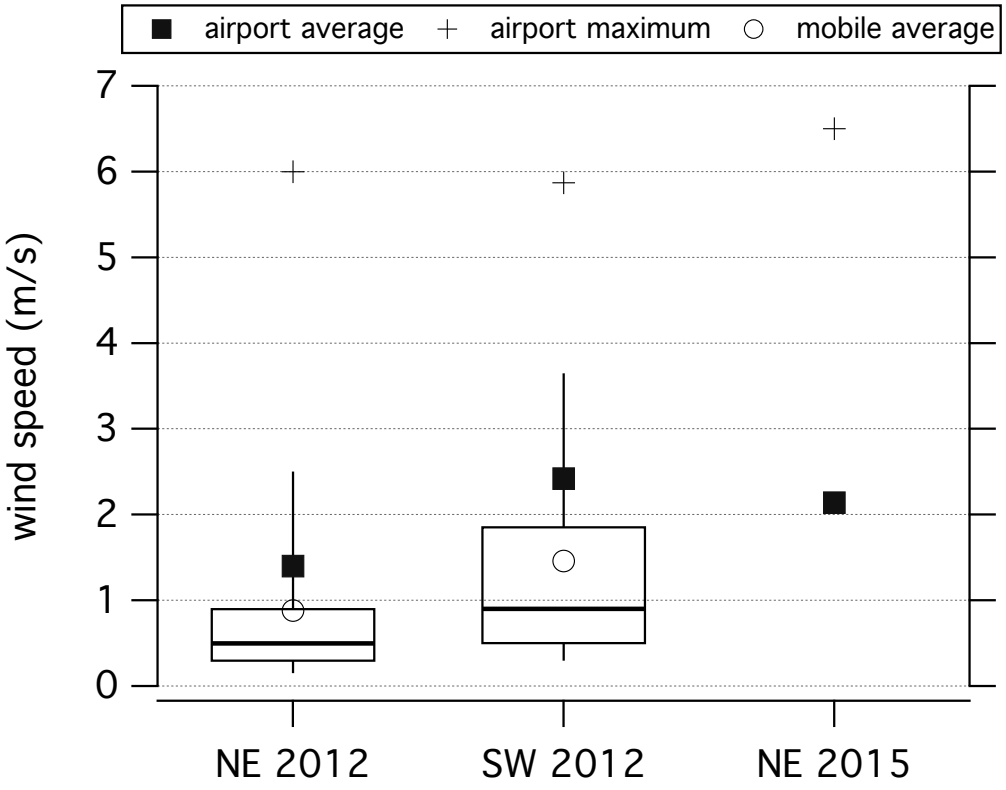


**Figure D.1.** Summary statistics of wind speed for the NE PA and SW PA study period in 2012 and the NEPA study period in 2015. The box and whisker plots represent the $10^{th}$, $25^{th}$, $50^{th}$, $75^{th}$, and $90^{th}$ percentiles of wind speeds measured by the AML. The mean wind speed estimated from the AML dataset in 2012 is displayed as open circles. Mean airport measured wind speeds from the Williamsport Regional Airport in NE PA and the Allegheny County Airport in SW PA are displayed as solid squares. Mean maximum wind speeds from the same airports are displayed as crosses.

# Appendix E: Back Trajectories Using HYSPLIT

The origin of each daily air mass was estimated using the NOAA Hybrid Single Particle Lagrangian Integrated Trajectory Model (HYSPLIT) back trajectories (Stein, 2015;Rolph, 2016). A 48-hour back trajectory was calculated for each sampling day with a midday (12:00) end time. Each trajectory was estimated at a height of 500 meter above ground level. For the NE PA study periods the start of each back trajectory was Laporte, PA (41.422 N, 76.488 W). The town of Laporte was chosen because it is centrally located in NE PA and because it was the location of NE PA nighttime measurements in 2012. In SW PA, Hidden Valley PA (40.024 N, 79.299 W) was chosen as the starting location of the daily back trajectories because it was the location of SW PA nighttime measurements in 2012.

The HYSPLIT back trajectory results are shown in Figure E.1. Based on the back trajectories it is clear that most of the air masses observed in each study period where from regions West of the Marcellus or from within the Marcellus region 48 hours prior to being measured. The NE PA 2012 study region, however, was found to have three daily trajectories from the East and two with 48-hour origins in the Atlantic Ocean (Figure E.1). Additionally, except for the two back trajectories originating in the Atlantic Ocean, the remainder of the trajectories in the NE PA 2012 study period generally covered a shorter distance than the trajectories calculated for the other two study periods. The unique back trajectories for the NE PA 2012 study period suggests that the air masses observed during that study period had different origins than the air masses observed during the other two study periods. The effect of air mass origin on the local background results in this work is uncertain.

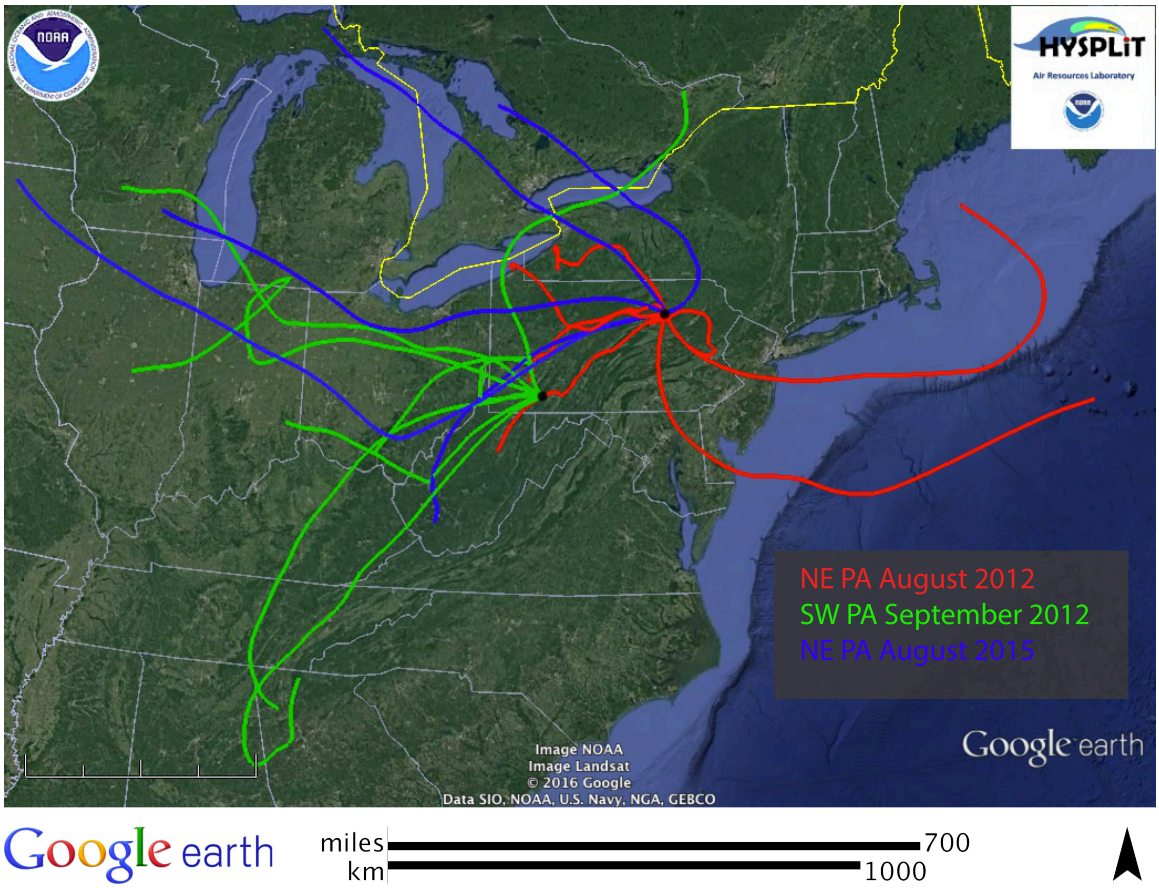


**Figure E.1.** Map of HYSPLIT back trajectories for the three study periods. Daily back trajectories for NE PA 2012, SW PA 2012, and NE PA 2015 are found as red, green, and blue lines, respectively. The starting point for the NE PA back trajectories (black circle) is Laporte, PA. The starting point for the SW PA back trajectories (black circle) is Hidden Valley, PA.

## Appendix F: NAMaSTE Organic Aerosol Emission Factor Distributions

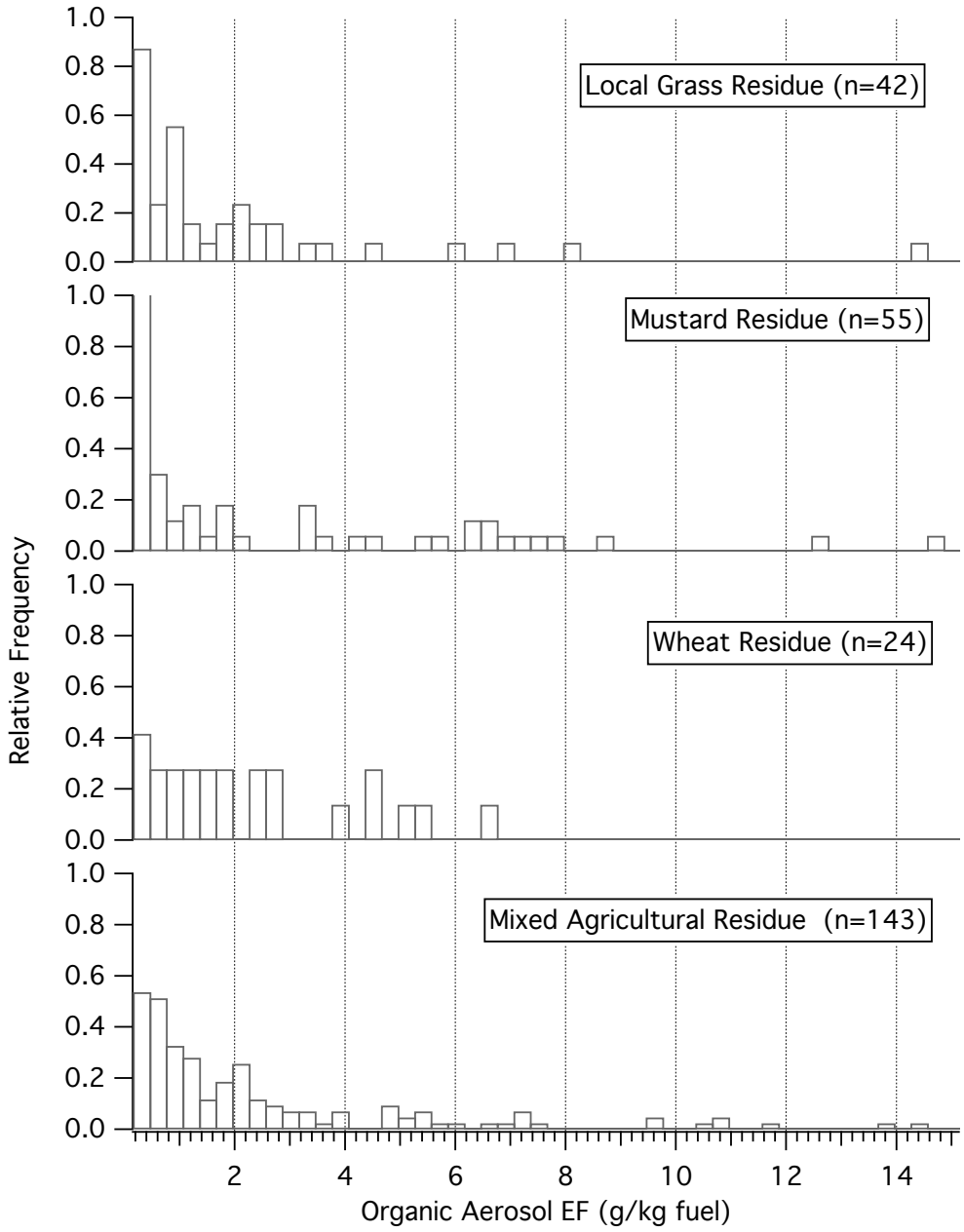


**Figure F1.** Probability density histograms of 10s organic aerosol emission factors from the crop residue burning experiments.

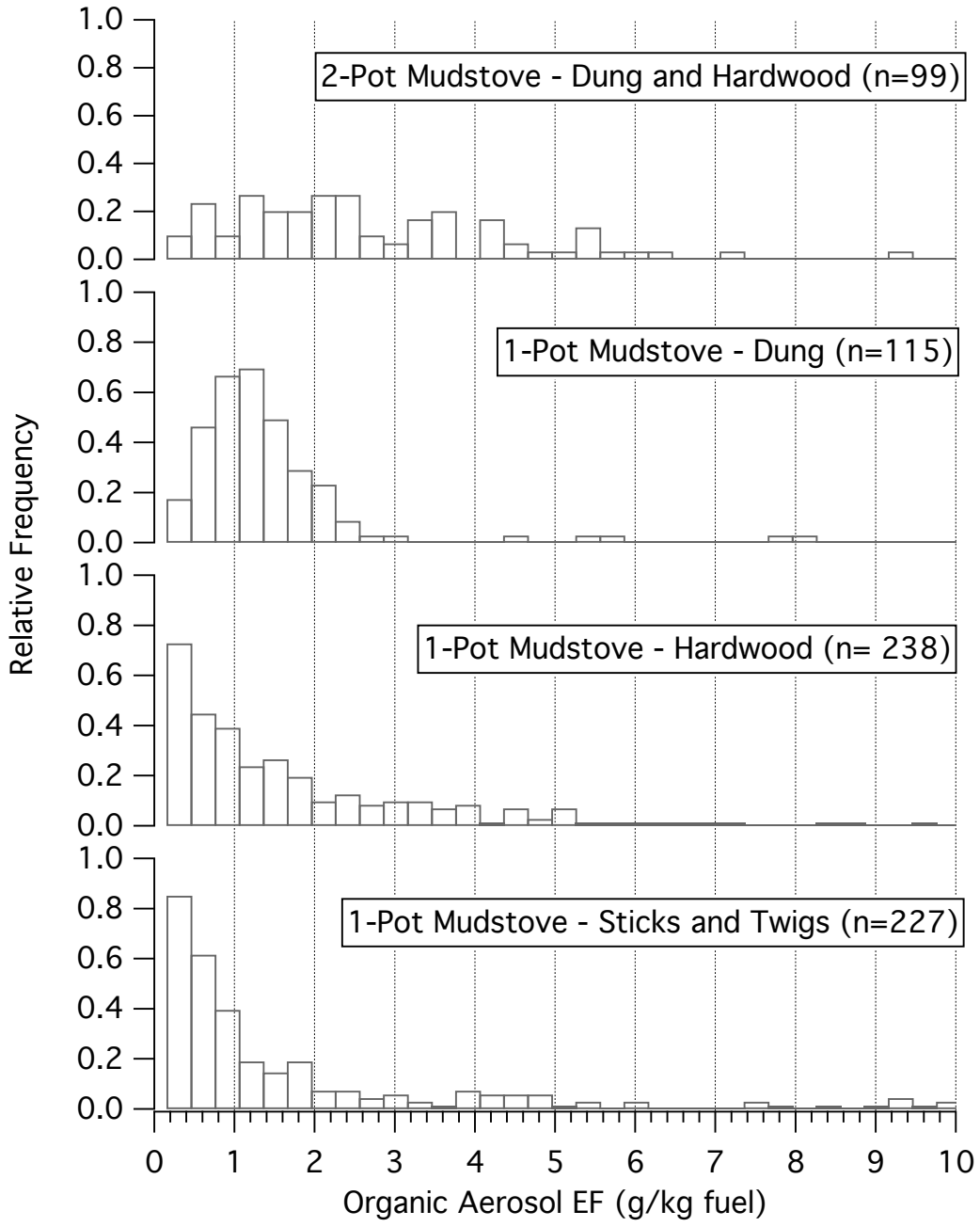


**Figure F2.** Probability density histograms of 10s organic aerosol emission factors from the field tested tradition mudstove experiments.

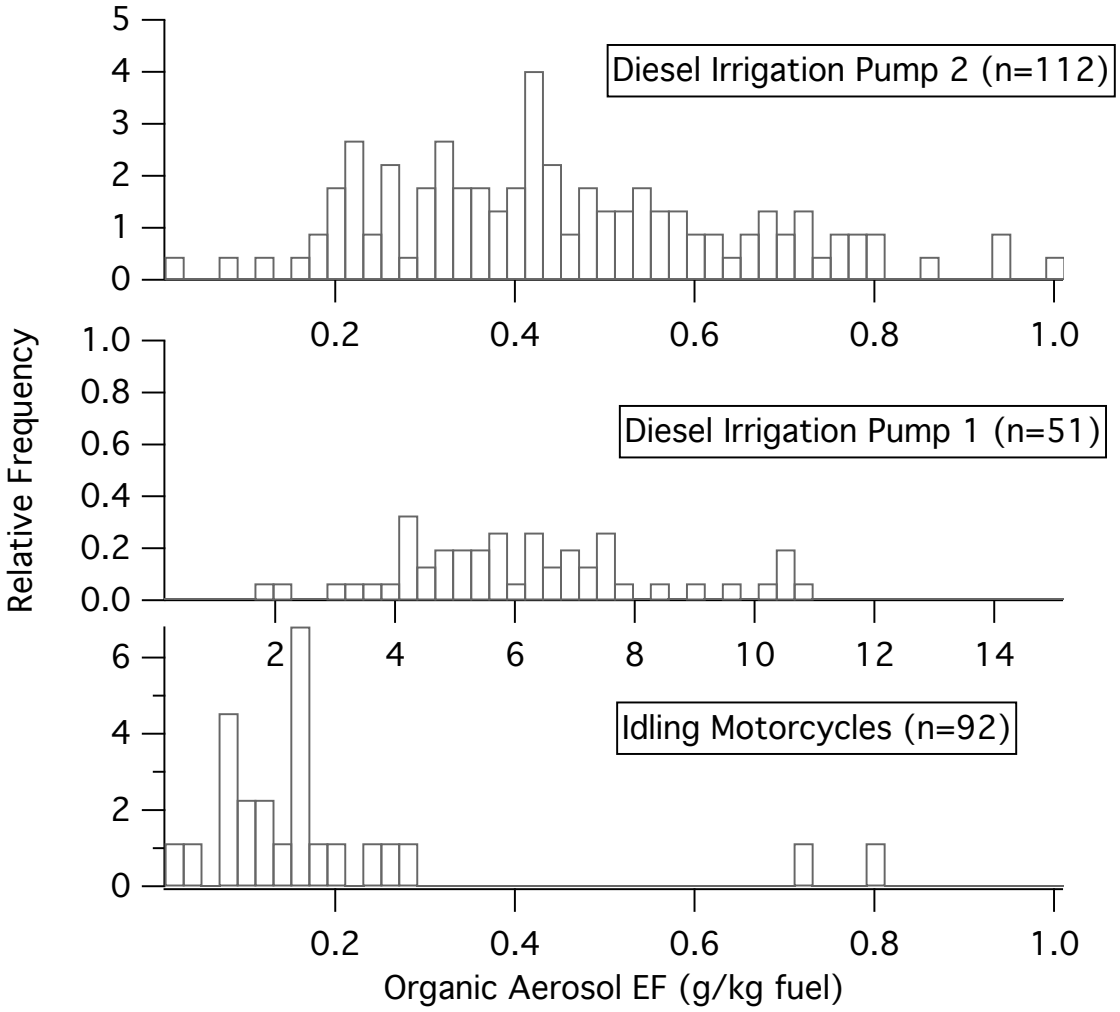


**Figure F3.** Probability density histograms of 10s organic aerosol emission factors from the NAMaSTE engine exhaust samples.

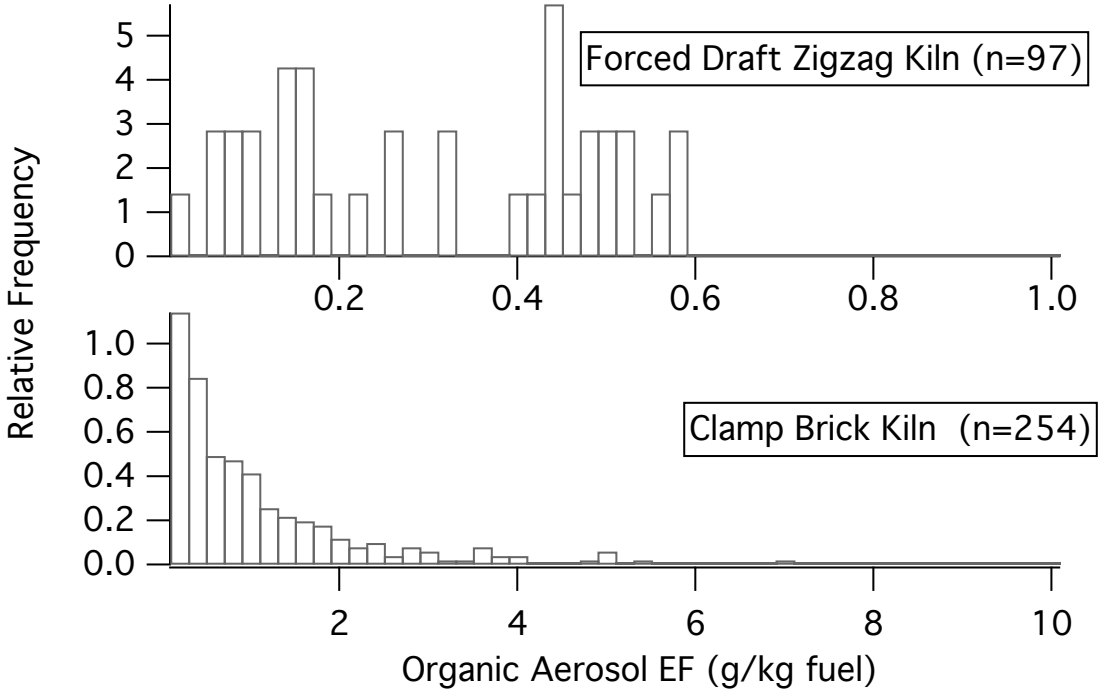


**Figure F4.** Probability density histograms of 10s organic aerosol emission factors from the tested brick kilns.

## Appendix G: NAMaSTE Summary Statistics of Speciated Fuel-based Emission Factors

(see following pages)

| Source Type | Fuel | $f$[a] | MCE[b] | | Fuel-based emission factor (g/kg fuel) | | | | | | | | |
|---|---|---|---|---|---|---|---|---|---|---|---|---|---|
| | | | | | $PM_1$[c] | OA[d] | BC | Delta-C[e] | $SO_4$ | $NO_3$ | Chloride | $NH_4$ | PAH |
| **1-pot traditional mudstove** | **dung** | **0.33** | **0.908** | **median** | **1.466** | **1.039** | **0.099** | **0.854** | **0.007** | **0.002** | **0.250** | **0.068** | **0.003** |
| | | | (0.945) | 25th (10th) | 0.973(0.530) | 0.701(0.365) | 0.057(0.035) | 0.531(0.356) | 0.004(0.003) | 0.002(0.001) | 0.162(0.099) | 0.047(0.027) | 0.002(0.001) |
| | | | | 75th (90th) | 2.232(3.237) | 1.576(2.283) | 0.189(0.340) | 1.427(2.099) | 0.011(0.017) | 0.004(0.006) | 0.358(0.471) | 0.095(0.120) | 0.006(0.015) |
| | | | | $\mu$ ($\sigma$) | 1.863(1.833) | 1.367(1.472) | 0.144(0.161) | 1.077(1.002) | 0.009(0.009) | 0.003(0.003) | 0.268(0.149) | 0.072(0.040) | 0.005(0.007) |
| | | | | integrated | 1.833 | 1.351 | 0.133 | 1.011 | 0.008 | 0.003 | 0.270 | 0.069 | 0.005 |
| | **hardwood**[f] | **0.5** | **0.914** | **median** | **1.421** | **1.070** | **0.279** | **0.783** | **0.011** | **-** | **0.062** | **-** | **0.007** |
| | | | (0.962) | 25th (10th) | 0.558(0.257) | 0.385(0.174) | 0.145(0.070) | 0.352(0.215) | 0.008(0.005) | | 0.021(0.009) | | 0.002(0.001) |
| | | | | 75th (90th) | 3.169(5.792) | 2.514(4.647) | 0.500(0.864) | 1.417(2.215) | 0.017(0.030) | | 0.138(0.252) | | 0.016(0.027) |
| | | | | $\mu$ ($\sigma$) | 2.406(3.166) | 1.916(2.685) | 0.377(0.355) | 1.028(0.960) | 0.017(0.022) | | 0.096(0.105) | | 0.011(0.012) |
| | | | | integrated | 2.827 | 2.370 | 0.321 | 0.971 | 0.016 | | 0.121 | | 0.012 |
| | **sticks and twigs**[g] | **0.5** | **0.933** | **median** | **1.265** | **0.777** | **0.453** | **0.597** | **0.009** | **0.003** | **0.022** | **-** | **0.008** |
| | | | (0.945) | 25th (10th) | 0.531(0.189) | 0.288(0.092) | 0.227(0.090) | 0.314(0.158) | 0.005(0.002) | 0.002(0.001) | 0.009(0.004) | | 0.003(0.001) |
| | | | | 75th (90th) | 3.403(9.526) | 2.286(7.263) | 1.054(2.147) | 1.017(1.653) | 0.015(0.030) | 0.007(0.014) | 0.042(0.073) | | 0.020(0.052) |
| | | | | $\mu$ ($\sigma$) | 3.271(5.767) | 2.444(4.880) | 0.777(0.828) | 0.772(0.702) | 0.014(0.020) | 0.006(0.008) | 0.030(0.032) | | 0.019(0.035) |
| | | | | integrated | 2.624 | 1.794 | 0.782 | 0.865 | 0.009 | 0.004 | 0.035 | | 0.025 |
| **2-pot traditional mudstove** | **dung and hardwood** | **0.4** | **0.912** | **median** | **3.151** | **2.417** | **0.321** | **0.840** | **0.014** | **0.005** | **0.325** | **0.070** | **0.019** |
| | | | (0.965) | 25th (10th) | 1.882(0.860) | 1.430(0.602) | 0.145(0.105) | 0.567(0.436) | 0.008(0.005) | 0.002(0.001) | 0.246(0.117) | 0.051(0.030) | 0.010(0.007) |
| | | | | 75th (90th) | 6.792(20.405) | 5.200(16.779) | 0.428(0.766) | 1.277(1.340) | 0.029(0.087) | 0.007(0.017) | 0.858(2.222) | 0.270(0.533) | 0.037(0.069) |
| | | | | $\mu$ ($\sigma$) | 6.025(6.936) | 4.836(5.750) | 0.320(0.218) | 0.860(0.360) | 0.026(0.031) | 0.006(0.007) | 0.676(0.749) | 0.160(0.181) | 0.027(0.023) |
| | | | | integrated | 4.187 | 3.303 | 0.253 | 0.712 | 0.018 | 0.005 | 0.501 | 0.107 | 0.020 |

a. Carbon mass fraction of fuel from Stockwell et al. (2016)
b. Average modified combustion efficiency ($\Delta CO2/(\Delta CO+\Delta CO2)$) from Stockwell et al. (2016)
c. Sum of detected species (Delta-C and PAH not included)
d. Primary organic aerosol measured with the mAMS
e. Ultraviolet absorbing brown carbon measured by the Aethalometer ($BC_{370nm}$-$BC_{880nm}$)
f. Baikano (*Melia azedarach*)
g. *Shorea robusta* is primary component.

| | | | | | Fuel-based emission factor (g/kg fuel) | | | | | | | | |
|---|---|---|---|---|---|---|---|---|---|---|---|---|---|
| Source Type | fuel | $f$[a] | MCE[b] | | $PM_1$[c] | OA[d] | BC | Delta-C[e] | $SO_4$ | $NO_3$ | Chl | $NH_4$ | PAH |
| **Crop Residue Burning** | **mixed residue** | **0.42** | **0.957** (0.943) | **median** | **1.958** | **1.244** | **0.516** | **0.693** | **0.020** | **0.008** | **0.170** | **-** | **0.004** |
| | | | | 25th (10th) | 0.729(0.260) | 0.439(0.153) | 0.216(0.072) | 0.339(0.125) | 0.008(0.004) | 0.003(0.001) | 0.064(0.030) | | 0.002(0.001) |
| | | | | 75th (90th) | 4.541(9.979) | 3.039(7.424) | 1.047(1.495) | 0.933(1.467) | 0.068(0.168) | 0.014(0.027) | 0.374(0.865) | | 0.010(0.018) |
| | | | | $\mu$ ($\sigma$) | 3.861(5.259) | 2.754(3.970) | 0.698(0.618) | 0.724(0.552) | 0.056(0.100) | 0.011(0.012) | 0.341(0.560) | | 0.007(0.007) |
| | | | | integrated | 3.745 | 2.641 | 0.720 | 0.736 | 0.019 | 0.008 | 0.358 | | 0.006 |
| | **wheat** | **0.42** | **0.949** (0.888) | **median** | **3.378** | **2.359** | **0.736** | **0.958** | **0.104** | **0.007** | **0.139** | **0.034** | **0.004** |
| | | | | 25th (10th) | 1.534(0.761) | 1.013(0.424) | 0.391(0.290) | 0.295(0.113) | 0.039(0.013) | 0.004(0.001) | 0.067(0.025) | 0.020(0.008) | 0.003(0.002) |
| | | | | 75th (90th) | 6.737(23.499) | 4.485(18.779) | 1.349(2.216) | 1.031(2.614) | 0.289(0.407) | 0.030(0.081) | 0.477(1.786) | 0.107(0.230) | 0.013(0.042) |
| | | | | $\mu$ ($\sigma$) | 4.134(5.048) | 2.850(3.849) | 0.794(0.540) | 0.932(0.805) | 0.121(0.120) | 0.013(0.018) | 0.301(0.463) | 0.056(0.059) | 0.007(0.009) |
| | | | | integrated | 4.872 | 3.339 | 0.964 | 1.128 | 0.051 | 0.010 | 0.446 | 0.062 | 0.009 |
| | **mustard** | **0.42** | **0.920** (0.902) | **median** | **2.136** | **1.061** | **0.860** | **3.36** | **0.145** | **0.009** | **0.060** | **-** | **0.004** |
| | | | | 25th (10th) | 0.562(0.277) | 0.230(0.107) | 0.296(0.153) | 1.980(0.670) | 0.025(0.014) | 0.002(0.001) | 0.009(0.002) | | 0.001(0.000) |
| | | | | 75th (90th) | 8.282(14.279) | 5.599(8.602) | 2.054(4.105) | 3.950(4.088) | 0.326(0.523) | 0.041(0.094) | 0.262(0.955) | | 0.011(0.020) |
| | | | | $\mu$ ($\sigma$) | 4.920(7.401) | 3.172(5.429) | 1.325(1.356) | 2.559(1.167) | 0.183(0.202) | 0.022(0.028) | 0.218(0.385) | | 0.006(0.007) |
| | | | | integrated | 4.609 | 3.217 | 0.991 | 1.415 | 0.111 | 0.021 | 0.269 | | 0.004 |
| | **grass** | **0.42** | **0.961** (0.866) | **median** | **2.091** | **1.150** | **0.381** | **0.714** | **-** | **0.005** | **0.475** | **0.080** | **0.003** |
| | | | | 25th (10th) | 0.792(0.238) | 0.404(0.175) | 0.215(0.030) | 0.187(0.045) | | 0.002(0.000) | 0.147(0.022) | 0.024(0.010) | 0.001(0.001) |
| | | | | 75th (90th) | 5.462(18.954) | 3.147(14.353) | 0.795(1.701) | 1.351(3.302) | | 0.009(0.023) | 1.290(2.540) | 0.222(0.337) | 0.008(0.029) |
| | | | | $\mu$ ($\sigma$) | 4.163(6.502) | 2.776(4.929) | 0.535(0.512) | 0.959(1.156) | | 0.006(0.007) | 0.735(0.906) | 0.111(0.149) | 0.007(0.011) |
| | | | | integrated | 2.912 | 1.817 | 0.508 | 0.692 | | 0.003 | 0.528 | 0.055 | 0.005 |

a. Carbon mass fraction of fuel from Stockwell et al. (2016)
b. Average modified combustion efficiency ($\Delta CO2/(\Delta CO+\Delta CO2)$) from Stockwell et al. (2016)
c. Sum of detected species (Delta-C and PAH not included)
d. Primary organic aerosol measured with the mAMS
e. Ultraviolet absorbing brown carbon measured by the Aethalometer ($BC_{370nm}$-$BC_{880nm}$)

| Source Type | Fuel | $f$ [a] | MCE[b] | | Fuel-based emission factor (g/kg fuel) | | | | | | | | |
|---|---|---|---|---|---|---|---|---|---|---|---|---|---|
| | | | | | $PM_1$[c] | OA[d] | BC | Delta-C[e] | $SO_4$ | $NO_3$ | Chl | $NH_4$ | PAH |
| **Open Garbage Burning** | **Mixed Refuse 1** | **0.5** | **0.937** (0.990) | **median** | **1.815** | **1.574** | **0.188** | **-** | **0.002** | **0.003** | **0.047** | **-** | **0.003** |
| | | | | 25th (10th) | 0.599(0.126) | 0.512(0.091) | 0.062(0.023) | | 0.001(0.001) | 0.002(0.001) | 0.016(0.009) | | 0.001(0.001) |
| | | | | 75th (90th) | 5.791(13.935) | 5.225(11.820) | 0.430(1.799) | | 0.004(0.005) | 0.005(0.008) | 0.124(0.242) | | 0.007(0.029) |
| | | | | $\mu$ ($\sigma$) | 3.742(5.150) | 3.277(4.513) | 0.355(0.514) | | 0.002(0.002) | 0.003(0.002) | 0.084(0.102) | | 0.006(0.010) |
| | | | | integrated | 3.855 | 3.497 | 0.263 | | 0.002 | 0.003 | 0.083 | | 0.004 |
| | **Mixed Refuse 2** | **0.5** | **0.980** (0.957) | **median** | **4.699** | **1.024** | **3.630** | **-** | **-** | **-** | **0.046** | **-** | **-** |
| | | | | 25th (10th) | 1.747(0.931) | 0.321(0.077) | 1.415(0.851) | | | | 0.011(0.003) | | |
| | | | | 75th (90th) | 9.667(14.044) | 3.076(5.416) | 6.479(8.385) | | | | 0.111(0.244) | | |
| | | | | $\mu$ ($\sigma$) | 6.195(5.914) | 2.032(2.922) | 4.087(2.902) | | | | 0.076(0.091) | | |
| | | | | integrated | 5.388 | 1.353 | 3.976 | | | | 0.059 | | |
| | **Mixed Refuse (1 and 2)** | **0.5** | **0.923** (0.976) | **median** | **3.168** | **1.148** | **1.970** | **-** | **0.003** | **0.002** | **0.045** | **-** | **0.002** |
| | | | | 25th (10th) | 0.936(0.174) | 0.448(0.077) | 0.472(0.093) | | 0.001(0.000) | 0.001(0.000) | 0.013(0.003) | | 0.001(0.000) |
| | | | | 75th (90th) | 8.915(14.557) | 3.424(6.499) | 5.369(7.800) | | 0.006(0.010) | 0.004(0.007) | 0.111(0.242) | | 0.005(0.010) |
| | | | | $\mu$ ($\sigma$) | 5.636(6.702) | 2.477(3.608) | 3.074(2.994) | | 0.004(0.003) | 0.003(0.002) | 0.079(0.095) | | 0.004(0.007) |
| | | | | integrated | 4.923 | 1.998 | 2.968 | | 0.000 | 0.002 | 0.066 | | 0.003 |
| | **Mixed Plastic** | **0.74** | **0.962** (0.987) | **median** | **13.727** | **11.047** | **2.335** | **-** | **0.014** | **-** | **0.331** | **-** | **0.017** |
| | | | | 25th (10th) | 5.503(3.148) | 4.719(2.785) | 0.615(0.237) | | 0.009(0.005) | | 0.160(0.121) | | 0.005(0.003) |
| | | | | 75th (90th) | 42.566(85.981) | 35.474(73.734) | 6.286(10.395) | | 0.025(0.045) | | 0.782(1.807) | | 0.030(0.080) |
| | | | | $\mu$ ($\sigma$) | 27.465(34.446) | 23.260(30.191) | 3.612(3.610) | | 0.018(0.015) | | 0.576(0.631) | | 0.026(0.040) |
| | | | | integrated | 20.976 | 16.590 | 3.869 | | 0.015 | | 0.502 | | 0.023 |
| | **Chip Bags** | **0.63** | **0.989** (0.986) | **median** | **4.827** | **2.456** | **2.355** | **-** | **0.004** | **-** | **0.012** | **-** | **0.004** |
| | | | | 25th (10th) | 1.827(0.769) | 1.238(0.567) | 0.583(0.198) | | 0.003(0.001) | | 0.004(0.002) | | 0.001(0.001) |
| | | | | 75th (90th) | 10.736(24.129) | 4.965(15.976) | 5.732(8.042) | | 0.007(0.013) | | 0.033(0.098) | | 0.006(0.024) |
| | | | | $\mu$ ($\sigma$) | 7.906(11.340) | 4.846(8.504) | 3.029(2.793) | | 0.005(0.004) | | 0.026(0.040) | | 0.008(0.018) |
| | | | | integrated | 6.763 | 3.484 | 3.255 | | 0.003 | | 0.021 | | 0.005 |

a. Carbon mass fraction of fuel from Stockwell et al. (2016)
b. Average modified combustion efficiency ($\Delta CO2/(\Delta CO+\Delta CO2)$) from Stockwell et al. (2016)
c. Sum of detected species (Delta-C and PAH not included)
d. Primary organic aerosol measured with the mAMS
e. Ultraviolet absorbing brown carbon measured by the Aethalometer ($BC_{370nm}$-$BC_{880nm}$)

| Source | Type (fuel) | $f$[a] | MCE[b] | | Fuel-based emission factor (g/kg fuel) | | | | | | | | |
|---|---|---|---|---|---|---|---|---|---|---|---|---|---|
| | | | | | $PM_1$[c] | OA[d] | BC | Delta-C[e] | $SO_4$ | $NO_3$ | Chl | $NH_4$ | PAH |
| **Motorcycles** | **idling (gasoline)** | **0.85** | **0.6** (0.678) | **median** | **0.067** | **0.067** | **-** | **-** | **-** | **-** | **-** | **-** | **-** |
| | | | | 25th (10th) | 0.024(0.010) | 0.024(0.010) | | | | | | | |
| | | | | 75th (90th) | 0.218(1.329) | 0.218(1.329) | | | | | | | |
| | | | | $\mu$ ($\sigma$) | 0.408(1.142) | 0.408(1.142) | | | | | | | |
| | | | | integrated | 0.127 | 0.127 | | | | | | | |
| **Irrigation pumps** | **Pump 1 (diesel)** | **0.87** | **0.987** (0.978) | **median** | **9.212** | **5.892** | **3.321** | **-** | **-** | **-** | **-** | **-** | **-** |
| | | | | 25th (10th) | 7.543(6.568) | 4.654(4.024) | 2.889(2.543) | | | | | | |
| | | | | 75th (90th) | 11.129(15.232) | 7.304(10.284) | 3.826(4.948) | | | | | | |
| | | | | $\mu$ ($\sigma$) | 9.337(3.046) | 5.983(2.167) | 3.354(0.879) | | | | | | |
| | | | | integrated | 8.108 | 5.178 | 2.931 | | | | | | |
| | **Pump 2 (diesel)** | **0.87** | **0.996** (0.997) | **median** | **5.248** | **0.419** | **4.823** | **-** | **0.006** | **-** | **-** | **-** | **0.003** |
| | | | | 25th (10th) | 4.059(3.506) | 0.309(0.203) | 3.748(3.302) | | 0.003(0.002) | | | | 0.002(0.001) |
| | | | | 75th (90th) | 7.453(9.151) | 0.583(0.759) | 6.862(8.382) | | 0.008(0.010) | | | | 0.005(0.015) |
| | | | | $\mu$ ($\sigma$) | 5.682(2.293) | 0.452(0.223) | 5.225(2.067) | | 0.005(0.003) | | | | 0.009(0.030) |
| | | | | integrated | 3.656 | 0.445 | 3.207 | | 0.004 | | | | 0.006 |
| **Brick Kilns** | **Batch Style Clamp Kiln (coal and harwood[f])** | **0.64** | **0.950** (0.961) | **median** | **1.153** | **0.604** | **0.028** | **0.213** | **0.353** | **-** | **0.042** | **0.126** | **-** |
| | | | | 25th (10th) | 0.474(0.205) | 0.231(0.113) | 0.015(0.006) | 0.065(0.022) | 0.158(0.059) | | 0.015(0.004) | 0.055(0.022) | |
| | | | | 75th (90th) | 2.439(4.545) | 1.341(2.587) | 0.055(0.099) | 0.430(0.704) | 0.700(1.239) | | 0.101(0.207) | 0.242(0.414) | |
| | | | | $\mu$ ($\sigma$) | 1.788(2.059) | 0.977(1.110) | 0.046(0.070) | 0.295(0.274) | 0.504(0.564) | | 0.082(0.113) | 0.179(0.202) | |
| | | | | integrated | 1.773 | 0.999 | 0.029 | 0.288 | 0.484 | | 0.094 | 0.168 | |
| | **Forced-draft Zig-zag Kiln (coal and bagasse[g])** | **0.72** | **0.994** (0.991) | **median** | **1.760** | **0.317** | **0.321** | **-** | **1.009** | **-** | **-** | **0.113** | **-** |
| | | | | 25th (10th) | 1.003(0.445) | 0.136(0.077) | 0.219(0.084) | | 0.582(0.229) | | | 0.066(0.055) | |
| | | | | 75th (90th) | 3.520(4.202) | 0.474(0.561) | 1.446(1.834) | | 1.458(1.628) | | | 0.142(0.179) | |
| | | | | $\mu$ ($\sigma$) | 1.961(1.393) | 0.295(0.183) | 0.648(0.637) | | 0.912(0.528) | | | 0.106(0.045) | |
| | | | | integrated | 2.126 | 0.294 | 0.769 | | 0.955 | | | 0.108 | |

a. Carbon mass fraction of fuel from Stockwell et al. (2016)
b. Average modified combustion efficiency ($\Delta CO2/(\Delta CO+\Delta CO2)$) from Stockwell et al. (2016)
c. Sum of detected species (Delta-C and PAH not included)
d. Primary organic aerosol measured with the mAMS
e. Ultraviolet absorbing brown carbon measured by the Aethalometer ($BC_{370nm}$-$BC_{880nm}$)
f. Kiln estimated to be co-fired with 10% hardwood
g. Used as a starter fuel

## List of References

Agrawal, S., and Yamamoto, S.: Effect of Indoor air pollution from biomass and solid fuel combustion on symptoms of preeclampsia/eclampsia in Indian women, Indoor Air, 25, 341-352, 10.1111/ina.12144, 2015.

Ahmadov, R., McKeen, S., Trainer, M., Banta, R., Brewer, A., Brown, S., Edwards, P. M., de Gouw, J. A., Frost, G. J., Gilman, J., Helmig, D., Johnson, B., Karion, A., Koss, A., Langford, A., Lerner, B., Olson, J., Oltmans, S., Peischl, J., Pétron, G., Pichugina, Y., Roberts, J. M., Ryerson, T., Schnell, R., Senff, C., Sweeney, C., Thompson, C., Veres, P. R., Warneke, C., Wild, R., Williams, E. J., Yuan, B., and Zamora, R.: Understanding high wintertime ozone pollution events in an oil- and natural gas-producing region of the western US, Atmos. Chem. Phys., 15, 411-429, 10.5194/acp-15-411-2015, 2015.

Aiken, A. C., DeCarlo, P. F., Kroll, J. H., Worsnop, D. R., Huffman, J. A., Docherty, K. S., Ulbrich, I. M., Mohr, C., Kimmel, J. R., Sueper, D., Sun, Y., Zhang, Q., Trimborn, A., Northway, M., Ziemann, P. J., Canagaratna, M. R., Onasch, T. B., Alfarra, M. R., Prevot, A. S. H., Dommen, J., Duplissy, J., Metzger, A., Baltensperger, U., and Jimenez, J. L.: O/C and OM/OC Ratios of Primary, Secondary, and Ambient Organic Aerosols with High-Resolution Time-of-Flight Aerosol Mass Spectrometry, Environmental Science & Technology, 42, 4478-4485, 10.1021/es703009q, 2008.

Akagi, S. K., Yokelson, R. J., Wiedinmyer, C., Alvarado, M. J., Reid, J. S., Karl, T., Crounse, J. D., and Wennberg, P. O.: Emission factors for open and domestic biomass burning for use in atmospheric models, Atmos. Chem. Phys., 11, 4039-4072, 10.5194/acp-11-4039-2011, 2011.

Alfarra, M. R., Prevot, A. S. H., Szidat, S., Sandradewi, J., Weimer, S., Lanz, V. A., Schreiber, D., Mohr, M., and Baltensperger, U.: Identification of the Mass Spectral Signature of Organic Aerosols from Wood Burning Emissions, Environmental Science & Technology, 41, 5770-5777, 10.1021/es062289b, 2007.

Allen, D. T., Torres, V. M., Thomas, J., Sullivan, D.W.,Harrison, M., Hendler, A., Herndon, S.C., Kolb, C.E., Fraser, M.P., Hill, A.D., Lamb, B.K., Miskimins, J., Sawyer, R.F., and Seinfeld, J.H.: Measurements of methane emissions at natural gas production sites in the United States, Proceedings of the National Academy of Sciences, 10.1073/pnas.1304880110, 2013.

Andreae, M. O.: Biomass burning - Its history, use, and distribution and its impact on environmental quality and global climate., MIT Press, USA, 1991.
Andreae, M. O., and Merlet, P.: Emission of trace gases and aerosols from biomass burning, Global Biogeochemical Cycles, 15, 955-966, 10.1029/2000GB001382, 2001.

Andreae, M. O.: Aerosols Before Pollution, Science, 315, 50-51, 10.1126/science.1136529, 2007.

Atkinson, R.: Atmospheric chemistry of VOCs and NOx, Atmospheric Environment, 34, 2063-2101, http://dx.doi.org/10.1016/S1352-2310(99)00460-4, 2000.

Baker, A. K., Beyersdorf, A. J., Doezema, L. A., Katzenstein, A., Meinardi, S., Simpson, I. J., Blake, D. R., and Sherwood Rowland, F.: Measurements of nonmethane hydrocarbons in 28 United States cities, Atmospheric Environment, 42, 170-182, http://dx.doi.org/10.1016/j.atmosenv.2007.09.007, 2008.

Beychock, M. R.: Fundamental of Stack Gas Dispersion, 5th ed., 2005.

Bhattacharyya, S. C.: Power sector reform in South Asia: Why slow and limited so far?, Energy Policy, 35, 317-332, http://dx.doi.org/10.1016/j.enpol.2005.11.028, 2007.

Bond, T. C., Streets, D. G., Yarber, K. F., Nelson, S. M., Woo, J.-H., and Klimont, Z.: A technology-based global inventory of black and organic carbon emissions from combustion, Journal of Geophysical Research: Atmospheres, 109, n/a-n/a, 10.1029/2003JD003697, 2004.

Bond, T. C., Wehner, B., Plewka, A., Wiedensohler, A., Heintzenberg, J., and Charlson, R. J.: Climate-relevant properties of primary particulate emissions from oil and natural gas combustion, Atmospheric Environment, 40, 3574-3587, http://dx.doi.org/10.1016/j.atmosenv.2005.12.030, 2006.

Brantley, H. L., Hagler, G. S. W., Kimbrough, E. S., Williams, R. W., Mukerjee, S., and Neas, L. M.: Mobile air monitoring data-processing strategies and effects on spatial air pollution trends, Atmos. Meas. Tech., 7, 2169-2183, 10.5194/amt-7-2169-2014, 2014a.

Brantley, H. L., Thoma, E. D., Squier, W. C., Guven, B. B., and Lyon, D.: Assessment of Methane Emissions from Oil and Gas Production Pads using Mobile Measurements, Environmental Science & Technology, 48, 14508-14515, 10.1021/es503070q, 2014b.

Brantley, H. L. T., Eben D.; Squier, WIlliam C.; Guven, Birnur B.; and Lyon, David Assessment of Methane Emissions from Oil and Gas Production Pads using Mobile Measurements, Environmental Science & Technology, 48, 14508-14515, dx.doi.org/10.1021/es503070q, 2014.

Brook, R. D., Franklin, B., Cascio, W., Hong, Y., Howard, G., Lipsett, M., Luepker, R., Mittleman, M., Samet, J., Smith, S. C., and Tager, I.: Air pollution and cardiovascular disease: a statement for healthcare professionals from the Expert Panel on Population and Prevention Science of the American Heart Association, Circulation, 109, 10.1161/01.cir.0000128587.30041.c8, 2004.

Bruns, E. A., Krapf, M., Orasche, J., Huang, Y., Zimmermann, R., Drinovec, L., Močnik, G., El-Haddad, I., Slowik, J. G., Dommen, J., Baltensperger, U., and Prévôt, A. S. H.: Characterization of primary and secondary wood combustion products generated under different burner loads, Atmos. Chem. Phys., 15, 2825-2841, 10.5194/acp-15-2825-2015, 2015.

Bukowiecki, N., Dommen, J., Prévôt, A. S. H., Richter, R., Weingartner, E., and Baltensperger, U.: A mobile pollutant measurement laboratory—measuring gas phase and aerosol ambient concentrations with high spatial and temporal resolution, Atmospheric Environment, 36, 5569-5579, http://dx.doi.org/10.1016/S1352-2310(02)00694-5, 2002.

Bureau, U. S. C.: Pennsylvania 2010: Population and Housing Unit Counts, 2012.

Burnham, A., Han, J., Clark, C. E., Wang, M., Dunn, J. B., and Palou-Rivera, I.: Life-Cycle Greenhouse Gas Emissions of Shale Gas, Natural Gas, Coal, and Petroleum, Environmental Science & Technology, 46, 619-627, 10.1021/es201942m, 2011.

Bush, S. E., Hopkins, F. M., Randerson, J. T., Lai, C. T., and Ehleringer, J. R.: Design and application of a mobile ground-based observatory for continuous measurements of atmospheric trace gas and criteria pollutant species, Atmos. Meas. Tech., 8, 3481-3492, 10.5194/amt-8-3481-2015, 2015.

Campuzano Jost, P., Jimenez, J.L., Kimmel, J., Day, D.A., Hu, W., Sueper, D., Knochenmuss, R., Worsnop, D.R., Jayne, J.T.: Particle Time-of-Flight by Hadamard Transform (ePTOF): A new high-duty-cycle approach to size-segregated and total aerosol mass measurements for the Aerodyne Aerosol Mass Spectrometer, American Geophysical Union Fall Meeting, San Francisco, 2014.

Canagaratna, M. R., Jayne, J. T., Ghertner, D. A., Herndon, S., Shi, Q., Jimenez, J. L., Silva, P. J., Williams, P., Lanni, T., Drewnick, F., Demerjian, K. L., Kolb, C. E., and Worsnop, D. R.: Chase Studies of Particulate Emissions from in-use New York City Vehicles, Aerosol Science and Technology, 38, 555-573, 10.1080/02786820490465504, 2004.

Canagaratna, M. R., Onasch, T. B., Wood, E. C., Herndon, S. C., Jayne, J. T., Cross, E. S., Miake-Lye, R. C., Kolb, C. E., and Worsnop, D. R.: Evolution of Vehicle Exhaust Particles in the Atmosphere, Journal of the Air & Waste Management Association, 60, 1192-1203, 10.3155/1047-3289.60.10.1192, 2010.

Canagaratna, M. R., Jimenez, J. L., Kroll, J. H., Chen, Q., Kessler, S. H., Massoli, P., Hildebrandt Ruiz, L., Fortner, E., Williams, L. R., Wilson, K. R., Surratt, J. D., Donahue, N. M., Jayne, J. T., and Worsnop, D. R.: Elemental ratio measurements of organic compounds using aerosol mass spectrometry: characterization, improved calibration, and implications, Atmos. Chem. Phys., 15, 253-272, 10.5194/acp-15-253-2015, 2015.

Cao, G., Zhang, X., Gong, S., and Zheng, F.: Investigation on emission factors of particulate matter and gaseous pollutants from crop residue burning, Journal of Environmental Sciences, 20, 50-55, http://dx.doi.org/10.1016/S1001-0742(08)60007-8, 2008.

Carlton, A. G., Little, E., Moeller, M., Odoyo, S., and Shepson, P. B.: The Data Gap: Can a Lack of Monitors Obscure Loss of Clean Air Act Benefits in Fracking Areas?, Environmental Science & Technology, 48, 893-894, 10.1021/es405672t, 2014.
Caulton, D. R. S., P.B.; Santoro, R.L.; Sparks, J.P.; Howarth, R.W.; Ingraffea, A.R.; Cambaliza, M.O.L.; Sweeney, C.; Karion, A.; Davis, K.J.; Stirm, B.H.; Montzka, S.A.; Miller, B.R.: Toward a better understanding and quantification of methane emissions from shale gas development, Proceedings of the National Academy of Sciences, 111, 6237-6242, 10.1073/pnas.1316546111, 2014.

Chafe, Z. A., Brauer, M., Klimont, Z., Van Dingenen, R., Mehta, S., Rao, S., Riahi, K., Dentener, F., and Smith, K. R.: Household Cooking with Solid Fuels Contributes to Ambient PM(2.5) Air Pollution and the Burden of Disease, Environmental Health Perspectives, 122, 1314-1320, 10.1289/ehp.1206340, 2014.

Chen, B. H., Hong, C. J., Pandey, M. R., and Smith, K. R.: Indoor air pollution in developing countries, World Health Stat Q, 43, 127-138, 1990.

Chen, Y., Sheng, G., Bi, X., Feng, Y., Mai, B., and Fu, J.: Emission Factors for Carbonaceous Particles and Polycyclic Aromatic Hydrocarbons from Residential Coal Combustion in China, Environmental Science & Technology, 39, 1861-1867, 10.1021/es0493650, 2005.

Chien, S. M., and Huang, Y. J.: Sizes and polycyclic aromatic hydrocarbon composition distributions of nano, ultrafine, fine, and coarse particulates emitted from a four-stroke motorcycle, Journal of Environmental Science and Health, Part A, 45, 1768-1774, 10.1080/10934529.2010.513289, 2010.

China, S., Mazzoleni, C., Gorkowski, K., Aiken, A. C., and Dubey, M. K.: Morphology and mixing state of individual freshly emitted wildfire carbonaceous particles, Nature Communications, 4, 2122, 10.1038/ncomms3122
http://www.nature.com/articles/ncomms3122#supplementary-information, 2013.

Chowdhury, Z., Zheng, M., Schauer, J. J., Sheesley, R. J., Salmon, L. G., Cass, G. R., and Russell, A. G.: Speciation of ambient fine organic carbon particles and source apportionment of PM2.5 in Indian cities, Journal of Geophysical Research: Atmospheres, 112, n/a-n/a, 10.1029/2007JD008386, 2007.

Christian, T. J., Kleiss, B., Yokelson, R. J., Holzinger, R., Crutzen, P. J., Hao, W. M., Saharjo, B. H., and Ward, D. E.: Comprehensive laboratory measurements of biomass-burning emissions: 1. Emissions from Indonesian, African, and other fuels, Journal of Geophysical Research: Atmospheres, 108, n/a-n/a, 10.1029/2003JD003704, 2003.

Christian, T. J., Yokelson, R. J., Cárdenas, B., Molina, L. T., Engling, G., and Hsu, S. C.: Trace gas and particle emissions from domestic and industrial biofuel use and garbage burning in central Mexico, Atmos. Chem. Phys., 10, 565-584, 10.5194/acp-10-565-2010, 2010.

Coleman, J. L., Milici, R.C., Cook, T.A., Charpentier, R.R., Kirschbaum, M., Klett, T.R., Pollastro, R.M., and Schenk, C.J.: Assessment of undiscovered oil and gas resources of the Devonian Marcellus Shale of the Appalachian Basin Province, 2011, U.S. Geological Survey Fact Sheet 2011–3092, 2, 2011.

Cubison, M. J., Ortega, A. M., Hayes, P. L., Farmer, D. K., Day, D., Lechner, M. J., Brune, W. H., Apel, E., Diskin, G. S., Fisher, J. A., Fuelberg, H. E., Hecobian, A., Knapp, D. J., Mikoviny, T., Riemer, D., Sachse, G. W., Sessions, W., Weber, R. J., Weinheimer, A. J., Wisthaler, A., and Jimenez, J. L.: Effects of aging on organic aerosol from open biomass burning smoke in aircraft and laboratory studies, Atmos. Chem. Phys., 11, 12049-12064, 10.5194/acp-11-12049-2011, 2011.

da Rocha, G. O., Allen, A. G., and Cardoso, A. A.: Influence of Agricultural Biomass Burning on Aerosol Size Distribution and Dry Deposition in Southeastern Brazil, Environmental Science & Technology, 39, 5293-5301, 10.1021/es048007u, 2005.
Dale, A. T., Khanna, V. Vidic, R. D., & Bilec, M. M.: Process Based Life-Cycle Assessment of Natural Gas from the Marcellus Shale, Environmental Science & Technology, 47, 5459-5466, 10.1021/es304414q, 2013.

Dallmann, T. R., DeMartini, S. J., Kirchstetter, T. W., Herndon, S. C., Onasch, T. B., Wood, E. C., and Harley, R. A.: On-Road Measurement of Gas and Particle Phase Pollutant Emission Factors for Individual Heavy-Duty Diesel Trucks, Environmental Science & Technology, 46, 8511-8518, 10.1021/es301936c, 2012.

de Gouw, J., and Warneke, C.: Measurements of volatile organic compounds in the earth's atmosphere using proton-transfer-reaction mass spectrometry, Mass Spectrometry Reviews, 26, 223-257, 10.1002/mas.20119, 2007.

de Gouw, J. A.: Emission sources and ocean uptake of acetonitrile (CH3CN) in the atmosphere, Journal of Geophysical Research, 108, 10.1029/2002jd002897, 2003.
de Gouw, J. A., Parrish, D. D., Frost, G. J., and Trainer, M.: Reduced Emissions of CO2, NOx and SO2 from U.S. Power Plants Due to the Switch from Coal to Natural Gas with Combined Cycle Technology, Earth's Future, n/a-n/a, 10.1002/2014EF000196, 2014.

DeCarlo, P. F., Ulbrich, I. M., Crounse, J., de Foy, B., Dunlea, E. J., Aiken, A. C., Knapp, D., Weinheimer, A. J., Campos, T., Wennberg, P. O., and Jimenez, J. L.: Investigation of the sources and processing of organic aerosol over the Central Mexican Plateau from aircraft measurements during MILAGRO, Atmos. Chem. Phys., 10, 5257-5280, 10.5194/acp-10-5257-2010, 2010.

Dockery, D. W.: Epidemiologic evidence of cardiovascular effects of particulate air pollution, Environ Health Perspect, 109, 10.1289/ehp.01109s4483, 2001.
Dominion Transmission, I.: Abbreviated Application for Certificate of Public Convenience and Necessity. Leidy South Project docket no. CP15-, Federal Energy Regulatory Commission (FERC), 2015.

Drewnick, F., Hings, S. S., DeCarlo, P., Jayne, J. T., Gonin, M., Fuhrer, K., Weimer, S., Jimenez, J. L., Demerjian, K. L., Borrmann, S., and Worsnop, D. R.: A New Time-of-Flight Aerosol Mass Spectrometer (TOF-AMS)—Instrument Description and First Field Deployment, Aerosol Science and Technology, 39, 637-658, 10.1080/02786820500182040, 2005.

Drewnick, F., Böttger, T., von der Weiden-Reinmüller, S. L., Zorn, S. R., Klimach, T., Schneider, J., and Borrmann, S.: Design of a mobile aerosol research laboratory and data processing tools for effective stationary and mobile field measurements, Atmos. Meas. Tech., 5, 1443-1457, 10.5194/amt-5-1443-2012, 2012.

Drinovec, L., Močnik, G., Zotter, P., Prévôt, A. S. H., Ruckstuhl, C., Coz, E., Rupakheti, M., Sciare, J., Müller, T., Wiedensohler, A., and Hansen, A. D. A.: The "dual-spot" Aethalometer: an improved measurement of aerosol black carbon with real-time loading compensation, Atmos. Meas. Tech., 8, 1965-1979, 10.5194/amt-8-1965-2015, 2015.

Dunlea, E. J. H., S. C.; Nelson, D. D.; Volkamer, R. M.; San Martini, F.; Sheehy, P. M.; Zahniser, M. S.; Shorter, J. H.; Wormhoudt, J. C.; Lamb, B. K.; Allwine, E. J.; Gaffney, J. S.; Marley, N. A.; Grutter, M.; Marquez, C.; Blanco, S.; Cardenas, B.; Retama, A.; Ramos Villegas, C. R.; Kolb, C. E.; Molina, L. T.; Molina, M. J.: Evaluation of nitrogen dioxide chemiluminescence monitors in a polluted urban environment, Atmos. Chem. Phys., 7, 2691-2704, 10.5194/acp-7-2691-2007, 2007.

Durant, J. L., Ash, C. A., Wood, E. C., Herndon, S. C., Jayne, J. T., Knighton, W. B., Canagaratna, M. R., Trull, J. B., Brugge, D., Zamore, W., and Kolb, C. E.: Short-term variation in near-highway air pollutant gradients on a winter morning, Atmospheric chemistry and physics (Print), 10, 5599-5626, 2010.

Durbin, T. D., Johnson, K., Miller, J.W., Maldonado, H., & Chernich, D.: Emissions from heavy-duty vehicles under actual on-road driving conditions, Atmospheric Environment, 42, 4812-4821, http://dx.doi.org/10.1016/j.atmosenv.2008.02.006, 2008.

Dzepina, K., Arey, J., Marr, L. C., Worsnop, D. R., Salcedo, D., Zhang, Q., Onasch, T. B., Molina, L. T., Molina, M. J., and Jimenez, J. L.: Detection of particle-phase polycyclic aromatic hydrocarbons in Mexico City using an aerosol mass spectrometer, International Journal of Mass Spectrometry, 263, 152-170, http://dx.doi.org/10.1016/j.ijms.2007.01.010, 2007.

Ellis, P., and Roberts, M.: Leveraging Urbanization in South Asia, World Bank Group, 2016.

Drilling Productivity Report, 2015b.

Field, R. A., Soltis, J., and Murphy, S.: Air quality concerns of unconventional oil and natural gas production, Environmental Science: Processes & Impacts, 16, 954-969, 10.1039/C4EM00081A, 2014.

Fröhlich, R., Cubison, M. J., Slowik, J. G., Bukowiecki, N., Prévôt, A. S. H., Baltensperger, U., Schneider, J., Kimmel, J. R., Gonin, M., Rohner, U., Worsnop, D. R., and Jayne, J. T.: The ToF-ACSM: a portable aerosol chemical speciation monitor with TOFMS detection, Atmos. Meas. Tech., 6, 3225-3241, 10.5194/amt-6-3225-2013, 2013.

Fullerton, D. G., Bruce, N., and Gordon, S. B.: Indoor air pollution from biomass fuel smoke is a major health concern in the developing world, Transactions of The Royal Society of Tropical Medicine and Hygiene, 102, 843-851, 10.1016/j.trstmh.2008.05.028, 2008.

Gautam, R., Hsu, N. C., Kafatos, M., and Tsay, S.-C.: Influences of winter haze on fog/low cloud over the Indo-Gangetic plains, Journal of Geophysical Research: Atmospheres, 112, n/a-n/a, 10.1029/2005JD007036, 2007.

Gilman, J. B., Lerner, B. M., Kuster, W. C., and de Gouw, J. A.: Source Signature of Volatile Organic Compounds from Oil and Natural Gas Operations in Northeastern Colorado, Environmental Science & Technology, 47, 1297-1305, 10.1021/es304119a, 2013.

Goetz, J. D., Floerchinger, C., Fortner, E. C., Wormhoudt, J., Massoli, P., Knighton, W. B., Herndon, S. C., Kolb, C. E., Knipping, E., Shaw, S. L., and DeCarlo, P. F.: Atmospheric Emission Characterization of Marcellus Shale Natural Gas Development Sites, Environmental Science & Technology, 49, 7012-7020, 10.1021/acs.est.5b00452, 2015.

Goetz, J. D., Giordano, M. R., Stockwell, C. E., Christian, T. J., Maharjan, R., Adhikari, S., Bhave, P. V., Praveen, P. S., Panday, A. K., Jayarathne, T., Stone, E. A., Yokelson, R. J., and DeCarlo, P. F.: Speciated On-line PM1 from South Asian Combustion Sources: Part II, AMS Mass Spectral Profiles and Wavelength Dependence, in preparation, 2017a.

Goetz, J. D., Giordano, M. R., Stockwell, C. E., Christian, T. J., Maharjan, R., Adhikari, S., Bhave, P. V., Praveen, P. S., Panday, A. K., Jayarathne, T., Stone, E. A., Yokelson, R. J., and DeCarlo, P. F.: Speciated

On-line PM1 from South Asian Combustion Sources: Part I, Fuel-based Emission Factors and Size Distributions, in preparation, 2017b.

Goldberg, M. S., Burnett, R. T., Yale, J. F., Valois, M. F., and Brook, J. R.: Associations between ambient air pollution and daily mortality among persons with diabetes and cardiovascular disease, Environ Res, 100, 10.1016/j.envres.2005.04.007, 2006.

Gong, X., Zhang, C., Chen, H., Nizkorodov, S. A., Chen, J., and Yang, X.: Size distribution and mixing state of black carbon particles during a heavy air pollution episode in Shanghai, Atmos. Chem. Phys., 16, 5399-5411, 10.5194/acp-16-5399-2016, 2016.
Graham, L. A., Rideout, G., Rosenblatt, D., and Hendren, J.: Greenhouse gas emissions from heavy-duty vehicles, Atmospheric Environment, 42, 4665-4681, http://dx.doi.org/10.1016/j.atmosenv.2008.01.049, 2008.

Gustafsson, Ö., Kruså, M., Zencak, Z., Sheesley, R. J., Granat, L., Engström, E., Praveen, P. S., Rao, P. S. P., Leck, C., and Rodhe, H.: Brown Clouds over South Asia: Biomass or Fossil Fuel Combustion?, Science, 323, 495-498, 10.1126/science.1164857, 2009.

Guttikunda, S. K., and Goel, R.: Health impacts of particulate pollution in a megacity—Delhi, India, Environmental Development, 6, 8-20, http://dx.doi.org/10.1016/j.envdev.2012.12.002, 2013.

Guttikunda, S. K., Goel, R., and Pant, P.: Nature of air pollution, emission sources, and management in the Indian cities, Atmospheric Environment, 95, 501-510, http://dx.doi.org/10.1016/j.atmosenv.2014.07.006, 2014.

Hagemann, R., Corsmeier, U., Kottmeier, C., Rinke, R., Wieser, A., and Vogel, B.: Spatial variability of particle number concentrations and NOx in the Karlsruhe (Germany) area obtained with the mobile laboratory 'AERO-TRAM', Atmospheric Environment, 94, 341-352, http://dx.doi.org/10.1016/j.atmosenv.2014.05.051, 2014.

Hakami, A., Bergin, M. S., and Russell, A. G.: Ozone Formation Potential of Organic Compounds in the Eastern United States: A Comparison of Episodes, Inventories, and Domains, Environmental Science & Technology, 38, 6748-6759, 10.1021/es035471a, 2004.

Hallquist, M., Wenger, J. C., Baltensperger, U., Rudich, Y., Simpson, D., Claeys, M., Dommen, J., Donahue, N. M., George, C., Goldstein, A. H., Hamilton, J. F., Herrmann, H., Hoffmann, T., Iinuma, Y., Jang, M., Jenkin, M. E., Jimenez, J. L., Kiendler-Scharr, A., Maenhaut, W., McFiggans, G., Mentel, T. F., Monod, A., Prévôt, A. S. H., Seinfeld, J. H., Surratt, J. D., Szmigielski, R., and Wildt, J.: The formation, properties and impact of secondary organic aerosol: current and emerging issues, Atmos. Chem. Phys., 9, 5155-5236, 10.5194/acp-9-5155-2009, 2009.

Hayhoe, K., Kheshgi, H.S., Jain, A.K., and Wuebbles, D.J.: Substitution of Natural Gas for Coal: Climatic Effects of Utility Sector Emissions, Climatic Change, 54, 107-139, 10.1023/A:1015737505552, 2002.

Hays, M. D., Fine, P. M., Geron, C. D., Kleeman, M. J., and Gullett, B. K.: Open burning of agricultural biomass: Physical and chemical properties of particle-phase emissions, Atmospheric Environment, 39, 6747-6764, http://dx.doi.org/10.1016/j.atmosenv.2005.07.072, 2005.

Heeb, N. V., Forss, A.-M., and Bach, C.: Fast and quantitative measurement of benzene, toluene and C2-benzenes in automotive exhaust during transient engine operation with and without catalytic exhaust gas treatment, Atmospheric Environment, 33, 205-215, http://dx.doi.org/10.1016/S1352-2310(98)00149-6, 1999.

Heeb, N. V., Forss, A.-M., Bach, C., Reimann, S., Herzog, A., and Jäckle, H. W.: A comparison of benzene, toluene and C2-benzenes mixing ratios in automotive exhaust and in the suburban atmosphere

during the introduction of catalytic converter technology to the Swiss Car Fleet, Atmospheric Environment, 34, 3103-3116, http://dx.doi.org/10.1016/S1352-2310(99)00446-X, 2000.

Hefley, W. E., Seydor, S.M., Bencho, M.K., Chappel, I., Dizard, M., Hallman, J., Herkt, J., Jiang, P.J., Kerec, M., Lampe, F., Lehner, C.L., Wei, T., Birsic, B., Coulter, E., Hatter, E.M., Jacko, D., Mignogna, S., Park, N., Riley, K., Tawoda, T., Clements, E., & Harlovic, R.: The Economic Impact of the Value Chain of a Marcellus Shale Well, Pitt Business Working Papers, 2011.

Herndon, S. C., Jayne, J. T., Zahniser, M. S., Worsnop, D. R., Knighton, B., Alwine, E., Lamb, B. K., Zavala, M., Nelson, D. D., McManus, J. B., Shorter, J. H., Canagaratna, M. R., Onasch, T. B., and Kolb, C. E.: Characterization of urban pollutant emission fluxes and ambient concentration distributions using a mobile laboratory with rapid response instrumentation, Faraday Discussions, 130, 327-339, 10.1039/B500411J, 2005a.

Herndon, S. C., Shorter, J. H., Zahniser, M. S., Wormhoudt, J., Nelson, D. D., Demerjian, K. L., and Kolb, C. E.: Real-Time Measurements of SO2, H2CO, and CH4 Emissions from In-Use Curbside Passenger Buses in New York City Using a Chase Vehicle, Environmental Science & Technology, 39, 7984-7990, 10.1021/es0482942, 2005b.

Holzinger, R., Williams, J., Salisbury, G., Klüpfel, T., de Reus, M., Traub, M., Crutzen, P. J., and Lelieveld, J.: Oxygenated compounds in aged biomass burning plumes over the Eastern Mediterranean: evidence for strong secondary production of methanol and acetone, Atmos. Chem. Phys., 5, 39-46, 10.5194/acp-5-39-2005, 2005.

Howarth, R. W., Santoro, R., and Ingraffea, A.: Methane and the greenhouse-gas footprint of natural gas from shale formations, Climatic Change, 106, 679-690, 10.1007/s10584-011-0061-5, 2011.

Hu, W. W., Hu, M., Yuan, B., Jimenez, J. L., Tang, Q., Peng, J. F., Hu, W., Shao, M., Wang, M., Zeng, L. M., Wu, Y. S., Gong, Z. H., Huang, X. F., and He, L. Y.: Insights on organic aerosol aging and the influence of coal combustion at a regional receptor site of central eastern China, Atmos. Chem. Phys., 13, 10095-10112, 10.5194/acp-13-10095-2013, 2013.

Huffman, J. A., Docherty, K. S., Aiken, A. C., Cubison, M. J., Ulbrich, I. M., DeCarlo, P. F., Sueper, D., Jayne, J. T., Worsnop, D. R., Ziemann, P. J., and Jimenez, J. L.: Chemically-resolved aerosol volatility measurements from two megacity field studies, Atmos. Chem. Phys., 9, 7161-7182, 10.5194/acp-9-7161-2009, 2009.

IPCC, I. P. o. C. C.: Climate Change 2013: The Physical Science Basis, 2013.

Jackson, R. B., Down, A., Phillips, N. G., Ackley, R. C., Cook, C. W., Plata, D. L., and Zhao, K.: Natural Gas Pipeline Leaks Across Washington, DC, Environmental Science & Technology, 48, 2051-2058, 10.1021/es404474x, 2014.

Jacob, D. J., Field, B. D., Jin, E. M., Bey, I., Li, Q., Logan, J. A., Yantosca, R. M., and Singh, H. B.: Atmospheric budget of acetone, Journal of Geophysical Research: Atmospheres, 107, ACH 5-1-ACH 5-17, 10.1029/2001JD000694, 2002.

J
ayarathne, T., Stockwell, C. E., Christian, T. J., Bhave, P. V., Praveen, P. S., Panday, A. K., Adhikari, S., Maharjan, R., Goetz, J. D., DeCarlo, P. F., Saikawa, E., Yokelson, R. J., and Stone, E. A.: Nepal Ambient Monitoring and Source Testing Experiment (NAMaSTE): Emissions of particulate matter from wood and dung cooking fires, brick kilns, generators, trash and crop residue burning, Submitted, 2017.

Jayne, J. T., Leard, D. C., Zhang, X., Davidovits, P., Smith, K. A., Kolb, C. E., and Worsnop, D. R.: Development of an Aerosol Mass Spectrometer for Size and Composition Analysis of Submicron Particles, Aerosol Science and Technology, 33, 49-70, 10.1080/027868200410840, 2000.

Jeong, C.-H., Hopke, P. K., Kim, E., and Lee, D.-W.: The comparison between thermal-optical transmittance elemental carbon and Aethalometer black carbon measured at multiple monitoring sites, Atmospheric Environment, 38, 5193-5204, http://dx.doi.org/10.1016/j.atmosenv.2004.02.065, 2004.

Jerrett , M., Burnett , R. T., Pope , C. A. I., Ito , K., Thurston , G., Krewski , D., Shi , Y., Calle , E., and Thun , M.: Long-Term Ozone Exposure and Mortality, New England Journal of Medicine, 360, 1085-1095, doi:10.1056/NEJMoa0803894, 2009.

Jiang, M., Marr, L. C., Dunlea, E. J., Herndon, S. C., Jayne, J. T., Kolb, C. E., Knighton, W. B., Rogers, T. M., Zavala, M., Molina, L. T., and Molina, M. J.: Vehicle fleet emissions of black carbon, polycyclic aromatic hydrocarbons, and other pollutants measured by a mobile laboratory in Mexico City, Atmos Chem Phys, 5, 10.5194/acp-5-3377-2005, 2005.

Jobson, B. T., Alexander, M. L., Maupin, G. D., and Muntean, G. G.: On-line analysis of organic compounds in diesel exhaust using a proton transfer reaction mass spectrometer (PTR-MS), International Journal of Mass Spectrometry, 245, 78-89, http://dx.doi.org/10.1016/j.ijms.2005.05.009, 2005.

Jordan, C., Fitz, E., Hagan, T., Sive, B., Frinak, E., Haase, K., Cottrell, L., Buckley, S., and Talbot, R.: Long-term study of VOCs measured with PTR-MS at a rural site in New Hampshire with urban influences, Atmos. Chem. Phys., 9, 4677-4697, 10.5194/acp-9-4677-2009, 2009.

Kargbo, D. M., Wilhelm, R. G., and Campbell, D. J.: Natural Gas Plays in the Marcellus Shale: Challenges and Potential Opportunities, Environmental Science & Technology, 44, 5679-5684, 10.1021/es903811p, 2010.

Karion, A., Sweeney, C., Pétron, G., Frost, G., Michael Hardesty, R., Kofler, J., Miller, B. R., Newberger, T., Wolter, S., Banta, R., Brewer, A., Dlugokencky, E., Lang, P., Montzka, S. A., Schnell, R., Tans, P., Trainer, M., Zamora, R., and Conley, S.: Methane emissions estimate from airborne measurements over a western United States natural gas field, Geophysical Research Letters, 40, 4393-4397, 10.1002/grl.50811, 2013.

Kebabian, P. L., Wood, E. C., Herndon, S. C., and Freedman, A.: A Practical Alternative to Chemiluminescence-Based Detection of Nitrogen Dioxide: Cavity Attenuated Phase Shift Spectroscopy, Environmental Science & Technology, 42, 6040-6045, 10.1021/es703204j, 2008.

Keene, W. C., Lobert, J. M., Crutzen, P. J., Maben, J. R., Scharffe, D. H., Landmann, T., Hély, C., and Brain, C.: Emissions of major gaseous and particulate species during experimental burns of southern African biomass, Journal of Geophysical Research: Atmospheres, 111, n/a-n/a, 10.1029/2005JD006319, 2006.

Kemball-Cook, S., Bar-Ilan, A., Grant, J., Parker, L., Jung, J., Santamaria, W., Mathews, J., and Yarwood, G.: Ozone Impacts of Natural Gas Development in the Haynesville Shale, Environmental Science & Technology, 44, 9357-9363, 10.1021/es1021137, 2010.

Kleeman, M. J., Schauer, J. J., and Cass, G. R.: Size and Composition Distribution of Fine Particulate Matter Emitted from Wood Burning, Meat Charbroiling, and Cigarettes, Environmental Science & Technology, 33, 3516-3523, 10.1021/es981277q, 1999.

Kolb, C. E., Herndon, S.C., McManus, J.B., Shorter, J.H., Zahniser, M.S., Nelson, D.D., Jayne, J.T., Canagaratna, M.R.,and Worsnop, D.R.: Mobile Laboratory with Rapid Response Instruments for Real-Time Measurements of Urban and Regional Trace Gas and Particulate Distributions and Emission Source Characteristics, Environmental Science & Technology, 38, 5694-5703, 10.1021/es030718p, 2004.

Kolb, C. S., McManus, J. B., Shorter, J. H., Zahniser, M. S., Nelson, D. D., Jayne, J. T., Canagaratha, M. R., and Worsnop, M. D. R.: Mobile laboratory with rapid response instruments for real-time measurments

of urban and regional trace gas and particulate distributions and emission source characteristics, Environ Sci Technol, 38, 10.1021/es030718p, 2004.

Kondo, Y., Matsui, H., Moteki, N., Sahu, L., Takegawa, N., Kajino, M., Zhao, Y., Cubison, M. J., Jimenez, J. L., Vay, S., Diskin, G. S., Anderson, B., Wisthaler, A., Mikoviny, T., Fuelberg, H. E., Blake, D. R., Huey, G., Weinheimer, A. J., Knapp, D. J., and Brune, W. H.: Emissions of black carbon, organic, and inorganic aerosols from biomass burning in North America and Asia in 2008, Journal of Geophysical Research: Atmospheres, 116, n/a-n/a, 10.1029/2010JD015152, 2011.

Kortelainen, A., Joutsensaari, J., Hao, L., Leskinen, J., Tiitta, P., Jaatinen, A., Miettinen, P., Sippula, O., Torvela, T., Tissari, J., Jokiniemi, J., Worsnop, D. R., Smith, J. N., Laaksonen, A., and Virtanen, A.: Real-Time Chemical Composition Analysis of Particulate Emissions from Woodchip Combustion, Energy & Fuels, 29, 1143-1150, 10.1021/ef5019548, 2015.

Kumar, R., Barth, M. C., Nair, V. S., Pfister, G. G., Suresh Babu, S., Satheesh, S. K., Krishna Moorthy, K., Carmichael, G. R., Lu, Z., and Streets, D. G.: Sources of black carbon aerosols in South Asia and surrounding regions during the Integrated Campaign for Aerosols, Gases and Radiation Budget (ICARB), Atmos. Chem. Phys., 15, 5415-5428, 10.5194/acp-15-5415-2015, 2015.

Kurokawa, J., Ohara, T., Morikawa, T., Hanayama, S., Janssens-Maenhout, G., Fukui, T., Kawashima, K., and Akimoto, H.: Emissions of air pollutants and greenhouse gases over Asian regions during 2000–2008: Regional Emission inventory in ASia (REAS) version 2, Atmos. Chem. Phys., 13, 11019-11058, 10.5194/acp-13-11019-2013, 2013.

Laden, F., Neas, L. M., Dockery, D. W., and Schwartz, J.: Association of fine particulate matter from different sources with daily mortality in six U.S. cities, Environ Health Perspect, 108, 10.1289/ehp.00108941, 2000.

Lamb, B. K., Edburg, S. L., Ferrara, T. W., Howard, T., Harrison, M. R., Kolb, C. E., Townsend-Small, A., Dyck, W., Possolo, A., and Whetstone, J. R.: Direct Measurements Show Decreasing Methane Emissions from Natural Gas Local Distribution Systems in the United States, Environmental Science & Technology, 49, 5161-5169, 10.1021/es505116p, 2015.

Lamb, B. K., McManus, J.B., Shorter, J.H., Kolb, C.E., Mosher, B., Harriss, R.C., Allwine, E., Blaha, D., Howard, T., Guenther, A., Lott, R.A., Siverson, R., Westburg, H., and Zimmerman, P.: Development of Atmospheric Tracer Methods To Measure Methane Emissions from Natural Gas Facilities and Urban Areas, Environmental Science & Technology, 29, 1468-1479, 10.1021/es00006a007, 1995.

Lawrence, M. G., and Lelieveld, J.: Atmospheric pollutant outflow from southern Asia: a review, Atmos. Chem. Phys., 10, 11017-11096, 10.5194/acp-10-11017-2010, 2010.

Lelieveld, J., Crutzen, P. J., Ramanathan, V., Andreae, M. O., Brenninkmeijer, C. A. M., Campos, T., Cass, G. R., Dickerson, R. R., Fischer, H., de Gouw, J. A., Hansel, A., Jefferson, A., Kley, D., de Laat, A. T. J., Lal, S., Lawrence, M. G., Lobert, J. M., Mayol-Bracero, O. L., Mitra, A. P., Novakov, T., Oltmans, S. J., Prather, K. A., Reiner, T., Rodhe, H., Scheeren, H. A., Sikka, D., and Williams, J.: The Indian Ocean Experiment: Widespread Air Pollution from South and Southeast Asia, Science, 291, 1031-1036, 2001.

Lim, S. S., Vos, T., Flaxman, A. D., Danaei, G., Shibuya, K., Adair-Rohani, H., Amann, M., Anderson, H. R., Andrews, K. G., Aryee, M., Atkinson, C., Bacchus, L. J., Bahalim, A. N., Balakrishnan, K., Balmes, J., Barker-Collo, S., Baxter, A., Bell, M. L., Blore, J. D., Blyth, F., Bonner, C., Borges, G., Bourne, R., Boussinesq, M., Brauer, M., Brooks, P., Bruce, N. G., Brunekreef, B., Bryan-Hancock, C., Bucello, C., Buchbinder, R., Bull, F., Burnett, R. T., Byers, T. E., Calabria, B., Carapetis, J., Carnahan, E., Chafe, Z., Charlson, F., Chen, H., Chen, J. S., Cheng, A. T., Child, J. C., Cohen, A., Colson, K. E., Cowie, B. C., Darby, S., Darling, S., Davis, A., Degenhardt, L., Dentener, F., Des Jarlais, D. C., Devries, K., Dherani, M., Ding, E. L., Dorsey, E. R., Driscoll, T., Edmond, K., Ali, S. E., Engell, R. E., Erwin, P. J., Fahimi, S., Falder, G., Farzadfar, F., Ferrari, A., Finucane, M. M., Flaxman, S., Fowkes, F. G., Freedman, G.,

Freeman, M. K., Gakidou, E., Ghosh, S., Giovannucci, E., Gmel, G., Graham, K., Grainger, R., Grant, B., Gunnell, D., Gutierrez, H. R., Hall, W., Hoek, H. W., Hogan, A., Hosgood, H. D., 3rd, Hoy, D., Hu, H., Hubbell, B. J., Hutchings, S. J., Ibeanusi, S. E., Jacklyn, G. L., Jasrasaria, R., Jonas, J. B., Kan, H., Kanis, J. A., Kassebaum, N., Kawakami, N., Khang, Y. H., Khatibzadeh, S., Khoo, J. P., Kok, C., Laden, F., Lalloo, R., Lan, Q., Lathlean, T., Leasher, J. L., Leigh, J., Li, Y., Lin, J. K., Lipshultz, S. E., London, S., Lozano, R., Lu, Y., Mak, J., Malekzadeh, R., Mallinger, L., Marcenes, W., March, L., Marks, R., Martin, R., McGale, P., McGrath, J., Mehta, S., Mensah, G. A., Merriman, T. R., Micha, R., Michaud, C., Mishra, V., Mohd Hanafiah, K., Mokdad, A. A., Morawska, L., Mozaffarian, D., Murphy, T., Naghavi, M., Neal, B., Nelson, P. K., Nolla, J. M., Norman, R., Olives, C., Omer, S. B., Orchard, J., Osborne, R., Ostro, B., Page, A., Pandey, K. D., Parry, C. D., Passmore, E., Patra, J., Pearce, N., Pelizzari, P. M., Petzold, M., Phillips, M. R., Pope, D., Pope, C. A., 3rd, Powles, J., Rao, M., Razavi, H., Rehfuess, E. A., Rehm, J. T., Ritz, B., Rivara, F. P., Roberts, T., Robinson, C., Rodriguez-Portales, J. A., Romieu, I., Room, R., Rosenfeld, L. C., Roy, A., Rushton, L., Salomon, J. A., Sampson, U., Sanchez-Riera, L., Sanman, E., Sapkota, A., Seedat, S., Shi, P., Shield, K., Shivakoti, R., Singh, G. M., Sleet, D. A., Smith, E., Smith, K. R., Stapelberg, N. J., Steenland, K., Stockl, H., Stovner, L. J., Straif, K., Straney, L., Thurston, G. D., Tran, J. H., Van Dingenen, R., van Donkelaar, A., Veerman, J. L., Vijayakumar, L., Weintraub, R., Weissman, M. M., White, R. A., Whiteford, H., Wiersma, S. T., Wilkinson, J. D., Williams, H. C., Williams, W., Wilson, N., Woolf, A. D., Yip, P., Zielinski, J. M., Lopez, A. D., Murray, C. J., Ezzati, M., AlMazroa, M. A., and Memish, Z. A.: A comparative risk assessment of burden of disease and injury attributable to 67 risk factors and risk factor clusters in 21 regions, 1990-2010: a systematic analysis for the Global Burden of Disease Study 2010, Lancet (London, England), 380, 2224-2260, 10.1016/s0140-6736(12)61766-8, 2012.

Lipsett, M. J., Ostro, B. D., Reynolds, P., Goldberg, D., Hertz, A., Jerrett, M., Smith, D. F., Garcia, C., Chang, E. T., and Bernstein, L.: Long-term Exposure to Air Pollution and Cardiorespiratory Disease in the California Teachers Study Cohort, Am J Respir Crit Care Med, 184, 10.1164/rccm.201012-2082OC, 2011.

Lipsky, E. M., and Robinson, A. L.: Effects of Dilution on Fine Particle Mass and Partitioning of Semivolatile Organics in Diesel Exhaust and Wood Smoke, Environmental Science & Technology, 40, 155-162, 10.1021/es050319p, 2006.

Litovitz, A., Curtright, A., Abramzon, S., Burger, N., & Samaras, C.: Estimation of regional air-quality damages from Marcellus Shale natural gas extraction in Pennsylvania, Environmental Research Letters, 8, 014017, 2013.

Lowenthal, D. H., Zielinska, B., Chow, J.C., Watson, J.G., Gautam, M., Ferguson, D.H., Neuroth, G.R., and Stevens, K.D.: Characterization of heavy-duty diesel vehicle emissions, Atmospheric Environment, 28, 731-743, http://dx.doi.org/10.1016/1352-2310(94)90050-7, 1994.

Manadhar, U. M., Dangol, S.B.: Study on Evaluating Energy Conservation Potential of Bricks Production in SAARC Countries: A Report for Nepal, SAARC Energy Centre, 2013.

Marr, L. C., Kirchstetter, T. W., Harley, R. A., Miguel, A. H., Hering, S. V., and Hammond, S. K.: Characterization of Polycyclic Aromatic Hydrocarbons in Motor Vehicle Fuels and Exhaust Emissions, Environmental Science & Technology, 33, 3091-3099, 10.1021/es981227l, 1999.

Massoli, P., Fortner, E. C., Canagaratna, M. R., Williams, L. R., Zhang, Q., Sun, Y., Schwab, J. J., Trimborn, A., Onasch, T. B., Demerjian, K. L., Kolb, C. E., Worsnop, D. R., and Jayne, J. T.: Pollution Gradients and Chemical Characterization of Particulate Matter from Vehicular Traffic near Major Roadways: Results from the 2009 Queens College Air Quality Study in NYC, Aerosol Science and Technology, 46, 1201-1218, 10.1080/02786826.2012.701784, 2012.

May, A. A., Levin, E. J. T., Hennigan, C. J., Riipinen, I., Lee, T., Collett, J. L., Jimenez, J. L., Kreidenweis, S. M., and Robinson, A. L.: Gas-particle partitioning of primary organic aerosol emissions: 3. Biomass burning, Journal of Geophysical Research: Atmospheres, 118, 11,327-311,338, 10.1002/jgrd.50828, 2013.

May, A. A., Nguyen, N. T., Presto, A. A., Gordon, T. D., Lipsky, E. M., Karve, M., Gutierrez, A., Robertson, W. H., Zhang, M., Brandow, C., Chang, O., Chen, S., Cicero-Fernandez, P., Dinkins, L., Fuentes, M., Huang, S.-M., Ling, R., Long, J., Maddox, C., Massetti, J., McCauley, E., Miguel, A., Na, K., Ong, R., Pang, Y., Rieger, P., Sax, T., Truong, T., Vo, T., Chattopadhyay, S., Maldonado, H., Maricq, M. M., and Robinson, A. L.: Gas- and particle-phase primary emissions from in-use, on-road gasoline and diesel vehicles, Atmospheric Environment, 88, 247-260, http://dx.doi.org/10.1016/j.atmosenv.2014.01.046, 2014.

McLafferty, F. W., and Turecek, A.: Interpretation of Mass Spectra, University Scientific Books, Mill Valley, CA, 1993.

Millet, D. B., Donahue, N. M., Pandis, S. N., Polidori, A., Stanier, C. O., Turpin, B. J., and Goldstein, A. H.: Atmospheric volatile organic compound measurements during the Pittsburgh Air Quality Study: Results, interpretation, and quantification of primary and secondary contributions, Journal of Geophysical Research: Atmospheres, 110, n/a-n/a, 10.1029/2004JD004601, 2005.

Mohan, J., Griffin, W. M., Chris, H., Paulina, J., Jeanne, V., and Aranya, V.: Life cycle greenhouse gas emissions of Marcellus shale gas, Environmental Research Letters, 6, 034014, 2011.

Mohr, C., Huffman, J. A., Cubison, M. J., Aiken, A. C., Docherty, K. S., Kimmel, J. R., Ulbrich, I. M., Hannigan, M., and Jimenez, J. L.: Characterization of Primary Organic Aerosol Emissions from Meat Cooking, Trash Burning, and Motor Vehicles with High-Resolution Aerosol Mass Spectrometry and Comparison with Ambient and Chamber Observations, Environmental Science & Technology, 43, 2443-2449, 10.1021/es8011518, 2009.

Monod, A., Sive, B. C., Avino, P., Chen, T., Blake, D. R., and Sherwood Rowland, F.: Monoaromatic compounds in ambient air of various cities: a focus on correlations between the xylenes and ethylbenzene, Atmospheric Environment, 35, 135-149, http://dx.doi.org/10.1016/S1352-2310(00)00274-0, 2001.
Moore, C. W., Zielinska, B., Pétron, G., and Jackson, R. B.: Air Impacts of Increased Natural Gas Acquisition, Processing, and Use: A Critical Review, Environmental Science & Technology, 48, 8349-8359, 10.1021/es4053472, 2014.

Nair, V. S., Moorthy, K. K., Alappattu, D. P., Kunhikrishnan, P. K., George, S., Nair, P. R., Babu, S. S., Abish, B., Satheesh, S. K., Tripathi, S. N., Niranjan, K., Madhavan, B. L., Srikant, V., Dutt, C. B. S., Badarinath, K. V. S., and Reddy, R. R.: Wintertime aerosol characteristics over the Indo-Gangetic Plain (IGP): Impacts of local boundary layer processes and long-range transport, Journal of Geophysical Research: Atmospheres, 112, n/a-n/a, 10.1029/2006JD008099, 2007.

Ng, N. L., Canagaratna, M. R., Jimenez, J. L., Zhang, Q., Ulbrich, I. M., and Worsnop, D. R.: Real-Time Methods for Estimating Organic Component Mass Concentrations from Aerosol Mass Spectrometer Data, Environmental Science & Technology, 45, 910-916, 10.1021/es102951k, 2011.

Ogneva-Himmelberger, Y., and Huang, L.: Spatial distribution of unconventional gas wells and human populations in the Marcellus Shale in the United States: Vulnerability analysis, Applied Geography, 60, 165-174, http://dx.doi.org/10.1016/j.apgeog.2015.03.011, 2015.

Ohara, T., Akimoto, H., Kurokawa, J., Horii, N., Yamaji, K., Yan, X., and Hayasaka, T.: An Asian emission inventory of anthropogenic emission sources for the period 1980–2020, Atmos. Chem. Phys., 7, 4419-4444, 10.5194/acp-7-4419-2007, 2007.

Olson, M. R., Victoria Garcia, M., Robinson, M. A., Van Rooy, P., Dietenberger, M. A., Bergin, M., and Schauer, J. J.: Investigation of black and brown carbon multiple-wavelength-dependent light absorption from biomass and fossil fuel combustion source emissions, Journal of Geophysical Research: Atmospheres, 120, 6682-6697, 10.1002/2014JD022970, 2015.

Onasch, T. B., Jayne, J. T., Herndon, S., Worsnop, D. R., Miake-Lye, R. C., Mortimer, I. P., and Anderson, B. E.: Chemical Properties of Aircraft Engine Particulate Exhaust Emissions, Journal of Propulsion and Power, 25, 1121-1137, 10.2514/1.36371, 2009.

Onasch, T. B., Trimborn, A., Fortner, E. C., Jayne, J. T., Kok, G. L., Williams, L. R., Davidovits, P., and Worsnop, D. R.: Soot Particle Aerosol Mass Spectrometer: Development, Validation, and Initial Application, Aerosol Science and Technology, 46, 804-817, 10.1080/02786826.2012.663948, 2012.

Palit, D., and Chaurey, A.: Off-grid rural electrification experiences from South Asia: Status and best practices, Energy for Sustainable Development, 15, 266-276, http://dx.doi.org/10.1016/j.esd.2011.07.004, 2011.

Panday, A. K., and Prinn, R. G.: Diurnal cycle of air pollution in the Kathmandu Valley, Nepal: Observations, Journal of Geophysical Research: Atmospheres, 114, n/a-n/a, 10.1029/2008JD009777, 2009.

Pandey, A., Sadavarte, P., Rao, A. B., and Venkataraman, C.: Trends in multi-pollutant emissions from a technology-linked inventory for India: II. Residential, agricultural and informal industry sectors, Atmospheric Environment, 99, 341-352, http://dx.doi.org/10.1016/j.atmosenv.2014.09.080, 2014.

Pandis, S. N., Harley R.A., Cass, G.R., Seinfeld, J.H.: Secondary organic aerosol formation and transport, Atmospheric Environment, Part A. General Topics, 10.1016/0960-1686(92)90358-R, 1992.

Parrish, D. D., Trainer, M., Young, V., Goldan, P. D., Kuster, W. C., Jobson, B. T., Fehsenfeld, F. C., Lonneman, W. A., Zika, R. D., Farmer, C. T., Riemer, D. D., and Rodgers, M. O.: Internal consistency tests for evaluation of measurements of anthropogenic hydrocarbons in the troposphere, Journal of Geophysical Research: Atmospheres, 103, 22339-22359, 10.1029/98JD01364, 1998.

Peischl, J., Ryerson, T. B., Aikin, K. C., de Gouw, J. A., Gilman, J. B., Holloway, J. S., Lerner, B. M., Nadkarni, R., Neuman, J. A., Nowak, J. B., Trainer, M., Warneke, C., and Parrish, D. D.: Quantifying atmospheric methane emissions from the Haynesville, Fayetteville, and northeastern Marcellus shale gas production regions, Journal of Geophysical Research: Atmospheres, 120, 2119-2139, 10.1002/2014JD022697, 2015.

Pekney, N. J., Veloski, G., Reeder, M., Tamilia, J., Rupp, E., and Wetzel, A.: Measurement of atmospheric pollutants associated with oil and natural gas exploration and production activity in Pennsylvania's Allegheny National Forest, Journal of the Air & Waste Management Association, 64, 1062-1072, 10.1080/10962247.2014.897270, 2014.

Pétron, G., Frost, G., Miller, B.R., Hirsch, A.I., Montzka, S.A., Karion, A., Trainer, M., Sweeney, C., Andrews, A.E., Miller, L., Kofler, J., Bar-Ilan, A., Dlugokencky, E.J., Patrick, L., Moore, C.T., Ryerson, T.B., Siso, C., Kolodzey, W., Lang, P.M., Conway, T., Novelli, P., Masarie, K., Hall, B., Guenther, D., Kitzis, D., Miller, J., Welsh, D., Wolfe, D., Neff, W., and Tans, P.: Hydrocarbon emissions characterization in the Colorado Front Range: A pilot study, Journal of Geophysical Research: Atmospheres, 117, D04304, 10.1029/2011JD016360, 2012.

Phillips, N. G., Ackley, R., Crosson, E. R., Down, A., Hutyra, L. R., Brondfield, M., Karr, J. D., Zhao, K., and Jackson, R. B.: Mapping urban pipeline leaks: Methane leaks across Boston, Environmental Pollution, 173, 1-4, http://dx.doi.org/10.1016/j.envpol.2012.11.003, 2013.

Pope, C. A., Burnett, R. T., Thurston, G. D., Thun, M. J., Calle, E. E., Krewski, D., and Godleski, J. J.: Cardiovascular mortality and long-term exposure to particulate air pollution: epidemiological evidence of general pathophysiological pathways of disease, Circulation, 109, 10.1161/01.cir.0000108927.80044.7f, 2004.

Pope , C. A. I., Ezzati , M., and Dockery , D. W.: Fine-Particulate Air Pollution and Life Expectancy in the United States, New England Journal of Medicine, 360, 376-386, doi:10.1056/NEJMsa0805646, 2009.

Putero, D., Cristofanelli, P., Marinoni, A., Adhikary, B., Duchi, R., Shrestha, S. D., Verza, G. P., Landi, T. C., Calzolari, F., Busetto, M., Agrillo, G., Biancofiore, F., Di Carlo, P., Panday, A. K., Rupakheti, M., and Bonasoni, P.: Seasonal variation of ozone and black carbon observed at Paknajol, an urban site in the Kathmandu Valley, Nepal, Atmos. Chem. Phys., 15, 13957-13971, 10.5194/acp-15-13957-2015, 2015.

Ramanathan, V., Chung, C., Kim, D., Bettge, T., Buja, L., Kiehl, J. T., Washington, W. M., Fu, Q., Sikka, D. R., and Wild, M.: Atmospheric brown clouds: Impacts on South Asian climate and hydrological cycle, Proceedings of the National Academy of Sciences of the United States of America, 102, 5326-5333, 10.1073/pnas.0500656102, 2005.

Reddy, M. S., and Venkataraman, C.: Inventory of aerosol and sulphur dioxide emissions from India: I—Fossil fuel combustion, Atmospheric Environment, 36, 677-697, http://dx.doi.org/10.1016/S1352-2310(01)00463-0, 2002.

Rich, A., Grover, J. P., and Sattler, M. L.: An exploratory study of air emissions associated with shale gas development and production in the Barnett Shale, Journal of the Air & Waste Management Association, 64, 61-72, 10.1080/10962247.2013.832713, 2014.

Roden, C. A., Bond, T. C., Conway, S., and Pinel, A. B. O.: Emission Factors and Real-Time Optical Properties of Particles Emitted from Traditional Wood Burning Cookstoves, Environmental Science & Technology, 40, 6750-6757, 10.1021/es052080i, 2006.

Roden, C. A., Bond, T. C., Conway, S., Osorto Pinel, A. B., MacCarty, N., and Still, D.: Laboratory and field investigations of particulate and carbon monoxide emissions from traditional and improved cookstoves, Atmospheric Environment, 43, 1170-1181, http://dx.doi.org/10.1016/j.atmosenv.2008.05.041, 2009.

Rogers, T. M., Grimsrud, E. P., Herndon, S. C., Jayne, J. T., Kolb, C. E., Allwine, E., Westberg, H., Lamb, B. K., Zavala, M., Molina, L. T., Molina, M. J., and Knighton, W. B.: On-road measurements of volatile organic compounds in the Mexico City metropolitan area using proton transfer reaction mass spectrometry, International Journal of Mass Spectrometry, 252, 26-37, http://dx.doi.org/10.1016/j.ijms.2006.01.027, 2006.

Rolph, G. D.: Real-time Environmental Applications and Display sYstem (READY) Website (http://www.ready.noaa.gov), NOAA Air Resources Laboratory, 2016.

Roscioli, J. R., Yacovitch, T. I., Floerchinger, C., Mitchell, A. L., Tkacik, D. S., Subramanian, R., Martinez, D. M., Vaughn, T. L., Williams, L., Zimmerle, D., Robinson, A. L., Herndon, S. C., and Marchese, A. J.: Measurements of methane emissions from natural gas gathering facilities and processing plants: measurement methods, Atmos. Meas. Tech., 8, 2017-2035, 10.5194/amt-8-2017-2015, 2015.

Roy, A. A., Adams, P.J., & Robinson, A.L.: Air pollutant emissions from the development, production and processing of Marcellus Shale natural gas, Journal of the Air & Waste Management Association, null-null, 10.1080/10962247.2013.826151, 2013.

Rupakheti, D., Adhikary, B., Praveen, P. S., Rupakheti, M., Kang, S., Mahata, K. S., Naja, M., Zhang, Q., Panday, A. K., and Lawrence, M. G.: Pre-monsoon air quality over Lumbini, a world heritage site along the Himalayan foothills, Atmos. Chem. Phys. Discuss., 2016, 1-46, 10.5194/acp-2016-430, 2016.

Sahai, S., Sharma, C., Singh, D. P., Dixit, C. K., Singh, N., Sharma, P., Singh, K., Bhatt, S., Ghude, S., Gupta, V., Gupta, R. K., Tiwari, M. K., Garg, S. C., Mitra, A. P., and Gupta, P. K.: A study for development of emission factors for trace gases and carbonaceous particulate species from in situ burning of wheat straw in agricultural fields in india, Atmospheric Environment, 41, 9173-9186, http://dx.doi.org/10.1016/j.atmosenv.2007.07.054, 2007.

Salcedo, D., Laskin, A., Shutthanandan, V., and Jimenez, J. L.: Feasibility of the Detection of Trace Elements in Particulate Matter Using Online High-Resolution Aerosol Mass Spectrometry, Aerosol Science and Technology, 46, 1187-1200, 10.1080/02786826.2012.701354, 2012.

Saleh, R., Robinson, E. S., Tkacik, D. S., Ahern, A. T., Liu, S., Aiken, A. C., Sullivan, R. C., Presto, A. A., Dubey, M. K., Yokelson, R. J., Donahue, N. M., and Robinson, A. L.: Brownness of organics in aerosols from biomass burning linked to their black carbon content, Nature Geosci, 7, 647-650, 10.1038/ngeo2220 http://www.nature.com/ngeo/journal/v7/n9/abs/ngeo2220.html#supplementary-information, 2014.

Sarkar, C., Sinha, V., Kumar, V., Rupakheti, M., Panday, A., Mahata, K. S., Rupakheti, D., Kathayat, B., and Lawrence, M. G.: Overview of VOC emissions and chemistry from PTR-TOF-MS measurements during the SusKat-ABC campaign: high acetaldehyde, isoprene and isocyanic acid in wintertime air of the Kathmandu Valley, Atmos. Chem. Phys., 16, 3979-4003, 10.5194/acp-16-3979-2016, 2016.

Schneider, J., Weimer, S., Drewnick, F., Borrmann, S., Helas, G., Gwaze, P., Schmid, O., Andreae, M. O., and Kirchner, U.: Mass spectrometric analysis and aerodynamic properties of various types of combustion-related aerosol particles, International Journal of Mass Spectrometry, 258, 37-49, http://dx.doi.org/10.1016/j.ijms.2006.07.008, 2006.

Schnell, R. C., Oltmans, S. J., Neely, R. R., Endres, M. S., Molenar, J. V., and White, A. B.: Rapid photochemical production of ozone at high concentrations in a rural site during winter, Nature Geosci, 2, 120-122, 2009.

Shah, S. D., Johnson, K. C., Wayne Miller, J., and Cocker III, D. R.: Emission rates of regulated pollutants from on-road heavy-duty diesel vehicles, Atmospheric Environment, 40, 147-153, http://dx.doi.org/10.1016/j.atmosenv.2005.09.033, 2006.

Shahid, I., Kistler, M., Mukhtar, A., Ramirez-Santa Cruz, C., Bauer, H., and Puxbaum, H.: Chemical composition of particles from traditional burning of Pakistani wood species, Atmospheric Environment, 121, 35-41, http://dx.doi.org/10.1016/j.atmosenv.2015.01.041, 2015.

Sheesley, R. J., Schauer, J. J., Chowdhury, Z., Cass, G. R., and Simoneit, B. R. T.: Characterization of organic aerosols emitted from the combustion of biomass indigenous to South Asia, Journal of Geophysical Research: Atmospheres, 108, n/a-n/a, 10.1029/2002JD002981, 2003.

Shields, K. N., Cavallari, J. M., Hunt, M. J. O., Lazo, M., Molina, M., Molina, L., and Holguin, F.: Traffic-related air pollution exposures and changes in heart rate variability in Mexico City: A panel study, Environmental Health, 12, 1-14, 10.1186/1476-069x-12-7, 2013.

Shorter, J. H., Herndon, S., Zahniser, M. S., Nelson, D. D., Wormhoudt, J., Demerjian, K. L., and Kolb, C. E.: Real-Time Measurements of Nitrogen Oxide Emissions from In-Use New York City Transit Buses Using a Chase Vehicle, Environmental Science & Technology, 39, 7991-8000, 10.1021/es048295u, 2005.

Simoneit, B. R. T., Schauer, J. J., Nolte, C. G., Oros, D. R., Elias, V. O., Fraser, M. P., Rogge, W. F., and Cass, G. R.: Levoglucosan, a tracer for cellulose in biomass burning and atmospheric particles, Atmospheric Environment, 33, 173-182, http://dx.doi.org/10.1016/S1352-2310(98)00145-9, 1999.

Simoneit, B. R. T., Medeiros, P. M., and Didyk, B. M.: Combustion Products of Plastics as Indicators for Refuse Burning in the Atmosphere, Environmental Science & Technology, 39, 6961-6970, 10.1021/es050767x, 2005.

Simpson, I. J., Sulbaek Andersen, M. P., Meinardi, S., Bruhwiler, L., Blake, N. J., Helmig, D., Rowland, F. S., and Blake, D. R.: Long-term decline of global atmospheric ethane concentrations and implications for methane, Nature, 488, 490-494,

http://www.nature.com/nature/journal/v488/n7412/abs/nature11342.html#supplementary-information, 2012.

Singh, H., Chen, Y., Tabazadeh, A., Fukui, Y., Bey, I., Yantosca, R., Jacob, D., Arnold, F., Wohlfrom, K., Atlas, E., Flocke, F., Blake, D., Blake, N., Heikes, B., Snow, J., Talbot, R., Gregory, G., Sachse, G., Vay, S., and Kondo, Y.: Distribution and fate of selected oxygenated organic species in the troposphere and lower stratosphere over the Atlantic, Journal of Geophysical Research: Atmospheres, 105, 3795-3805, 10.1029/1999JD900779, 2000.

Stein, A. F., Draxler, R.R., Rolph, G.D., Stunder, B.J.B., Cogen, M.D., and Ngan, F.: NOAA's HYSPLIT atmospheric transport and dispersion modeling system, Bull., American Meteological Society, 96, 2059-2077, http://dx.doi.org/10.1175/BAMS-D-14-00110.1, 2015.

Stein, S., Mirokhin, D., Tchekhovskoi, D., and Mallard, G.: The NIST Mass Spectral Search Program for the NIST/EPA/NIH Mass Spectral Library, The Standard Referecne Data Program of NIST, 2001.

Stephenson, T., Valle, J. E., and Riera-Palou, X.: Modeling the Relative GHG Emissions of Conventional and Shale Gas Production, Environmental Science & Technology, 45, 10757-10764, 10.1021/es2024115, 2011.

Stockwell, C. E., Yokelson, R. J., Kreidenweis, S. M., Robinson, A. L., DeMott, P. J., Sullivan, R. C., Reardon, J., Ryan, K. C., Griffith, D. W. T., and Stevens, L.: Trace gas emissions from combustion of peat, crop residue, domestic biofuels, grasses, and other fuels: configuration and Fourier transform infrared (FTIR) component of the fourth Fire Lab at Missoula Experiment (FLAME-4), Atmos. Chem. Phys., 14, 9727-9754, 10.5194/acp-14-9727-2014, 2014.

Stockwell, C. E., Veres, P. R., Williams, J., and Yokelson, R. J.: Characterization of biomass burning emissions from cooking fires, peat, crop residue, and other fuels with high-resolution proton-transfer-reaction time-of-flight mass spectrometry, Atmos. Chem. Phys., 15, 845-865, 10.5194/acp-15-845-2015, 2015.

Stockwell, C. E., Christian, T. J., Goetz, J. D., Jayarathne, T., Bhave, P. V., Praveen, P. S., Adhikari, S., Maharjan, R., DeCarlo, P. F., Stone, E. A., Saikawa, E., Blake, D. R., Simpson, I., Yokelson, R. J., and Panday, A. K.: Nepal Ambient Monitoring and Source Testing Experiment (NAMaSTE): Emissions of trace gases and light-absorbing carbon from wood and dung cooking fires, garbage and crop residue burning, brick kilns, and other sources, Atmos. Chem. Phys. Discuss., 2016, 1-57, 10.5194/acp-2016-154, 2016.

Stone, E. A., Schauer, J. J., Pradhan, B. B., Dangol, P. M., Habib, G., Venkataraman, C., and Ramanathan, V.: Characterization of emissions from South Asian biofuels and application to source apportionment of carbonaceous aerosol in the Himalayas, Journal of Geophysical Research: Atmospheres, 115, n/a-n/a, 10.1029/2009JD011881, 2010.

Streets, D. G., Bond, T. C., Carmichael, G. R., Fernandes, S. D., Fu, Q., He, D., Klimont, Z., Nelson, S. M., Tsai, N. Y., Wang, M. Q., Woo, J. H., and Yarber, K. F.: An inventory of gaseous and primary aerosol emissions in Asia in the year 2000, Journal of Geophysical Research: Atmospheres, 108, n/a-n/a, 10.1029/2002JD003093, 2003.

Subramanian, R., Williams, L. L., Vaughn, T. L., Zimmerle, D., Roscioli, J. R., Herndon, S. C., Yacovitch, T. I., Floerchinger, C., Tkacik, D. S., Mitchell, A. L., Sullivan, M. R., Dallmann, T. R., and Robinson, A. L.: Methane Emissions from Natural Gas Compressor Stations in the Transmission and Storage Sector: Measurements and Comparisons with the EPA Greenhouse Gas Reporting Program Protocol, Environmental Science & Technology, 49, 3252-3261, 10.1021/es5060258, 2015.

Swarthout, R. F., Russo, R. S., Zhou, Y., Miller, B. M., Mitchell, B., Horsman, E., Lipsky, E., McCabe, D. C., Baum, E., and Sive, B. C.: Impact of Marcellus Shale Natural Gas Development in Southwest

Pennsylvania on Volatile Organic Compound Emissions and Regional Air Quality, Environmental Science & Technology, 49, 3175-3184, 10.1021/es504315f, 2015.

Tao, L., Sun, K., Miller, D. J., Pan, D., Golston, L. M., and Zondlo, M. A.: Low-power, open-path mobile sensing platform for high-resolution measurements of greenhouse gases and air pollutants, Applied Physics B, 119, 153-164, 10.1007/s00340-015-6069-1, 2015.

Thoma, E. a. B. S.: OTM 33 Geospatial Measurement of Air Pollution, Remote Emissions Quantification (GMAP-REQ) and OTM33A Geospatial Measurement of Air Pollution-Remote Emissions Quantification-Direct Assessment (GMAP-REQ-DA), US Environmental Protection Agency, 2014.

Timko, M. T., Yu, Z., Kroll, J., Jayne, J. T., Worsnop, D. R., Miake-Lye, R. C., Onasch, T. B., Liscinsky, D., Kirchstetter, T. W., Destaillats, H., Holder, A. L., Smith, J. D., and Wilson, K. R.: Sampling Artifacts from Conductive Silicone Tubing, Aerosol Science and Technology, 43, 855-865, 10.1080/02786820902984811, 2009.

Torvela, T., Tissari, J., Sippula, O., Kaivosoja, T., Leskinen, J., Virén, A., Lähde, A., and Jokiniemi, J.: Effect of wood combustion conditions on the morphology of freshly emitted fine particles, Atmospheric Environment, 87, 65-76, http://dx.doi.org/10.1016/j.atmosenv.2014.01.028, 2014.

Transcontinental Gas Pipe Line Company, L.: Application for Certificate of Public Convenience and Necessity (Leidy Souteast Project) docket no. CP13-, Federal Energy Regulatory Commission (FERC), 2013.

Hazardous Air Pollutants: http://www.epa.gov/haps, 2015.

Ulbrich, I. M., Canagaratna, M. R., Zhang, Q., Worsnop, D. R., and Jimenez, J. L.: Interpretation of organic components from Positive Matrix Factorization of aerosol mass spectrometric data, Atmos. Chem. Phys., 9, 2891-2918, 10.5194/acp-9-2891-2009, 2009.

United Nations: Demographic Yearbook 2014, Statistics Division, 2014.

Venkataraman, C., and Rao, G. U. M.: Emission Factors of Carbon Monoxide and Size-Resolved Aerosols from Biofuel Combustion, Environmental Science & Technology, 35, 2100-2107, 10.1021/es001603d, 2001.

Venkataraman, C., Habib, G., Eiguren-Fernandez, A., Miguel, A. H., and Friedlander, S. K.: Residential Biofuels in South Asia: Carbonaceous Aerosol Emissions and Climate Impacts, Science, 307, 1454-1456, 10.1126/science.1104359, 2005.

Vinciguerra, T., Yao, S., Dadzie, J., Chittams, A., Deskins, T., Ehrman, S., and Dickerson, R. R.: Regional air quality impacts of hydraulic fracturing and shale natural gas activity: Evidence from ambient VOC observations, Atmospheric Environment, 110, 144-150, http://dx.doi.org/10.1016/j.atmosenv.2015.03.056, 2015.

von der Weiden-Reinmüller, S. L., Drewnick, F., Crippa, M., Prévôt, A. S. H., Meleux, F., Baltensperger, U., Beekmann, M., and Borrmann, S.: Application of mobile aerosol and trace gas measurements for the investigation of megacity air pollution emissions: the Paris metropolitan area, Atmos. Meas. Tech., 7, 279-299, 10.5194/amt-7-279-2014, 2014.

Wang, M., Zhu, T., Zheng, J., Zhang, R. Y., Zhang, S. Q., Xie, X. X., Han, Y. Q., and Li, Y.: Use of a mobile laboratory to evaluate changes in on-road air pollutants during the Beijing 2008 Summer Olympics, Atmos. Chem. Phys., 9, 8247-8263, 10.5194/acp-9-8247-2009, 2009.

Wang, Y., Hopke, P. K., Rattigan, O. V., Chalupa, D. C., and Utell, M. J.: Multiple-year black carbon measurements and source apportionment using Delta-C in Rochester, New York, Journal of the Air & Waste Management Association, 62, 880-887, 10.1080/10962247.2012.671792, 2012.

Ward, D. E.: Factors Influencing the Emissions of Gases and Particulate Matter from Biomass Burning, in: Fire in the Tropical Biota: Ecosystem Processes and Global Challenges, edited by: Goldammer, J. G., Springer Berlin Heidelberg, Berlin, Heidelberg, 418-436, 1990.

Warneke, C., Geiger, F., Edwards, P. M., Dube, W., Pétron, G., Kofler, J., Zahn, A., Brown, S. S., Graus, M., Gilman, J. B., Lerner, B. M., Peischl, J., Ryerson, T. B., de Gouw, J. A., and Roberts, J. M.: Volatile organic compound emissions from the oil and natural gas industry in the Uintah Basin, Utah: oil and gas well pad emissions compared to ambient air composition, Atmos. Chem. Phys., 14, 10977-10988, 10.5194/acp-14-10977-2014, 2014.

Weber, C. L., and Clavin, C.: Life Cycle Carbon Footprint of Shale Gas: Review of Evidence and Implications, Environmental Science & Technology, 46, 5688-5695, 10.1021/es300375n, 2012.

Weimer, S., Alfarra, M. R., Schreiber, D., Mohr, M., Prévôt, A. S. H., and Baltensperger, U.: Organic aerosol mass spectral signatures from wood-burning emissions: Influence of burning conditions and wood type, Journal of Geophysical Research: Atmospheres, 113, n/a-n/a, 10.1029/2007JD009309, 2008.

Wells, K. C., Millet, D. B., Hu, L., Cady-Pereira, K. E., Xiao, Y., Shephard, M. W., Clerbaux, C. L., Clarisse, L., Coheur, P. F., Apel, E. C., de Gouw, J., Warneke, C., Singh, H. B., Goldstein, A. H., and Sive, B. C.: Tropospheric methanol observations from space: retrieval evaluation and constraints on the seasonality of biogenic emissions, Atmos. Chem. Phys., 12, 5897-5912, 10.5194/acp-12-5897-2012, 2012.

Weyant, C., Athalye, V., Ragavan, S., Rajarathnam, U., Lalchandani, D., Maithel, S., Baum, E., and Bond, T. C.: Emissions from South Asian Brick Production, Environmental Science & Technology, 48, 6477-6483, 10.1021/es500186g, 2014.

Wiedinmyer, C., Yokelson, R. J., and Gullett, B. K.: Global Emissions of Trace Gases, Particulate Matter, and Hazardous Air Pollutants from Open Burning of Domestic Waste, Environmental Science & Technology, 48, 9523-9530, 10.1021/es502250z, 2014.

Winijkul, E., and Bond, T. C.: Emissions from residential combustion considering end-uses and spatial constraints: Part II, emission reduction scenarios, Atmospheric Environment, 124, Part A, 1-11, http://dx.doi.org/10.1016/j.atmosenv.2015.10.011, 2016.

Wood, E. C., Herndon, S. C., Fortner, E. C., Onasch, T. B., Wormhoudt, J., Kolb, C. E., Knighton, W. B., Lee, B. H., Zavala, M., Molina, L., and Jones, M.: Combustion and Destruction/Removal Efficiencies of In-Use Chemical Flares in the Greater Houston Area, Industrial & Engineering Chemistry Research, 51, 12685-12696, 10.1021/ie202717m, 2012.

World Health Organization: Fuel For Life: Houshold Energy and Health, http://www.who.int/indoorair/publications/fuelforlife/en/, 2006.

World Meterological Organization, W.: Volume IV - Greenhouse Gases and Other Atmospheric Gases, 2013.

Yacovitch, T. I., Herndon, S. C., Pétron, G., Kofler, J., Lyon, D., Zahniser, M. S., and Kolb, C. E.: Mobile Laboratory Observations of Methane Emissions in the Barnett Shale Region, Environmental Science & Technology, 49, 7889-7895, 10.1021/es506352j, 2015.

Yacovitch, T. I., Herndon, Scott C., Roscioli, Joseph R., Floerchinger, Cody, McGovern, Ryan M., Agnese, Michael, Petron, Gabrielle, Kofler, Jonathan, Sweeney, Colm, Karion, Anna, Conley, S. A., Kort, Eric A., Nähle, Lars, Fischer, Marc, Hildebrandt, Lars, Koeth, Johannes, McManus, Barry J., Nelson, David D., Zahniser, Mark, Kolb, Charles E.: Demonstration of an Ethane Spectrometer for Methane Source Identification, Environmental Science & Technology, 10.1021/es501475q, 2014.

Yang, H.-H., Chien, S.-M., Chao, M.-R., and Lin, C.-C.: Particle size distribution of polycyclic aromatic hydrocarbons in motorcycle exhaust emissions, Journal of Hazardous Materials, 125, 154-159, http://dx.doi.org/10.1016/j.jhazmat.2005.05.019, 2005.

Yuan, B., Kaser, L., Karl, T., Graus, M., Peischl, J., Campos, T. L., Shertz, S., Apel, E. C., Hornbrook, R. S., Hills, A., Gilman, J. B., Lerner, B. M., Warneke, C., Flocke, F. M., Ryerson, T. B., Guenther, A. B., and de Gouw, J. A.: Airborne flux measurements of methane and volatile organic compounds over the Haynesville and Marcellus shale gas production regions, Journal of Geophysical Research: Atmospheres, 120, 6271-6289, 10.1002/2015JD023242, 2015.

Zavala, M., Herndon, S. C., Wood, E. C., Jayne, J. T., Nelson, D. D., Trimborn, A. M., Dunlea, E., Knighton, W. B., Mendoza, A., Allen, D. T., Kolb, C. E., Molina, M. J., and Molina, L. T.: Comparison of emissions from on-road sources using a mobile laboratory under various driving and operational sampling modes, Atmos. Chem. Phys., 9, 1-14, 10.5194/acp-9-1-2009, 2009.

Zavala-Araiza, D., Lyon, D., Alvarez, R. A., Palacios, V., Harriss, R., Lan, X., Talbot, R., and Hamburg, S. P.: Toward a Functional Definition of Methane Super-Emitters: Application to Natural Gas Production Sites, Environmental Science & Technology, 49, 8167-8174, 10.1021/acs.est.5b00133, 2015a.

Zavala-Araiza, D., Lyon, D. R., Alvarez, R. A., Davis, K. J., Harriss, R., Herndon, S. C., Karion, A., Kort, E. A., Lamb, B. K., Lan, X., Marchese, A. J., Pacala, S. W., Robinson, A. L., Shepson, P. B., Sweeney, C., Talbot, R., Townsend-Small, A., Yacovitch, T. I.,
Zimmerle, D. J., and Hamburg, S. P.: Reconciling divergent estimates of oil and gas methane emissions, Proceedings of the National Academy of Sciences, 112, 15597-15602, 10.1073/pnas.1522126112, 2015b.

Zhang, Q., Alfarra, M. R., Worsnop, D. R., Allan, J. D., Coe, H., Canagaratna, M. R., and Jimenez, J. L.: Deconvolution and Quantification of Hydrocarbon-like and Oxygenated Organic Aerosols Based on Aerosol Mass Spectrometry, Environmental Science & Technology, 39, 4938-4952, 10.1021/es048568l, 2005a.
Zhang, Q., Worsnop, D. R., Canagaratna, M. R., and Jimenez, J. L.: Hydrocarbon-like and oxygenated organic aerosols in Pittsburgh: insights into sources and processes of organic aerosols, Atmos. Chem. Phys., 5, 3289-3311, 10.5194/acp-5-3289-2005, 2005b.

Zhang, Q., Jimenez, J. L., Canagaratna, M. R., Ulbrich, I. M., Ng, N. L., Worsnop, D. R., and Sun, Y.: Understanding atmospheric organic aerosols via factor analysis of aerosol mass spectrometry: a review, Analytical and Bioanalytical Chemistry, 401, 3045-3067, 10.1007/s00216-011-5355-y, 2011.

Zhang, X., Smith, K. A., Worsnop, D. R., Jimenez, J. L., Jayne, J. T., Kolb, C. E., Morris, J., and Davidovits, P.: Numerical Characterization of Particle Beam Collimation: Part II Integrated Aerodynamic-Lens–Nozzle System, Aerosol Science and Technology, 38, 619-638, 10.1080/02786820490479833, 2004.

Zhu, D., Nussbaum, N. J., Kuhns, H. D., Chang, M. C. O., Sodeman, D., Uppapalli, S., Moosmüller, H., Chow, J. C., and Watson, J. G.: In-Plume Emission Test Stand 2: Emission Factors for 10- to 100-kW U.S. Military Generators, Journal of the Air & Waste Management Association, 59, 1446-1457, 10.3155/1047-3289.59.12.1446, 2009.

# Vita

## Education

**Ph.D. Candidate, Environmental Engineering** Expected March 2017
Department of Civil, Architectural, and Environmental Engineering
College of Engineering, Drexel University, Philadelphia, PA

**Bachelor of Science in Environmental Geoscience** December 2009
Department of Geology, Geography, and the Environment
College of Arts and Science, Slippery Rock University, Slippery Rock, PA

## Research Experience

**Drexel Air Resources Research Laboratory, Drexel University** July 2012 – Present
**Graduate Research Assistant – DeCarlo Group**

- Participated in atmospheric measurement campaigns in:
    - McMurdo Sound, Antarctica, 2ODIAC (http://www.2odiac.com/) – Fall 2015
    - Marcellus Shale region of Northwestern Pennsylvania – Summer 2015
    - Kathmandu Valley and Terai Regions, Nepal, NAMaSTE – Spring 2015
    - Marcellus Regions of Pennsylvania – Summer 2012
    - Philadelphia, Pennsylvania – various mobile monitoring – 2012-2016
- Designed and constructed the Drexel Mobile Lab, a mobile measurement platform implemented for near-source atmospheric surveying, emissions characterization, and ambient surveying in Philadelphia and broader regions of Pennsylvania
- Programmed software tools for the analysis of tracer ratio and point source Gaussian emissions data collected by ground-based mobile measurement platforms to characterize emission rates from natural gas infrastructure
- Assisted in the design, construction, and programming of CLEARPM, a suite of air quality instrumentation designed to educate all age groups about air quality, atmospheric science, and environmental engineering principles
- Performed lab and field experiments with research grade instrumentation:
    - Soot-particle Aerosol Mass Spectrometer (SP-AMS)
    - Mini Aerosol Mass Spectrometer (mAMS)
    - Scanning Particle Sizers (TSI, Cambustion, Brechtel)
    - Magee Scientific AE33 aethalometer
    - Picarro Cavity Ring Down Spectrometer
    - Aerodyne TILDAS Trace Gas Monitors
    - Aerodyne CAPS $NO_2$ monitor

**NASA Student Airborne Research Program, Irvine, California** Summer 2009
**Student Researcher**

- Participated in a NASA funded undergraduate research experience through the National Suborbital Education and Research Center
- Conducted hydrological research on agriculture in water scarce areas using the MASTER aerial hyperspectral remote sensing instrument installed on the NASA DC-8
- Gained understanding and practice of how to conduct a scientific research project from the starting proposal to the final written and oral communication of findings

## Publications

**Goetz, J. D.**, Giordano, M. R., Stockwell, C. E., Christian, T. J., Maharjan, R., Adhikari, S., Bhave, P. V., Praveen, P. S., Panday, A. K., Jayarathne, T., Stone, E. A., Yokelson, R. J., and DeCarlo, P. F.: Speciated On-line PM1 from South Asian Combustion Sources: Part I, Fuel-based Emission Factors and Size Distributions, in prep., 2017.

**Goetz, J. D.**, Giordano, M. R., Stockwell, C. E., Christian, T. J., Maharjan, R., Adhikari, S., Bhave, P. V., Praveen, P. S., Panday, A. K., Jayarathne, T., Stone, E. A., Yokelson, R. J., and DeCarlo, P. F.: Speciated On-line PM1 from South Asian Combustion Sources: Part II, AMS Mass Spectral Profiles and Wavelength Dependence, in prep., 2017.

**Goetz, J. D.**, Avery A., Werden, B., Floerchinger, C., Fortner, E. C., Wormhoudt, J., Massoli, P., Herndon, S. C., Kolb, C., Knighton, W. B, Peischl, J., Warneke, C., de Gouw, J.A., Shaw, S. L., DeCarlo, P. F.: Analysis of local-scale background concentrations of methane and other gas-phase species in the Marcellus Shale, *Elem Sci Anth,* 2017;5:1. DOI:http://doi.org/10.1525/elementa.182

Giordano, M. R., Kalnajs, L. E., Avery, A., **Goetz, J. D.**, Davis, S. M., and DeCarlo, P. F.: A missing source of aerosols in Antarctica – beyond long-range transport, phytoplankton, and photochemistry, *Atmos. Chem. Phys. Discuss*, doi:10.5194/acp-2016-606, Accepted

Stockwell, C. E., Christian, T. J., **Goetz, J. D.**, Jayarathne, T., Bhave, P. V., Praveen, P. S., Adhikari, S., Maharjan, R., DeCarlo, P. F., Stone, E. A., Saikawa, E., Blake, D. R., Simpson, I. J., Yokelson, R. J., and Panday, A. K.: Nepal Ambient Monitoring and Source Testing Experiment (NAMaSTE): emissions of trace gases and light-absorbing carbon from wood and dung cooking fires, garbage and crop residue burning, brick kilns, and other sources, *Atmos. Chem. Phys.*, 16, 11043-11081, doi:10.5194/acp-16-11043-2016, 2016.

**Goetz, J. D.**, Floerchinger, C., Fortner, E. C., Wormhoudt, J., Massoli, P., Knighton, W. B., Herndon, S. C., Kolb, C. E., Knipping, E., Shaw, S. L., DeCarlo, P. F.: Atmospheric Emission Characterization of Marcellus Shale Natural Gas Development Sites. *Environmental Science & Technology* 2015, 49, (11), 7012-7020.

## Recent Presentations

**Goetz, J.D**, Giordano, M.R., Stockwell, C.E., Christian, T.J., Maharjan, R., Adhikari, S., Bhave, P.V., Praveen, P.S., Panday, A.K., Jayarathne, T., Stone, E.A., Yokelson, R.J., DeCarlo, P.F.: Speciated PM1 Emission Factors and AMS Mass Spectral Profiles of South Asian Combustion Sources, *American Association of Aerosol Research,* October 2016

**Goetz, J.D**, Giordano, M.R., Stockwell, C.E., Christian, T.J., Maharjan, R., Adhikari, S., Bhave, P.V., Praveen, P.S., Panday, A.K., Jayarathne, T., Stone, E.A., Yokelson, R.J., DeCarlo, P.F.: Mass Spectral Characterization of Aerosol Emissions from South Asian Combustion Sources, *American Chemical Society Annual Meeting,* August 2016

**Goetz, J. D.**, Floerchinger, C., Fortner, E. C., Wormhoudt, J., Massoli, P., Knighton, W. B., Herndon, S. C., Kolb, C. E., Knipping, E., Shaw, S. L., DeCarlo, P. F: Characterization of Early Stage Marcellus Shale Development Atmospheric Emissions and Regional Air Quality Impacts using Fast Mobile Measurements, *American Geophysical Union Fall Meeting*, December 2014

**Goetz, J. D.**, Floerchinger, C., Fortner, E. C., Wormhoudt, J., Massoli, P., Knighton, W. B., Herndon, S. C., Kolb, C. E., Knipping, E., Shaw, S. L., DeCarlo, P. F: Site Specific Emission Characterization of Marcellus Shale Development using Fast Mobile Measurements, *American Geophysical Union Fall Meeting*, December 2013

## Awards and Funding

| | |
|---|---|
| Koerner Family Award | Spring 2014 |
| Matthew Veltri Environmental Science Scholarship | Spring 2008 |
| Member of Sigma Gamma Epsilon, an earth science honor society | Spring 2007 |
| Research Assistant Funding - Electric Power Research Institute | 2012 –2015 |
| Research Assistant Funding – National Science Foundation | 2015-2017 |